Development of stationary phase gradients and multi-functional stationary phases in capillary formats.

Sinéad Ann Currivan BSc.

Student Number: 53391698

Under the Supervision of Prof. Brett Paull

(ACROSS, University of Tasmania, Australia)

and Dr. Damian Connolly

(School of Chemical Sciences, DCU)

A thesis submitted to Dublin City University for consideration

for the degree of:

Doctor of Philosophy.

Dublin City University

School of Chemical Sciences

September 2012

I hereby certify that this material, which I now submit for assessment on the programme of study leading to the award of *Doctor of Philosophy* is entirely my own work, and that I have exercised reasonable care to ensure that the work is original, and does not to the best of my knowledge breach any law of copyright, and has not been taken from the work of others save and to the extent that such work has been cited and acknowledged within the text of my work.

Signed: _____ (Candidate) ID No.: _____ Date: _____

Table of contents

List of Abbreviations.

AIBN	α,α'-azoisobutyronitrile.
AMPS	2-acrylamido-2-methyl-1-propanesulphonic acid.
BSA	Bovine serum albumin.
BuMA	Butyl methacrylate.
C^4D	Capacitively coupled contactless conductivity detector.
CA	Carrier ampholyte.
CE	Capillary electrophoresis.
CEC	Capillary electrochromatography.
CZE	Capillary zone electrophoresis.
COC	Cyclic olefin co-polymer.
CTAB	Cetytrimethyl ammonium bromide.
DAP	2,2-dimethoxy-2-phenylacetophenone.
DOSS	Sodium dioctyl sulfosuccinate.
EDMA	Ethylene dimethacrylate.
EOF	Electro osmotic flow.
EDX	Energy dispersive X-ray spectroscopy.
FE-SEM	Field emission scanning electron microscopy.
GMA	Glycidyl methacrylate.
HEMA	2-hydroxyethyl methacrylate.
HPLC	High performance liquid chromatography.
IC	Ion chromatography.
IEX	Ion exchange chromatography.
IEF	Isoelectric focusing.
IDA	Iminodiacetic acid.
IMAC	Immobilised metal affinity chromatography.
ISEC	Inverse size exclusion chromatography.
LMA	Lauryl methacrylate.
META	Methacryloyloxyethyl trimethylammonium chloride.
MudPIT	Multi dimensional protein identification technology.
ODS	Octadecylsilane.

PC	Poly carbonate.
PEEK	Polyether ether ketone.
PEG	Poly(ethylene glycol)
PEGMA	Poly(ethylene glycol) methyl ether methacrylate.
PET	Polyethylene terephthalate.
PDMA	Polydimethoxysilane.
PMMA	Polymethylmethacrylate.
PTFE	Poly(tetrafluoroethylene).
sC^4D	Scanning C^4D.
SCX	Strong cation exchange.
SDS	Sodium dodecyl sulphate.
SEM	Scanning electron microscopy.
SPE	Solid phase extraction.
SPM	Sulphopropyl methacrylate.
TES	2-[(2-hydroxy-1,1-bis(hydroxymethyl)ethyl)amino]ethanesulphonic acid.
THF	Tetrahydrofuran.
VAL	4,4-Dimethyl-2-vinyl-2-oxazolin-5-one (synonym Vinyl Azlactone).

List of Figures

Figure 4.4: *%T for increasing film thickness (a), optical density for 13 layers of 40 µm COC film (b). Insert; film thickness of 200 µm, as indicated by red box, expanded to show error bar.*

Figure 4.5: *Schematic of the application of the COC film optical filter. Optical density increases from left to right as indicated by grey scaling.*

Figure 4.6*:* *Columns 1 (-♦-), 2 (-■-) and 3 (-▲-) profiled using sC^4D prior to surface grafting of VAL. Flow rate 1 µL/min, 2.5 m*M*, TES 3 m*M *ethanolamine. Columns scanned in triplicate as indicated by error bars. Column signals have been offset by +50 mV each for illustrative purposes only. Column 1 measured 150 mm, columns 2 and 3 measured 140 mm in length.*

Figure 4.7*:* *sC^4D profiles of a BuMA-co-EDMA monolithic column prior to grafting of PEGMA (a), and following the grafting of PEGMA (b). Column scanned in 2.5 m*M *TES, 3 m*M *ethanolamine at a flow rate of 1 µL/min. Insert, structure of PEGMA.*

Figure 4.8: *sC^4D profiles prior to and following grafting of VAL and immobilisation of IDA for Column 1 (a), Column 2 (b), and Column 3 (c). Scanning buffer 2.5 m*M *TES 3 m*M *ethanolamine at 1 µL/min. Measurements for sC^4D taken at 5 mm for blank columns conditions and 1 mm for grafted gradient column conditions. Gradient columns were normalised to blank columns by subtraction of excess signal generated by the buffer, for illustrative purposes only.*

Figure 4.9: *Plot of C^4D response versus temperature for deionised water. Temperature controlled by column oven heater. C^4D response measured at 16 °C, 18 °C, 20 °C, 25 °C and 30 °C. Flow rate of 1 µL/min.*

Figure 4.10: *sC^4D profiles of Column 1 in IDA form (a)(i), and following complex formation (b)(i). Change in conductive response versus detector position along column, difference between (i) and (ii) of part (a), (b). Plots measured in triplicate, error bars included. Scan performed in 2.5 m*M *TES, 3 m*M *ethanolamine at a flow rate of 1 µL/min.*

Figure 4.11: *sC^4D profile of Column 3 in IDA form (a), following complex formation using dynamic (b) and static immobilisation (c). The difference between the final data points in (b) and (c) was used to*

List of Tables

List of Publications.

Sinéad Currivan, Damian Connolly, Brett Paull, *Microchemical Journal*, accepted August 2012.

Title: *Production of polymer monolithic capillary columns with integrated gold nano-particle modified segments for on-capillary extraction.*

Damian Connolly, Sinéad Currivan, Brett Paull, *Proteomics*, invited review, accepted, April 2012.

Title: *Polymeric monoliths modified with nano-particles for separation and detection of biomolecules.*

Sinead Currivan, Damian Connolly, Brett Paull, *Analyst*, 137, 2012, 2559.

Title: *Production of novel polymer monolithic columns, with stationary phase gradients, using cyclic olefin co-polymer (COC) optical filters.*

Sinéad Currivan, Damian Connolly, Eoin Gillespie, Brett Paull, *Journal of Separation Science*, 33, 2010, 484-492.

Title: *Fabrication and characterisation of capillary polymeric monoliths incorporating continuous stationary phase gradients.*

List of Poster Presentations.

- International Conference of Trends in Bioanalytical Sciences and Biosensors, 26th - 27th of January 2009, Crown Plaza Hotel, Dublin, Ireland.
  "*Use of contactless conductivity detection for the direct visualisation of stationary phase gradients on polymer monoliths.*"

Sinéad Currivan, Damian Connolly, Eoin Gillespie, Brett Paull.

- Analytical Research Forum 13th-15th July 2009, University of Canterbury, Kent and Pfizer global R+D Labs, Sandwich, Kent, United Kingdom.
  "Use of on-column scanning contactless conductivity detection for the direct visualisation of stationary phase gradients on polymer monoliths."
  Sinéad Currivan, Damian Connolly, Eoin Gillespie, Brett Paull.
- Euroanalysis 2009, Innsbruck Congress Centre, Innsbruck, Austria, Septemeber 6th-10th.
  "Use of on-column scanning contactless conductivity detection for the direct visualisation of stationary phase gradients on polymer monoliths."
  Sinéad Currivan, Damian Connolly, Eoin Gillespie, Brett Paull.
- International Ion Chromatography Symposium (IICS) 2009, The Grand Hotel, Malahide, September 21st-24th 2009 .
  "On-column visualisation of stationary phase gradients in polymer monoliths using scanning contactless conductivity."
  Sinéad Currivan, Damian Connolly, Eoin Gillespie, Brett Paull.
- UNCSR 1st Annual Symposium, the Helix, DCU, October 22nd 2009.
  "Use of contactless conductivity detection for the direct visualisation of stationary phase gradients on polymer monoliths."
  Sinéad Currivan, Damian Connolly, Eoin Gillespie, Brett Paull.
- HPLC 2010, Hynes Convention Centre, Boston, MA, USA, June 19th-24th 2010.
  "Production of functional gradients on monolithic rods via photografting, characterisation with scanning contactless conductivity detection and investigations into on-column focusing."
  Sinéad Currivan, Damian Connolly, Brett Paull.
- Analytical Research Forum 2010, Loughborough University, UK, July 26th-28th 2010.
  "Production and non-invasive visualisation of stationary phase gradients on capillary monoliths for on-column focusing of selected analytes."
  Sinéad Currivan, Damian Connolly, Brett Paull.
- International Symposium on Chromatography, Valencia Conference Centre, Valencia, Spain, September 12th-16th 2010.

"Use of scanning contactless conductivity detection (sC^{4}D) for the visualisation of stationary phase gradients in capillary polymeric monolithic rod columns."

Sinéad Currivan, Damian Connolly, Brett Paull.

- Conference on Analytical Sciences Ireland, the Helix, DCU, February 21st-22nd 2011.

  "Fabrication of novel monolithic stationary phases incorporating a gradient of bonded iminodiacetic acid for potential IMAC or bio-affinity applications."

  Sinéad Currivan, Damian Connolly, Paul Clarke, Róisín Thompson, Brendan O'Connor and Brett Paull**.**

List of Honours and Awards.

Analytical Chemistry Trust Fund bursary for attendance to the RSC Analytical Research Forum 2010.

Analytical Chemistry Trust Fund bursary for attendance to the RSC Analytical Research Forum 2009.

Acknowledgements

Firstly, I would like to extend my gratitude to Prof. Brett Paull, and Dr. Damian Connolly for giving me the chance to obtain my PhD, and for their guidance throughout the course of the project. I would also like to thank Prof. Pavel Nesterenko, for his advice throughout my PhD (большое спасибо). I wish to thank all my colleagues within the ISSC and the NCSR, especially those in S205D. Through all the morning coffees, evening teas, and summer ice creams, you have made these past three years wonderful, I am sincerely grateful to you all. The amazing technical staffs in the School of Chemical Sciences and the National Centre for Sensor Research deserve a resounding thank you also, for all their support.

To my parents Ann and Des, my brother David, and to my partner James Spencer, without the emotional and physical support I would have crashed out long ago. Thank you all for the late night lifts, the hugs, and the many, many cups of tea (and perhaps one too many cupcakes??). Go raibh míle maith agat, ar fad. Gan sibh ní ba mhaith liom a bheith críochnaithe ar an gcúrsa.

Most importantly, I wish to thank my former class mate, the late Deirdre Gallagher, for her amazing spirit and courage which she exhibited throughout her life. Without her inspiration I would not have come this far.

Of course there will be the inevitable person who was not listed. To you, thank you.

Abstract

The following thesis provides an extensive study into the fabrication of polymer monolithic columns in capillary housing, their modification and subsequent characterisation. The fabricated columns, in all instances, were profiles using scanning capacitively coupled contactless conductivity detection (sC^4D), a non-invasive method of characterisation, which can provide information on the density of the monolithic column, and the distribution of charged functional groups within the column.

Using thermally initiated co-monomer polymerisation, monolithic columns were fabricated within fused silica capillaries. The resulting distribution of charged functional groups was monitored using sC^4D. Thermally initiated gradient monolithic columns produced linear gradients, however, the capacity produced was sufficiently low, as determined by the retention factor, k ($k < 1$). Alternatively photo-initiated modification of polymer monoliths was investigated using commercially available optical filters, with a gradient of optical density. However, due to the optical density of the filter, the gradient did not span the desired length of the column.

In the place of a linear gradient, a photo-grafted stepped gradient was produced and characterised using sC^4D. The column was successfully applied to the separation of two metal cations. However, the resulting stepped gradient was not ideal for separations. To resolve this problem, an optical filter was developed (in-house). The filter was comprised of commercially available COC films which demonstrated attenuation of UV energy with increasing thickness, resulting in a linear photo-grafted gradient. The column was profiled using sC^4D, thus providing a novel, indirect characterisation of the optical filter (complementary to UV/VIS analysis).

Using photo-grafting techniques, a gold nano-particle agglomerated segment of a monolithic column was created. This provided a stationary phase with dual-functionality, which was applied to the on-line extraction of proteins, followed by reversed-phase chromatography. The columns were characterised using techniques such as field emission SEM and sC^4D. This provided a novel application of sC^4D.

Chapter 1.0

Literature Review

"To raise new questions, new possibilities, to regard old problems from a new angle, requires creative imagination and marks real advance in science"

Albert Einstein

1.1. Monolithic stationary phases

Monolithic stationary phases are relatively new materials, developed in the early 1990's, for separation science. They consist of a single piece of porous material (either polymer or silica), through which all mobile phase flows. Moving away from slower diffusion processes, as experienced in particulate columns, mass transfer in monolithic columns is dominated by convection. In traditional separation columns, packed with small particles, two main problems arise; the slow diffusion of solutes into pores wherein stagnant mobile phase is present, and the large interstitial volume between particles [1,2]. Monolithic columns have been developed primarily to overcome these issues, to ultimately provide an alternative separation phase, useful in many applications such as capillary electrochromatography (CEC) [3]. This is illustrated in Figure 1.1, where Van Deemter curves of a fabricated silica monolithic column versus that of a commercial particulate silica column were compared [4].

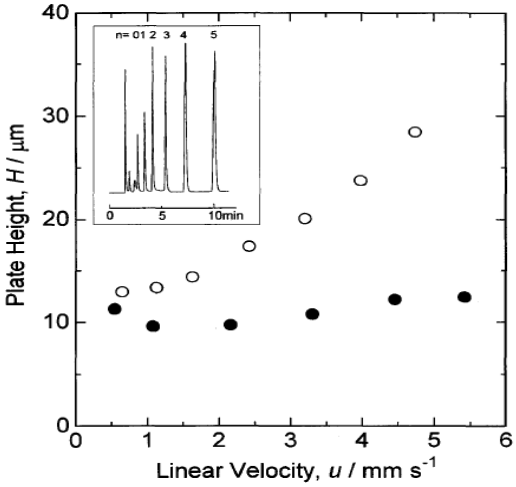

Figure 1.1: *Dependence of plate height on linear mobile phase velocity for an ODS C_{18} modified silica monolithic column (●) versus a CAPCELL PAK C_{18} UG column (5 µm particle diameter with 12 nm meso-pores) (○), using a mobile phase of 80 % methanol and an analyte of amylbenzene. Insert contains a chromatogram of a number of alkyl benzenes obtained on the monolithic column [4].*

The silica monolithic column exhibited a more desirable dependence of plate height on linear flow velocity, with a decrease in resistance to mass transfer with increasing linear velocity, with respect to the packed column [4].

1.2. Advantages of monolithic columns

With respect to particulate stationary phases, monolithic columns have a number of advantages. Packing capillary columns requires a slurry consisting of particles suspended in an inert solvent. This procedure requires a high pressure delivery system and retaining frits to contain the packed particles. Compared to the packing process of particulate columns, monolithic columns are prepared *in-situ* in the presence of monomer, porogenic solvent(s), cross-linking monomer and initiator (discussed in detail later in the text). In polymer monolithic columns, the monolith polymer is anchored to the column housing wall (usually a fused silica capillary) following a pre-treatment step [5], resulting in no need for retaining frits. Monolithic columns function with convective flow rather than traditional diffusive flow, resulting in improved mass transfer kinetics [1,2,6], and lower contributions to eddy diffusion in the Van Deemter equation [7]. Due to the macro-porous structure in polymer monoliths, they exhibit low back pressures, which enable them to be used at high flow rates [8]. The selectivity of the monolith can be easily changed *in-situ* (especially in the case of polymer monolithic columns) where reactions such as (a) co-polymerisation of functional monomer [9], (b) post polymerisation chemical modification of reactive sites [10], or (c) surface grafting using photo-initiated processes [11] can be used to introduce specific selectivities, all of which will be discussed later in the text in detail.

Some monolithic columns are formed in “needles” suitable for electrospray ionisation [12]. Due to the low volumes used in monolithic chromatography, a significant reduction in solvent use is apparent. Correspondingly, a reduction in waste is also observed. In using monolithic columns, with flow characteristics of convection, faster separations occur, reducing analysis time.

Monolithic columns are available in a wide range of formats such as disks (Convective Interaction Media, CIM®) [13,14], capillary column dimensions [3,15], integrated into electrospray needles [11,16], standard bore column dimensions [17,18], micro-fluidic chips [19,20], in 96 well plates [21,22], pipette tips, (both inorganic [23,24] and organic based monoliths [25,26]), and also in syringe barrels [27,28] for solid phase extraction (SPE).

1.3. Monolithic columns in the literature

Monolithic columns are generally classified into two categories, silica (inorganic) or polymer (organic) monoliths. The fabrication processes of monolithic columns, both silica and polymer based, have been reviewed extensively in the literature. Silica monolithic columns emerged later in the literature, with polymer monoliths being the forerunner in the field. Svec provided the primary review into such fabrication processes in 1996 [29]. Peters *et al*. reported on the advancements of monolithic structures in 1999 [6], focusing on fabrication, flow characteristics, and applications of polymeric monolithic rod columns. Svec and Fréchet also published a review in the same year [30], detailing the effect of varying factors (such as porogenic solvent concentration) upon the resulting porosity and morphology. Throughout the following ten years, numerous reviews had been provided on the fabrication [31,32,33] and application of monolithic columns to HPLC [34,35]. The merits of capillary scale separations, using both packed and monolithic columns (both silica and polymer), were recently reviewed by Saito *et al*. [36]. In this review the authors highlighted the lower contribution to terms in the Van Deemter equation for monolithic columns, versus conventional packed stationary phases. In 2007 Guichon provided an excellent report, highlighting the main attributes of monolithic columns in both silica and polymer monolithic materials, but also in varying column size ranges (i.e. capillary and analytical scales) [37]. Due to the variation of available surface chemistries on monolithic columns, numerous applications exist.

Affinity chromatography is a popular technique suited to monolithic columns, out of which a new technique was described. Affinity monolithic chromatography (AMC) was reviewed by Mallik *et al*. in 2006 [38], wherein a number of ligand immobilisation techniques, and chromatographic methods were examined. Predominately, silica monolithic columns exhibit an increased surface area with respect to polymer monoliths. This is due to the presence of meso-pores (2-50 nm) and micro-pores (< 2 nm), which contribute greatly to the surface area [39]. These pores are generally not present in polymer monolithic columns, resulting in columns with significantly reduced surface areas [32,40]. As a result, silica monolithic columns have found a greater success towards the separations of small molecules, (e.g. ion chromatography). A dedicated review to the use of monolithic columns in

ion chromatography was published by Schaller *et al*. in 2006 [41], shortly followed by Chambers *et al*. in 2007 [42]. Both reviews detailed surfactant modification of commercially available silica monoliths, as well as in-house fabricated polymer monolithic columns. Ion exchange chromatography using monolithic columns was reviewed by Nordberg *et al*. in 2009 [43], describing extensively the numerous modification techniques available to polymer monolithic columns, including co-polymerisation of functional monomer and post polymerisation modifications. Other unusual applications of monolithic columns have also been reported by Svec, involving the use of monolithic columns in proteomics and peptide mapping [44], micro solid phase extraction (μSPE) and pre-concentration [45], gas chromatography [46], and finally the advancement of micro-reactors involving immobilised enzymes [47]. Following Svec's review on μSPE in 2006 [45], Potter *et al*. published another review on the topic in 2008 [48]. Moving from monolithic materials in column format, extraction techniques involving the use of monolithic materials in polypropylene tips was reviewed by Blomberg in 2009 [49]. Monolithic materials may also be used as short monolithic columns or disks. Tennikova *et al*. reviewed the transition from membrane to monolithic disk chromatography with comparisons to other packed columns (e.g. non-porous beads) [50]. Barut *et al*. in 2005 further reviewed the subject with respect to bio-purification methods for short monolithic columns, with consideration to scale-up methods and applications [51]. Another popular format of monolithic columns is in micro-fluidic chip systems. Separation media in this format can range from membranes to monolithic materials, which was reviewed in detail by Peterson in 2005 [52]. Later in 2010, Vázquez and Paull reviewed the advancements made in porous materials and monoliths in micro-fluidic devices, from 2005 to 2010 [53]. These types of monolith devices are beyond the scope of this chapter.

1.4. Silica monolithic columns

Most silica based monolithic columns originate from a sol-gel synthesis route, resulting in a bi-modal pore morphology as described by Nakanishi *et al.* in 1997 [4]. Silica monoliths are formed through the mixing of reactants, the production of a colloidal solution (sol), the transition to a gel, aging, drying, surface modification (if any), and finally the column is clad [4,54]. In the preparation of silica monoliths, the

polymerisation of alkoxysilanes occurs. The sol is formed with water, trimethoxysilane (TMOS), acid (e.g. acetic acid), and a polymer (e.g. Poly(ethylene glycol), PEG) at 0° C. The sol is poured into a mould and kept at room temperature for 2 days for gelation and aging. Following solvent exchange, the material is dried at 60 °C for 3 days, and then subjected to heat treatment at 600 °C for 2 hours. With the production of silica monoliths in a mould, the entire volume of silica is reduced, and as a result the structure must be encased in polytetrafluoroethylene (PTFE, Teflon®) or a poly ether ether ketone (PEEK) resin to be suitable for use in HPLC [55].The fabrication of a silica monolith is illustrated in Figure 1.2.

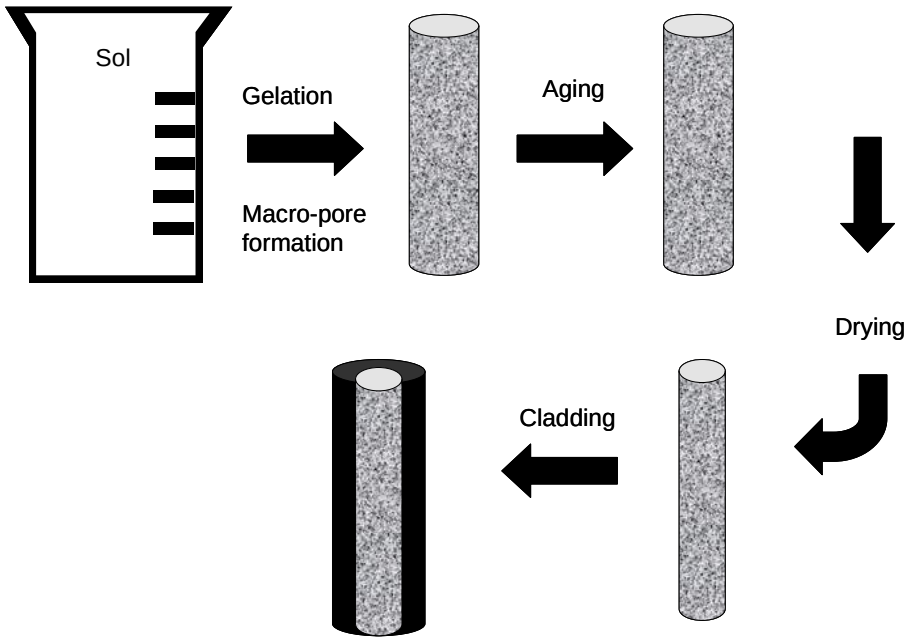

Figure 1.2: *Schematic diagram of silica monolith formation.*

The control of porous properties is a function of temperature, porogen concentration, and control of phase separation. Shrinking of the monolithic structure occurs, and can be minimised if the silica monolith is attached chemically to the inner walls of the column housing [55,56]. It should be noted that the use of PEEK cladding on silica monoliths is a limiting factor of the linear velocities applied, due to the low back pressure capabilities of PEEK, which cannot achieve pressures of 200 Bar or above [37].

Silica monoliths may only be used between pH 2 and 8. Below pH 2 the organic chains of bonded ligand such as C_{18}, separates from the silica surface. Above

pH 8, silica becomes hydrolysed and dissolves. The incorporation of organic monomers can be useful, as an increase in monolith stability can be obtained, i.e. an increase in working pH range [57]. Other types of inorganic monolithic columns have been produced and incorporate materials such as tin oxide [58], zirconium [59], and titanium [60] to prepare alternative inorganic columns. Other columns exist comprising of organic and inorganic materials, such as a hybrid silica column composing of octadecyl and sulphonic acid groups [57], and also, the incorporation of silyl C_{60} into the sol-gel matrix [61]. Bare silica monolithic columns have also been modified with surfactant coatings [62,63] to change selectivity e.g. from reversed phase to ion exchange [64].

Sugrue *et al.* [65] covalently attached imminodiacetate (IDA) onto commercially available silica monolith to evaluate the use of a silica monolithic column in weak cation exchange, and successfully separated alkaline earth metals and a selection of transition metals. Zajickova *et al.* [66] recently reported the modification of a silica based monolith with poly(pentyafluoropropyl) methacrylate via a single step photo-grafting procedure. The produced column was used successfully for the separation of benzene derivatives, using the column in reversed phase liquid chromatography. By using a photo-grafting procedure, the time required to functionalise the column was reduced with respect to thermal grafting (1 hour versus 24 hours, respectively). Silica monolithic columns provide a high surface area [67] (surface areas up to 300 m^2/g reported for silica monolithic columns [68,65]), and can produce a higher plate count per column for the analysis of small molecules e.g. >100, 000 N/m for silica monolith [69].

Silica monolithic columns are commercially available in a number of formats. Silica monolithic columns for HPLC and semi-preparative steps are available from Phenomenex as Onyx® monolithic columns, in varying column lengths (5 - 100 mm) and inner diameters (i.d), encompassing both capillary (0.1 – 0.2 mm i.d), standard bore (4.6 mm i.d), and larger column widths (3.0 and 10.0 mm i.d) for semi-preparative chromatography. The surface chemistries available include bare silica, C_8 and C_{18} modifications [70]. An example of which is shown below in Figure 1.3 (a). Chromolith® CapRod (Figure 1.3 (b)) is a silica monolith commercially available from Merck, and is available in capillary bore (0.05 mm, 0.1 mm, 0.2 mm i.d), standard bore (4.6 mm i.d), and larger as guard columns (10 mm i.d, 25 mm i.d), in a

variety of column lengths (5 - 300 mm long). The available surface chemistries are bare silica, C_8, and C_{18} [71].

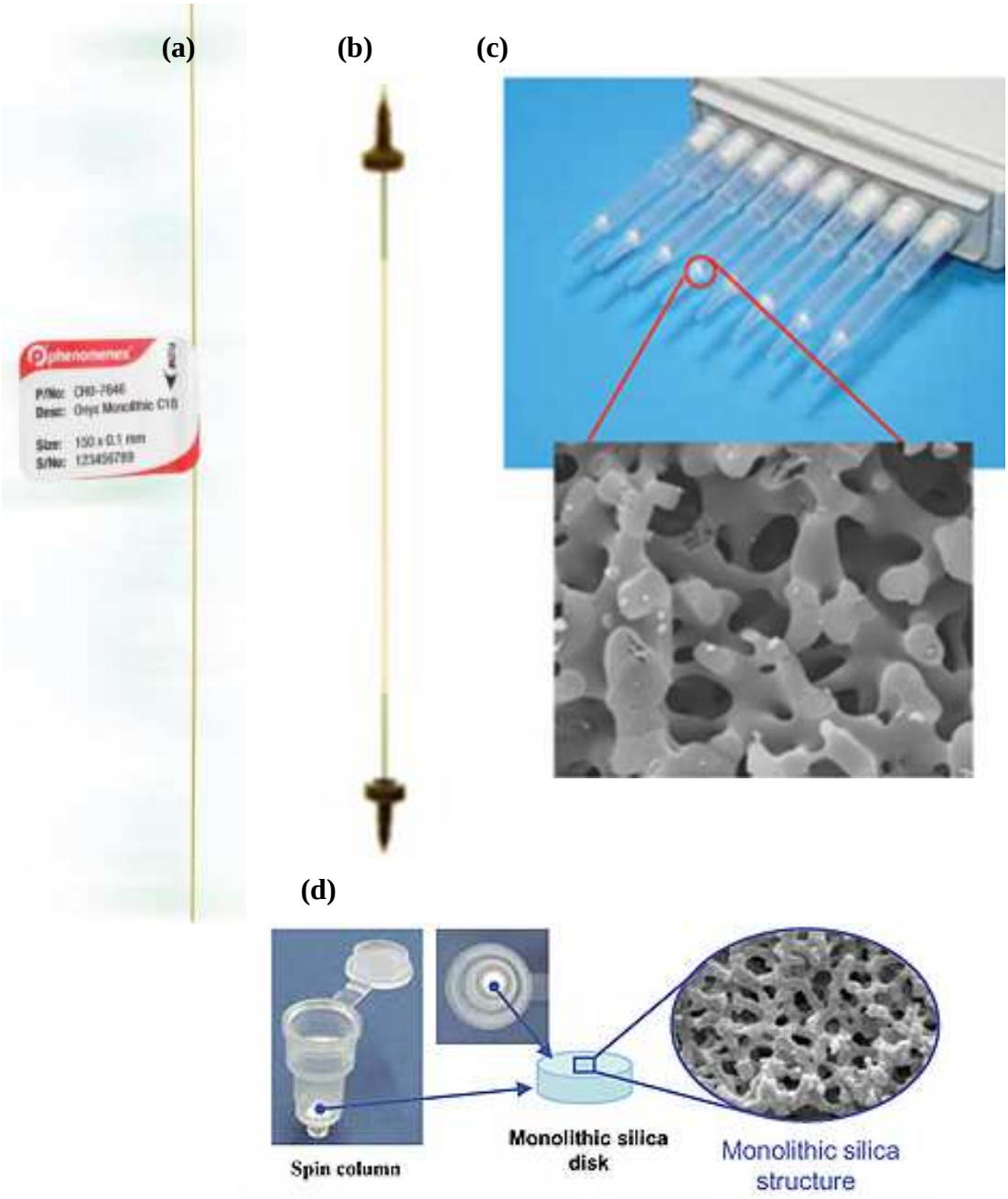

Figure 1.3: *Examples of commercial silica monolithic materials, Onyx® (a), Chromolith® (b), MonoTip® (c), MonoSpin® (d).*

As mentioned above in Section 1.3, monolithic materials can also be found in solid phase extraction techniques. For rapid extraction methods, cartridges having monolithic silica are available from GL Sciences (MonoSpin®), for use with centrifugation based extraction methods, as shown in Figure 1.3 (c). Pipette tips

containing monolithic silica, MonoTip®, are also available from this company, of which the surface chemistries include C_{18}, titanium oxide coated, and immobilised trypsin, for rapid sample throughput (Figure 1.3 (d)). Details of monolithic phases manufactured by GL Sciences can be found here [72].

1.5. Polymer monolithic columns

Polymer monolithic columns have a number of advantages over their silica based counterparts. The major advantage of polymer monolithic columns over silica particulate columns is that polymer monolithic columns exhibit excellent pH stability over a wide pH range [8]. They can be more easily fabricated easily *in-situ*, and can be further modified using a wide variety of chemistries [73]. The spatial location of polymer monolithic columns in micro-fluidic devices, and capillary housings, can be easily controlled using photo-initiated polymerisations incorporating photo-masks [74,75].

As polymer monoliths suffer from poor surface area, some groups have tried to resolve this issue by incorporating materials such as nano-particles, into the monolith pre-cursor monomer solution, or via surface modification. For example, Hilder *et al.* [76] attached latex nano-particles (60 nm) to a butyl methacrylate-*co*-ethylene dimethacrylate-*co*-2-acrylamido-2-methyly-1-propanesulphonic acid (BuMA-*co*-EDMA-*co*-AMPS) monolithic column, via coloumbic interactions. In doing so, an increase of approximately 30 % was observed in the specific surface area following nano-particle immobilisation. Functionalisation processes involving nano-particles are further detailed in Chapter 5. Alternatively, in an attempt to increase surface area, a process of hyper-cross-linking on monolithic columns was investigated by Urban *et al*. [40,77], where poly(styrene-*co*-divinyl chloride-*co*-divinyl benzene) monolithic columns were hyper-cross-linked resulting in staggering surface areas for polymer monoliths (600 m^2/g), twice that of available silica monolithic columns. The obvious presence of smaller pores had a negative effect on the separation of proteins, resulting in poor resolution [40]. However, the separation of small molecules with efficiencies of up to 80, 000 N/m for separations of uracil and alkyl benzenes, could be achieved [77].

1.6. The polymerisation process

In order to understand the polymerisation process involved in polymer monolith fabrication, it is useful to discuss the mechanism of suspension polymerisation first. The process for monolith formation was developed from the fabrication of macro-porous polymer beads, in which suspension polymerisation is used [56]. In the production of polymer beads for stationary phases, a bi-phase system is used, usually with the incorporation of temperature and stirring [78]. In suspension polymerisation, the monomer is suspended in an inert diluent, usually water, with added suspension agents. Each micro-droplet is a micro-reactor for bulk polymerisation. The polymerisation process used in the bulk polymerisation of polymer beads was adopted for monolithic columns [1]. The main difference in the procedure is the mould used for the monolith formation, which is unstirred. Using the same materials in a stirred and unstirred bulk polymerisation, the macro-pores are much larger in the unstirred environment [39] e.g. a monolithic column in capillary format. Reasons for this deviation have been discussed in the literature, and include the lack of interfacial tension between the organic and aqueous phases, and the lack of dynamic stirring. In suspension polymerisation a constant pressure is exerted by interfacial tension on the micro-globules forming in solution. With the synergistic effect of the pressure on the particles and the shrinkage of the undiluted monomer, the nuclei forming in solution are brought closer together. This results in smaller particles, and thus, smaller pores. The interfacial tension present in the fabrication of beads is absent in the fabrication of monoliths and may be the predominant factor in the change of porous properties between beads and monoliths [56].

An organic monolith consists of a functional monomer and a cross-linking monomer, polymerised in the presence of an initiator and a porogenic solvent. Dissolved oxygen must be removed from the monomer solution to prevent the interference of oxygen with the generation of polymer. Dissolved oxygen can scavenge radical species in solution, reducing the rate of polymerisation, and so it is important to remove dissolved oxygen [79]. After the removal of dissolved oxygen (via nitrogen sparging or sonication in some instances), the column housing is filled with the monomer mixture and the column is subjected to initiation energy, usually UV or thermal energy. The formed monolith is washed with an appropriate solvent (usually methanol or acetonitrile (ACN)).

The fabrication method is represented by the diagram below (Figure 1.4). The precursor solution comprising of functional monomer, cross-linking monomer, pore forming solvents (porogens), and initiator is added to a mould. Energy is supplied to the system in a suitable form (e.g. thermal or UV irradiation). Thermal initiation can occur between temperatures of 60 °C and 90 °C, whilst photo-initiation can occur over a range of wavelengths such as in the UV 254 nm [11], 365 nm [80], and visible light range [120]. These initiation systems vary with the initiating mechanism used, (e.g. benzophenone vs. AIBN). The polymerisation of monolithic columns is based upon chain polymerisation initiated by free radicals. This type of polymerisation occurs in three steps; initiation, propagation and termination. Over the course of the polymerisation, the concentration of monomer steadily decreases with the production of polymer. Chain polymerisation occurs with unsaturated monomers. Initiation involves the generation of highly energetic radicals, provided by a free-radical initiator. The radicals readily react with other monomers, without quenching the active centre. The monomer is then transformed into a new radical species, responsible for the continuous growth of the polymer chain [78].

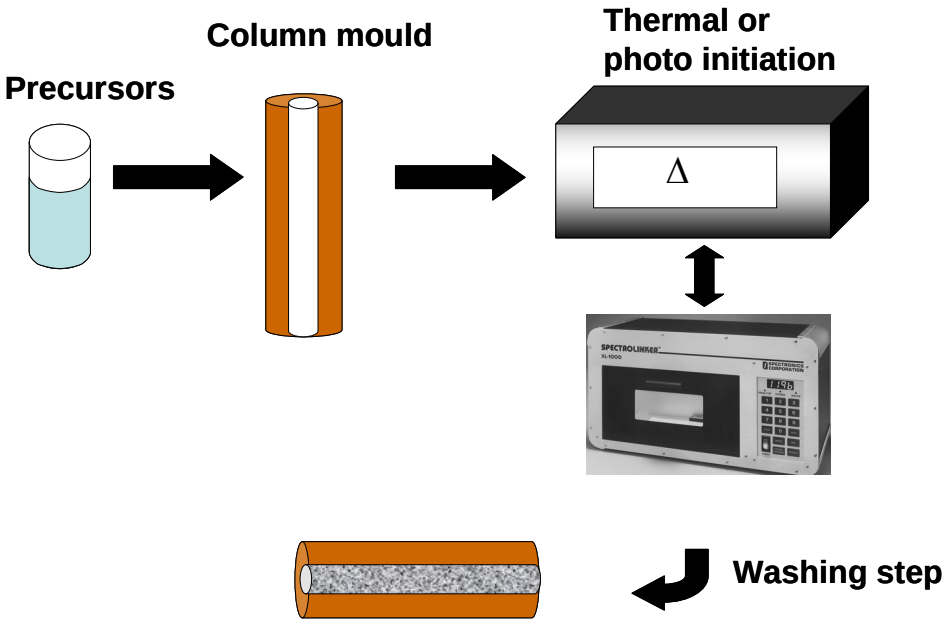

Figure 1.4: *Schematic of polymer monolith formation via thermal or photo-initiated polymerisation, where Δ indicates temperature applied during polymerisation, between 55 °C and 70 °C.*

As the polymerisation proceeds, a gel-like polymer species (nuclei) is formed, which is insoluble in the porogen [32]. The nuclei form clusters, and as polymerisation progresses, the clusters increase in size and come into contact with other clusters. The porous structure of polymeric monolithic columns consists of an interconnected network of irregular voids between these clusters of polymeric globules [1].

To control the porous properties, a deeper understanding of the factors involved in pore formation is required. The morphology of the resulting polymer is highly dependent on the timing of phase separation (precipitation of polymer). Variables such as the type and concentration of porogenic solvents, the polymerisation initiation energy, and the amount of cross-linking monomer can all affect the resulting porous nature of the polymeric support [1,30]. In an endeavour to understand the individual affects of these variables on the resulting monolith, Viklund *et al*. performed in depth studies on each variable [39,81], in the preparation of monolithic columns of varying functionality.

1.7. Porogenic solvent composition and concentration

The initial monolith pre-cursor solution is a homogeneous mixture of monomer (functional monomer and cross-linking monomer), porogenic solvents, and a free radical initiator. The porogen system can compose of a single solvent or a mixture of a number of solvents, to create an optimised average pore size. Such solvents can be a single organic solvent, a mixture of organic solvents, or indeed polymers (such as PEG). The porogen does not react during the polymerisation, it remains in solution surrounded by polymer until it is removed through a washing step [81]. The resulting porous properties can be controlled by the porogen through solvation of growing polymer nuclei, in the early stages of polymerisation [39].

The porogen(s) can be either solvating (thermodynamically good, micro-porogen) or non-solvating (thermodynamically poor, macro-porogen) solvents for the resulting polymer. By varying the ratio of solvating and non-solvating porogenic solvents, the timing of phase separation, and thus globule formation can be controlled. In the case of a solvating solvent, phase separation occurs later. In this case following the formation of polymer nuclei, the solvent competes with the remaining monomers for the solvation of the newly formed nuclei; the solvent competes increasingly with

the monomer localised around the nuclei, imparting a preferential bias on the formation of nuclei in solution. Due to the low concentration of monomer within the nuclei, attraction between the nuclei is limited, and so, a larger number of smaller micro-globules are formed [81]. This results in a smaller pore size. Conversely in the case of a non-solvating solvent (thermodynamically poor solvent), where the remaining monomer is a better solvating solvent for the resulting polymer, phase separation occurs earlier.

As the growing nuclei swell with monomer, the local concentration of monomer is higher within the nuclei than in the surrounding solution, and so, the polymerisation is preferred to occur here. As the globules coalesce, the growing nuclei are captured, further increasing the size of the globules. Consequently, the resulting globules are therefore much larger. This shifts the resulting average pore size to larger pores.

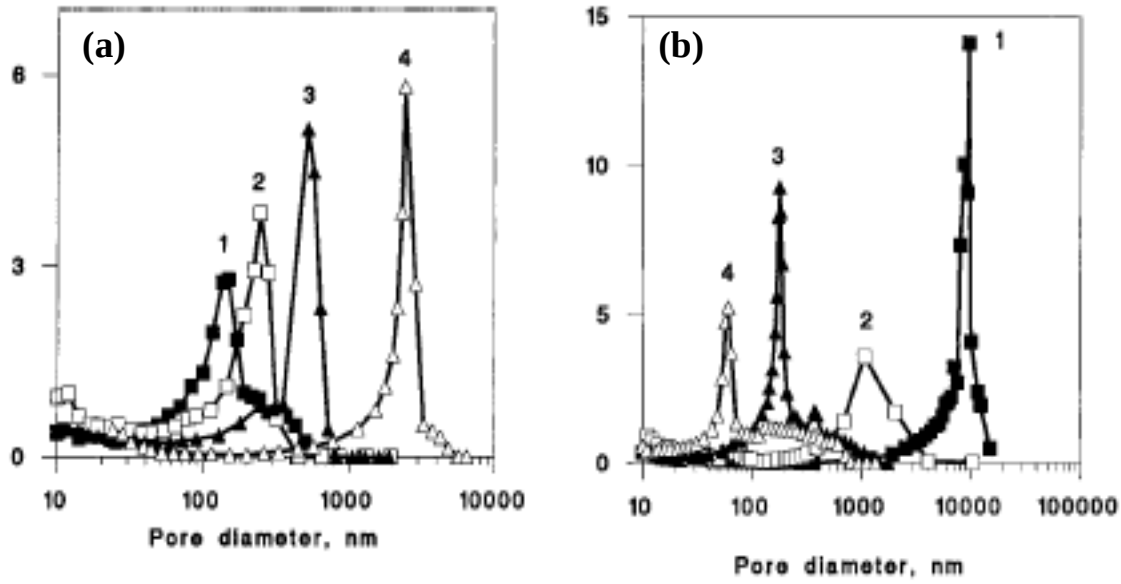

Figure 1.5: *Effect of porogenic solvent composition on the average pore size distribution curve. GMA-co-EDMA monolith (a), prepared with varying concentrations of cyclohexanol and dodecanol in porogen (increasing non-solvating solvent concentration); 60 + 0 % (1), 57 + 3 % (2), 54 + 6 % (3), and 45 + 15 % (4). PSDVB monolith (b) prepared with varying concentrations of dodecanol and toluene (increasing solvating solvent concentration); 60 + 0 % (1), 50 + 10 % (2), 45 + 15 % (3), 40 + 20 % (4) [39].*

The porosity of the monolith may be changed by varying porogenic composition whilst maintaining the chemistry of the resulting column. For example, Viklund *et al*. discovered that in adjusting the ratio of porogenic solvents, a shift in average pore size was observed [39]. For a GMA-*co*-EDMA monolithic column, dodecanol was the non-solvating solvent. As the ratio of dodecanol to cyclohexanol increased, a shift to greater pore sizes was observed, as seen in Figure 1.5 (a). For a poly(styrene-*co*-divinyl benzene) (PSDVB) monolith prepared in the presence of dodecanol and toluene, the solvating solvent is toluene. In increasing the toluene ratio in the porogenic mixture, a shift to smaller pore sizes was observed. This effect is seen in Figure 1.5 (b). The monomer to porogen ratio must also be considered. As the porogen is pivotal in the formation of pores, it is only logical that as the porogen concentration is decreased, the resulting pore volume is also decreased. This is indeed the case as determined by Viklund *et al*. [81]. A decrease in average pore size was also observed with decreasing porogen concentration (e.g. from 70 % to 50 %).

Porogenic solvents usually consist of alcohols or polymers and may contain water, especially in the production of co-polymer monolithic columns, wherein a charged monomer is required. With the demands of novel monolithic materials, porogenic systems are needed for a number of chemistries. For example a porogen system was developed for a BuMA-*co*-EDMA-*co*-AMPS monolith, for which the porogenic system needed to dissolve both hydrophilic, and hydrophobic monomers, and so incorporated water, 1,4-butanediol and 1-propanol [3]. Many organic solvents are used for pore formation, namely toluene [82], decanol [83,84], propanol and 1,4-butanediol mixture [85,86,87,88,89], and a combination of cyclohexanol and decanol [74,90,91]. Porogenic solvents can vary from aqueous to organic solvents [3,82-92], super critical fluids [93,94], and can even include polymers [95-97]. Generally large average molecular weight polymers are used. For the production of glycerol dimethacrylate monolithic columns, Aoki *et al*. used polystyrene standards of 50, 000, 600, 000, and 3, 840, 000 g/mol, with low polydispersity, as porogenic solvents [95]. This resulted in macroporous monoliths suitable for chromatography. A glycerol dimethacrylate (GDMA) monolith prepared in 250 μm i.d. capillaries, using the largest polystyrene standard as a porogenic solvent, exhibited a higher efficiency in the separation of benzene (~34,000 N/m), compared to the columns prepared in the presence of lower molecular weight standards. It would be expected that in using the larger polystyrene standard a predominantly macro-porous structure would result. The

group suggested that the presence of the polystyrene porogen resulted in a staggered phase separation, where GDMA had a later onset of phase separation with the solvent chlorobenzene. Later phase separation results in the formation of smaller globules, and thus average pore size [81]. Liu *et al*. used a 20,000 average molecular weight PEG polymer as a porogen in the fabrication of acrylamide monolithic columns [96]. They investigated the use of 10,000 and 20,000 molecular weight polymer standards as porogens, with desirable pore structure resulting from the latter. Kubo *et al*. also used PEG polymer to produce diacrylate monolithic columns, with the desired porous structure [97].

1.8. Effect of functional monomer

The functional monomer is generally the monomer used to determine the selectivity of the monolith e.g. for non-polar characteristics required, stearyl methacrylate can be used. The functional monomer must contain at least one vinyl bond for polymerisation. Common organic monoliths originate from monomers of acrylates [98,99], methacrylates [100,101], styrenes [1,39], or acrylamides [102,103]. Structures of some common monomers are illustrated below in Figure 1.6.

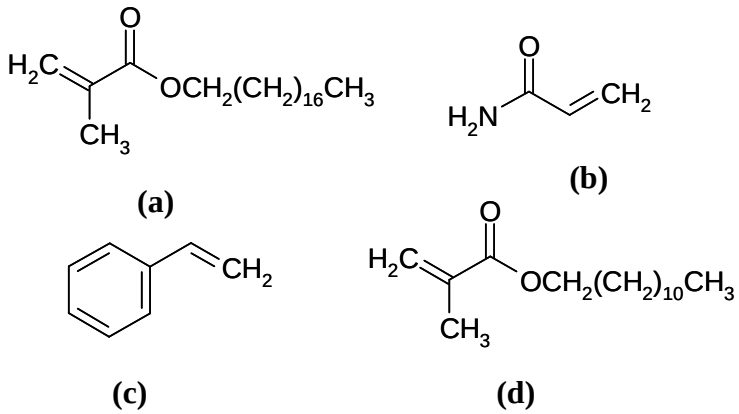

Figure 1.6: *Structures of monomers used in monolith fabrication, stearyl methacrylate (C_{18}) (a), acrylamide (b), styrene (c), and lauryl methacrylate (C_{12}) (d).*

Co-polymerisation of two or more functional monomers can result in a monolith exhibiting more than one functional group [104]. This is extremely useful for monolithic columns where a low surface expression of a particular surface chemistry is required. Such an example consists of a neutral functional monomer such

as BuMA, which can be co-polymerised with a charged functional monomer, such as AMPS, resulting in acidic sulphonate groups presented at the surface of the monolithic column [105]. A hydrophobic functional monomer can be co-polymerised with a hydrophilic monomer, to produce a hydrophilic monolith with a low surface expression of hydrophobic moieties, suitable for hydrophobic interaction chromatography (HIC) [100].

1.9. The cross-linking monomer

The amount of cross-linking monomer present during the polymerisation step can have a profound affect on the mechanical properties of the resulting polymer [56]. The cross-linker consists of a monomer containing one or two double bonds. With a high concentration of cross-linker present the thermal stability of the polymer is increased. The cross-linker adds rigidity to the structure. Highly cross-linked materials also exhibit a hard and brittle structure [78]. Increasing the concentration of cross-linker affects both the chemical composition of the resulting polymer and the porosity [32,56]. With an increase in cross-linker concentration, phase separation can occur earlier. If a nucleus is highly cross-linked, it will show a lower tendency to swell with monomer or solvent, resulting in smaller globules. With a decrease in globule size, the pore size is also smaller. As a result of the smaller pore size, an increase in surface area is observed. By varying the concentration of cross-linking monomer, the porous structure of the resulting monolith can be changed, but changes in the resulting composition may have negative effects on the monolith selectivity in chromatographic applications [39]. Santora *et al*. [106] demonstrated that in using a precursor solution of 100 % divinylbenzene (cross-linker), a surface area of 800 m^2/g was obtainable, as illustrated in Figure 1.7 .

The greater the proportion of smaller pore sizes, the greater the surface area [39]. Consequently, for a column of such properties, the column back pressure would be unreasonably high, with significantly reduced permeability [56]. Figure 1.8 illustrates the structure of some regularly used cross-linking molecules.

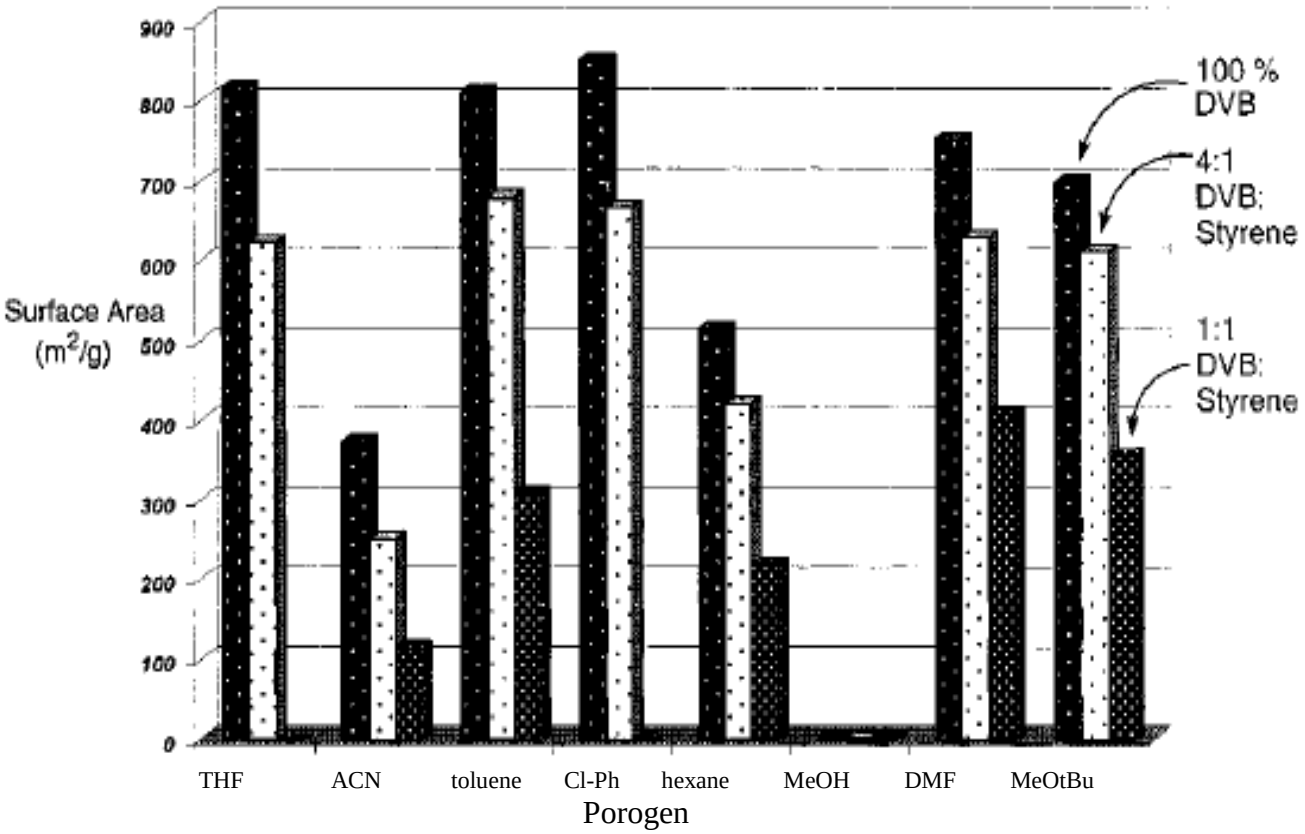

Figure 1.7: *BET surface area measurements for monolithic columns consisting of differing cross-linker concentrations and porogenic solvents, adapted from [106].*

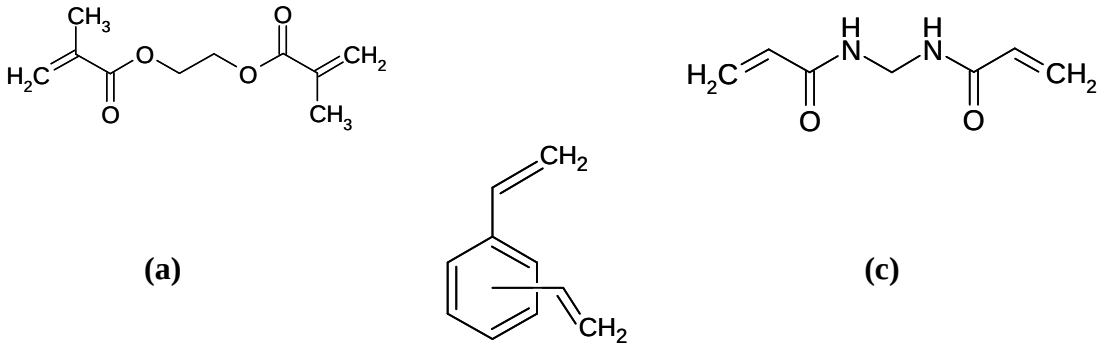

(a) **(b)** **(c)**

Figure 1.8: *Structures of some common cross-linking monomers, ethyleneglycol dimethacrylate (a), divinyl benzene (b), and N, N'- methylenebis(acrylamide) (c).*

1.10. The free-radical initiator and initiation

Most polymer monolithic columns are prepared by free radical initiation performed *in-situ*. Polymer monoliths may be formed using a number of different polymerisation initiation methods. Thermal energy [107], γ radiation [108], and UV energy [81] can be used in conjunction with specific initiators for polymerisation. The polymerisation conditions also play a vital role in control of pore size. The initiation of the free radical requires high activation energy. The amount of radicals produced is dependant on the half life of the initiator itself. The structure of two common free radical initiators, α,α'-azoisobutyronitrile (AIBN) and 2,2-dimethoxy-2-phenylacetophenone (DAP), can be seen below in Figure 1.9.

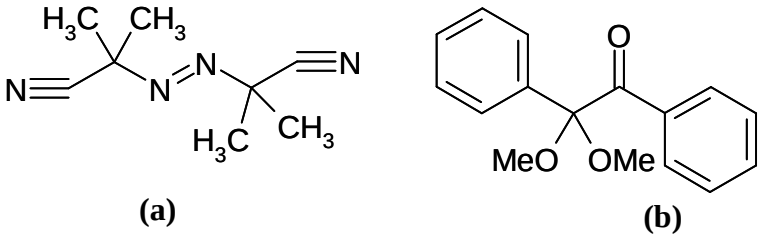

(a) **(b)**

Figure 1.9: *Structures of two popular initiating compounds, AIBN which is used for thermal polymerisation and UV initiation at 365 nm (a), DAP which is predominantly used in UV initiated polymerisations at 254 nm (b).*

Other thermally initiated polymerisations, known as living polymerisations, have been investigated as an approach to improve the fine control of porous properties in polymer monolithic columns. A polymerisation that can restart chain growth upon the addition of new monomer is called "living". During the polymerisation process the stable free radicals are combined with the growing polymer chains. A functional monomer can then be added to the structure, and with the activation of latent dormant radicals, surface localised grafting can occur, upon the application of temperature [109]. In terms of monolithic columns, this may provide a method for controlling the phase separation, resulting in a more homogeneous monolithic structure [32]. There are numerous types of living polymerisations such as nitroxide mediated polymerisation [109,110], ring opening metathesis polymerisation (ROMP) [111,112], atom transfer radical polymerisation (ATRP) [113,114], and reversible addition fragment transfer polymerisation (RAFT) [115]. Some of these methods have

been used in the fabrication of cross-linked gels [113], polymer beads [114], and polymer monoliths [109,116]. Temperatures above 100 °C are generally used, while termination of the growing polymer is mediated by decreasing the temperature [116]. These methods of living polymerisations are worth noting, they are, however, beyond the scope of the material presented herein.

1.10.1. Variation in initiating energy

The first monolithic columns were prepared using thermal polymerisation over 24 hours [117,1]. Viklund *et al*. investigated the use of temperature in the fine control of porous properties [39]. They postulated that by increasing temperature, there would be a similar increase in the rate of nucleation. Higher reaction temperatures lead to the formation of a larger number of free radicals, and thus, resulted in the formation of a larger number of growing nuclei. Consequently, a larger number of globules form at once, resulting in smaller globule size, and hence smaller pores. The change in average pore size with temperature can be seen below in Figure 1.10.

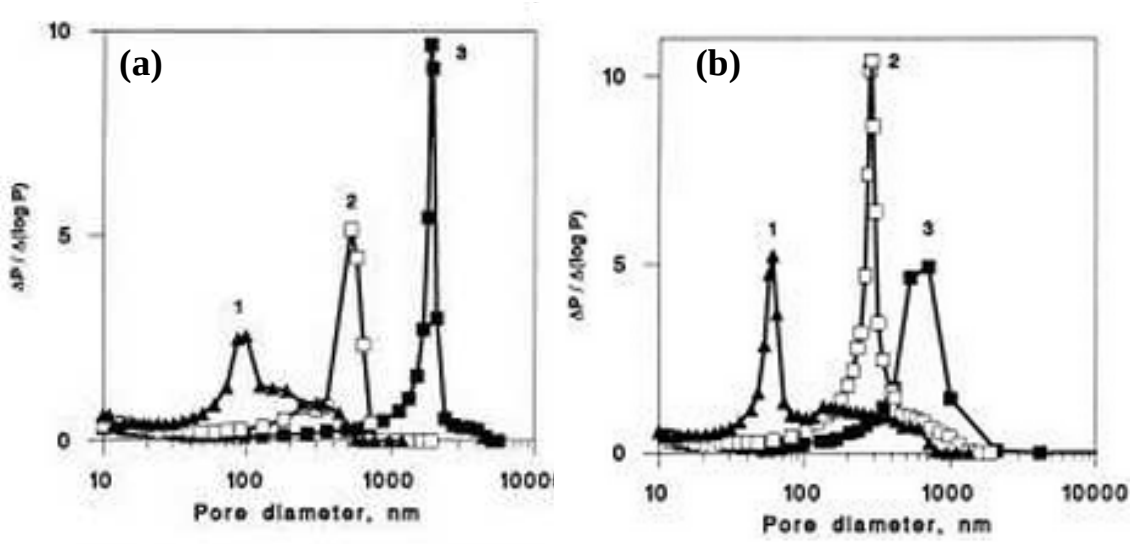

Figure 1.10: *Average pore size distribution curves for monoliths prepared using varying temperatures over a 24 hour polymerisation time. GMA-co-EDMA (40 %) with cyclohexanol (54 %) and dodecanol (6 %) polymerised at 80 (1), 70 (2), and 55 °C (3) (a). PSDVB (40 %) with dodecanol (40 %) and toluene (20 %) polymerised at 80 (1), 70 (2), and 60 °C (3) (b) [39].*

For example, AIBN is regularly used in the production of monolithic columns via thermal initiation [56], which has a half life of 37 hours, at a temperature of 55 ˚C. However, at 70 ˚C the half life is significantly reduced to only 6 hours. Most

monolithic columns prepared using thermal initiation, are prepared between 60 and 70 ˚C over a range of 16 to 24 hours, depending on the desired porous properties. At elevated temperatures, the rate of generation of radicals is higher due to the increase in the rate of decomposition. Due to the resulting increased rate of nucleation, more nuclei are formed at once, in a short time period, and so, a large proportion of globules are formed, which remain small in size with small interstitial voids [32,56].

1.10.2. Photo-initiated polymerisation.

An alternative to thermally initiated reactions is photo-polymerisation. This is performed *in-situ* using a UV light source and is a faster method for initiation. The first photo-initiated monolith was produced in 1997 by Vicklund *et al.* using glycidyl methacrylate as a backbone monomer and trimethylolpropane tri-methacrylate as a cross-linker [81]. Photo-polymerisation occurs at room temperature, which permits the use of solvents with low boiling points (e.g. methanol, ethanol *etc*.) [32], for use in the porogenic solvent. The polymerisation can be achieved in a matter of minutes as compared to hours with thermal initiation [81]. In comparing columns prepared using UV and thermal initiation, chromatographically only small variances in retention are observed, as determined by Geiser *et al.* [118]. In their experiments, two columns were prepared from the same monomer pre-cursor solution with differing initiation mechanisms. From their results, photo-polymerised columns exhibited higher column back pressures compared to those prepared under thermally initiated polymerisation. This is suggestive of a change in the porous structure; in which smaller pore sizes can be acquired by using this method of polymerisation initiation. This may be explained by the increase in kinetics for UV polymerisation over those of thermal polymerisation [81].

Photo-initiated methods are ideal for the specific spatial placement of a monolith within a micro-fluidic chip or capillary column by using photo-masking methods [11]. For photo-polymerisation, an initiator such as 2,2-dimethoxy-2-phenylacetophenone (DAP) would be used (Figure 1.9 b) at a wavelength of 254 nm. AIBN has also been used for UV initiation at a wavelength of 365 nm [119]. Walsh *et al.* also reported the use of visible light at a wavelength of 470 nm, for the production of PSDVB monolithic columns, using a range of initiating compounds including (1)-(S)-camphorquinone, ethyl-4-dimethylaminobenzoate, and N-methoxy-4-phenylpyridinium tetrafluoroborate [120]. This resulted in the formation of PSDVB

polymer monoliths with successful application to the separation of proteins in the reversed-phase under gradient elution.

1.11. Commercially available polymer monoliths

Thermo Scientific Dionex is the predominant manufacturers of rod polymer monolithic columns, producing a wide range of surface chemistries. Methacrylate monomers feature in the fabrication of ProSwift weak anion exchange (WAX), strong anion exchange (SAX), weak cation exchange (WCX) and strong cation exchange (SCX) columns, which are available in 1 mm and 4.6 mm i.d dimensions, at 50 mm in length. Similarily a ProSwift column immobilised with Concavalin A (Con A) is fabricated from methacrylate monomers, which is available in 5 mm i.d, with a length of 50 mm. The ProSwift column advertised for reversed-phase LC comprises of a PSDVB polymer phase, available in column widths of 4.6 mm i.d and 1 mm i.d, with varying column lengths of 50 to 250 mm long. The IonSwift range of polymer monoliths comprises of a divinyl benzene cross-linker, however, the functional monomer is not specified. The DNASwift monolithic column, is fabricated from methacrylate monomers, and is available with 5 mm i.d, with a length of 150 mm. Details on the variety of stationary phases offered by Thermo Scientific Dionex can be found at the following website [121]. Monolithic phases also appear in disk format, known as Convective Interaction Media® or CIM. Bia Separations manufacture disk monolithic columns, predominantly using GMA-*co*-EDMA polymers. The resulting surface chemistries range from WAX, SAX, SCX, affinity phases (e.g. IDA, Protein A etc.), activated disks (e.g. bare epoxide groups), enzyme immobilised disks (e.g. trypsin), C_4, and hydroxyl surface chemistry. The monolithic phases are available in dimensions such as 12-16 mm in diameter, with 2.5-3 mm in thickness. The monolithic disks are also available in much larger dimensions such as 65 mm i.d, with a length of 150 mm. Additional information can be found on their website [122]. An image of a monolithic CIM® disk for HPLC can be seen below in Figure 1.11.

Figure 1.11: *Image of a quaternary ammonium CIMac™ monolithic disk. Each monolith housing tube has a coloured band, indicating the surface chemistry (a), diagram of flow through CIM disk (b) [122].*

1.12. Modification of monolith selectivity

The following section will contain a discussion on a variety of methods used in the control of surface chemistry of both silica and polymer monoliths. In all cases, the desired outcome is to separate the control of monolith morphology, from the modification and tailoring of the surface chemistry into distinct steps. In doing so, the surface chemistry can be modified without the need to re-optimise the pore morphology. [123]

1.12.1. Surfactant modification of silica monolithic columns

One of the most straightforward methods of semi-permanent surface modification is the coating of a reversed-phase substrate with an ionic surfactant. This results in stationary phases which can be used for ion exchange chromatography. In previous works involving C_{18} modified silica stationary phases, either an ion interaction reagent (IIR) was added to the eluent [124,125], or coated onto the stationary phase [126,127]. The stationary phase coating was facilitated by flushing the column with a highly aqueous solution of surfactant (<< critical micellar concentration), containing a percentage of organic solvent (either methanol or ACN in the range of 5 to 20 %) [124-126]. A surfactant modified silica-C_{18} monolithic column was reported in 2003 by Hatsis and Lucy [127], whose method was based upon the coating procedure outlined for short packed (3 μm particles) silica-C_{18} columns, outlined by Connolly *et al.* [125,126]. A C_{18} modified silica column was flushed with 10 m*M* didodecyldimethylammonium bromide (DDAB) in 5 % ACN until breakthrough was achieved. The column was then flushed with water to remove

excess surfactant. The column was applied to the successful separation of 7 anions in < 60 seconds.

Similarly Connolly *et al.* [128] developed an IC system for the dual separation of both anions and cations. To achieve this, the group used two separate silica monolithic columns connected in parallel. Each monolithic column was coated with either a cationic or anionic surfactant for the respective ion separations. Using a 1 m*M* solution of DDAB (cationic suractant) in 5% ACN, a 25 mm monolithic column was modified, with unbound surfactant removed using a water washing step. The anionic surfactant sodium dioctyl sulfosuccinate (DOSS) was prepared at 1 m*M* in 5 % ACN. The surfactant was flushed across the column followed by a water washing step to remove any unbound surfactant. A 50:50 flow splitter followed the injector port delivering mobile phase to each column. For optimum separations (i.e. with no interference to peaks from either column) a flow rate of 0.5 mL/min through the anion exchange column and a flow rate of 1.5 mL/min through the cation exchange column was necessary. Prior to detection the eluent flow was combined resulting in a single chromatograph for the analysis. Analysis of water samples could be achieved in relatively short analysis times (< 2 mins each), for both anions and cations, with efficiencies ranging from 23, 000 N/m to 62, 000 N/m for anions, and 36, 000 N/m to 58, 000 N/m for cations. A sample chromatogram is shown below in Figure 1.12.

An example of surfactant interactions with a hydrophobic substrate (e.g. C_{18} chain from silica monolith) is shown below in Figure 1.13. Permanent modifications of the stationary phase would be more desirable, as they would be more stable than surfactant coatings which can desorb from the surface if organic modifiers are used in the mobile phase. Coatings can also exhibit non-homogeneous coverage, which is discussed later in Section 1.19.5.

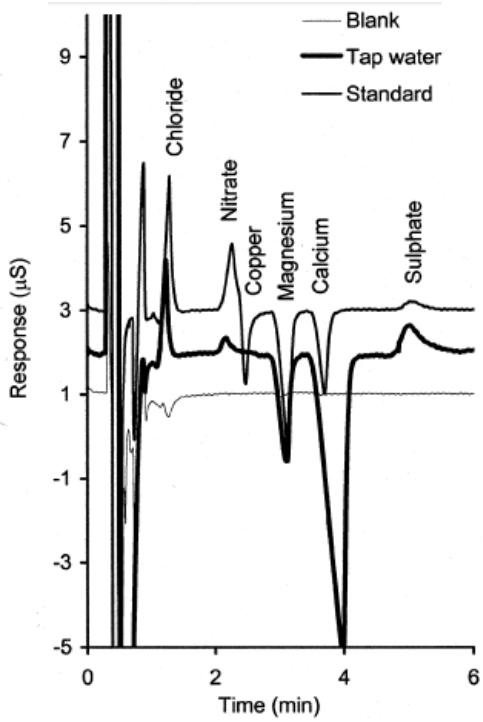

Figure 1.12: *Chromatogram of cation and anion analysis from a tap water sample using surfactant modified Silica-ODS monolithic columns. Eluent 2.5 m*M *phthalate/1.5 m*M *ethylenediamine pH 4.5, flow rate 0.5 mL/min through anion column, 1.5 mL/min through cation column, column temperature 30 °C, direct (anions) and indirect (cations) conductivity detection, injection loop 100 µL [128].*

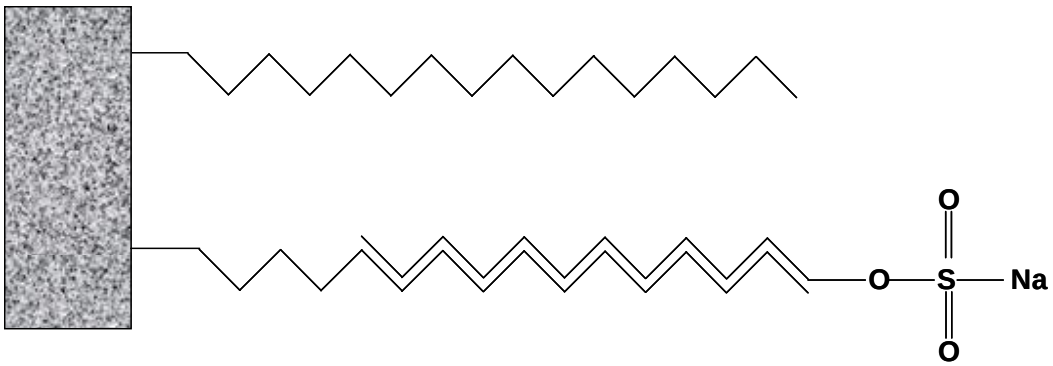

Figure 1.13: *Schematic of the interaction of a common surfactant, sodium dodecylsulphate (SDS) with a non-polar (C_{18}) stationary phase.*

1.12.2. Chemical formation of functional groups via reactive chemistry on polymer monolithic columns

Polymer monolithic columns can be prepared to incorporate a reactive functional monomer within the monolith matrix. Following polymerisation, surface expressed reactive functional groups can be further reacted with subsequent chemical

modifications to yield the desired surface chemistry. Chemical reactions have been used for the immobilisation of functional groups via epoxide rings. Wieder *et al.* prepared a quaternary ammonium, strong anion exchange column (SAX), through amination of the epoxide group, and further alkylation of the tertiary amino group [129]. The majority of chemical modifications involve the use of epoxide rings [130,131,132]. Usually the epoxide group is hydrolysed using a strong acid at room temperature, or a base with added heat (≥ 60 ˚C). For example, the first monolithic type columns prepared by Svec *et al*. [117] incorporated GMA which contains an oxirane or epoxide ring. Using this chemistry, diol functional groups could be formed on the surface, resulting from the ring opening reaction of epoxide ring with sulphuric acid. Similarly, amino based functionalities can be added following the ring opening reaction of the epoxide group with a base such as diethylamine, or ethylenediamine. Examples of these reactions on GMA monolithic columns can be seen below in Figure 1.14. More complex reactions can be performed in order to produce selectivies such as SCX sulphonic acid groups [105].

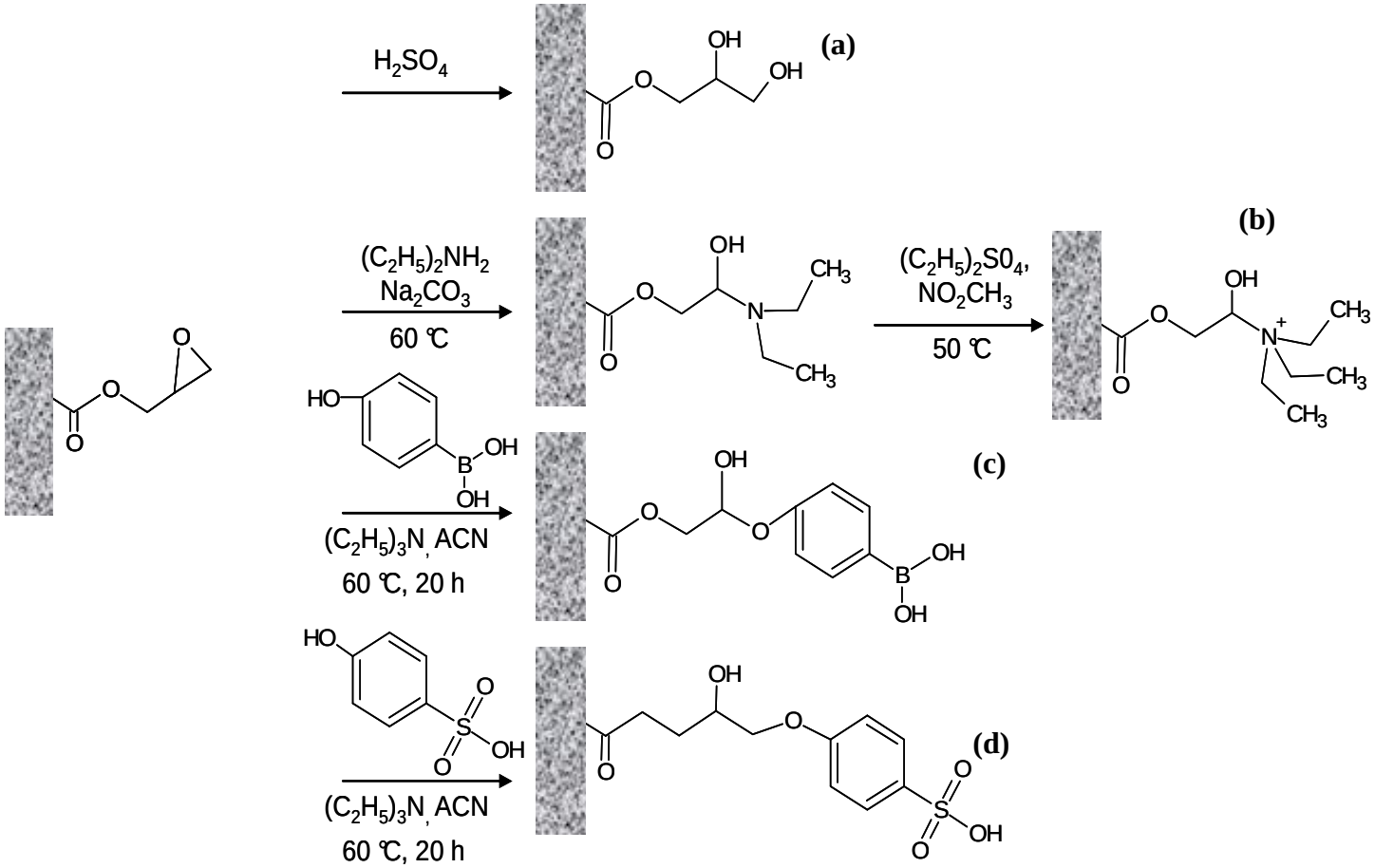

Figure 1.14: *Some reactions of GMA monoliths, production of diols (a), amination (b), boronic acid groups (c), sulphonic acid groups (d).*

The immobilisation of biomolecules such as enzymes and proteins, for affinity chromatography upon monolithic columns exhibiting an epoxide ring, can occur using a number of methods. Complex immobilisation techniques of biomolecules onto GMA monolithic columns, was reviewed by Mallik *et al*. [38], and involve the Schiff base method, glutaraldehyde immobilisation, and the disuccinimidyl carbonate method. These are highlighted below in Figure 1.15

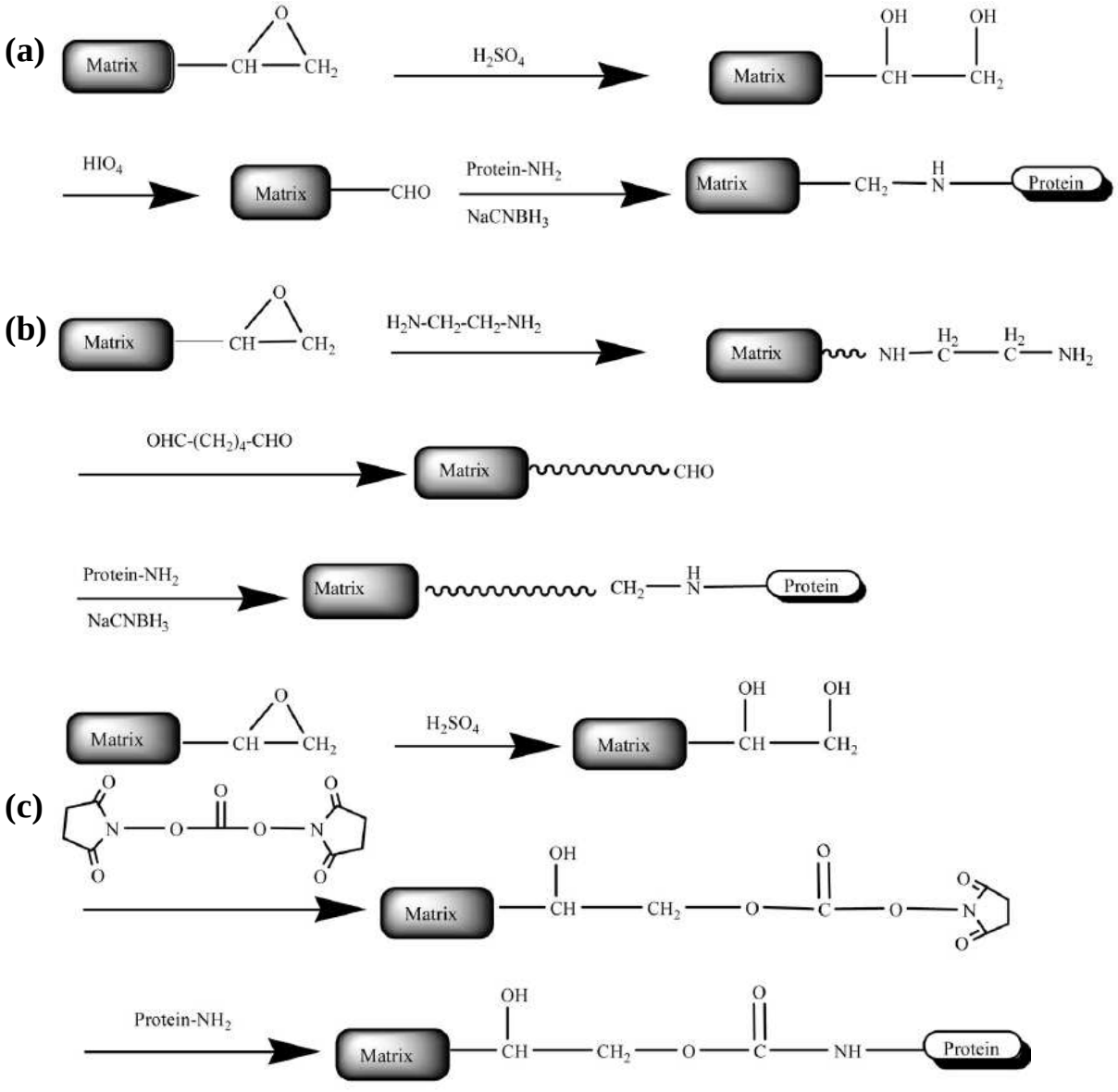

Figure 1.15: *Schematic of techniques for biomolecule immoblisation onto epoxide expressing monolithic columns, Schiff base method (a), glutaraldehyde method (b), disuccinimidyl carbonate method (c), [38].*

In 1999, Xie *et al*. [102] prepared a monolithic column in the presence of the reactive monomer 2-vinyl-4,4-dimethylazlactone (vinyl azlactone (VAL)). The monolith comprised of acrylamide functional monomer, ethylene dimethacrylate (EDMA) cross-linker, and VAL. This resulted in reactive VAL groups presented at the surface. The groups utilised the rapid room temperature reactions of this molecule to covalently attach trypsin, for enzyme digestion. The azlactone ring is susceptible to nucleophilic attack from the lone pair of incoming amines, resulting in the covalent attachment of the amine containing group as seen in Figure 1.16.

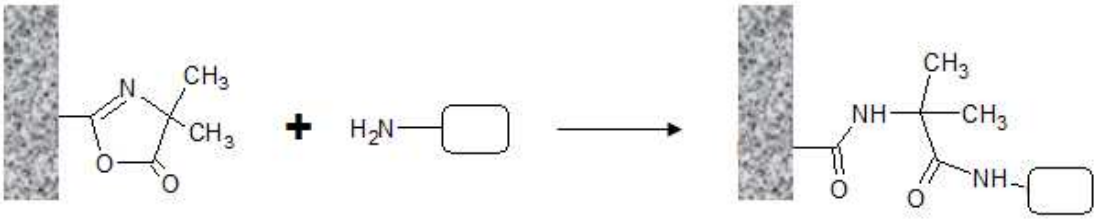

Figure 1.16: *Ring opening reaction of VAL from incoming amine lone pair, of a biomolecule such as an enzyme or a protein (as indicated by white box). Adapted from [102].*

Another type of reactive monolith can be formed using N-acryloxysuccinimide (NAS) as a functional monomer. Guerouache *et al.* [133] prepared a monolith of poly(NAS-*co*-EDMA) within 75 μm i.d. capillaries. The succinimide groups on the monolith surface provided reactive sites for nucleophile chemistry to occur. Using an amine based alkyne, the surface was functionalised with propargylamine. The monolith was further reacted to express β cyclodextrin for chiral analysis.

These types of reactive monolithic columns formed via co-polymerisation of functional monomer are useful, however, some disadvantages exist. For example, the capacity is dictated by the surface available functional groups, the amount of which may be small due to the nature of the co-polymerisation method, as illustrated below in Figure 1.17. As this type of surface modification is based on the concentration of functional monomer incorporated into the monolith structure, attempting to adjust the concentration of the functional monomer will require the re-optimisation of the monolith morphology. Also in utilising these reactive methods, only a single site with functional group may be prepared,. The resulting surface expression is dependent on

the concentration of functional monomer in the monolith precursor solution, and also on the surface expression of the resulting functional groups. For example, in the co-polymerisation of a reactive monomer such as glycidyl methacrylate (GMA), epoxide groups emanate from the surface. Upon reaction of these groups, such as amination, a single site would react for that location. As the bulk of the functional monomer is contained within the globule structure, the surface expression can be sporadic. In UV initiated photo-grafting, a highly cross-linked network of functional monomer is produced, resulting in a dense presence of functional monomer per unit area unlike co-polymerisation [31]

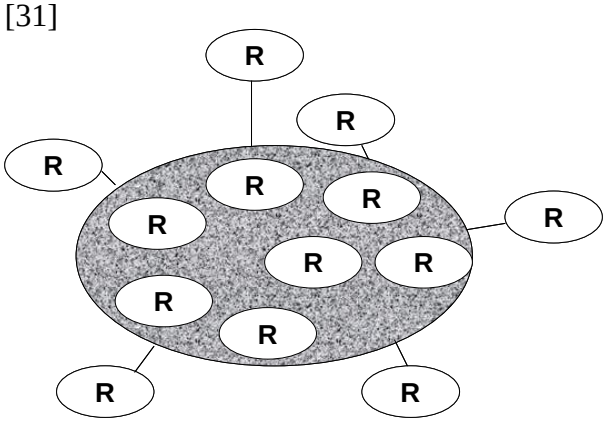

Figure 1.17: *Schematic of co-polymerisation of a monomer with a functional monomer, expressing a functional group (R). The diagram illustrates that not all the functional monomer is exposed on the surface of the monolithic pore, leading to a limit of the subsequent ligand density following reaction.*

1.12.3. Photo-grafting on polymer monolithic columns

The following section describes the grafting procedures performed on polymer films as a method of lamination with polymer films. In 2003 a number of research groups published works [11,12,134,135] on the photo-grafting of desired surface chemistries in monolithic columns. Photo-grafting procedures can be achieved using a single, or a two step method. One problem encountered in single step photo-grafting is the polymerisation of monomer not only on the surface, but in solution [73]. If the functional monomer solution contained an initiator, the growth of chains would not only occur on the surface, but also in solution suspended in the pores of the monolith, as shown in Figure 1.22 Reaction (3) and (4). This can lead to the blocking of pores as the polymer to be removed can be very viscous, also resulting in high column back pressures. To counter this, a two step photo-grafting procedure was devised by Stachowiak *et al*. [73]. By exposing benzophenone to UV irradiation, its excited state

(T_1) removes a hydrogen atom from the surface of a preformed monolith, leaving a surface bound free radical. In the absence of monomers, the surface bound radical binds to the semi-pinacol radical formed by the absorption of UV light by benzophenone. Upon irradiation a second time, in the presence of monomers, the benzophenone radical is released from the surface, dimerising in solution, exposing the surface bound free radical for graft chain growth. From these sites, the chain polymerisation grafting process propagates [136]. This is illustrated in Figure 1.18, below.

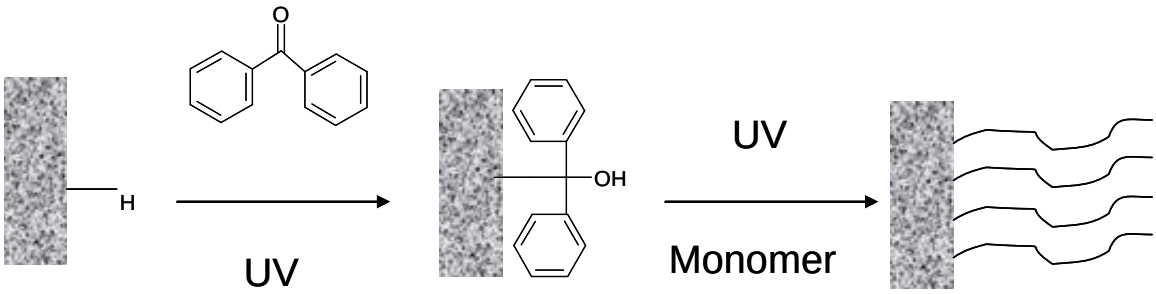

Figure 1.18: *Schematic of photo-grafting in two steps [73]. Diagram illustrates the covalent attachment of the ketyl radical to the polymer surface, prior to the grafting of monomer.*

Using photo-grafting, chains of the desired surface chemistry can be produced with a dense surface coverage. The extremely cross-linked and branched homopolymer chains continue to grow until the reaction is terminated. The density of grafting is easily controlled by irradiation time. Rohr *et al*. illustrated that control of the density of grafted chains is highly dependent on the irradiation time [11]. This is illustrated below in Figure 1.19.

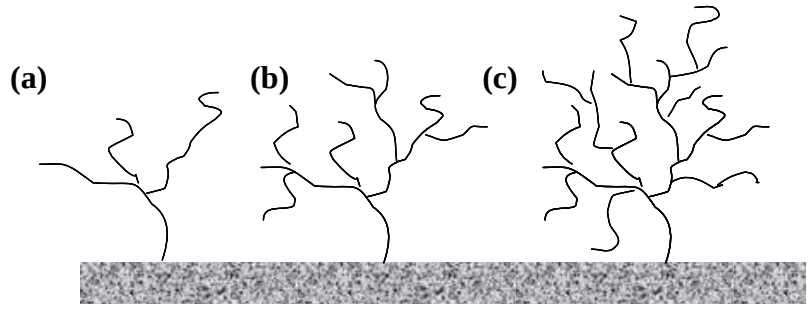

Figure 1.19: *Schematic of graft chain branching and cross-linking with increased irradiation time from (a) to (c) [11].*

Using a two step grafting procedure the percentage of monomer grafted to the surface is increased when compared to a single grafting step [73]. Photo-grafting can be used for the introduction of charged chains of grafted polymer onto an otherwise neutral monolith. For example, Eeltink *et al.* [137] used this photo-grafting method also for the introduction of AMPS onto the surface of BuMA-*co*-EDMA monolithic columns producing a negative charge on an otherwise neutral monolithic column.

1.12.4. Mechanism of photo-grafting using benzophenone

The grafting reactions used regularly for the modification of monolithic substrates, was developed by Rånby and co-workers [138,139], which was further developed in the late 1990's [140-142,144-146]. From their work on the grafting mechanism in the development of lamination techniques for polymer films, this method of post polymerisation modification was devised [11]. Rånby *et al.* [140] originally postulated that the primary excited state of benzophenone was the S_1 singlet state, formed by absorption of light at a wavelength of 376 nm. From here, the transition to triplet states T_2 (at 400 nm) and T_1 (414 nm) were spontaneous. However, their excitation energies at 71 and 69 kcal/mol respectively, were too low for hydrogen abstraction to occur. Yang *et al*. deduced that the energetically feasible transitions from the highest energy state, the S_2 singlet, were responsible for the abstraction mechanism [138]. The abstraction of a hydrogen atom could not be performed by this singlet excited state alone. The singlet S_2 is formed upon the irradiation of benzophenone in the deep UV spectrum, at a wavelength of approximately 250 nm [141]. The maximum absorbance for benzophenone is shown in the following spectrum (Figure 1.20).

Ground state benzophenone molecules absorb light and are promoted to the excited singlet state, S_2, which has an activation energy of 110 kcal/mol. This singlet state is extremely short lived (10^{-12} seconds). Via a non-radiative transition, the S_2 state undergoes transition to a "super heated" singlet state, S_1 [142]. This energy (34 kcal/mol) is transferred to the substrate by non-elastic collisions, resulting in some surface excited polymer (PH) groups. Following the release of this energy, the first triplet state is formed (T_2) and the reactive species T_1, is also formed.

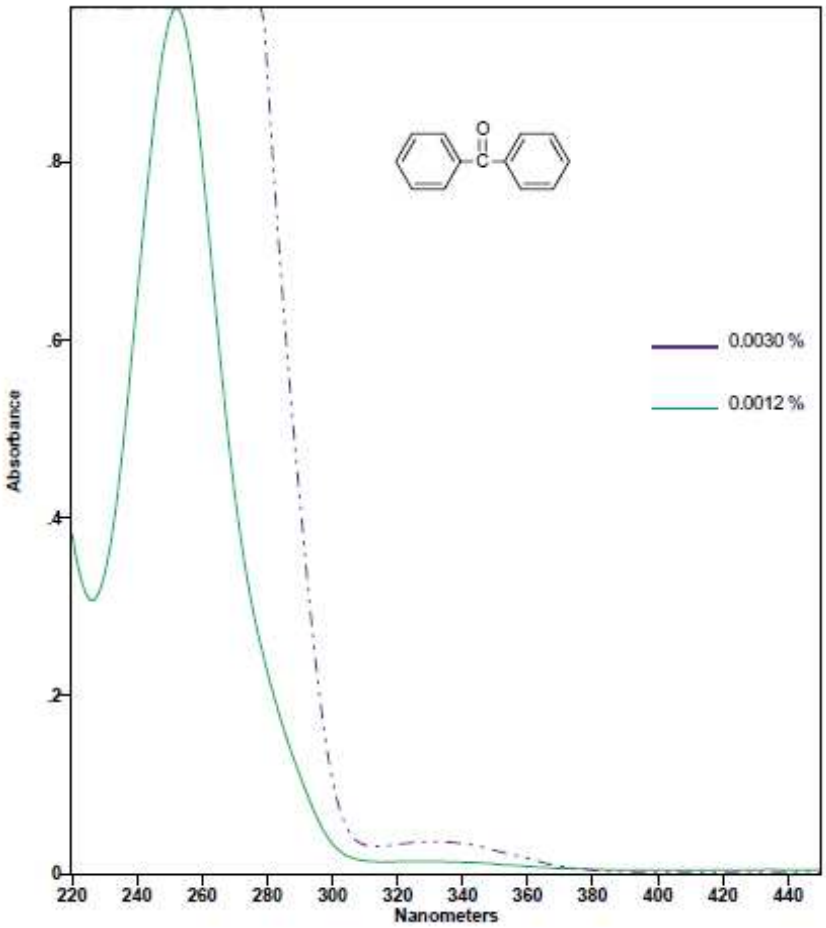

Figure 1.20: *Absorbance spectrum for benzophenone, demonstrating a maximum absorbance value (λ_{max}) between wavelength of 240 nm and 260 nm [143].*

This is highlighted in the Jablonski diagram below in Figure 1.21. It is with the triplet state of benzophenone that the hydrogen abstraction step occurs [140]. The triplet states are long lived (10^{-2}, 10^{-3} seconds respectively) in comparison to the singlet states S_2 and S_1 (10^{-12}, 10^{-9} seconds respectively) [140,143]. Following hydrogen abstraction, a free radical is left on the polymer surface ($P^{\bullet}$), from which chain growth is possible. Semi-pinacol molecules resulting from the benzophenone photolysis and initiation, dimerise, forming pinacol type molecules [140].

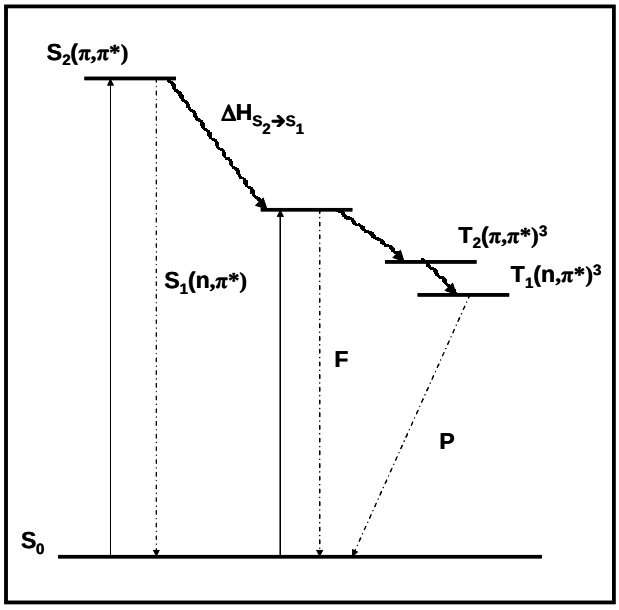

Figure 1.21: *Jablonski diagram for benzophenone. S is a singlet state, T is a triplet state. F is fluorescence and P is phosphorescence. Adapted from [145].*

Not all allylic hydrogen atoms can be easily extracted. Tertiary, secondary, and primary hydrogen atoms have decreasing bond strengths in alkanes (93 kcal/mol, 96 kcal/mol, 100 kcal/mol, respectively) [143,144]. The lower the bond strength, the higher the reactivity for hydrogen abstraction [139], for example, in the case of hydrogen abstraction of acrylic acid, which contains an ethylenic hydrogen carbon bond (106 kcal/mol), compared with methacrylate monomers such as butyl methacrylate (containing primary, secondary and tertiary bonded hydrogen atoms), reacted faster in hydrogen abstraction thus producing higher amounts of homopolymer [138]. This is due to the lower energy requirements for radical formations, particularly in the case of tertiary bonded hydrogen atoms (as seen above). Predominantly methacrylic monomers contain secondary and primary bonded hydrogen atoms, with a lack of tertiary bonded hydrogen atoms present. However, acrylate monomers in general have a higher reactivity in hydrogen abstraction compared to methacrylates [145], due to the absence of tertiary hydrogen bonded atoms in the newly formed polymer. It has been noted that primary and secondary bonded hydrogen atoms also form homopolymer in such reactions, however, it is in significantly lower proportions [138].

In the formation of grafted polymer, a number of steps are involved as outlined in Figure 1.22. For those reactions performed in the presence of both initiator and monomer in solution, a number of side reactions can occur, other than the desired polymer chain grafting. There are six main reaction types outlined in this schematic [146]. Reactions (1) and (2) outline the possibility of no grafting reaction occurring, following photolysis of the initiator molecule upon irradiation with UV light. Reactions (3) and (4) are of particular interest, as they illustrate the primary grafting step. Reaction (3) illustrates the formation of homopolymer (Mn) in solution, i.e. not localised to a polymer substrate surface. However, reaction (4) illustrates the generation of the polymer bound radical (P$^{\bullet}$), and its reaction producing a homopolymer grafted to the polymer substrate (PMn). Reactions (5) and (6) detail the growth of homopolymer in solution (5), and upon the polymer substrate (6).

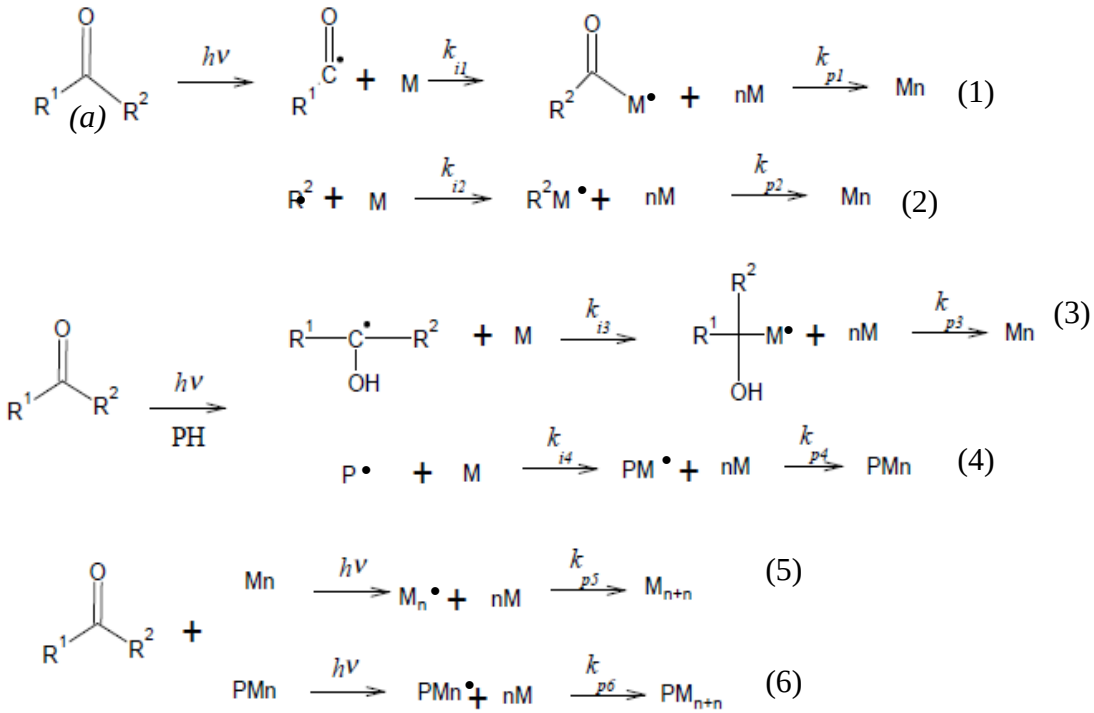

Figure 1.22: *Reaction scheme of the individual reactions of benzophenone (a) in monomer solution following UV irradiation. Where k = rate, i= initiation, p= propogation, M = vinyl monomer, Mn = homopolymer, PH = polymer substrate donating hydrogen atom, $R^{1,2}$ indicate phenyl rings of benzophenone [146].*

Any vinylic bonds (C=C) are reduced to form more stable moieties in which secondary and tertiary hydrogen bonded atoms are produced. These new hydrogen bonds will be the sites for future branches of homopolymer. When reactions (4) and (6) occur simultaneously, a high amount of grafting is achieved [146].

This type of grafting procedure can result in grafted layers of < 10 nm [141]. If a two step grafting procedure is performed, in the absence of monomer in the bulk solution during the initial excitation of benzophenone, a semi-pinacol radical is covalently attached to the substrate site. Upon irradiation of the attached radical, reactions (4) and (6) should predominate, with any semi-pinacol radicals forming dimmers (i.e. pinacol type compound) [140]. This is shown in Figure 1.23.

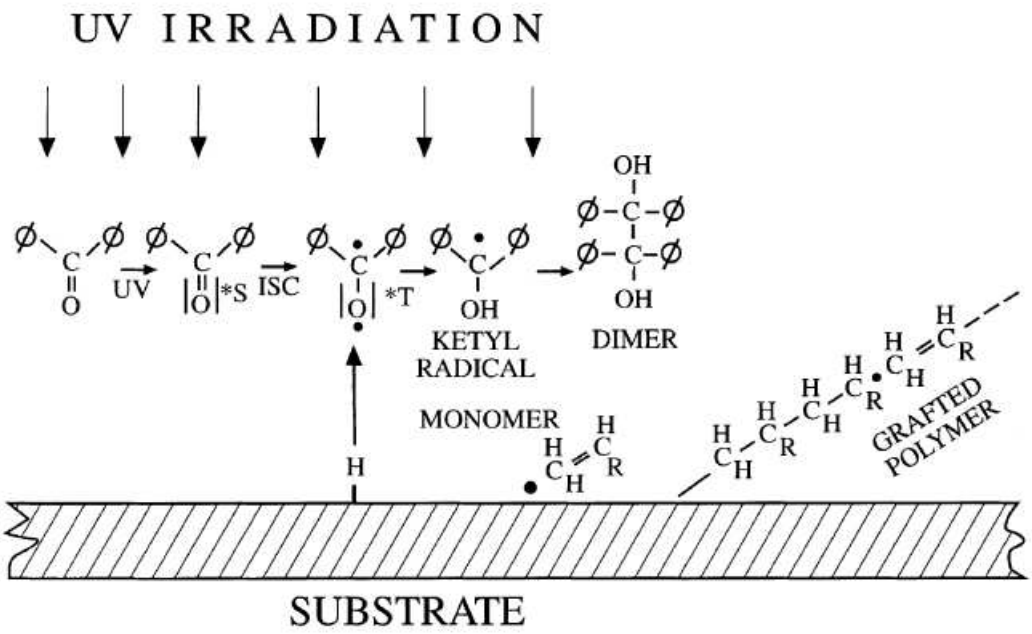

Figure 1.23: *Schematic of overall grafting process. ISC stands for intersystem crossing for the transition of S_1 to T_2 via radiationless transfer [140].*

1.12.5. Photo-masking polymer monoliths

Methods which involve thermal grafting of polymer chains are not site specific, resulting in the grafting of the entire column length [11]. The spatial location of desired functional groups within a monolithic column can be facilitated by photo-masking methods. By using site specific photo-grafting procedures, columns can be produced easily to contain a number of different surface chemistries in specific areas [11,12]. This technique is illustrated below for photo-grafting in methacrylate based monolithic columns in Figure 1.24.

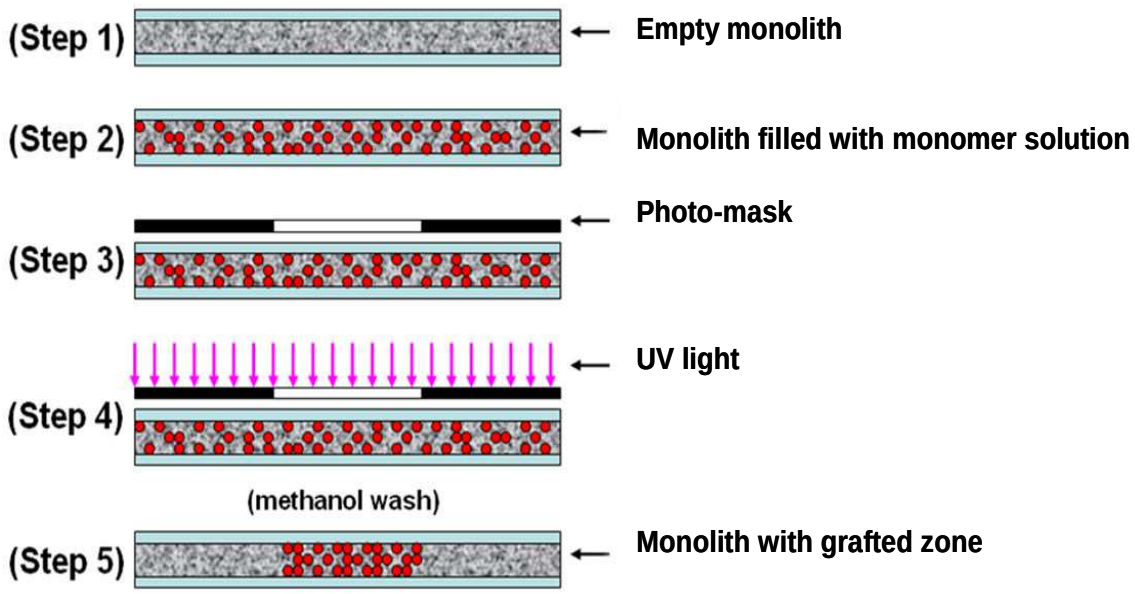

Figure 1.24: *Schematic of photo-masking on a polymer monolithic column for photo-initiated grafting.*

Photo-masking was utilised by Pederson *et al.* [12] in the production of a dual function micro-analytical device, for combined solid phase extraction and tryptic digestion of proteins for peptide mapping. This consisted of the production of a hydrophobic base monolith of which a 20 mm section was grafted with vinyl azlactone (VAL) via benzophenone initiation. Trypsin was immobilised onto the VAL sites and provided a platform for enzymatic digestion. As a cross validation of the non-grafted zone of SPE material, a fluorescence microscope image was taken of the boundary between the two distinct zones, following the SPE capture of fluorescent peptides. This is shown in Figure 1.25 below.

The resulting image showed a distinct boundary between the grafted and non-grafted zones, indicating a successful photo-masking procedure. The ability to visualise the boundary of the grafted and non-grafted zone using fluorescence has its benefits, however, as noted by Stachowiak *et al.* [73] the fluorescence imaging is not strictly quantitative, as the surface concentration of the tagged protein is not correlated to the fluorescence intensity. The method is useful for the visualisation of relative protein adsorption along the column length.

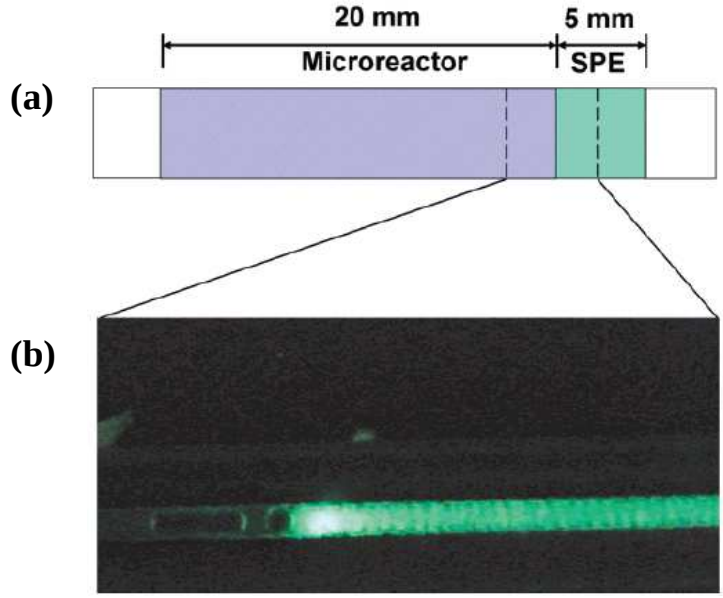

Figure 1.25: *Schematic of the dual function device (a), fluorescence microscope image of digestion-SPE boundary, with captured fluorescent peptides in the SPE segment (b) [12].*

Stachowiak *et al.* [73] prepared two separate BuMA-*co*-EDMA monolithic columns, Column 1 and Column 2. Column 1 was subjected to the photo-grafting of spatially separated zones of the hydrophilic monomer, poly(ethylene glycol methacrylate) (PEGMA), via photo-masking. In this method sections of the column were covered with a mask to prevent exposure to UV irradiation. This resulted in zones of grafted PEGMA, separated by zones of non-grafted monolith. Following grafting a solution of fluorescently tagged protein, bovine serum albumin (BSA), was flushed across the column. The grafted zones of PEGMA provided a resistance to the non-specific binding of the protein to the hydrophobic monolith. An image taken on a fluorescence microscope can be seen in Figure 1.26 (A), where the dark zones represent the grafted sections of PEGMA, which resist non-specific protein binding, due to the hydrophilic nature of the polymer graft.

Column 2 was grafted entirely with the hydrophilic monomer, PEGMA (i.e. without a photo-mask). Using the photo-patterning technique, zones of the reactive monomer VAL were grafted upon the PEGMA grafted BuMA-*co*-EDMA monolith. The VAL zones were reacted with the fluorescently tagged BSA. The resulting fluorescence (Figure 1.26 (B)) was due to the BSA covalently attached to the grafted

sites of VAL. Using imaging software the intensity of fluorescence was measured relative to both columns. The grafting of the hydrophilic monomer PEGMA reduced non-specific bonding of protein to the column by a figure of 98 %.

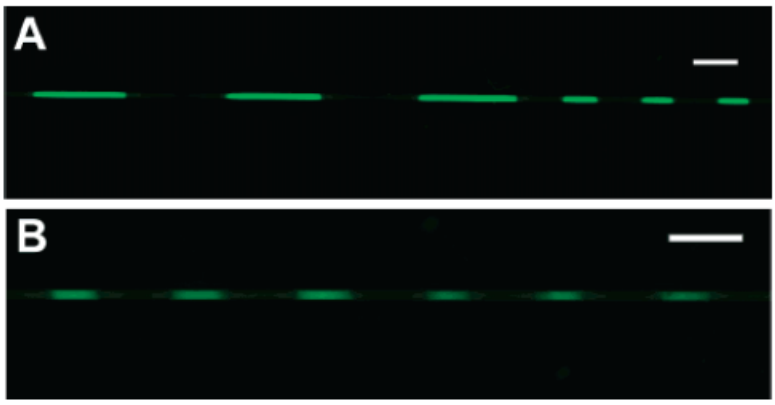

Figure 1.26: *Column grafted with PEGMA zones (dark region) and treated with fluorescently tagged BSA (A), Column grafted with PEGMA, followed by grafting of VAL zones which were treated with fluorescently tagged BSA (B) [73].*

This method has been used since, in a study of the hydrophilisation of a hydrophobic monolith substrate [74,86]. Logan *et al*. produced a column expressing three different enzymatic systems, each specifically placed using photo-grafting of the reactive monomer, VAL [74]. The monolith was grafted first with PEGMA along the column, producing a hydrophilised surface. Further to this, the column was then grafted with VAL using a single photo-grafting step, and the biomolecule was immobilised. A schematic of the monolith patterning is illustrated below in Figure 1.27.

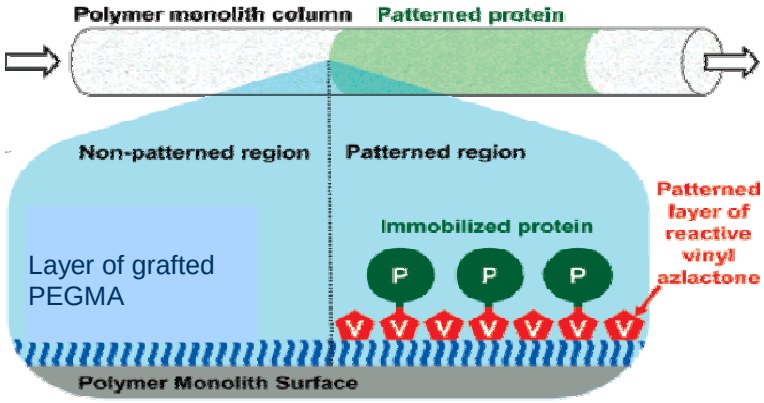

Figure 1.27: *Schematic of the resulting photo-patterned monolith, following grafting steps [74].*

The surface was further grafted with discrete zones of a VAL. Altogether, three separate enzymes (glucose oxidase, horseradish peroxidise, and invertase) were immobilised to the monolith surface via sequential grafting steps of VAL. A fluorescent protein was then covalently bonded to the VAL sites producing a visual cross validation of VAL zones. The group grafted VAL in three sequential steps, each following the immobilisation of enzyme. In step one VAL was grafted onto the column and green fluorescent protein (GFP) was immobilised to the active zones. This was repeated in the second step, with new zones of GFP created [74]. This is shown below in Figure 1.28.

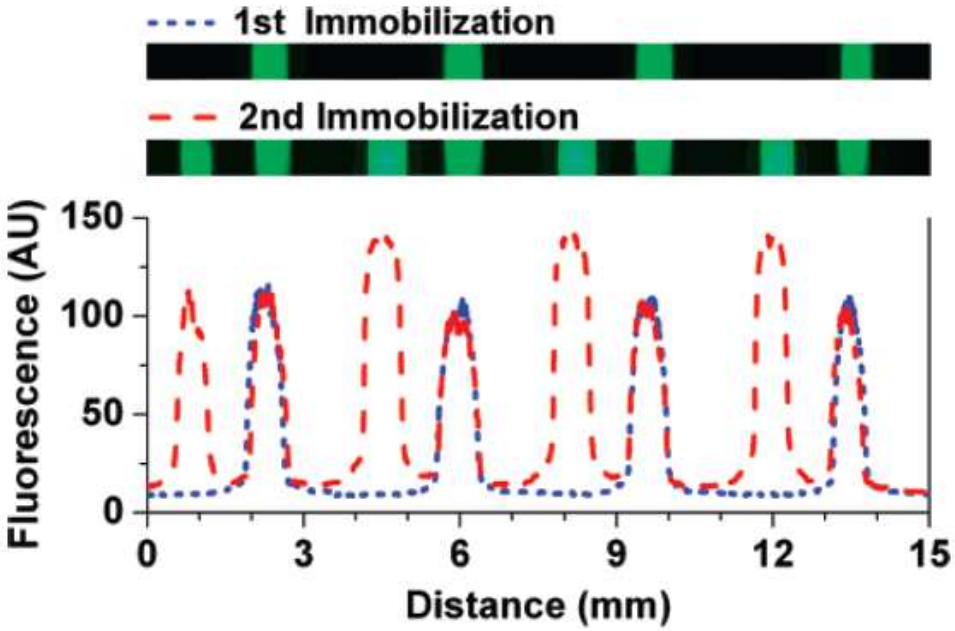

Figure 1.28: *Fluorescence imaging of immobilised GFP on a VAL grafted monolithic column. Two distinct VAL grafting steps used to illustrate the ability of sequential grafting [74].*

This method illustrated no reduction in the fluorescence of the first GFP zones following the second step of photo-grafting, thus indicating no significant interference on the immobilised groups during a secondary grafting step. This demonstrates the versatility of the photo-masking technique to graft monolithic columns within a single column housing, with a variety of different chemistries via subsequent steps.

1.13. Stationary phase gradients

Gradient elution is used in chromatography to aid in the elution of highly retained compounds and those of similar properties within a reasonable run time. The advantages associated with gradient elution include an increase in peak capacity, improvement in peak shape, and on-column chromatographic band focusing. However, using a mobile phase gradient, sophisticated pumps are required. The transfer of one gradient method to another instrumental system can also prove difficult as delay volume between chromatographic instruments can differ, i.e. the time taken for re-equilibration may be different, and the formation of the gradient may not be accurate. Creating a mobile phase gradient in nano and micro-flow devices can be extremely difficult, as highlighted by Brennan *et al*. [147]. The group investigated the use of a very sophisticated device, capable of delivering a gradient of mobile phase composition to a nano-flow chip used for LC.

A number of commercially available nano-flow pumps exist. Some instruments have a split flow system, wherein to generate the micro- or nano-flow a larger volume is split into a ratio suitable for the application. Such a system is the Dionex Ultimate 3000 standard LC system. In this system a split flow is created by a specifically designed cartridge which controls the flow to the column. Mobile phase gradients can be performed, however, delay time can be long in comparison to the separation time when using nano-flow. Other systems, such as the RSLC model, have a splitless flow offering direct and continuous flow from 20 nL/min to 50 µL/min, with the ability to perform mobile phase gradients [148]. Waters also offers nano-pumps, the nanoAquity UPLC, which is capable of splitless flow from 200 nL/min to 100 µL/min. this pump is also capable of performing mobile phase gradients, however, due to the flow calibration of set mobile phases via mobile phase viscosity, the range of possible gradient compositions can be limited [149]. Thermo Scientific also provide a nano LC chromatography system called the Easy-nLC, with flow range between 20-2,000 nL/min or 100-1,000 nL/min. Gradient elution is also possible for this system, advertising a high precision due to integrated flow sensors prior to the mixing chamber [150].

The complexity of this work illustrates the difficulty in controlling flow under such low flow rates, however, an alternative method to produce a gradient in micro-

and nano-flow systems is the use of an immobilised gradient situated, within or on, a stationary phase.

1.14. Stationary phase gradients in particulate columns

"Pseudo" stationary phase gradients have been investigated by a number of research groups [151-154], using particulate columns. In these methods, numerous columns are connected in series, to produce an overall gradient of selectivity, using multiple coupled columns [151,152]. Sreedhara *et al*. [151] used columns coupled in series to achieve this change in selectivity, and compared their work to 2D chromatography. Unlike two dimensional (2D) chromatography, whereby two columns are coupled together, switching valves are not used [153,154] as mobile phases were changed following the separation on each in-series column [151]. In coupling columns together, a true stationary phase gradient is not constructed, and with dead volume introduced from extra inter-column connections, band broadening issues may arise. Desirably, a stationary phase gradient should be produced within *a single* column housing.

In an attempt to produce a 2D stationary phase Link *et al*. [155] packed a single capillary (of 100 μm i.d) column using two types of stationary phase; ion exchange and reversed-phase. The capillary was pulled, for use as an electro-spray tip, thus reducing the need of a frit in the capillary. Firstly, 8 cm of a 5 μm C_{18} particles were packed into the column. Secondly, 4 cm of the same capillary column was packed with 5 μm SCX particles. This method has its disadvantages, as packing a capillary from two different particle slurry preparations can be technically difficult. For example, capillary columns are packed under pressure, with the packing material suspended in a solvent (slurry). In order to change the packing slurry to add another slurry of differing selectivity, the pressure would have to be disengaged, resulting in the decompression of particles in the column. Inevitably, this would result in a diffused boundary between the two stationary phases. Nonetheless, this procedure named multidimensional protein identification technology (MudPIT), was repeated by Washburn *et al*. [156] and Wolters *et al.* [157], for total analysis of complex biological samples with subsequent MS/MS detection. Producing a packed stationary phase gradient comprising of *n* selectivities will ultimately prove difficult, as an

infinite amount of stationary phase selectivities would be needed in order to produce a linear stationary phase of continuously changing selectivity.

The ease of *in-situ* polymerisation and post polymerisation modifications of polymer monolithic columns makes them an ideal candidate for the development of a stationary phase gradient. A number of methods can be explored in order to produce such a column; co-polymerisation, thermally induced reactions, and photo-grafting.

1.15. Co-polymerisation of functional monomers

Maruška and co-workers [158] fabricated monolithic stationary phase gradients using a co-polymerisation method, using hydrophilic and hydrophobic constituents, to enhance separation performance in reversed-phase chromatography. In the preparation of columns, the capillary housing was marked to a designated "zone" length. The capillary was to be filled with a number of monomer mixtures. Each monomer mixture contained an increasing concentration of functional monomer. During the filling step for the capillaries, the capillary was placed into the desired monomer solution, until the meniscus met the predetermined mark of the capillary. The capillary was then moved to the next monomer solution (ideally one of higher functional monomer concentration) until the capillary was full, and then the column was sealed and subjected to thermal polymerisation. This fabrication procedure is outlined in Figure 1.29 below.

Columns were prepared for both capillary LC methods, and capillary electrochromatography (CEC). For the CEC separations, the columns were prepared with total monomer concentration held constant. For columns used in capillary LC mode, the columns were composed of a hydrophobic monomer, diluted with a 50 m*M* sodium phosphate buffer to varying concentrations for each "zone" of the column. Obviously, this results in a column of varying morphology, with some segments of the column exhibiting lower polymer density. This can have a negative effect upon the separation efficiency, and thus the true effect of the gradient of hydrophobicity may be masked. Sections comprising of 100 % buffer may not exhibit a stable polymer scaffold, and so may result in an open tubular type capillary segment.

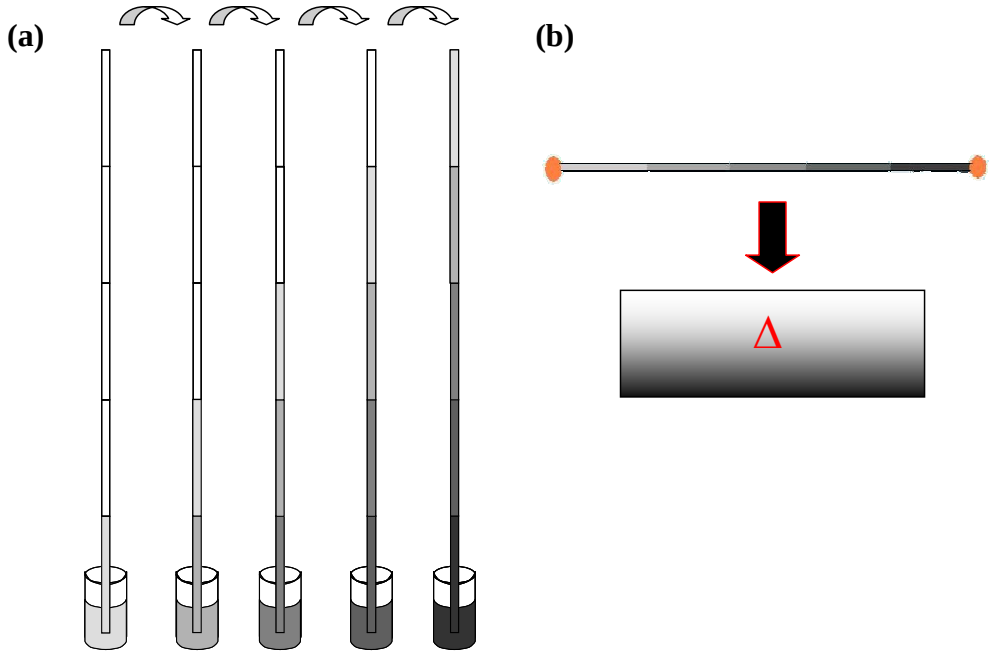

Figure 1.29: *Schematic of co-polymerised gradient; Capillary with predetermined "zone" lengths (a), the column was sealed and subjected to thermal energy (Δ) for polymerisation (b). Increasing functional monomer concentration illustrated by darker shades.*

In LC mode, an increase in efficiency was observed when comparing an isotropic column to a gradient column (9, 703 N/m versus 83, 300 N/m respectively), for the same analyte peak. The direction of the gradient was not highlighted in this report, however, upon analysis of reported chromatograms, a decrease in run time of approximately 2 mins, was observed for the column in the plumbing orientation of high to low hydrophobicity [158]. This may be due to sections of capillary with lower polymer density, as discussed above.

This reported method was an elegant approach to produce a stationary phase gradient, however, in the case of the addition of a functional/charged monomer, the gradient may be of a low capacity, and the morphology of the resulting column may not be constant. The true concentration of monomer expressed on the surface of the pore would be rather low. As the functional monomer is added to the monolith pre-cursor solution during fabrication, a large proportion of the functional monomer would then be contained within the monolith structure itself, upon polymerisation. The bulk of the functional monomer is concealed from the surface, within the globules, thus presenting a low concentration of functionality on the surface. This is

an obvious disadvantage to the use of co-polymerisation in the production of a stationary phase gradient.

1.16. Production of stationary phase gradients using UV polymerisation techniques

Due to the ease of surface modification of polymer monolithic columns, the development of a gradient of functionality has been mainly studied in this format. Stationary phase gradients can be produced rapidly *in-situ* using UV grafting [135,159] or by thermal methods [158]. For applications on a capillary scale, Pucci *et al.* [135] investigated the use of a photo-grafted gradient of sulphonic acid groups upon a monolithic column. The group used a number of methods in their investigations; (a) a commercially available neutral density gradient filter, (b) a moving shutter composed of polycarbonate, and (c) a moving shutter in conjunction with a length of polyester film (Mylar ®) to attenuate UV light transmission reaching the column during the photo-grafting procedure. They observed that the extent of photo-grafting depends on the total energy or UV dose used. In order to produce a gradient of photo-grafted surface functional groups, the UV dose had to be attenuated using irradiation time and intensity.

A commercially available neutral density gradient filter with a set optical density (absorption) which gradually changed along the length of the filter was used to produce an attenuation in UV grafting intensity along the column length. The OD is related to the percent transmission (% T) of light as shown in equation (1.1):

$$\%T = 10^{-OD} \times 100 \qquad \text{(Eq. 1.1)}$$

Such a gradient filter is shown in Figure 1.30 below. The filter is comprised of a fused silica substrate, with either a continuous or stepwise deposition of metallic particles.

Figure 1.30: *Neutral density gradient filter, commercially available with a defined optical density setting [160].*

Alternatively, the group used a moving shutter whilst the column was irradiated, producing a linear increase in graft density along the column. By further reducing light intensity with the aid of a polyester film, the irradiation time could be increased whilst maintaining control over the density of the resulting grafted layer. From their results, an improvement in separation performance was achieved, when comparing an isotropically (i.e. homogeneous graft density, across the entire column length) modified column to that of a gradient modified column. The group analysed the separation of acetylsalicylic acid and salicylic acid, both separations performed in CEC mode, on an isotropic column and two gradient columns (Figure 1.31 (b & c)).

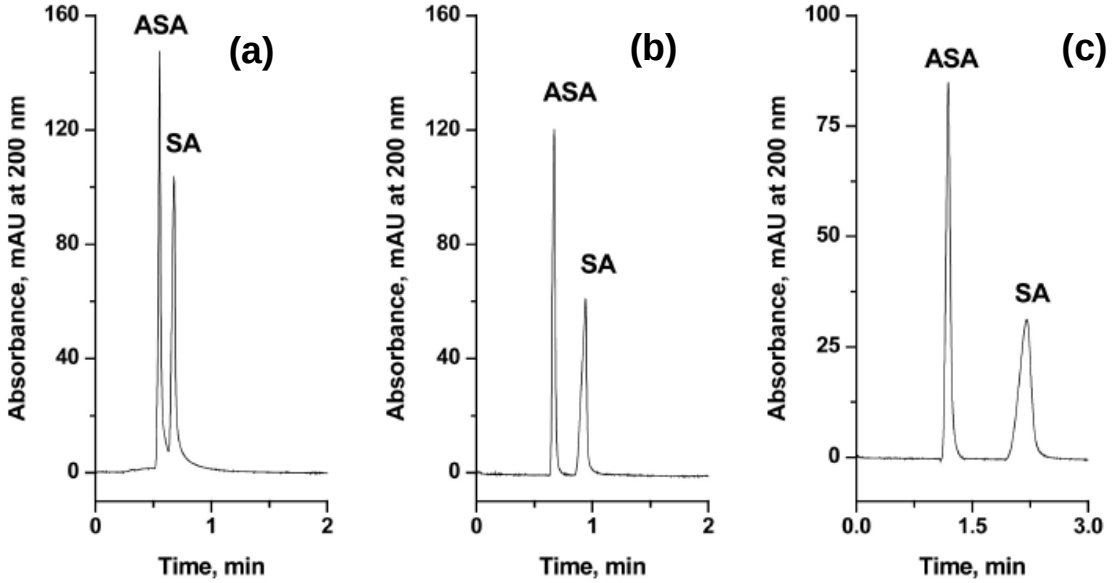

Figure 1.31: *Chromatograms generated on an isotropic column (a), a gradient prepared using moving shutter (b), and a gradient produced using a neutral density filter (c). Analytes ASA = acetylsalicylic acid, SA = salicylic acid. Mobile phase 80:20 ACN:10 mM phosphate buffer pH 2.5. Separation voltage = 25 kV, electrokinetic injection at 5 kV for 5 s. UV detection at a wavelength of 200 nm [135].*

Superior separation was exhibited by the 2-acrylamide-2-methyl-1-propanesulphonic acid (AMPS) gradient prepared in the format as seen in Figure 1.31, when compared to the isotropic column (homogeneous distribution of functional groups). Resolution is increased in the gradient formats of the column, with the moving shutter gradient producing good baseline resolution within a reasonable run time (~1 min). The isotropic column produced a separation efficiency of 34, 600 N/m, whilst the neutral density gradient filter produced a column with a plate count of 79, 500 N/m. The gradient column fabricated using moving shutter produced a higher efficiency of 85, 900 N/m (Figure 1.31 (b)). An increase in peak capacity was also observed, from 25 (isotropic) to 31 (gradient, moving shutter) [135].

To characterise the gradient of sulphonate groups along the column, cross sections of the monolith were subjected to electron probe microscopy and analysed for sulphur. From the results, plots of % capillary length versus % sulphur were constructed. For the column grafted using a moving shutter, the resulting plot was linear, whereas for the column grafted with a neutral density gradient filter, the resulting plot was exponential (Figure 1.32). However, this may not be an accurate representation of the exact functional group distribution across the column. Only certain intervals of the column could be visualised using this method, and so sections of column existing between these cross sectional sampling points may have been missed. In addition, the invasive nature of the characterisation process resulted in the destruction of the column.

Figure 1.32 (a) and (b) illustrate the expected results from the two methods of gradient production where, the first method incorporated the use of a moving shutter to vary exposure time along the column, and the second method utilised a commercially available optical filter. In Figure 1.32, plots (c) and (d), the experimentally determined % sulphur concentration at selected intervals along the columns using both methods are shown. Whilst the plot (c) resembles plot (a), there are only 4 data points reported, indicating a large amount of the column remained un-profiled for sulphur content. In plot (d), the profile is similar to that of (b), however, the reported sulphur content (which is dependant on exposure dose), increases to a point where it begins to plateau. This indicates a maximum of grafting has been achieved under the experimental conditions.

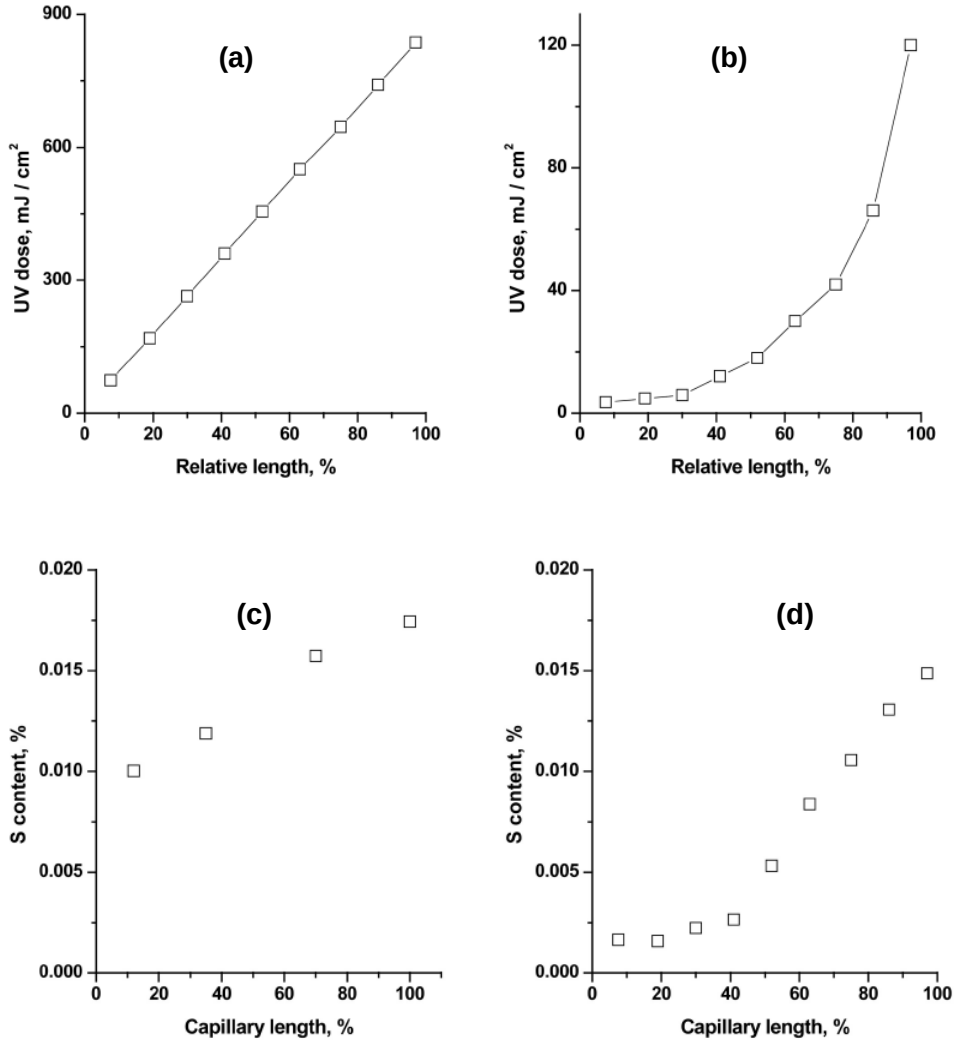

Figure 1.32*: Calculated UV dose profiles for a stationary phase gradient produced using a moving shutter (a), and using a neutral density filter (b), Sulphur content on a column produced using a moving shutter (c), and using a neutral density filter (d) [135]. The columns were destroyed for sulphur characterisation via electron probe microscopy.*

In a similar study, Urbanova *et al*. [159] applied the moving shutter technique to the fabrication of photo-grafted TLC plates expressing a porous polymer layer, to incorporate a gradient of hydrophobic polymer for two-dimensional separations. The presence of the gradient was validated visually using a fluorescent dye as shown in Figure 1.33. Contact angles across the gradient were also measured.

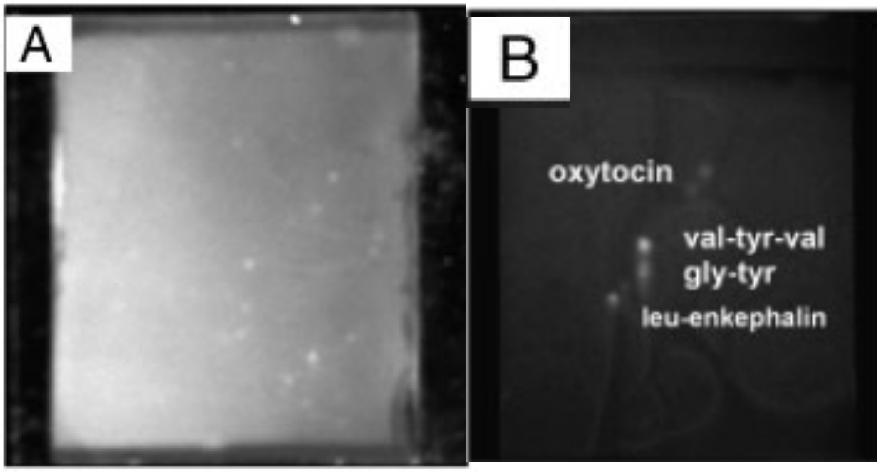

Figure 1.33: *Visualisation of the gradient using fluorescent labelling with 1-anilinonaphthalene-8-sulphonic acid (A), separation of oxytocin, leu-enkephalin, Val-Try-Val, and Gly-Try, on a hydrophilised monolithic layer with a diagonal surface photo-grafted layer of poly(LMA) (B). Mobile phase in first dimension 0.1 % trifluoroacetic acid (TFA) in 30% ACN- water, second dimension 0.1 % TFA in 50 % methanol-water [159].*

.

1.17. Immobilised pH gradients

Isoelectric focusing (IEF) is a technique which exploits the migration of an amphoteric molecule in a pH gradient, to a position of zero migration which is stable under an electric field [161]. In IEF, a pH gradient is produced with the appropriate catholyte, anolyte, and the addition of carrier ampholytes (CA). These carrier ampholytes consist of a large number of poly amino-poly carboxylic acid aggregates. The concentration of carboxylic acids, or amino groups in the ampholyte dictate the resultant pH. The exact structure of these compounds is unclear as it is proprietary information. Under the electric field they migrate to an area of zero mobility (p*I*) forming a stable pH gradient. Using IEF, molecules such as proteins are separated on a stable pH gradient exploiting the differences in p*I*. This occurs by an overlap of protein concentration at each differing p*I*.

In conventional IEF procedures in CE, the ampholyte carrier is added to the sample and buffer vials to maintain the stable gradient, which can be a costly procedure. Every protein is an ampholyte, and as such, has an isoelectric point, p*I*. A

reported method to produce immobilised pH gradients on a column for capillary isoelectric focusing (cIEF) uses the process of IEF itself [162]. This method of immobilised pH gradient formation is based on the immobilisation of carrier ampholytes. The use of a monomer with an accessible epoxide ring (such as GMA), is a straightforward method of producing the desired pH gradient. In acidic/basic solution under thermal conditions, the epoxide ring would react, forming diols. Once the appropriate monolithic substrate was formed, a solution of ampholyte was injected onto the column. A voltage was applied over a period of time which provided enough current to separate the CA's into areas of differing p*I*. When the current was stabilised, the focusing procedure was complete, and the column was sealed. Subsequently, the column was subjected to thermal functionalisation for 20 hours at 60˚ C. A number of variations exist for immobilisation of CA's, including, the use of an amination reaction followed by addition of glutaraldehyde, and immobilisation of ampholytes. This method is outlined in Figure 1.34 below. The sodium borohydride step was included to reduce any R-C=N-R groups, to diminish their reactivity. The immobilisation reaction can also occur via a nucleophilic addition of the amino groups from the ampholyte solution, at the reactive epoxide group [119,163,164].

Recently Liang *et al.* [165] reported the use of photo-grafting in the preparation of immobilised pH gradients. Monoliths were prepared in UV transparent capillaries using acrylamide and N,N'-methylenebisacrylamide monomers, producing a hydrophilic monolith. In a separate vial, GMA was reacted with ampholine at 40 °C for 1 hour. The solution was cooled and benzophenone was added to the solution containing methanol, water, GMA, and ampholine. The solution was injected onto the column following degassing, and was subjected to focussing until a stable current was achieved. The monolith was then sealed and irradiated at a wavelength of 254 nm for 20 minutes. This novel production method indicated higher resolution and sharper peaks, when compared to the thermally grafted ampholine as previously described, under the same experimental conditions. When using a GMA co polymerised monolith, a large proportion of the GMA epoxide ring may be embedded in the monolith structure, not available for ampholine immobilisation.

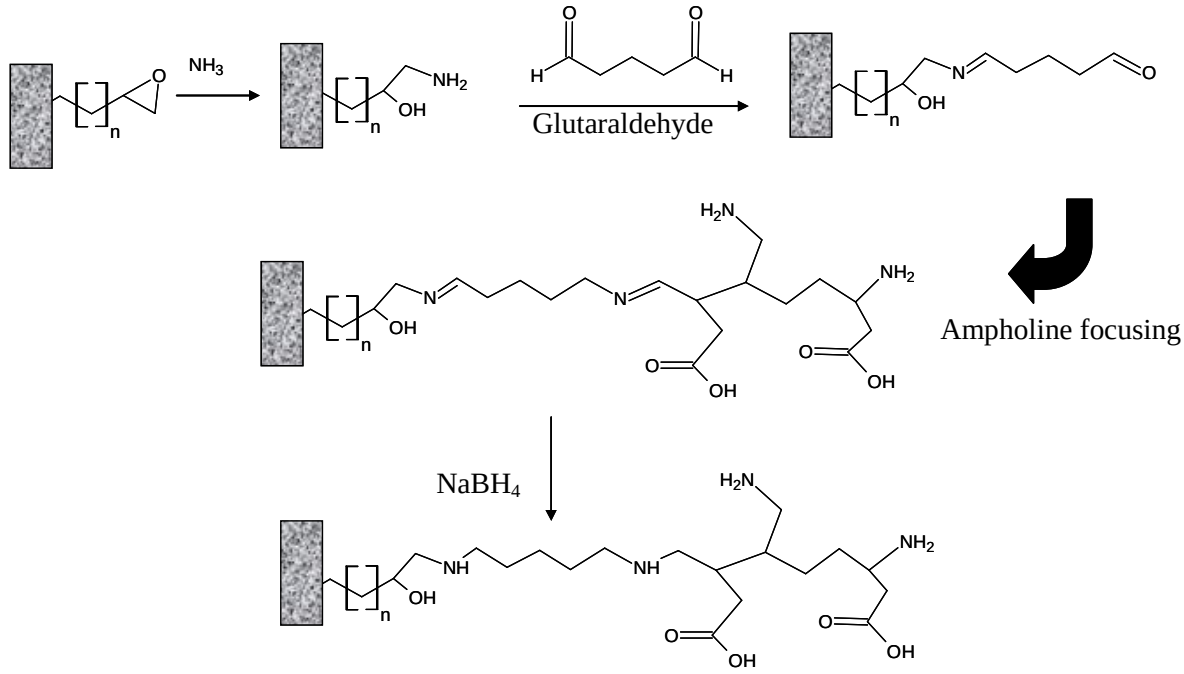

Figure 1.34*: Schematic of the immobilisation of glutaraldehyde on GMA and subsequent immobilisation of CA's. Adapted from [119]. The structure of ampholine included is not confirmed, as this is under patent control.*

In using photo-grafting procedures, chain polymerisation of GMA occurred, where a higher surface density of GMA would be expected. Due to the presence of ampholine on the GMA monomer, this may have inhibited the density of the final grafted layer. However, if secondary branching points appeared along the ampholine chain, a highly branched network of GMA-ampholine would have been produced. A higher proportion of surface available GMA-ampholine groups would account for the increase in efficiencies observed by the group.

1.18. Characterisation methods

The methods of characterisation most commonly used with monolithic column fabrication include contact angle [166,167], , FT-IR spectroscopy [168], inverse size exclusion chromatography [169,170], surface area measurements [171,172]. These methods, while important in characterisation, are beyond the scope of the work presented here. In this presented work, scanning electron microscopy (SEM) with

energy dispersive X-rays (EDX) chromatographic methods and sC^4D were used for characterisation purposes.

1.18.1. Scanning electron microscopy

SEM is used to characterise the pore size and monolithic skeleton characteristics in monolithic columns. However, the need to provide cross sections of the column is destructive and invasive. In slicing a sample monolith for cross-sectional samples, large sections of the monolith are not fully characterised. Also as imaging occurs only from the surface to 2 µm deep into the sample, a large proportion of the monolith would not be characterised. There are three different methods in which SEM can be used for analysis; (i) secondary electron (SE) for imaging, (ii) back scattered electron (BSE) mode for differences in atomic weight, and (iii) energy dispersive x-ray mode for elemental analysis. In most circumstances secondary electrons are used in imaging of monolithic columns. For observing a change in atomic weight, e.g. for visualising metal nano particles on a specimen, BSE mode is used [173]. A larger area is used to produce an image in BSE mode and as such sacrifices resolution (1µm compared to 10 nm in SE mode). BSE's are generated further below the surface compared to SE's and so can provide information on features not found on the surface.

Another useful method of characterisation is the use of characteristic x-rays emitted from specimens. This occurs when an inner shell electron is displaced by an electron, and an outer shell electron may fall into the inner shell in order to maintain charge balance after an ionisation event. The emission of an x-ray facilitates the returning of the ionised atom to ground state. Field emission SEM is a SE mode of detection, however, due to its advanced beam source it is used for imaging nano structures [174].

Many research articles utilise SEM for characterisation of pore size, and monolithic structure, and even for elemental analysis. In Figure 1.35, an example is shown of SEM and EDX of a 2-hydroxyethyl methacrylate (HEMA)-*co*-EDMA monolith, to which varying amounts of hydroxyapatite nano-particles were added to the pre-cursor monolith solution.

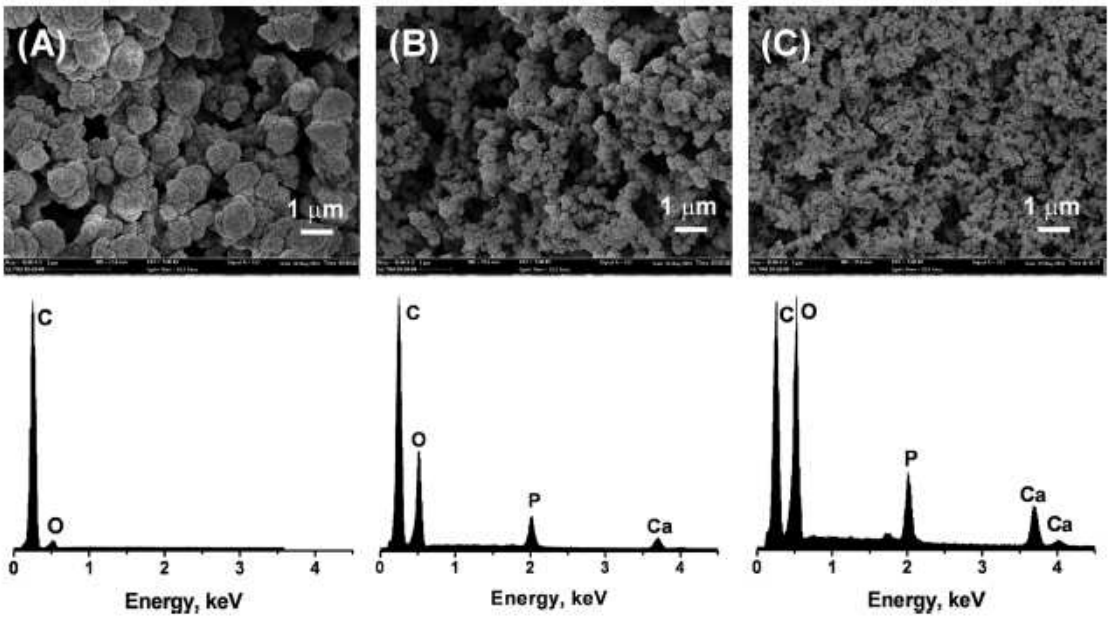

Figure 1.35: *SEM images of a HEMA-co-EDMA-co-hydroxyapatite nano-particle monolithic column; SEM images of sampled monolithic columns with corresponding EDX spectra beneath (A-C) [175].*

A sample was cut from the monolith and was taken for analysis. Under a high accelerating voltage (20-30 kV), the sample was scanned and produced characteristic X-rays. The elemental analysis showed an increase of phosphorous and calcium concentration, with an increase in monomer to nano-particle ratio [175]. This analysis method, along with chromatographic methods, and mercury intrusion porosimetry, is usually used to characterise homogeneity of monolith material, and the average pore size of a monolith.

1.19. Capacitively coupled contactless conductivity detection (C^4D)

1.19.1. Capacitance

Capacitance is the ability to store charge in an electro-static field. This phenomenon is present when two conductors are separated by an insulator. The insulator consists of a dielectric material while the capacitors are generally metal plates. The dielectric material can prevent, or facilitate charge transfer between the

plates, which is dependent on the dielectric constant. Capacitance is directly proportional to the size of the capacitor, and is inversely proportional to the distance between the plates. When a direct current (DC) voltage is applied current flows until the capacitor is charged, and the current stops. This results in an excess of negative charge on one plate, and an excess of positive charge on the other. The insulator prevents the passing of electrons from one plate to another. Capacitors charged with DC are suited to storage of energy, and do not allow the passage of DC [176].

Alternatively, when an alternating current (AC) is applied to the circuit, the capacitor is charged and discharged. Unlike a DC, the voltage and current are 90° out of phase. As soon as the capacitor charges to the peak voltage, the charging current drops to zero. As the voltage begins to decrease the capacitor begins discharging. The current begins to increase in a negative direction. When this current is at a maximum, the voltage is zero. In a capacitive AC circuit the voltage is constantly changing, charging, and discharging the capacitor. Electrons pass from one side of the capacitor to the other, but not through the insulator.

1.19.2. Capacitance in the capacitively coupled contactless conductivity (C^4D) cell

A C^4D cell consists of two cylindrical electrodes, which surround the capillary, separated by a distance, *d*. The two electrodes form capacitors with the inside of the capillary, directly below the electrodes, on the inner walls of capillaries. The electrodes are connected by a resistor formed by the material in the detection gap. This can vary between applications. In capillary electrophoresis an electrolytic buffer would provide the resistance, where in chromatography or CEC, the resistance would be due to the presence of both stationary phase and mobile phase (e.g. electrolyte and/or stationary phase) [177].

Upon the application of an AC voltage, a capacitive transfer with charged ions in the capillary bore beneath the ring electrode occurs, resulting in the generation of current. The analytical signal is generated by the resistance (conductivity) of the solution in the capillary between the detection gap.

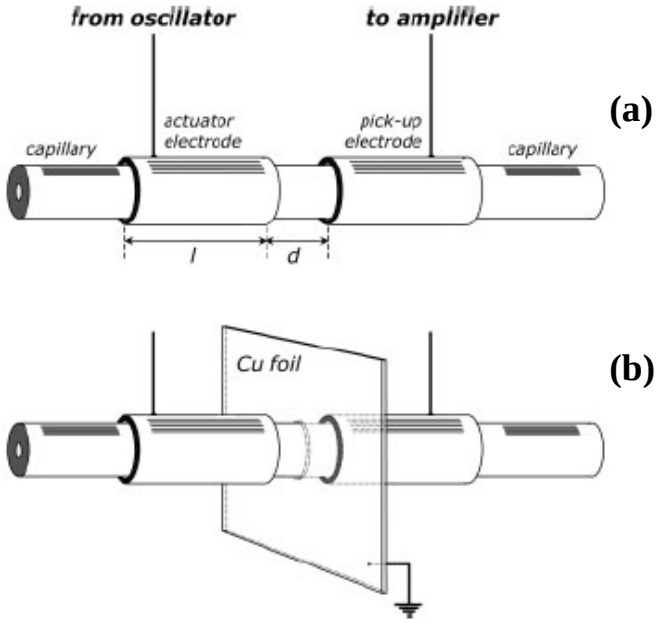

Figure 1.36: *C^4D cell without shield, where possible coupling (stray capacitance) between electrodes can occur (a), cell with shield connected to ground preventing stray capacitance between electrodes (b), l = length of electrode, d = detection gap [178].*

The analyte progresses through the detection gap, resulting in a secondary capacitive event with the pick-up electrode [178]. As an analyte proceeds through the detection gap (in the case of separation processes) a reduction in resistance results in an increase in current, as determined by Ohms law:

$$V = IR \qquad \text{(Equation 1.2)}$$

V= voltage, I = current (A), R= resistance (Ω).

The signal passing through the detection gap is a current and so, is converted to Volts using a pick-up amplifier. The C^4D measurements are generally recorded in millivolts (mV). The output current is converted by the amplifier to voltage using the following equation [177]:

$$V_{out} = -iR_f \qquad \text{(Equation 1.3)}$$

V_{out} = output current (V), i = current (A), R_f = feedback resistor value on the pick up amplifier (Ω).

Da Silva *et al*. [179] defined a complex series of capacitors and resistors in the C^4D system, including the resistance of the polyimide capillary coating, the resistance of the electrical double layer etc. However, for practical purposes the behaviour of the cell can be approximated reasonably well using a circuit of two capacitors, separated by a resistor. By focusing on the main contributions to the detector response from a detector, the group produced the following circuit diagram in Figure 1.37.

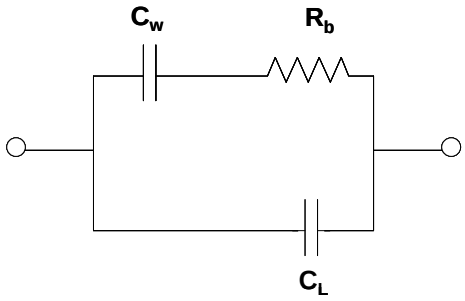

Figure 1.37: *Circuit diagram of the simplified C^4D cell, as developed by Da Silva and co-workers [179]. The wall capacitance is represented as C_W, the resistance of the bulk solution is represented by R_b, and capacitance from between the electrodes (e.g. edge effect where electrodes may couple together) is represented by C_L..*

To prevent capacitive transfer between electrodes (also known as stray capacitance), a grounded plane must be inserted between the electrodes. Generally a thin film of copper foil (faraday shield) is placed between the electrodes and is connected to ground. This ensures that the capacitive transfer occurs only from electrode to the inner bore of the capillary [180]. The difference between shielded and non-shielded detector cells is illustrated in Figure 1.36. Shielding plays a significant role in maintaining good signal to noise ratios. Kuban *et al*. [181] discovered deteriorated signal to noise ratios in the absence of a faraday shield, (six times lower than with a cell incorporating a shield). A log-log plot of voltage output versus frequency is usually constructed to ascertain the optimum excitation voltages. The voltage output (V_{out}) is measured over a range of frequencies (e.g. 10 Hz to 1000 Hz). This plot is termed a Bode plot, an example of which is shown below in Figure 1.38. It is within the plateau region that the optimum operating frequency has been achieved [177]. The V_{out} increases linearly until a plateau region is seen.

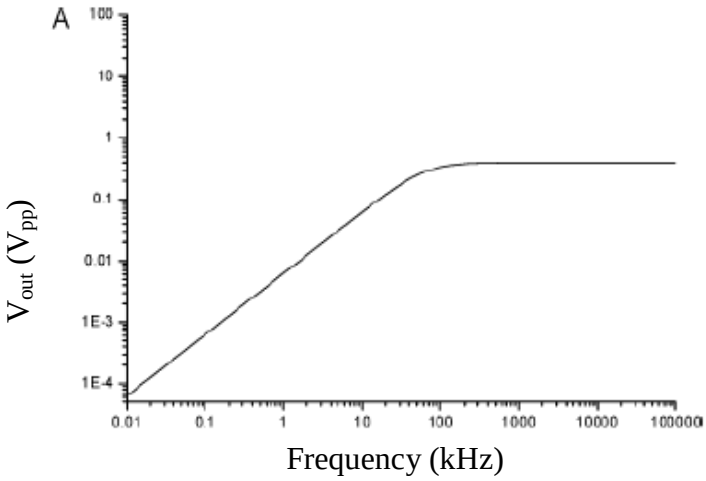

Figure 1.38: *Model Bode plot for a shielded C^4D cell [177].*

For detectors exhibiting stray capacitance the plateau region is shortened, and can be completely obscured [177]. An example of such a plot is shown below in Figure 1.39.

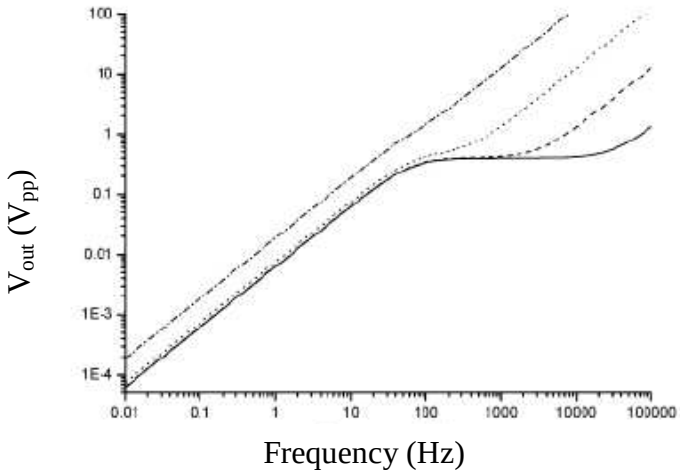

Figure 1.39: *Modelled Bode plot for a C^4D cell with no shielding. Capacitance C = 0.0001 pF (—), C = 0.001 pF (- - -), C = 0.01 pF (…), C = 0.1 pF (•-•-•-•), [177].*

As seen in Figure 1.39, the presence of stray capacitance can significantly affect the signal of interest. As capacitance is proportional to the size of the capacitor, smaller capacitances are seen in this method of detection. To increase signal, higher excitation frequencies are required (~300 kHz). For small capillary diameters (e.g. 10 μm i.d),

the plateau region of the Bode plot is shifted to lower frequencies, and vice versa for capillaries of larger diameter [177].

1.19.3. Operation of a C^4D cell

Figure 1.40 (a) shows a photograph of the C^4D cell used for capillary scale detection. In part (b), a schematic of the C^4D circuit is shown, which includes the actuator/excitation electrode, the detection gap (resistor) and the pick up electrode. With this type of detection, a double layer of capacitance is present between the electrode and the capillary, which is separated by a macroscopic insulation layer. Due to the smaller capacitances observed with this method of detection, excitation frequencies are required [182]. Other models of C^4D cells have included the use of stationary electrodes which were painted onto the polyimide coated capillary [183]. Again the system contains two electrodes each of which forms a capacitor with the solution inside the capillary [184]. Due to the layout of on-chip C^4D, a faraday shield cannot be used, which reduces the limits of detection [185]. The length of the detection gap is described as the length of cross sectional area between the electrodes (~1 mm). From experiments conducted by Kuban *et al*., the lengths of the electrodes have no effect on the resulting Ohmic resistance, whilst maintaining a length of the detection gap.

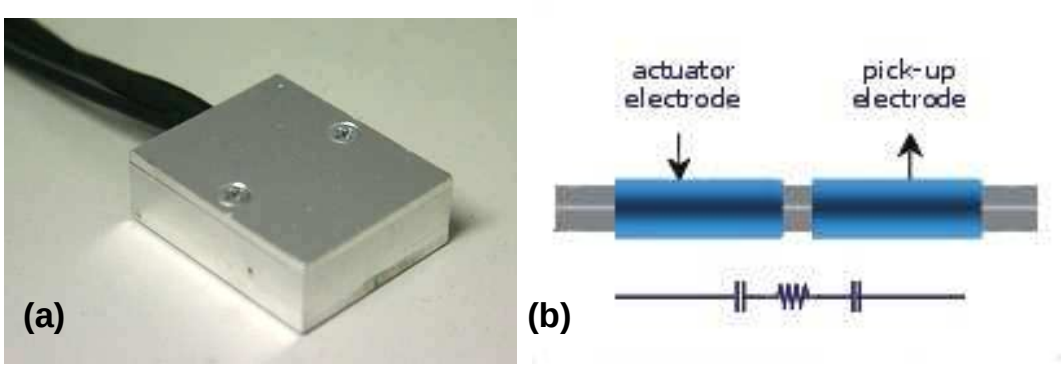

Figure 1.40: *Detector cell (a), schematic of basic C^4D cell (b) [186]. Actuator electrode is also known as the excitation electrode.*

By increasing the cell length, a deviation in the resulting Bode plot was observed. Therefore, the behaviour of the cell can be determined by the cell path length, which lies between the electrodes [177].

Capacitively coupled contactless conductivity detection (C^4D) has been used primarily as a detection method with CE instrumentation [178,179]. In 1998 C^4D was first coupled to a CE system using axial electrodes. The electrodes consisted of two syringe cannulae with a gap of 2 mm between them. The detector was described as a series of two capacitors and two resistors. The liquid between the gap served as an "internal wire" [178]. The C^4D cell has since been used in varying applications such as on-column non-suppressed conductivity detection, as well as profiling capillary columns.

1.19.4. On-column detection using C^4D

Contactless conductivity has been used extensively in the literature as an on-column detector for a number of different analytes in a number of different formats. In 2001, Hilder *et al.* [187] performed the separation of anions on a packed capillary column prepared from Dionex Ionpac® particles (latex agglomerated quaternary ammonium particles) under CEC conditions. In this work they compared the use of UV detection with on-column non-suppressed C^4D. From their separations, C^4D resulted in more sensitive detection compared to indirect UV detection. This was reflected in the limits of detection (LOD) where, for example, for a chloride peak in indirect UV the LOD was 11 μg/L compared to 5 μg/L for C^4D. In contrast Duc Mai *et al.* [188] used an ODS modified silica monolithic column for the separation of organic and inorganic cations, under CEC using C^4D on-column detection. C^4D has also been used in size exclusion electrokinetic chromatography of polystyrene standards [189] and in capillary zone electrophoresis (CZE), as an on-column detector of synthetic pharmaceuticals [190].Vásquez *et al.* [191] have also reported the use of C^4D on micro-fluidic chip platforms, wherein separations of cations (potassium, sodium and lithium) and anions (chloride, nitrate and perchlorate) were performed using electrophoretic methods, incorporating C^4D as an on-chip detector. Examples of on-column C^4D are shown below in Figure 1.41. These examples show the versatility of the C^4D as an on-column sensor.

1.19.5. Scanning C^4D (sC^4D)

The C^4D cell used in a scanning mode can be a useful evaluation technique in determining the longitudinal homogeneity of a capillary containing a coating, or the longitudinal density of a stationary phase (either packed or monolithic). The detector

measures capacitance as a function of voltage, resulting in a location specific current, measured inversely by resistance. The resulting voltage from the detector will be henceforth called detector response (mV). The advantage of using circular electrodes is the ability to move the electrodes along a capillary, facilitating the construction of a profile of detector response versus detector position on-column. This type of column profiling provides a non-invasive and non-destructive method of visualising a column, along the length of a capillary.

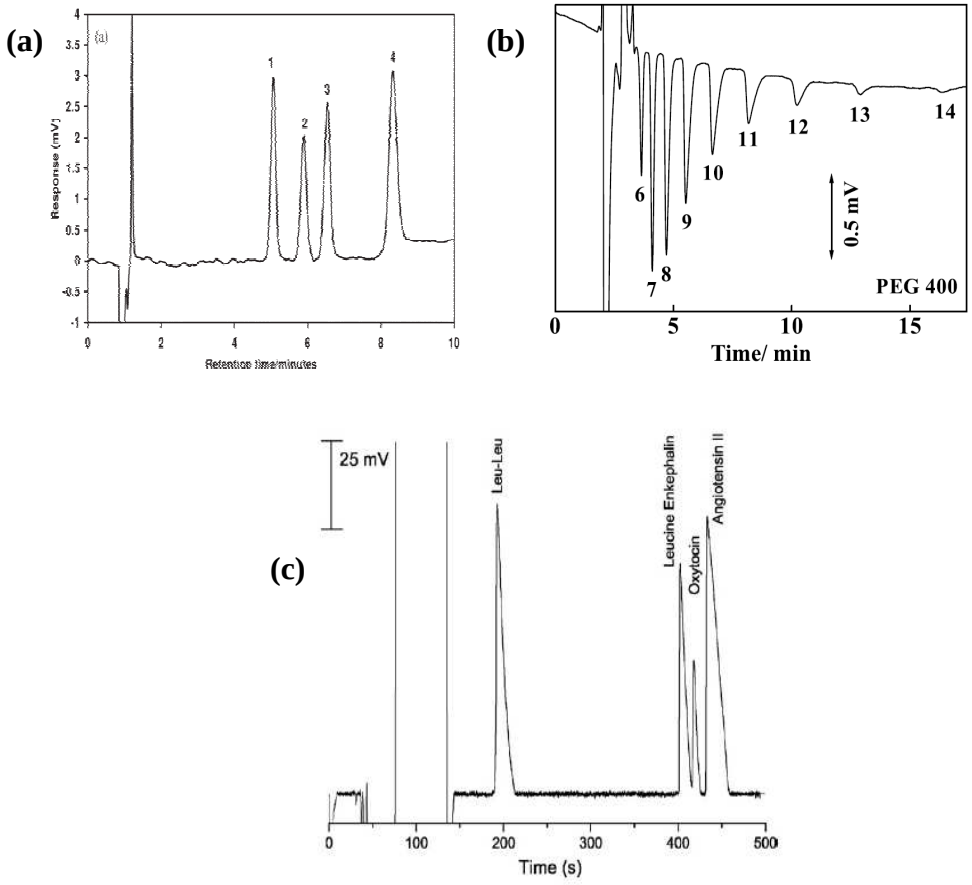

Figure 1.41: *On-column C^4D detection of cations on a surfactant modified silica capillary column, analytes 1-4 are Mg, Ca, Sr, and Ba respectively, in an 0.5 mM ethylenediamine (pH 4.5) eluent [192] (a), separation of polymer oligomers using indirect on-column C^4D with a sodium nitrate and ACN mobile phase [193] (b), separation of peptides using a mobile phase gradient of 0-100 % B in 14 min, mobile phase A 0.15 % acetic acid in deionised water, mobile phase B 0.5 % acetic acid in 24 % ACN, detection with on-column C^4D [194] (c).*

In this procedure a distance reference must be used, and in general, an immobilised ruler is used with 1 mm increment measurements. Figure 1.42

demonstrates the process of scanning C^4D on a capillary column. The detector response is recorded at each data point on the column (e.g. 1 mm, 5 mm etc). For sC^4D measurements, a steady background must be observed. In using a HPLC pump, it is essential that a steady flow is available, and thus used. This will eliminate any pump noise observed from pump stroke action. The pump must also be well primed with solvent, this will ensure no air bubbles are present, which can interfere with detector response.

Alternatively a column can be scanned in the absence of flow, however, the column must be filled with a suitable scanning solution. If an air pocket is present in the column, it can be evident in the resulting profile as a sharp change in detector response, relative to the length of the air pocket. Any contamination caused by the presence of contaminated monomer (i.e. during monolith synthesis), or ions within the column would be detected due to unexpected changes in ionic conductances. Temperature can also cause changes in background detector response, as ionic conductivity is affected by temperature fluctuations. As such, small deviations in detector response can be seen from column to column, with columns of similar dimension.

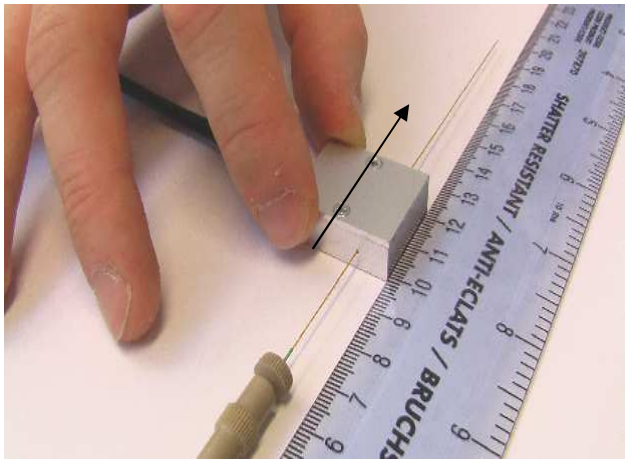

Figure 1.42: *Schematic of scanning C^4D (sC^4D.) Detector cell is moved at mm increments, against a ruler, whilst recording detector response.*

For the application of column profiling, not only is sC^4D useful in determining the distribution of a monolithic stationary phase in a capillary column, but it is also useful in the evaluation of grafting and modification reactions. This versatility of the detector cell has opened new avenues for characterisation for column coatings. The

homogeneity of surfactant coatings was investigated by Gillespie *et al.* [192,195]. Due to the external and non-contact nature of the C^4D detector the effective column length (L_{eff}) could be altered with no destructive effect on the column or the coating, and so, a plot of detector response versus detector position on-column could be generated. Prior to and following a number of coating procedures (DOSS on capillary monolithic silica-C_{18}), the detector response generated by charged groups on the surfactant could be monitored. Following a temporal study with constant water flushing, following an 18 hour window, the detector response of the column (generated by the ionised surfactant), was significantly reduced indicating a reduction in immobilised surfactant across the column over time. In another study, O' Riordáin *et al*. coated a silica based C_{18} column using a N-dodecyl-N,N-(dimethylammonio)undecanoate (DDMAU) surfactant, towards the analysis of anions [63]. Following a study of retention factor, *k*, across the column, deviations in the resulting *k*, led the authors to the conclusion that bleeding of the surfactant from the column over time was evident, which would result in an uneven coating of surfactant over time. This confirms the results observed by Gillespie *et al*. [195]. This inherently affects the resulting retention of analytes on column, and thus will cause a decrease in efficiency. This highlights one of the disadvantages of this method of stationary phase modification.

This type of column profiling may also be used to determine the density of column packing material, or indeed the density of monolithic columns. Connolly *et al.* reported the use of C^4D for the characterisation of a capillary packed column [196]. An increase in stationary phase density (whether packed or monolithic) resulted in a decrease in C^4D signal intensity, as the detector response is directly proportional to the fluid volume between the electrodes [196]. Using this technique, voids in the packing material were identified, which were due to poor packing of the stationary phase. This is shown below in Figure 1.43. This was confirmed by Walsh *et al*., in the investigation of column homogeneity, following the polymerisation of PSDVB monolithic columns using an LED array at a wavelength of 470 nm [120].

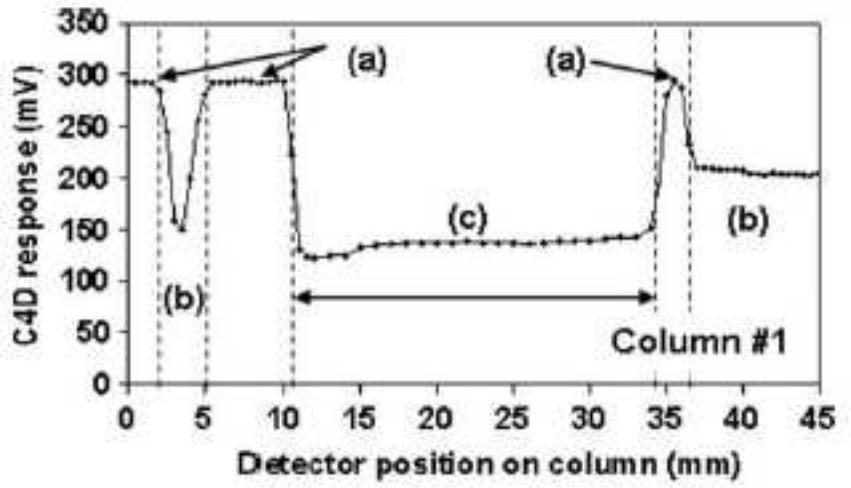

Figure 1.43: *sC^{4}D profile of a capillary column packed with Dionex PAX100 resin. Column void (a), monolithic frit (b), and packed bed of resin (c) [196].*

Connolly *et al*. [197] produced monolith columns expressing zones of charged functional groups, prepared using photo-masking. In one column, zones of AMPS were grafted onto the monolith surface via a single step photo-grafting reaction, to assess the efficiency of the grafting step. Following washing, the column was scanned using a contactless conductivity detector (sC^{4}D), wherein the charge density of the grafted AMPS groups, could be visualised. A profile of detector response at on-column detector positions could be constructed, an example of which is shown in Figure 1.44.

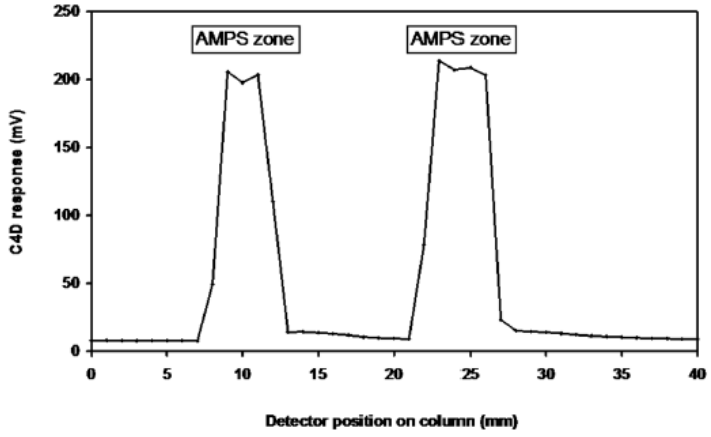

Figure 1.44: *sC^{4}D profile of charged zones of AMPS on a BuMA-co-EDMA monolith. Scan performed at 1 mL/min in deionised water [197].*

Zones of VAL were produced on a BuMA-*co*-EDMA monolithic column, and following covalent immobilisation of green fluorescent protein (GFP), the column profile was again constructed. The resulting profile again showed three distinct zones corresponding to the immobilised protein zones. As GFP is fluorescent, a digital photography image was taken of the column. The three fluorescent zones seen on the column correspond to the three zones of increased charge, seen with sC^4D. This is shown below in Figure 1.45.

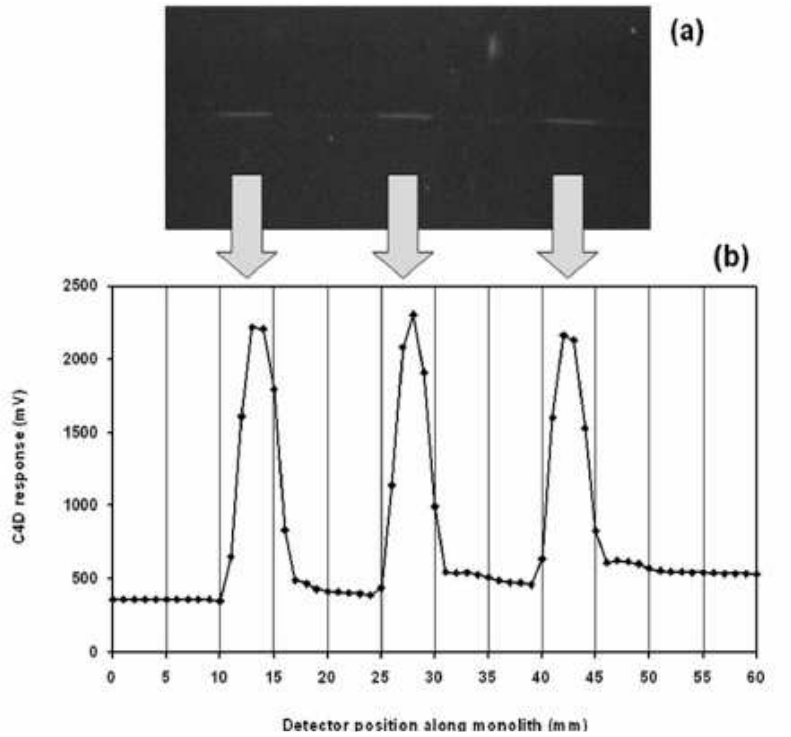

Figure 1.45: *Digital photography image of VAL-GFP zones (a), sC^4D profile of VAL-GFP zones upon a BuMA-co-EDMA monolithic column. Column scanned in water at a flow rate of 1 mL/min (b) [197].*

Photo-masking has been used extensively in the preparation of monolithic columns [73,74,151]. The technique of sC^4D has been used in the understanding of fundamentals of immobilised ligand chemistry [198,199]. For example, Gillespie *et al.* [199] were able to produce zones of amino-carboxylate molecules such as iminodiacetate, upon BuMA-*co*-EDMA monolithic columns. By grafting zones of ligand onto an otherwise neutral monolith (non-charged monomer precursors), the change in detector response of the ligand zone could be determined with respect to the ungrafted monolith sections. By using sC^4D a shift in detector response of the grafted zone was detected using scanning buffers which spanned the pH range of pH 3 to pH

9. By plotting the change on detector response with increasing pH, the authors could visualise the effect of pH on the immobilised ligand. Following identification of the on-column pK_a's of the immobilised ligands, the authors reported that a shift in ligand pK_a's occurred following immobilisation onto the monolith surface.

The detector has also been used for the optimisation of grafting procedures. Gillespie *et al*. [200] prepared BuMA-*co*-EDMA monolithic columns with grafted zones of AMPS. In using C^4D to profile the column, the grafting density and hence ion exchange capacity could be monitored. The group correlated the energy dose used for grafting of zones, with the resulting detector response for the respective zones.

The scanning C^4D method has also been used by Hilder *et al.* [201] to study the reproducibility of monolith formation. The authors fabricated monolithic columns via thermal polymerisation which were subsequently profiled using sC^4D. Columns that exhibited inhomogeneous conductive profiles along the column length, led to poor chromatographic separations, compared to columns exhibiting a flat horizontal type profile. The applications of C^4D are covered in detail in an excellent review [202], published in 2010, in which the characterisation of stationary phase gradients using sC^4D is also mentioned.

This type of detection is not limited to fused silica based capillaries. A form of C^4D can also be used in conjunction with micro-fluidic chips either for the characterisation of columns in micro-fluidic chips, or for separations. An example of the electrode layout is shown in Figure 1.46. In planar models, the electrode position denies the use of a faraday shield. This results in a lower limit of detection. A detailed discussion on cell geometry and electrode placement was provided by Kuban and Hauser [203]. Using the optimised electrode layout (Figure 1.46), Walsh *et al.* [204] packed micro-fluidic channels with a poly(styrene-divinyl benzene) stationary phase, and examined the packed channels using sC^4D profiling for possible applications in quality control of mass produced micro-fluidic chips, with packed stationary phases. In using this method, the packing density of the stationary phase could be ascertained along the column. This method was similarly repeated with monolithic columns fabricated within the channels of micro-fluidic chips. For this experiment the column was filled with deionised water and the ends were sealed to prevent drying of the monolith, providing a steady background detector response.

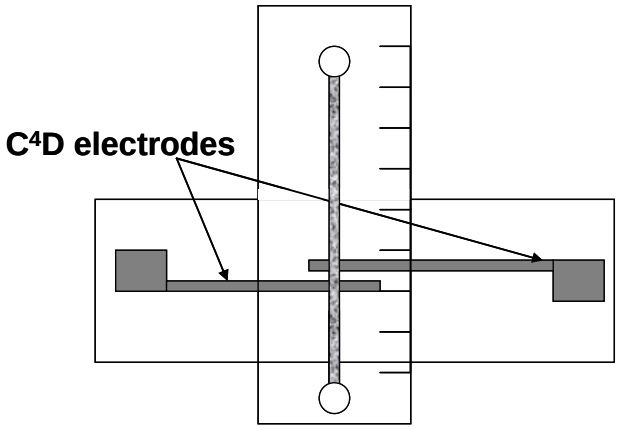

Figure 1.46: *Schematic of C^{4}D for planar measurements adapted from [204].*

Gillespie *et al.* moved one step further with the production of a C^{4}D cell which was not based on capillary format. This new cell had dimensions suitable for columns produced in PEEK tubing of 1.6 mm outer diameter, as shown in Figure 1.47 [205]. The larger tubing format may prove useful in the profiling of silica monolithic columns (1.6 mm outer diameter), which were clad in PEEK following synthesis. Packed columns of these dimensions may also benefit from this novel design of the C^{4}D cell.

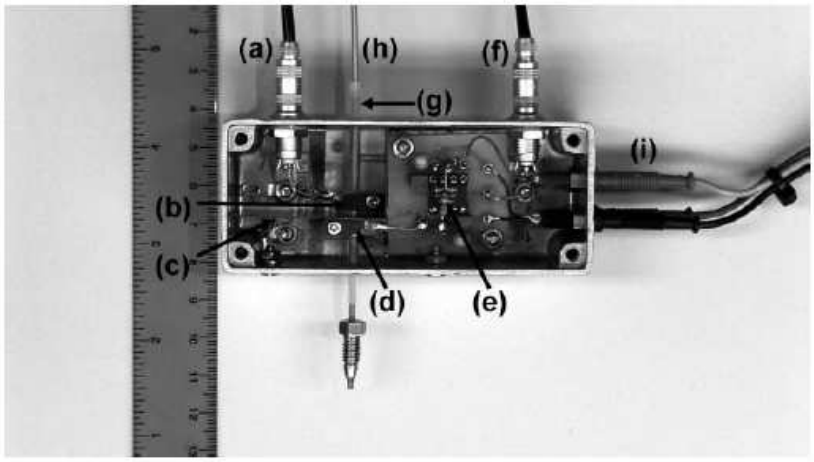

Figure 1.47: *Diagram of a C^{4}D cell suitable for PEEK (1.6 mm o.d.) tubing formats. Components; excitation lead (a), excitation electrode (b), faraday shield (c), pick up electrode (d), feedback resistor (e), signal output lead (f), Teflon sleeve (g), column (h), cell power leads (i) [205].*

The aim of this presented thesis was to demonstrate the versatility of the sC^{4}D profiling technique, in the investigation of emerging and novel monolithic column fabrication techniques. This thesis presents some novel applications of both photo-grafting techniques and characterisation via sC^{4}D profiling. Columns expressing gradients were fabricated with strong cation exchange and affinity/chelating functionalities using both thermal initiation and photo-initiated approaches. In an extension of the photo-grafting techniques developed herein, a nano-agglomerated stationary phase was also produced, which was subsequently followed by a reversed-phase functionality for dual function separations. In all instances of this work, the sC^{4}D method was used to profile columns prior to any grafting or further reaction, to investigate the distribution of the graft or chemical modification. Further reaction of grafted groups was required in some instances in order to produce a column of specific functionality, or to increase the detector response along the column. In the case of co-polymerised columns, wherein a charged functional group was added to the monolithic matrix, no blank could be prepared and thus profiled. The benefits of using such a visualisation method are the non-destruction of the monolith, and no fouling of electrodes due to the non-contact nature of the cell. The distribution of grafts could be directly measured non-invasively and non-destructively.

In addition to the development experiments in this thesis, the detector (C^{4}D) was also used in stationary mode to produce chromatograms in on-column non-suppressed conductivity detection. Due to the variable position nature of the C^{4}D cell, the effective column length could be varied, having no effect upon the on-going separation, and without the need for cutting the column.

1.20. References

[1] Wang, X., Svec, F., Fréchet, J., *Anal. Chem*., 65, 1993, 2253.

[2] Svec, F., Fréchet, J., *J. Mol. Rec*., 9, 1999, 326.

[3] Peters, E., Petro, M., Svec, F., Fréchet, J., *Anal. Chem*., 69, 1997, 3646.

[4] Nakanishi, K., Minakuchi, H., Soga, N., Tanaka, N., *Journal of Sol-Gel and Science Technology*, 8, 1997, 547.

[5] Gibson, G., Mugo, S., Oleschuk, R., *Polymer*, 49, 2008, 3084

[6] Peters, E., Svec, F., Fréchet, J., *Adv. Mater*., 11, 1999, 1169.

[7] Eeltink, S. Decrop, W., Rozing, G., Schoenmakers, P., Kok, W., *J. Sep. Sci*., 27, 2004, 1431.

[8] Xu, Y., Cao, Q., Svec, F., Fréchet, J., *Anal. Chem*., 82, 2010, 3352.

[9] Yu, C., Xu, M., Svec, F., Fréchet, J., *J. Polym. Sci. Part A, Polym. Chem*., 40, 2002, 755.

[10] Ueki, Y., Umemura, T., Li, J., Odake, T., Tsunoda, K., *Anal. Chem*., 76, 2004, 7007.

[11] Rohr, T., Hilder, E., Donovan, J., Svec, F., Fréchet, J., *Macromolecules*, 36, 2003, 1677.

[12] Peterson, D., Rohr, T., Svec, F., Fréchet, J., *Anal. Chem*., 75, 2003, 5328.

[13] Štrancar, A., Koselj, P., Schwinn, H., Josic, D., *Anal. Chem*., 68, 1996, 3843.

[14] Podgornik, A., Barut, M., Jančar, J., Štrancar, A., *J. Chromatogr. A*, 848, 1999, 51.

[15] Peters, E., Petro, M., Svec, F., Fréchet, J., *Anal. Chem*., 70, 1998, 2288.

[16] Moore, R., Licklider, L, Schumann, D., Lee, T., *Anal. Chem*., 70, 1998, 4879.

[17] Xie, S., Allington, R., Svec, F., Fréchet, J. *J. Chromatogr. A*, 865, 1999, 169.

[18] Jančo, M., Xie, S., Peterson, D., Allington, R., Svec, F., Fréchet, J., *J. Sep. Sci.*, 25, 2002, 909.

[19] Rohr, T., Yu, C., Davey, M., Svec, F., Fréchet, J., *Electrophoresis*, 22, 2001, 3959.

[20] Yu, C., Davey, M., Svec, F., Fréchet, J., *Anal. Chem*., 73, 2001, 5088.

[21] Pflegerl, K., Podgornik, A., Berger, E., Jungbauer, A., *Biotech. Bioeng*., 79, 2002, 733.

[22] Galaev, I., Dainiak, M., Plieva, F., Hatti-Kaul, R., Mattiasson, B., *J. Chromatogr. A*, 1065, 2005, 169.

[23] Miyazaki, S., Morisato, K., Ishizuka, N., Minakuchi, H., Shintani, Y., Furuno, M., Nakanichi, K., *J. Chromator. A*, 1043, 2004, 19.

[24] Ota, S., Miyazaki, S., Matsuoka, H., Morisato, K., Shintani, Y., Nakanishi, K., *J. Biochem. Biophys. Methods*, 70, 2007, 57.

[25] Altun, Z., Hjelmström, A., Abdel-Rehim, M., Blomberg, L., *J. Sep. Sci*., 30, 2007, 1964.

[26] Altun, Z., Skoglund, C., Abdel-Rehim, M., *J. Chromatogr. A*, 1217, 2010, 2581.

[27] Altun, Z., Blomberg, L., Jagerdeo, E., Abdel-Rehim, M., *Journal of Liquid Chromatography and Related Techniques*, 29, 2006, 829.

[28] Rahmi, D., Takasaki, Y., Zhu, Y., Kobayashi, H., Konagaya, S., Haraguchi, H., Umemura T., *Talanta*, 81, 2010, 1438.

[29] Svec, F., Fréchet, J., *Science*, 273, 205, 1996.

[30] Svec, F., Fréchet, J., *Ind. Eng. Chem Res*., 38, 1999, 34.

[31] Svec, F., *J. Sep. Sci*., 27, 2004, 747.

[32] Svec, F., *J. Chromatogr. A*, 1217, 2010, 902.

[33] Vlakh, E.G., Tennikova, T.B., *J. Sep. Sci*., 30, 2007, 2801.

[34] Svec, F., *J. Sep. Sci*., 27, 2004, 1419.

[35] Smith, N., Jiang, Z., *J. Chromatogr. A*, 1184, 2008, 416.

[36] Saito, Y., Jinno, K., Greibrokk, T., *J. Sep. Sci*., 27, 2004, 1379.

[37] Guichon, G., *J. Chromatogr. A*, 1168, 2007, 101.

[38] Mallik, R., Hage, D., *J. Sep. Sci*., 29, 2006, 1686.

[39] Viklund, C., Svec, F., Fréchet, J., *Chem. Mater*., 8, 1996, 744.

[40] Urban, J., Svec, F., Fréchet, J., *Anal. Chem*., 82, 2010, 1621.

[41] Schaller, D., Hilder, E., Haddad, P., *J. Sep. Sci*., 29, 2006, 1705.

[42] Chambers, S., Glenn, K., Lucy, C., *J. Sep. Sci*., 30, 207, 1628.

[43] Nordberg, A., Hilder, E., *Anal. Bioanal. Chem*., 394, 2009, 71.

[44] Svec, F., *Electrophoresis*, 27, 2006, 947.

[45] Svec, F., *J. Chromatogr. B*, 841, 2006, 52.

[46] Svec, F., Kurganov, A., *J. Chromatogr. A*, 1184, 2008, 281.

[47] Krenkova, J., Svec, F., *J. Sep. Sci*., 32, 2009, 706.

[48] Potter, O., Hilder, E., *J. Sep. Sci*., 31, 2008, 1881.

[49] Blomberg, L., *Anal. Bioanal. Chem*., 393, 2009, 797.

[50] Tennikova, T., Frietag, R., *J. High Resol. Chromatogr*., 23, 2000, 27.

[51] Barut, M., Podgornik, A., Brne, P., Štrancar, A., *J. Sep. Sci*., 28, 2005, 1876.

[52] Peterson, D., *Lab Chip*, 5, 2005, 132.

[53] Vázquez, M., Paull, B., *Anal. Chim. Acta*., 668, 2010, 100.

[54] Siouffi, A., Ziarelli, F., Caldarelli, S., *J. Chromatogr. A*, 1109, 2006, 26.

[55] Rieux, L., Niederlander, H., Verpoorte, E., Bischoff, R., *J. Sep. Sci*., 28, 2005, 1628.

[56] Svec, F., Tennikova, T., Deyl, Z., *Journal of Chromatography Library, Monolithic Materials*, Vol. 67, First edition, 2003.

[57] Chen, M., Zheng, M., Feng, Y., *J. Chromatogr. A*, 1217, 2010, 3457.

[58] Koboyasi , Y., Okamoto M., Tomita, A., *J. Mat. Sci*., 31, 1996, 6125.

[59] Shi, Z., Feng, Y., Xu, L., Zhang, M., Da, S., *Talanta*, 63, 2004, 593.

[60] Hou, C., Ma, J., Tao, D., Shan, Y., Liang, Z., Zhang, L., Zhang, Y., *Journal of Proteome Research*, 9, 2010, 4093.

[61] Gunji, t., Ozawa, M., Abe, Y., West, R., *Journal of Sol Gel Science and Technology*, 22, 2001, 219.

[62] Nesterenko, E., Guivarc'h, C., Duffy, C., Paull, B., *J. Sep. Sci*., 30, 2007, 2910.

[63] O' Riordáin, C., Gillespie, E., Connolly, D., Nesterenko, P., Paull, B., *J. Chromatogr. A*, 1142, 2007, 185.

[64] Greiderer, A., Ligon, S., Huck, C., Bonn, G., *J. Sep. Sci.*, 32, 2009, 2510.

[65] Sugrue, E., Nesterenko, P., Paull, B., *Analyst*, 128, 2003, 417.

[66] Zajickova, Z, Luna, J., Svec, F., *Journal of Chromatography and Related Technologies*, 33, 2010, 1640.

[67] Wang, P., *Monolithic Chromatography and its Modern Applications*, 2010.

[68] Minakuchi, H., Nakanishi, K., Soga, N., Ishizuka, N., Tanaka, N., *Anal. Chem*., 68, 1996, 3498.

[69] Preinerstofer, B., Hoffman, C., Ludba, D., Lammerhofer, M., Lidner, W., *Electrophoresis*, 2008, 29, 1626.

[70] http://www.phenomenex.com/Products/HPLCDetail/Onyx/Monolithic% 20C18?returnURL=/Products/Search/HPLC (accessed 09th Jan 2012).

[71] http://www.merck-chemicals.com/chromolith-hplc-columns/c_oUeb. s1LrkgAAAEWq.AfVhTl?back=true (accessed 09th Jan 2012)

[72] http://www.glsciences.com/products/monolithic_products/dna_and_peptide_ tools.html (accessed 09th Jan 2012)

[73] Stachowiak, T., Svec, F., Frechet, J., *Chem. Mater*., 18, 2006, 5950.

[74] Logan, T., Clark, D., Stachowiak, T., Svec, F., Frechét, J., *Anal. Chem.*, 79, 2007, 6592.

[75] Potter, O., Breadmore, M., Hilder, E., *Analyst*, 131, 2006, 1094.

[76] Hilder, E., Svec, F.,. Fréchet J., *J. Chromatogr., A*, 1053, 2004, 101.

[77] Urban, J., Svec, F., Fréchet, J., *J. Chromatogr. A*, 1217, 2010, 8212.

[78] Nicholson, J., *The Chemistry of Polymers*, Second Edition, RSC publications, 1997.

[79] Fouassier, J.P., *Kluwer Academic Publishers*, Radiation Curing in Polymer Science and Technology, Volume 3, 1993.

[80] . Bernabé -Zafón, V., Cantó -Mirapeix, A., Simó –Alfonso, E., Ramis-Ramos, G., Herrero Martínez, J., *Electrophoresis* 30, 2009, 1929

[81] Vicklund, C., Pontén, E., Glad, B., Irgum, K., Svec, F., *Chem. Mater*, 9, 1997, 463.

[82] Carbonnier, B., Guerrouache, M., Denoyel, R., Millot, M., *J. Sep. Sci*., 30, 2007, 3000.

[83] Connolly, D., Twamley, B., Paull, B., *Chem. Comm*., 46, 2010, 2109.

[84] Li, Y., Tolley, H., Lee, M., *J. Chromatogr. A*, 1218, 2011, 1399.

[85] Gillespie, E., Connolly, D., Paull, B., *Analyst*, 134, 2009, 1314.

[86] Krenkova, J., Lacher, N., Svec, F., *Anal. Chem*., 81, 2009, 2004.

[87] Buszewski, B., Szumski, M., *Chromatographia*, 60, 2004, S261.

[88] Gu, C., He, J., Jia, J., Fang, N., Shamsi, S., *Electrophoresis*, 30, 2009, 3814.

[89] Eeltink, S., Geiser, L., Svec, F., Fréchet, J., *J. Sep. Sci*., 30, 2007, 2814.

[90] Hoegger, D., Frietag, R., *J. Chromatogr. A*, 914, 2001, 211.

[91] Lammerhofer, M., Peters, E., Yu, C., Svec, F., Fréchet, J., *Anal. Chem*., 72, 2000, 4614.

[92] Danquah, M., Forde, G., *Chemical Engineering Journal*, 140, 2008, 593.

[93] Cooper, A., *J. Mater. Chem*., 10, 2000, 207.

[94] Cooper, A., Holmes, A., *Adv. Mater*., 11, 1999, 1270.

[95] Aoki, H., Kubo, T., Ikegami, T., Tanka, T., Hosoya, K., Tokuda, D., Ishizuka, N., *J. Chromatogr. A*, 1119, 2006, 66.

[96] Liu, M., Liu, H., Liu, Y., Bai, L., Yang, G., Yang, C., Cheng, J., *J. Chromatogr. A*, 1218, 2011, 286.

[97] Kubo, T., Watanabe, F., Kimura, N., Kaya, K., Hosoya, K., *Chromatographia*, 70, 2009, 527.

[98] Fintschenko, Y., Choi, W., Ngola, S., Shepodd, T., *Fresenius J. Anal. Chem*., 371, 2001, 174.

[99] Bedair, M., Rassi, Z., *Electrophoresis*, 23, 2002, 2938.

[100] Merhar, M., Podgornik, A., Barut, M., Zigon, M., Strancar, A., *J. Sep. Sci.*, 26, 2003, 322.

[101] Viklund, C., Svec, F., Fréchet, J., Irgum, K., *Biotechnol. Prog*., 13, 1997, 597.

[102] Xie, S., Svec, F., Fréchet, J., *J. Polym. Sci. Part A: Polym. Chem*., 35, 1997, 1013.

[103] Stulik, K., Pacáková, V., Suchánková, J., Coufal, P., *J. Chromatog. B*, 841, 2006, 79.

[104] Yu, C., Svec, F., Frechét, J., *Electrophoresis*, 21, 2000, 120.

[105] Hutchinson, J., Hilder, E., Shellie, R., Smith, J., Haddad, P., *Analyst*, 2006, 131, 215.

[106] Santora, B., Gagne, M., Moloy, K., Radu, N., *Macromolecules*, 34, 2001, 658.

[107] Smigol, V., Svec, F., *Journal of Applied Polymer Science*, 46, 1992, 1439.

[108] Beiler, B., Vincze, Á., Svec, F., Sáfrány, Á., *Polymer*, 48, 2007, 3033.

[109] Meyer, U., Svec, F., Fréchet, J., Hawker, C., Igrum, K., *Macromolecules*, 33, 2000, 7769.

[110] Georger, M., Veregin, R., Kazmaeir, P., Hamer, G., *Macromolecules*, 26, 1993, 2987.

[111] Buchmeiser, M., Sinner, F., Mupa, M., Wurst, K., *Macromolecules*, 33, 2000, 32.

[112] Sinner, F., Buchmeiser, M., *Macromolecules*, 33, 2000, 5777.

[113] Kanamori, K., Hasegawa, J., Nakanishi, K., Hanada, T., *Macromolecules*, 41, 2008, 7186.

[114] Limé, F., Igrum, K., *J. Polym. Sci.: Part A, Polym. Chem*., 47, 2009, 1259.

[115] Liu, H., Zhuang, X., Turson, M., Zhang, M., Dong, X., *J. Sep. Sci*., 31, 2008, 1694.

[116] Viklund, C., Nordström, A., Igrum, K., *Macromolecules*, 34, 2001, 4361.

[117] Svec, F., Fréchet, J., *Anal. Chem.*, 64, 1992, 820.

[118] Geiser, L., Eeltink, S., Svec, F., Fréchet, J., *J. Chromatogr. A*, 1140, 2007, 140.

[119] Han, B., Wang, P., Zhu, G., Zhang, L., Qu, F., Deng, Y., Zhang, Y., *J. Sep. Sci*., 32, 2009, 1211.

[120] Walsh, Z., Levkin, P., Jain, V., Paull, B., Svec, F., Macka, M., *J. Sep. Sci*., 33, 2010, 61.

[121] http://www.dionex.com/en-us/products/columns/lp-81265.html

(accessed 09th Jan 2012).

[122] http://www.biaseparations.com/sp/210/products, (accessed 09 Jan 2012).

[123] Hutchinson, J., Zakaria, P., Bowie, A., Macka, M., Avdalovic, N., Haddad, P., *Anal. Chem.*, 77, 2005, 407.

[124] Connolly, D., Paull, B., *J. Chromatogr. A*., 917, 2001, 353.

[125] Connolly, D., Paull, B., *Anal. Chim. Acta.*, 441, 2001, 53.

[126] Connolly, D., Paull, B., *J. Chromatogr. A*, 953, 2002, 299.

[127] Hatsis, P., Lucy, C., *Anal. Chem*., 75, 2003, 995.

[128] Connolly, D., Victory, D., Paull, B., *J. Sep. Sci*., 27, 2004, 912.

[129] Wieder, W., Bisjack, C, Huck, C, Bakry, R., Bonn, G., *J. Sep. Sci*., 29, 2006, 2478.

[130] Plieva, F., Bober, B., Dainiak, M., Galaev, I., Mattiasson, B., *J. Mol. Recognit.*, 19, 2006, 305.

[131] Lou, Q., Zou, H., Xiao, X., Gou, Z., Kong, L., Mao, X., *J. Chromatogr. A*, 926, 2001, 255.

[132] Bisjak, C., Bakry, R., Huck, C., Bonn, G., *Chromatographia*, 2005, 62, S31.

[133] Guerrouache, M., Millot, M., Carbonnier, B., *Macromol. Rapid. Commun*., 30, 2009, 109.

[134] Rohr, T., Ogletree, D., Svec, F., Fréchet, J., *Adv. Funct. Mater*.,13, 2003, 264.

[135] Pucci, V., Raggi, M.A., Svec, F., Fréchet, J., *J. Sep. Sci*., 27, 2004, 779.

[136] Stachowiak, T., Mair, D., Holden, T., Lee, J., Svec, F., Fréchet, J., *J. Sep. Sci*., 30, 2007, 1088.

[137] Eeltink, S., Hilder, E., Geiser, L., Svec, F., Fréchet, J., Rozing, G., Schoenmakers, P., Kok, W., *J. Sep. Sci*., 30, 2007, 407.

[138] Yang, W., Rånby, B., *Journal of Applied Polymer Science*, 62, 1996, 533.

[139] Yang, W., Rånby, B., *Journal of Applied Polymer Science*, 62, 1996, 545.

[140] Rånby, B., *Polym. Eng. Sci*., 38, 1998, 1229.

[141] Rånby, B., *Int. J. Adh. Adh*., 19, 1999, 337.

[142] Rånby, B., Yang, W., Tretinnikov, O., *Nucl. Instr. And Meth. In Phys. Res. B*, 151, 1999, 301.

[143] Sigma Aldrich, al_pp_spectra.pdf (accessed April 2011).

[144] Rånby, B., *Mat. Res. Innovat*., 2, 1998, 64.

[145] Yang, W., Rånby, B., *Journal of Applied Polymer Science*, 62, 1996, 545.

[146] Yang, W., Rånby, B., *Eurpoean Polymer Journal*, 35, 1999, 1557.

[147] Brennan, R., Yin, H., Kllleen., K., *Anal. Chem*., 79, 2007, 9302.

[148] http://www.dionex.com/en-us/products/liquid-chromatography/lp-71340.html (access 20 Jan 2012).

[149] http://www.waters.com/waters/nav.htm?cid=514210&locale=en_US (access 20 Jan 2012).

[150] http://www.thermoscientific.com/ecomm/servlet/productsdetail _11152_L10416_80573_13901133_-1 (access 20 Jan 2012).

[151] Sreedhara B., Seidel-Morgenstern, A., *J. Chromatogr. A*, 1215, 2008, 133.

[152] Chen, K., Lynen, F., De Beer, M., itzel, L., Ferguson, P., Hanna-Brown, M., Sandra, P., *J. Chromatogr. A*, 1217, 2010, 7222.

[153] Nyiredy, S., Szűcs, Z., Szepesy, L., *J. Chromatogr. A*, 1157, 2007, 122.

[154] Nyiredy, S., Szűcs, Z., Szepesy, L, *Chromatographia*, 63, 2006, S3.

[155] Link, A., Eng, J., Schieltz, D., Carmack, E., Mize, G., Morris, D., Garvik, B., Yates, J., *Nat. Biotechnol*., 17, 1999, 676.

[156] Washburn, M., Wolters, D., Yates, J., *Nat. Biotechnol.*, 19, 2001, 242.

[157] Wolters, D., Washburn, M., Yates, J., *Anal. Chem.*, 73, 2001, 5683.

[158] Maruška, A., Rocco, A, Kornysova, O., Fanali, S., *J. Biochem, Biophys. Methods*, 70, 2007, 47.

[159] Urbanova, I., Svec, F., *J. Sep. Sci*., 34, 2011, 2345.

[160] http://www.thorlabs.com/NewGroupPage9.cfm?ObjectGroup_ID=1623 (access 03 March 2012)

[161] Deyl, Z., *Journal of Chromatography Library*, Volume 18, Electrophoresis.

[162] Yang, C., Zhu, G., Zhang, L., Zhang, W., Zhang, Y., *Electrophoresis*, 25, 2004, 1729

[163] Zhu, G., Yuan, H., Zhao, P., Zhang, L, Liang, Z., Zhang, W., Zhang, Y., *Electrophoresis*, 27, 2006, 3578.

[164] Liang, Y., Cong, Y., Liang, Z., Zhang, L., Zhang, Y., *Electrophoersis*, 30, 2009, 4034.

[165] Liang, Y., Zhu, G., Wang, T., Zhang, X., Liang, Z., Zhang, L., Zhang, Y., *Electrophoresis*, 32, 2011, 2911.

[166] Altun, Z., Hjelmstrom, A., Abdel-Rehim, M., Blomberg, L., *J. Sep. Sci*., 30, 2007, 1964.

[167] Kubo, T., Kimura, N., Hosoya, K., Kaya, K., *Journal of Polymer Science Part A: Polym. Chem.*, 45, 2007, 3811.

[168] Ma, X., Sun, H., Yu, P., *J. Mater. Sci.*, 43, 2008, 887.

[169] Urban, J., Eeltink, S., Jandera, P., Schoenmakers, P., *J. Chromatogr. A*, 1182, 2008, 161.

[170] Urban J., Jandera, P., Schoenmakers, P., *J. Chromatogr. A*, 1150, 2007, 279.

[171] Bechtle, M., Butté, A., Storti, G., Morbidelli, M., *J. Chromatogr. A*, 1217, 2101, 4675.

[172] Eltmimi, A., Baron, L., Rafferty, A., Hanrahan, J., Fedyanina, O., Nesterenko, E., Nesterenko, P., Paull, B., *J. Sep. Sci.*, 33, 2010, 1231.

[173] Xu, Y., Cao, Q., Svec, F., Fréchet, J., *Anal. Chem.*, 82, 2010, 3352.

[174] Zhou, W., Wang, Z., *Scanning Microscopy for Nanotechnology*, 2007, Springer.

[175] Krenkova, J., Lacher, N., Svec, F., *Anal. Chem.*, 82, 2010, 8335.

[176] Gates, E., Introduction to Electronics, 6th Edition, 2012.

[177] Kuban, P., Hauser, P., *Electrophoresis*, 25, 2004, 3387.

[178] Zeeman, A., *Electrophoresis*, 24, 2003, 2125.

[179] Da Silva, J., do Lago, C., *Anal. Chem.*, 70, 1998, 4339.

[180] Mayrhofer, K., Zeeman, A., Schnell, E., Bonn, G., *Anal. Chem.*, 71, 1999, 3828.

[181] Kuban, P., Hauser, P., *Electrophoresis*, 25, 2004, 3398.

[182] Kuban, P., Hauser, P., *Electrophoresis*, 30, 2009, 176.

[183] Zeeman, A., Schnell, E., Vlogger, D., Bonn, G., *Anal. Chem*. 70, 1998, 563.

[184] Kuban, P., Hauser, P., *Electrophoresis*, 30, 2009, 3305.

[185] Kuban, P., Hauser, P., *Electroanalysis*, 18, 2006, 1289.

[186] http://www.istech.at/product.htm (access 08 November 2011).

[187] Hilder, E., Zeeman, A., Macka, M., Haddad, P., *Electrophoresis*, 22, 2001, 1273.

[188] Duc Mai, T., Viet Pham, H., Hauser, P., *Anal. Chim Acta*., 653, 2009, 228.

[189] Oudhoff, K., Macka, M., Haddad, P., Shoenmakers, P., Kok, W., *J. Chromatogr. A.*, 1068, 2005, 183.

[190] De Carvalho, L., M., Martini, M., Moreira, A., Garcia, S., Nascimento, P., Bohrer, D., *Microchemical journal*, 9, 2010, 114.

[191] Vasquez, M., Frankenfeld, C., Coltro, W., Carrilho, E., Diamond, D., Lunte, S., *Analyst*, 135, 2010, 96.

[192] Gillespie, E., Connolly, D., Macka, M., Nesterenko, P., Paull, B., *Analyst*, 132, 2007, 1238.

[193] Takeuchi, T., Sedyohutomo, A., Lim, L., *Anal. Sci*., 25, 2009, 851.

[194] Kuban, P., Hauser, P., *J. Chromatogr*. A., 1176, 2007, 185.

[195] Gillespie, E., Macka, M., Connolly, D., Paull, B., *Analyst*, 131, 2006, 886.

[196] Connolly, D., Barron, L., Gllespie, E., Paull, B., *Chromatographia*, 70, 2009, 915.

[197] Connolly, D., O' Shea, V., Clark, P., O' Connor, B., Paull, B., *J. Sep. Sci*., 30, 2007, 3060.

[198] Gillespie, E., Connolly, D., Nesterenko, P., Paull, B., *Analyst*, 131, 2008, 874.

[199] Gillespie, E., Connolly, D., Nesterenko, P., Paull, B., *J. Sep. Sci*., 32, 2009, 2659.

[200] Gillespie, E., Connolly, D., Paull, B., *Analyst*, 134, 2009, 1314.

[201] Hilder, E., Schaller, D., Evenhuis, C., Nesterenko, P., Haddad, P., *21st International Ion Chromatography Symposium 2009*.

[202] Connolly, D., Floris, P., Paull, B., Nesterenko, P., *Trends in Analaytical Chemistry*, 29, 2010, 870.

[203] Kuban, P., Hauser, P. *Lab Chip*, 5, 2005, 407.

[204] Walsh, Z., Vasquez, M., Benito-Lopez, F., Paull, B., Svec, F., Diamond, D., *Lab Chip*, 10, 2010 1777.

[205] Gillespie, E., Connolly, D., Hauser, P., Paull, B., *Analyst*, 133, 2008, 1104.

Chapter 2.0

Fabrication and characterisation of capillary housed polymeric monoliths incorporating continuous stationary phase gradients.

“The most exciting phrase to hear in science, the one that heralds the most discoveries, is not "Eureka!”, but "That's funny..."

Isaac Asimov

2.1. Introduction

The formation of stationary phase gradients has been reported in the literature for both photo-initiation [1], and thermal polymerisation texhniques [2]. Gradient elution is a known method in chromatographic separations, in which a change in mobile phase content is introduced over time in the chromatographic separation. This technique can result in advantages such as decreased band widths, an increase in peak capacity, and a decrease in chromatographic run time. As mentioned in Chapter 1, Section 1.13, there are some disadvantages associated with gradient elution, such as the difficulty in method transfer from one HPLC instrument to another. Commercially available gradient pumps can be sophisticated and costly. In nano-fluidic devices the generation of a mobile phase gradient is technically difficult due to variations in temperature and solvent compressibility [3], and so, using a gradient localised to the stationary phase offers an alternative approach to current traditional liquid chromatographic techniques. Such a separation column may allow the further study of peak focussing and zone isolation under isocratic mobile phase conditions. Thus producing gradients localised to a stationary phase rule out the need for sophisticated pumps.

Polymer monolithic columns can be modified easily using thermal or photo-initiated modifications. Stationary phase gradients have been developed primarily in polymer monolithic columns, due to the ease of preparation and stationary phase modification. To determine the success of photo-grafting, Rohr *et al.* [4], prepared two monolithic columns with zones of photo-grafted vinyl azlactone to which a fluorescent molecule (rhodamine 6G) was immobilised. Zones irradiated for 1 min exhibited lower fluorescence intensity when compared to columns irradiated for 3 mins. The exposure of the column to UV energy over longer periods or time resulted in a higher graft density. Using this information, Pucci *et al.* [1] reported a gradient of 2-acrylamido-2-methyl-1-propanesulphonic acid (AMPS), produced through photo-grafting methods. Using methacrylate based monolithic columns, a gradient of a sulphonated monomer (AMPS) was produced using a neutral density gradient filter and, alternatively, a moving shutter of a polymer film. By changing the intensity of UV energy applied to the column, gradually, an increase in graft density was achieved, resulting in a gradient of grafted charged groups. The group also used a

moving shutter, where the shutter exposed more of the column over time, resulting in sections of the column with increasing UV irradiation, thus resulting in a gradient of grafted groups. The gradient was validated using electron probe microscopy, with the results shown in Figure 2.1. However, this method required the total destruction of the monolithic column for analysis.

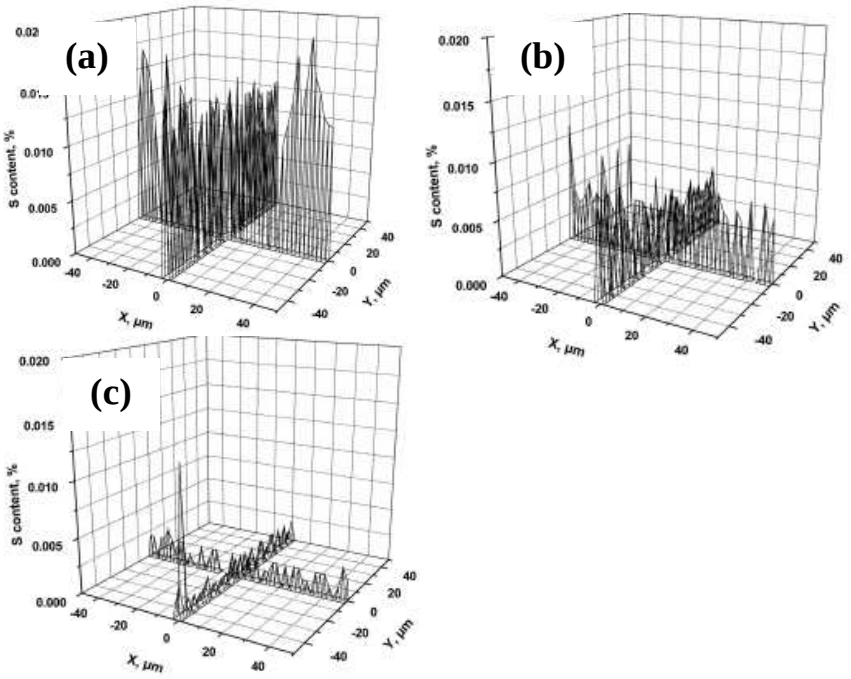

Figure 2.1*: Sulphur content for a BuMA-*co*-EDMA monolith grafted with AMPS. Samples taken at 1 cm (a), 5 cm (b), and 9 cm (c) of the stepped gradient filter. This Figure illustrates a change in sulphur concentration along the column, but is not conclusive of a linear gradient as it is not representative of the column as a whole. Adapted from [1].*

In a similar report, Maruška *et al.* [2] used co-polymerisation to produce a gradient of varying hydrophobic monomer content, along the length of a number of capillary columns. In the report, the columns produced for capillary LC did not contain a constant monomer concentration, which would result in an inhomogeneous monolithic structure. The density of polymer throughout the column was not examined, and so, the resulting chromatograms may not be solely due to the performance of the stationary phase gradient.

Characterisation techniques, such as scanning electron microscopy (SEM), and separation techniques do not illustrate the homogeneity of the monolith bed. Characterisation technique of SEM requires the destruction of the column where

sections of the monolith are cut to the desired length, with the resulting image examined to a depth of ~ 2μm. A large proportion of the monolith would therefore not be fully characterised, and so, stationary phase voids or sections of increased polymer density may not be discovered. Only with luck, in providing cross sections of the monolith for SEM analysis would a void in the separation bed be evident. In the following Chapter, the utility and advantage of column profiling using sC^4D is demonstrated, using both thermal initiated polymerisation and photo-grafting processes.

In this work, the use of scanning capacitively coupled contactless conductivity detection (sC^4D) is shown for the first time, as a tool for the characterisation of charged stationary phase gradients. Polymeric monoliths in capillary format have been fabricated incorporating a gradient of charged functional groups along their length. A photo-grafted gradient of poly(2-acrylamido-2-methyl-1-propanesulphonic acid) (AMPS) was produced using a commercially available optical filter, suited to absorption in the deep UV range (190-400 nm). Alternatively, a gradient was produced by filling a capillary with segmented plugs of monomer mixtures, each containing incrementally higher concentrations of functional monomer, with subsequent thermal polymerisation. This "co-polymerisation" method was also applied to the fabrication of a stationary phase gradient incorporating the chelating ligand and ion exchange group, iminodiacetic acid (IDA). The utility of sC^4D as a rapid and non-invasive tool for the assessment of the slope of various gradient configurations was demonstrated. Due to the complexing nature of the IDA ligand, the detector response was measured prior to and following complexation with Cu^{2+} ions, via a reduction in detector response. The effect of change in co-monomer conditions during fabrication was also studied. Following the production of the gradient column, retention studies were performed using the transition metal zinc. Finally, the morphology of the co-polymerised columns was analysed using scanning electron microscopy (SEM).

2.2. Experimental

2.2.1. Instrumentation

Thermally initiated monoliths were prepared using a GFL water bath (MSC Medical Supply, Dublin, Ireland). Photo-polymerisation of monoliths and all photo-

grafting steps were performed in a Spectrolinker Crosslinker Model XL1000 (Spectronics, Westbury, NY, USA). For photo-grafting studies, a neutral density filter (optical density from 0.04 to 4.0) was supplied by Edmund Optics (Edmund Optics, Barrington, NJ, USA). The balance used was a Sartorius Extend (Sartorius, Goettingen, Germany). The pH meter used was an Orion 2-Star pH meter (Thermo Orion, Beverly, MA, USA). A Harvard Apparatus PHD 2000 syringe pump (Harvard Apparatus, Holliston, MA, USA) was used to introduce monomer solutions into the pre-formed monoliths for photo-grafting. In all other instances, a Knauer Smartline 100 V 5010 pump (Knauer, Berlin, Germany) was used to pump through monoliths at flow rates ranging from 1 to 5 µL/min. For chromatographic separations, a Dionex Ultimate 3000 HPLC system was used, which contained a split flow cartridge with a split ratio of 101:1. The column flow rate was set at 1 µL/min, with an eluent consisting of 0.025 m*M* nitric acid. A TraceDec capacitively coupled contactless conductivity detector (Innovative Sensor Technologies, GmbH, Innsbruck, Austria) was used in scanning mode for monolith characterisation with settings of 0dB, 0% gain and 0 offset (unless otherwise stated). For SEM images, a Hitachi S3400N VP was used for characterisation of morphology in co-polymerised monolithic columns.

2.2.2. Materials and reagents

Butyl methacrylate (BuMA), ethylene glycol dimethacrylate (EDMA), glycidyl methacrylate (GMA), 2,2-dimethoxy-2-phenylacetophenone (DAP), 2-acrylamido-2-methyl-1-propanesulphonic acid (AMPS), benzophenone, 1,4-butanediol, 1-propanol, decanol, 3(trimethoxysilyl)-propyl methacrylate, α,α'-azoisobutyronitrile (AIBN), iminodiacetic acid (IDA), ethanolamine, 2-[(2-hydroxy-1,1-bis(hydroxymethyl)ethyl)amino]ethanesulphonic acid (TES), copper sulphate pentahydrate, nitric acid, sodium hydroxide pellets and hydrochloric acid were purchased from Sigma-Aldrich (Dublin, Ireland), and used as supplied. Vinyl azlactone (VAL) was purchased from TCI Europe (Boerenveldseweg, Belgium). Acetone and methanol were supplied by Labscan (Stillorgan, Dublin, Ireland). Deionised water was provided by a MilliQ Direct Q5 water purification system was from Millipore (Millipore Bedford, MA, USA). PTFE-coated fused silica capillary (100 µm i.d., 360 µm o.d.) was purchased from Composite Metal Services (Shipley, West Yorkshire, UK).

2.2.3. Scanning C^4D (sC^4D)

sC^4D was performed as described previously in Chapter 1, Section 1.19.5 and within reference [5]. For the profiling procedure, the capillary monolith was threaded through the cell of the C^4D detector which was then physically scanned along the length of the column at millimetre increments with the capacitive response recorded at each millimetre location. During the acquisition of sC^4D profiles, either water or a low-conductivity buffer (as indicated later in the text) was pumped through the column at a constant flow rate of 1 µL/min. The detector is constructed with a 1 mm gap between the electrodes. It must be noted that due to the length of column fittings, and the size of the detection cell some areas of columns could not be measured; ~ 5 mm from the end of the column, and ~15-20 mm at the column head.

2.2.4. Vinylisation of fused silica capillary

Fused silica capillary was vinylised using a procedure described previously [6]. The capillary was washed with acetone at a flow rate of 10 µL/min for 10 mins. Following drying with nitrogen flow, the capillary was washed with water for 10 mins at a flow rate of 10 µL/min. The capillary was flushed with 200 m*M* NaOH for 30 mins, followed by flushing with water until the effluent was neutral. The capillary was then flushed with 200 m*M* HCl for 5 mins, followed by flushing with water until effluent was neutral. The capillary was again washed with acetone, and dried using nitrogen. A solution of 50 % 3(trimethoxysilyl)-propyl methacrylate (also known as γ-maps) was prepared in acetone, and flushed through the empty capillary. The capillary was sealed with rubber septa, and placed in a thermostated water bath at 60 °C for 20 hours. Following the reaction, the capillary was flushed with acetone and dried under nitrogen flow for 10 mins.

2.2.5. Fabrication of methacrylate based monolithic columns incorporating stationary phase gradients

2.2.5.1. Photo-grafted stationary phase gradients using a neutral density gradient filter

Firstly, a polymer monolithic column was produced using a mixture of 24 % BuMA, 16% EDMA, and a porogen of decanol, present at 60%. A photo-initiator,

2,2-dimethoxy-2-phenylacetophenone (DAP), was present at 1 % w.r.t. the total % of monomer present. The mixture was deoxygenated using nitrogen sparging for 10 mins. A piece of vinylised PTFE coated fused silica capillary was filled with the mixture via capillary action. Photo-polymerisation took place using a wavelength of 254 nm, with a final UV exposure of 2 J/cm^2. The monolith was washed for 3 hours with methanol. In the second step a concentration of 15 % AMPS was prepared in a solvent of 3:1 tert-butanol: water, containing benzophenone as grafting initiator at a concentration of 0.22 % (wt %) [4]. This mixture was deoxygenated via nitrogen sparging for 10 mins and was subsequently flushed though the column for 1 hour. The column was sealed using rubber septa and was irradiated through the neutral density gradient filter. This provided attenuation of UV energy along the column length in a continuous manner. A total UV exposure of 3 J/cm^2 was applied and the column was washed with methanol for 3 hours to remove any un-reacted monomer. The column was equilibrated with water for 2 hours, prior to sC^{4}D profiling. Alternatively, an irradiative dose of 6 J/cm^2 was applied to the column, the filter providing attenuation in irradiation energy. The un-reacted monomer and polymer chains suspended in solution were removed using a methanol wash (1 hour at 1 μL/min). The column was equilibrated with deionised water prior to sC^{4}D scanning.

2.2.5.2.Co-polymerised stationary phase gradients prepared via thermal polymerisation

Using a method described by Maruška *et al* [2], a stationary phase gradient was prepared *in-situ,* via the co-polymerisation of a charged or reactive functional monomer and a neutral or inert co-monomer. An empty, vinylised fused silica capillary was marked using a permanent marker, which divided the column into "zones" of specific length. The length of each zone could be varied to produce different gradient profiles. A number of different monomer mixtures were prepared incorporating an increasing concentration of functional monomer (AMPS or VAL) across a predefined range, as shown in Table 2.1.

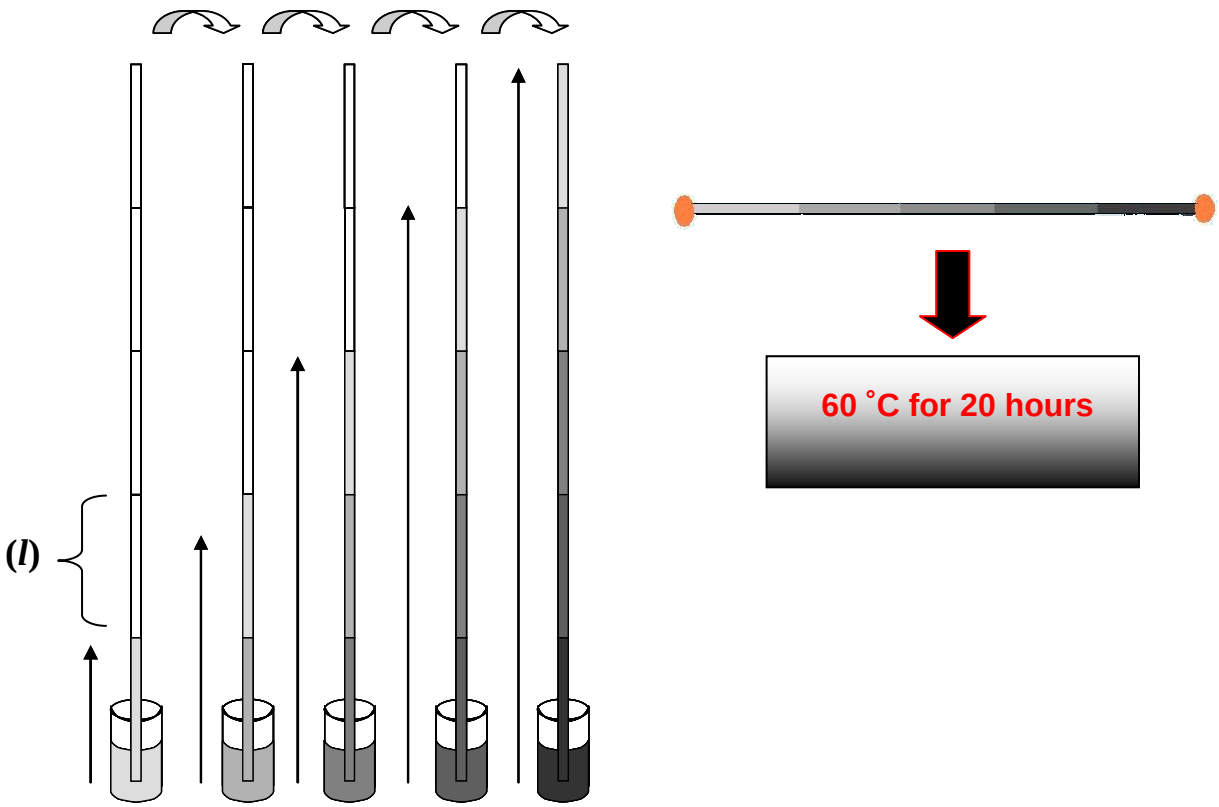

Figure 2.2: *Schematic of the method used for co-polymerised stationary phase gradient column production. The column housing was marked to a length of 10-50 mm (l), determining each zone length. An increase in the functional monomer concentration is indicated by darker shading. The column housing was successively placed into each solution until the meniscus reached each respective mark. The column was sealed and subjected to thermal initiation.*

The total monomer percent concentration was kept constant at 24 %, by adjusting the concentration of the base monomer (BuMA or GMA). The total porogen and crosslinker concentration were held constant at 60 % and 16 % respectively. The initiator was also held constant at 1 % w.r.t. total monomer concentration. The capillary was then filled (via capillary action) with each solution to the predefined mark on the capillary, as illustrated in Figure 2.2. The monomer preparations are listed in Table 2.1.

Table 2.1: *Composition of monomer mixtures used for fabrication of stationary phase gradients via co-polymerisation. Cross-linking monomer (EDMA) and porogen were held constant at 16 % and 60 % respectively. Porogenic system contained 21 % 1-propanol, 33 % 1,4-butanediol, and 6 % H_2O.*

Monomer mix	Monolithic Column SCX#1, SCX#2, SCX#3	
	BuMA (wt %)	AMPS (wt %)
AMPS (0)	24	0
AMPS (0.5)	23.5	0.5
AMPS (1)	23	1.0
AMPS (1.5)	22.5	1.5
AMPS (2)	22	2.0

Monomer mix	Monolithic Column IDA#1, IDA#2, IDA#3	
	BuMA (wt %)	VAL (wt %)
BVAL (0)	24	0
BVAL (0.5)	23.5	0.5
BVAL (1)	23	1.0
BVAL (1.5)	22.5	1.5
BVAL (2)	22	2.0
Monomer mix	Monolithic Column GIDA#1, GIDA#2	
	GMA (wt %)	VAL (wt %)
GVAL (0)	24	0
GVAL (0.5)	23.5	0.5
GVAL (1)	23	1.0
GVAL (1.5)	22.5	1.5
GVAL (2)	22	2.0
GVAL (2.5)	21.5	2.5
GVAL (5)	19	5.0
GVAL (7.5)	16.5	7.5
GVAL (10)	14	10.0

Once the capillary was filled, the ends were sealed with rubber septa and the column was placed in a water bath at 60 ˚C for 20 hours. Following polymerisation, the columns were washed with methanol for 3 hours at 1 µL/min, to remove any un-reacted monomer. The column was equilibrated with water for 2 hours at the same flow rate. Columns incorporating a gradient of AMPS were profiled using sC^4D without further reaction, whereas columns incorporating a gradient of VAL were further modified as specified below in Section 2.2.6. The distribution of monomer zones in filled capillaries prior to polymerisation is shown in Figure 2.3, along with a column naming convention. Each gradient column is referred to hereafter according to the nomenclature in Figure 2.3. A total of eight gradient columns were prepared using this protocol.

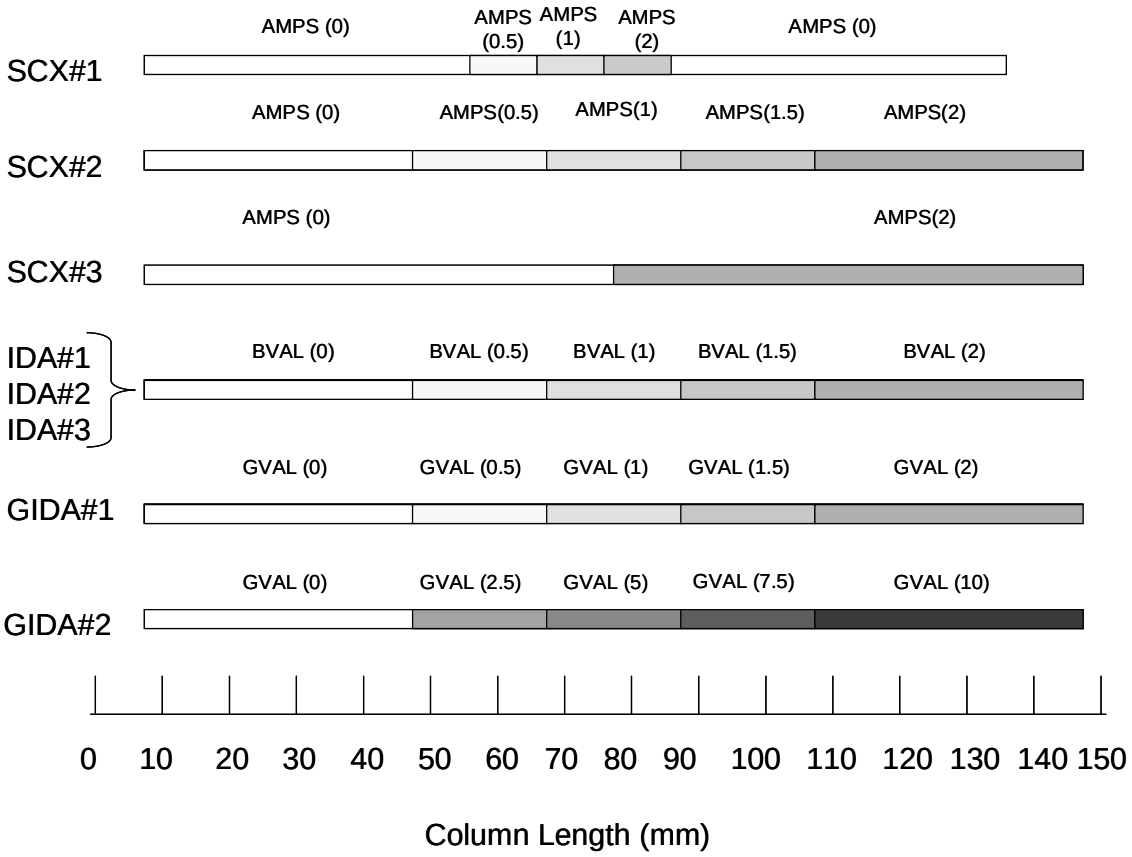

Figure 2.3: *Schematic diagram showing the distribution of monomer solutions in filled capillaries prior to polymerisation. Incremental shading represents higher concentrations of functional monomer. The composition of the monomer mixture in each zone is labelled and can be cross-referenced with Table 2.1.*

2.2.6. SEM analysis of co-polymerised columns

For columns SCX#3, and IDA#1, dry 5 mm cross sections from both ends of each column were removed. The monolithic samples were subjected to gold sputter coating for 2 mins. The samples were mounted, and were analysed using a low accelerating voltage (V_{acc}) in order to view surface features. For comparison, magnification was held constant for each sample.

2.2.7. Immobilisation of iminodiacetic acid on gradient vinyl azlactone monolithic columns

A solution of 1 mg/mL IDA was prepared in deionised water, and was subsequently pumped across the columns for 3 hours. Un-reacted IDA was removed using a water wash step, for 1 hour at 1 μL/min. The immobilisation reaction occurred via a ring opening reaction, following nucleophilic attack of the carbonyl by the incoming amine lone pairs. This is illustrated below in Figure 2.4 (a). A solution of 1 *M* ethanolamine was subsequently pumped across the column for 3 hours followed by a water wash until the effluent reached pH 7. The ethanolamine wash provided an end-capping procedure for un-reacted VAL groups, producing neutral 2-hydroxyethylamido groups (Figure 2.4 (b)).

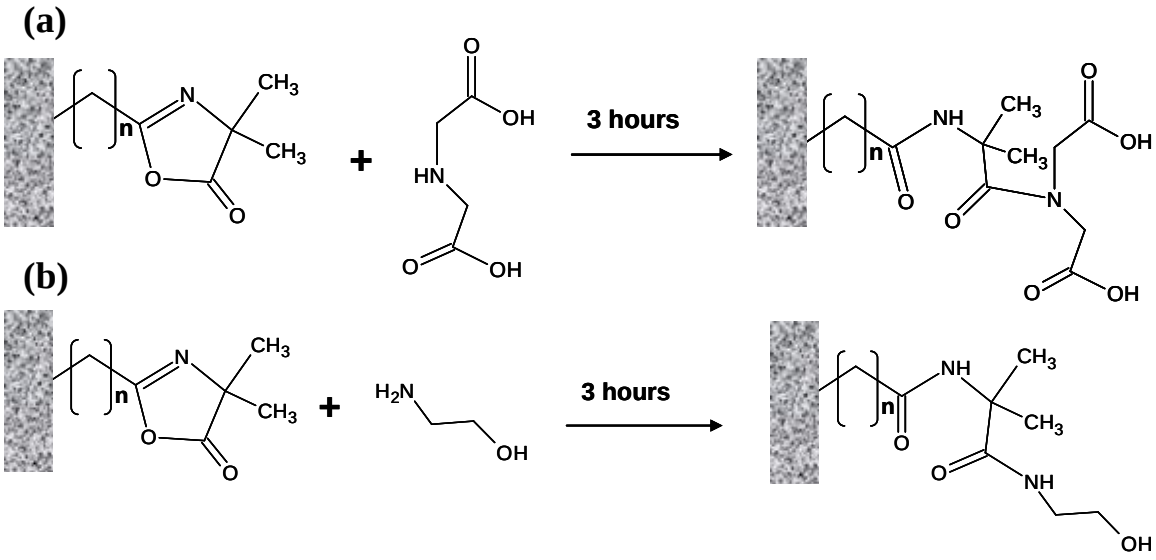

Figure 2.4: *Reaction scheme and molecular structures for the immobilisation of IDA onto VAL sites (a), and for the immobilisation of ethanolamine onto remaining VAL sites, producing neutral 2-hydroxyethylamido groups (b).*

2.2.8. Chromatographic evaluation of VAL-IDA stationary phase gradients

Using an eluent of 0.025 m*M* nitric acid, and an injection volume of 50 nL, standards of 10 ppm, 1 ppm and 0.1 ppm Zn^{2+} were injected onto the IDA functionalised column with the direction of flow opposite to that shown in Figure 2.3, i.e. the zone BVAL (2) was the column inlet, connected to the pump. The flow rate was constant at 1 µL/min. The method of detection was indirect non-suppressed on-column C^4D.

2.2.9. On-column complexation of Cu^{2+} on IDA stationary phase gradients

A selected IDA gradient column was profiled using sC^4D in a buffer consisting of 2.5 m*M* TES and 3 m*M* ethanolamine (Buffer 1). A second buffer (Buffer 2) was prepared using 2.5 m*M* TES, 3 m*M* ethanolamine and 1 m*M* copper sulphate. Buffer 2 was pumped across the column for 3 hours at a flow of 1 µL/min. The column was washed with water to remove any unbound Cu^{2+} ions and the column was scanned again in Buffer 1. The Cu^{2+} was removed from the IDA sites using 10 m*M* nitric acid (12 h at 1 µL/min).

2.3. Results and discussion

2.3.1. sC^4D characterisation of fabricated gradient columns

2.3.1.1. Photo-grafted gradient using a neutral density gradient filter

As mentioned in Chapter 1.0, Section 1.19.5, sC^4D is rapidly becoming a method of choice for characterisation of stationary phase coatings and stationary phase homogeneity. The sulphonated monomer, AMPS can be easily grafted onto polymeric columns as shown previously [5,6], and due to the presence of sulphonate groups, remains ionised at the pH of the scanning mobile phase (pH 7). This makes for an ideal model functional group for stationary phase gradient investigation. Using a neutral density filter as described previously [1], AMPS was grafted in such a way that a high graft density was anticipated in the region of the monolith corresponding to the area of high UV light transmission. The filter had an optical density ranging

from 4.0 to 0.04. The percent transmitted (%T) light is related to the optical density by the following equation;

$$T = 10^{-OD} \times 100 \qquad \text{(Equation 2.1)}$$

For an optical density of 4.0 the %T is 0.01%, and for an optical density of 0.04, the % T is ~91 %. The filter measured 100 mm in length, which was placed over a monolith of 130 mm in length. The first 10 mm of the monolith was masked to prevent photo-grafting. The equation above (2.1) is exponential in nature, and so, a linear gradient was not expected. This was also reported by Pucci *et al*. [1], wherein an exponential gradient of sulphur was measured (via electron probe microscopy) following grafting of a column through a neutral density gradient filter.

In Figure 2.5, the resulting sC^{4}D gradient profile can be seen. The low detector response along the first 10 mm of the column was due to photo-masking of this zone, as mentioned above. Following this point the detector response rises dramatically, resulting from grafting of the column through the area of highest transmittance of the filter.

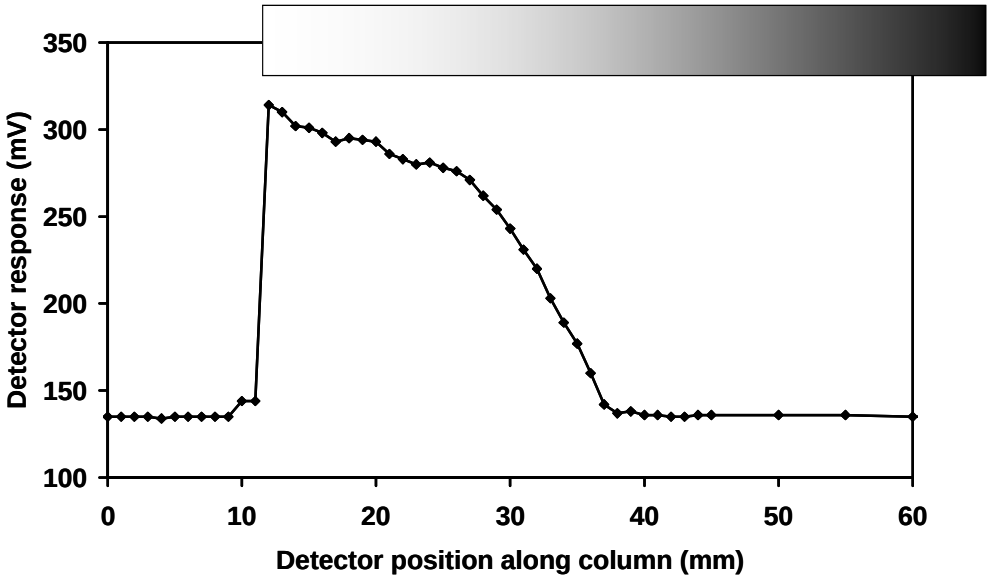

Figure 2.5: *sC^{4}D profile of a stationary phase gradient of AMPS grafted onto a BuMA-co-EDMA monolith via a neutral density filter using 3 J/cm^2 UV irradiation. Insert: schematic of placement of gradient filter during grafting. Column scanned in deionised water at a flow rate of 1 μL/min.*

The detector response begins to lower, due to the lower transmittance of the remainder of the gradient filter. This resulted in a lower activation energy transmitted to the column via the gradient filter, and thus little or no grafting occurred. The resulting gradient spans ~ 25 mm, much shorter than anticipated, given the 100 mm length of the filter.

In an attempt to increase graft density along the column, a BuMA-*co*-EDMA column was grafted using the same monomer solution, with a higher dose of UV energy (6 J/cm^2), to try to overcome the low activation energy resulting from the high optical density of the gradient filter. Following the grafting procedure, the column back pressure became very high during the wash step, and flushing the column became difficult due to the viscosity of polymer chains in solution. The exact column back pressure could not be determined as a manual split flow was used to obtain low micro litre flow. The column was scanned using sC^{4}D and a profile was constructed. The resulting profile can be seen below in Figure 2.6.

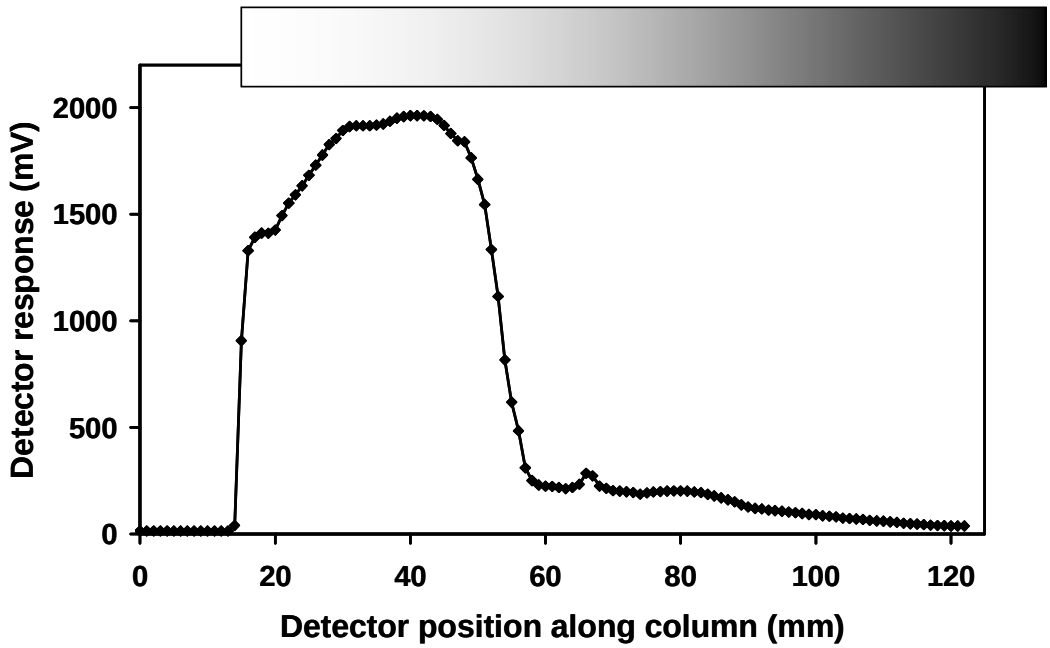

Figure 2.6: *sC^{4}D profile of BuMA-co-EDMA monolithic column grafted with AMPS, using 6 J/cm^2 UV irradiation, via a neutral density gradient filter. Column scanned in deionised water at 1 mm intervals. Single scan reported.*

In Figure 2.6, the section of the filter corresponding to the highest optical transmission resulted in the highest detector response. Unlike the plot in Figure 2.5, following the peak in detector response, a shallow gradient in detector response is

observed from 60 mm to 120 mm. The use of the neutral density gradient filter can provide a continuous gradient in UV transmission, and thus graft density, however, the optimum optical density must be chosen. An alternative method to produce stationary phase gradients is to use co-polymerisation of functional monomer. This is outlined in the following sections.

2.3.1.2.Co-polymerised gradient columns using thermal initiation

Using the method outlined by Maruška *et al.* [2], three cation exchange monoliths were fabricated using BuMA-*co*-EDMA-*co*-AMPS, in a co-polymerised gradient stationary phase, in which the longitudinal length of each zone and the concentration of functional monomer in each zone could be adjusted. The columns were denoted SCX#1, SCX#2, and SCX#3. By adjusting the length and concentration of functional monomer in each zone, the shape of the resulting gradient could be fine tuned. This is shown in Figure 2.3 and Table 2.1. Column SCX#1 consisted of 50 mm of a zone of 0 % AMPS (24 % BuMA) and three 10 mm zones of 0.5 %, 1 % and 2 % followed by 50 mm of 0 % AMPS. This can be seen clearly in Figure 2.7 (a). The detector response is very low corresponding to the zone of 0 % AMPS. The detector response increases rapidly according to the increased concentration of AMPS. Following the zone of 2 % AMPS, the detector response gradually decreases, with a shallower slope than the leading edge of the gradient. The resulting gradient spanned approximately 33 mm, longer then the expected 30 mm (as denoted in Figure 2.3). The detector response then declines gradually over the following 25 mm from the 2 % AMPS zone into the 0 % AMPS zone. The profiling tool, sC^4D, clearly shows the ability to map the distribution of charged monomer, and due to diffusion of monomers between adjacent zones, a stepped profile was not observed.

In SCX#2 (Figure 2.7 b) the zone lengths were increased to 20 mm (w.r.t. SCX#1, see Figure 2.3), and the functional monomer concentration was increased in smaller increments. This resulted in a close to ideal convex gradient profile. However, there was a decrease in the detector response towards the end of the column. This is likely due to a change in surface concentration of charged AMPS groups, or possibly, a decrease in monolith permeability (resulting in a lower volume between electrodes, thus a lower detector response). A void in the stationary phase would result in an increase in detector response due to the increased volume between the electrodes of

the detector. To understand the resulting column profiles (Figure 2.7), a discussion of the diffusion effects observed with the resulting monolithic columns is necessary.

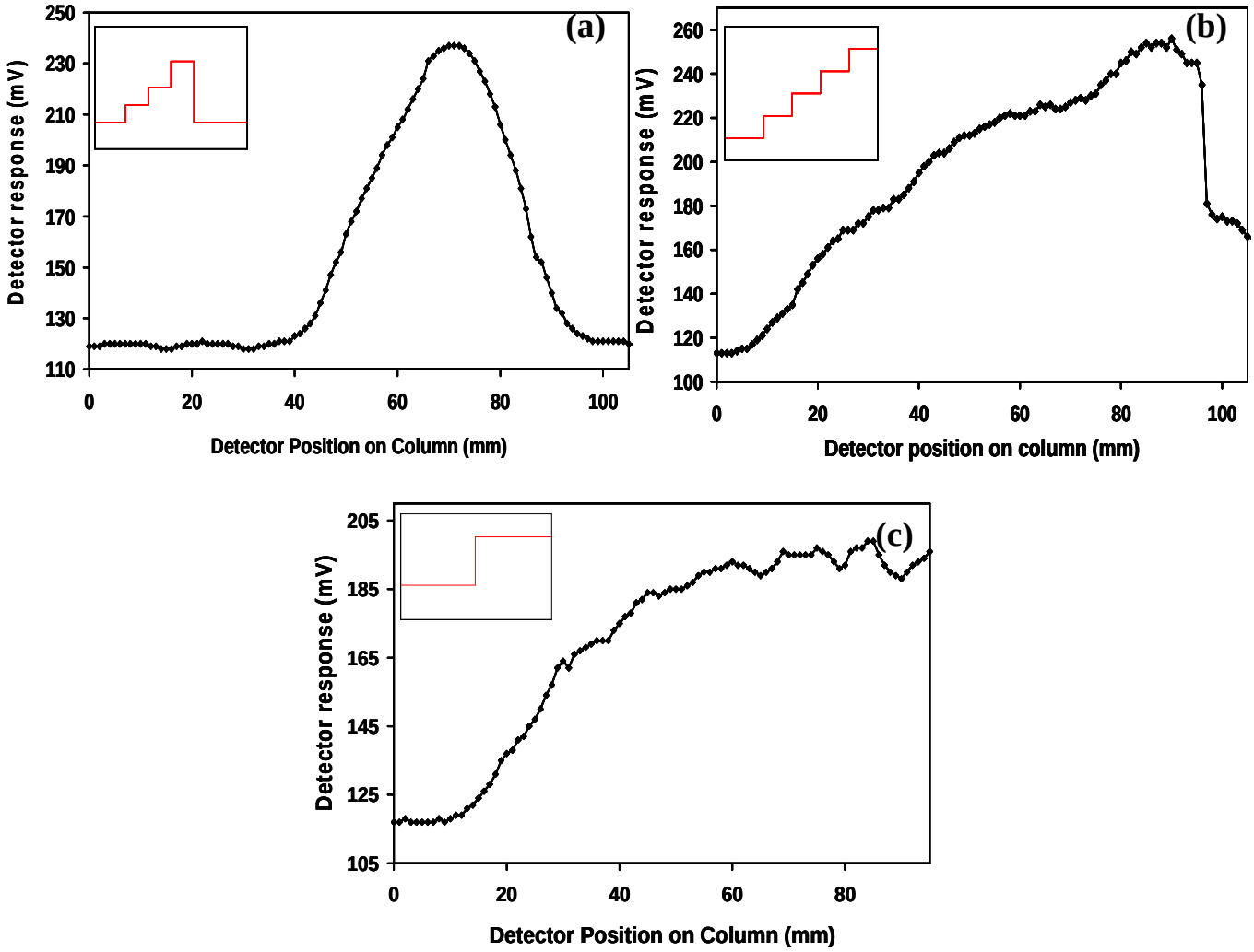

***Figure 2.7**: sC^{4}D profiles of SCX#1 (a), SCX#2 (b), and SCX#3 (c). Inserts: expected detector response with respect to concentration of functional monomer added. Columns scanned in deionised water.*

These columns were produced under thermal conditions where diffusion between zone boundaries was expected, following polymerisation. A stepped type gradient was expected, however, the resulting distribution of the gradient was linear, and extended into zones of lower functional monomer concentration. Fick's law states that the rate of flux (mass transfer, J) of a component of concentration C across a membrane of unit area A (in a predefined region) is proportional to the concentration differential across that plane. The theory of Fick's law assumes that the driving force of diffusion is based on the presence of a concentration gradient. Diffusion occurs

from a cross sectional area of high concentration to low concentration, creating a localised concentration gradient. The diffusion rate is dependant on the difference in concentration between two neighbouring zones. The higher the difference in concentration, the diffusion of functional monomer into an area of lower concentration is increased [7,8]. In this case, the zone of higher functional monomer concentration (Figure 2.8 (i)) is diffusing into the zone of lower functional monomer concentration, or no additional functional monomer (Figure 2.8 (ii)), at a rate depending on the concentration difference.

$$J = DA\frac{C_1 - C_2}{\Delta x} \qquad \text{(Equation 2.2)}$$

D = diffusion constant, J = mass movement per second, A = cross sectional area, Δx is length (in meters).

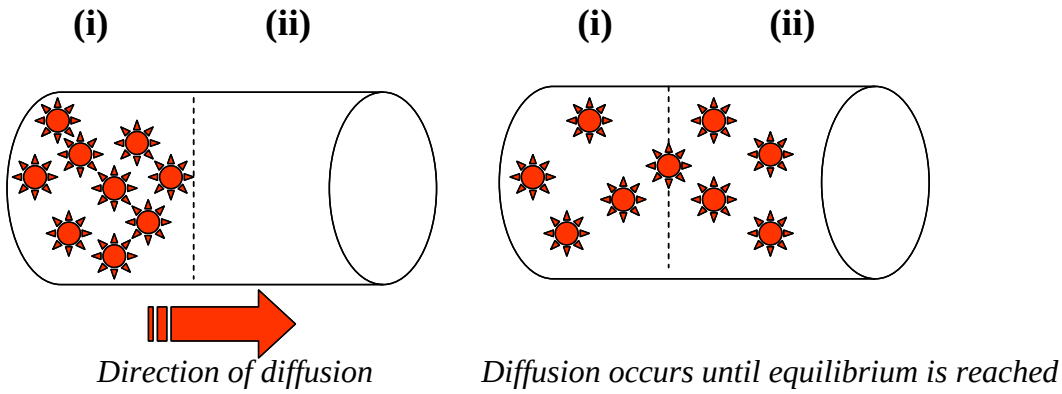

Figure 2.8: *Schematic illustrating Fick's law of diffusion.*

In Figure 2.7 (a), the resulting diffusion can be observed. In this column, three zones (each 10 mm) of increasing AMPS concentration, were sandwiched between two terminal zones of 0 % AMPS (50 mm each). The gradient measured 30 mm from baseline to apex, however, a sharp decrease in detector response was expected for the remaining 50 mm of 0 % AMPS monolith. Due to the diffusion outlined above, a gradual decrease in detector response, from the apex of the detector response back to baseline following the gradient was observed (across ~25 mm). Similarly in Figure 2.7 (b), a gradual increase in detector response is observed from 0 % AMPS zone to 2 % AMPS zone (from 6 mm to 90 mm). Following the apex of the gradient at

approximately 90 mm, a decrease in detector response was observed. In using the theory provided by Fick's law of diffusion, the decrease in detector response would indicate a section of lower or no functional monomer in the polymerisation mixture in this section of the column. The unexpected decrease in detector response may be due to changes in morphology, or possibly due to a decrease in surface available charged AMPS groups. However, this feature highlights the advantage of sC^4D as a simplistic means of non-invasive yet effective quality control test, following gradient fabrication.

To study the diffusion effects further, a column (SCX#3) measuring 140 mm in length, was prepared with 70 mm 0 % AMPS (i.e. 24 % BuMA) and 70 mm 2 % AMPS. Again the gradient had a smoothed profile (Figure 2.7 (c)). The detector response of the 0% AMPS region was much higher than expected due to the encroachment of the conductive monomer into the region. The solution of higher monomer concentration (2 % AMPS) diffused approximately 45 mm into the 0 % AMPS zone over a 20 hour period. This gave an average speed of 6.25×10^{-4} mm/sec. The profiles of SCX#2 and SCX#3 are very similar in shape, with no clear distinction of boundary between the zones. The detector response is much higher in SCX#2 than in SCX#3. The difference in detector response is due to the lower rate of diffusion seen for SCX#2 (i.e. lower change in concentration difference between each zone). As the change in AMPS concentration is higher in SCX#3 (0 to 2 %), the diffusion occurs at a higher rate as defined by Fick's law, the rate of diffusion is dependent on the concentration difference between zones. As a result, the remaining concentration of functional monomer within the zone is reduced, due to the migration of AMPS molecules to the zone of lower concentration and thus, causing a localised decrease in the detector response. The effects of diffusion on the formation of the gradient using the co-polymerisation method are inevitable, and as such, may be a problem in the fine control of stationary phase gradients. In the work performed by Maruška *et al*. [2], the exact shape of the resulting gradient columns was not determined, and so, any unexpected feature (e.g. diffusion of functional monomer or indeed a void between adjacent zones) could not be determined. The use of sC^4D in the work reported herein, clearly demonstrates the ability to fully visualise the shape of the gradient non-destructively and non-invasively.

2.3.2. Reproducibility of sC^{4}D profiling of stationary phase gradients

To study the reproducibility of sC^{4}D, column SCX#1 was taken for analysis. The column was scanned in triplicate. Error bars are included for each data point as shown in Figure 2.9. The conductivity profile was very reproducible with a standard deviation in response, of no greater than 2.4 % RSD.

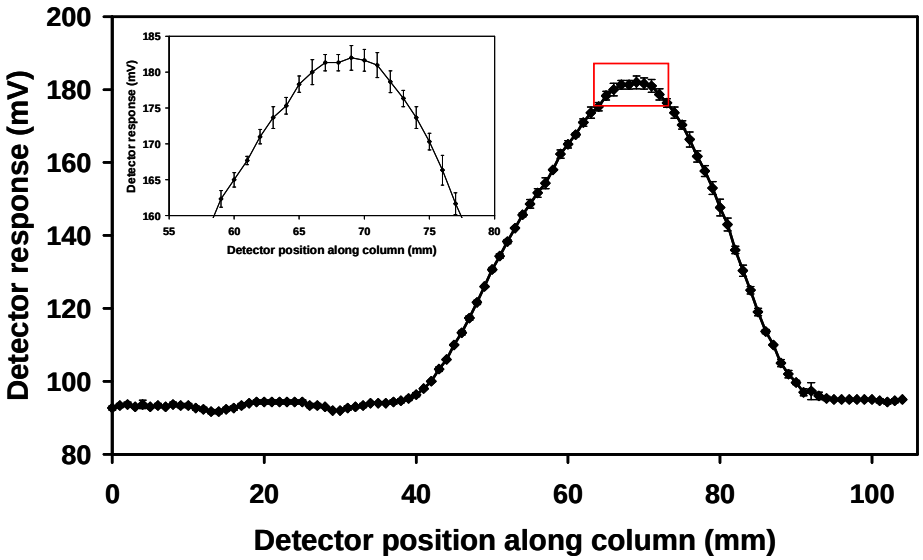

Figure 2.9: *sC^{4}D plot of entire column with error bars with the expanded area highlighted in the red box, measured from triplicate profiling scans. Insert: sC^{4}D plot of SCX#1 from 55 mm to 80 mm (detector position along column) to emphasise the presence of error bars.*

2.3.3. Fabrication and direct visualisation of immobilised metal affinity chromatography (IMAC) stationary phase gradients

2.3.3.1. Profiling of VAL-IDA gradient columns

A number of publications exist involving the immobilisation of IDA onto polymer monolith surfaces via epoxy groups on the monolith surface (GMA-*co*-EDMA) [9,10]. Immobilised metal affinity chromatography (IMAC) separations generally involve trap and release strategies, or in the case of histidine containing compounds, either an imidazole gradient [10], or a chaotropic gradient must be applied for an efficient separation [9]. Using a gradient of IDA immobilised onto a

separation column, on-column chromatographic zone focussing can potentially occur, without the need to deliver a mobile phase gradient.

Immobilisation via reaction of surface available epoxide groups is a common procedure in the immobilisation of amine containing compounds such as IDA. However, the lengthy reaction times required with thermal reaction, and the necessary temperatures make this immobilisation reaction less attractive. The use of microwaves can result in rapid polymerisation of monolithic columns [11], and may be useful for the thermal functionalisation of columns, however it is beyond the scope of this thesis. The use of VAL offers an attractive alternative where faster reactions times are achieved under milder conditions e.g. neither a catalyst nor extreme temperature conditions are required. VAL chemistry has been used recently in the immobilisation of proteins via pendant lysine groups [12].The immobilisation of small molecules has also been reported recently [13]. A rapid ring opening reaction occurs at the electrophilic C=O of VAL, with an incoming primary amine lone pair via a nucleophilic addition [14]. In this work, IDA was immobilised onto a BuMA-*co*-EDMA-*co*-VAL monolith, which incorporated a gradient of VAL. Using VAL chemistry, three columns were prepared via the co-polymerisation method as described above in Section 2.2.5.2. IDA was immobilised onto the VAL gradient columns using the method outlined above in Section 2.2.6. These columns were denoted as IDA#1, IDA#2, and IDA#3.

A blank scan of the monolithic columns prior to immobilisation of IDA was performed in water. This scan provided a profile of the overall monolithic structure and confirmed the absence of voids, or possible sections of monolith inhomogeneity. Obviously, the buffer could not be used on monolithic columns having exposed VAL sites, as irreversible binding would occur between the amine groups of the buffer constituent (ethanolamine) and the VAL ring. The column was therefore scanned in buffer <u>after</u> IDA immobilisation and normalised to the profile of the column in water. This effectively removes the background conductivity generated by the buffer. This can be seen in Figure 2.10.

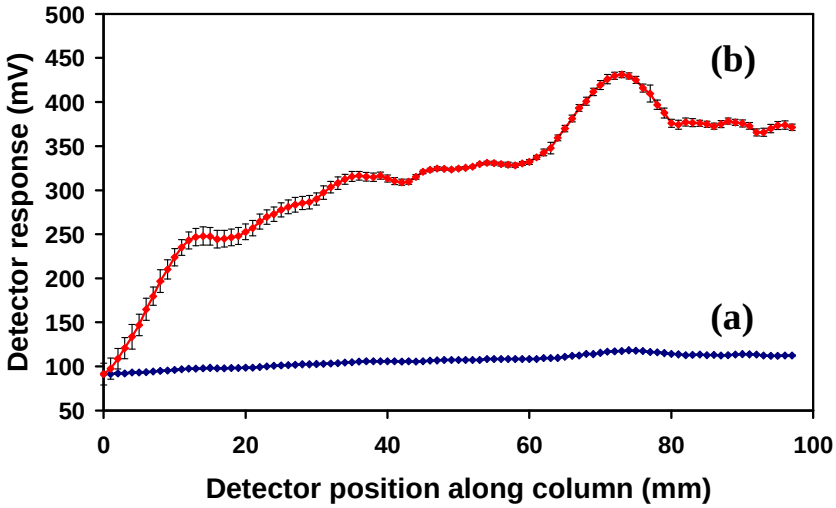

Figure 2.10: *sC^{4}D profile of IDA#1 in water (pH 7) (a), and in 2.5 mM TES, 3 mM ethanolamine buffer (pH 9) (b). Profile (b) normalised to profile (a) by removing background signal contributed by the scanning buffer.*

The scan of the column in water (Figure 2.10 (a)), illustrates that the monolith prior to deprotonation provides a somewhat homogeneous structure, with a low detector response (< 100 mV). There is a small increase in detector response across the column (~ +15 mV) indicating a small variation in monolith structure along the column. The amine lone pairs can be protonated for sC^{4}D profiling using an acid wash, however, the resulting signal was not sufficient, possibly due to low equivalent ionic conductance. In order to maximise the stationary phase charge, a buffer of 2.5 m*M* TES, 3 m*M* ethanolamine (pH ~9) was used to deprotonate the carboxylate groups of the immobilised IDA, as described by Gillespie *et al*. [12] (pK_a's 5.1, 6.9 when immobilised onto a polymer monolithic column). The resulting detector response can be seen in Figure 2.10 (b).

The detector response of the column in the TES, ethanolamine scanning buffer resulted in a close to ideal convex gradient shape. The incremental increase in detector response corresponding to surface localised IDA groups, demonstrates the presence of the gradient. From the first on-column data point the detector response increases gradually from 91 to 419 mV (0 mm to 70 mm respectively). At ~ 70 mm an increase in detector response was observed, resulting in a "humped" feature on the gradient profile. It can be concluded that this is due to a surface localised increase in VAL density (and thus IDA). The column was scanned in triplicate and this

"humped" increase was observed in each scan with an observed % RSD of less than 5.3 % for the data points located at the apex of this feature.

2.3.3.2. Reproducibility of VAL-IDA columns

To study the reproducibility of the co-polymerisation method of IDA gradient formation, two more columns were prepared (IDA#2, IDA#3). An overlay of the sC^4D profiles of these columns can be seen in Figure 2.11. It is evident from the profiles that the columns are largely similar; however, the last 20 mm of each column generated a different response. This phenomenon may be in part due to the preparation on separate days, and in part due to experimental error in monomer solution preparation. If C^4D had not been used in the characterisation of these columns, it would be assumed that the columns would follow exactly the same profile following preparation from the same protocol. The advantage of sC^4D is that the exact spatial distribution of the charged groups can be determined accurately. In column IDA#2 a large spike in detector response is seen. Upon further inspection of the monolith a void was seen in the stationary phase. A photograph of this void was taken (Figure 2.11 insert). Upon careful measurement it was observed that this void was indeed responsible for the large increase in detector response. The void stems from the sequential "dipping" of the capillary housing into different monomer solutions. For example the capillary is filled sequentially by capillary action. If the vacuum does not stop during the transfer of the capillary from monomer solutions, a pocket of air can be taken into the capillary, forming a void in the stationary phase. This is an obvious drawback of using the co-polymerisation method. This also illustrates the benefit of C^4D as a characterisation technique.

Furthermore, in column IDA#2 (Figure 2.11 (b)), the detector response is higher beyond the stationary phase void (70-95 mm) than for the corresponding columns (IDA#1,IDA#3). As an air gap was present in this particular column during the polymerisation, the diffusion processes as observed with the SCX columns (Figure 2.7), did not occur. This resulted in a higher detector response, correlated to a higher localised concentration of VAL-IDA. Some variation was expected as each column was prepared from a different monomer pre-cursor solution. Variations in sample preparation may account for some differences in the resulting gradient profile.

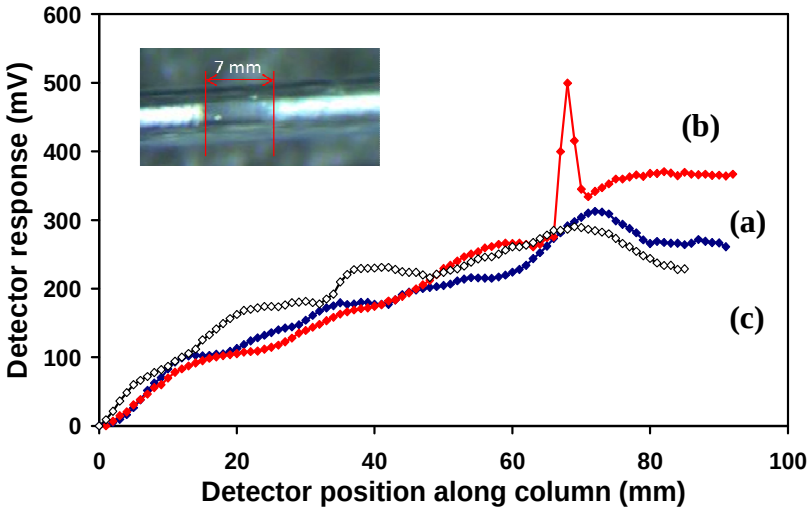

Figure 2.11: *sC^{4}D profiles of replicate columns IDA#1 (a), IDA#2 (b), and IDA#3 (c), following IDA immobilisation, columns scanned in 2.5 mM TES, 3 mM ethanolamine buffer and normalised to zero for comparative purposes only. The peak seen at ~ 70 mm in the profile of IDA#2, is due to break in stationary phase (~ 7mm). Insert: Photograph of void in monolith formation (IDA#2).*

2.3.3.3.On-column complexation of Cu^{2+} ions on an IDA stationary phase gradient

As stated previously, stationary phase gradients may prove useful for future applications in IMAC, upon further development. One of the most stable reactions in affinity chromatography is the Cu^{2+} histidine interaction [15]. To show the IDA selectivity for Cu^{2+}, the column was flushed with Buffer 2 for 3 hours. Interstitial Cu^{2+} was removed by pumping water across the column for 1 hour. The column was scanned in Buffer 1 (2.5 m*M* TES, 3 m*M* ethanolamine) before and after Cu^{2+} immobilisation. The resulting profiles are shown in Figure 2.12, below.

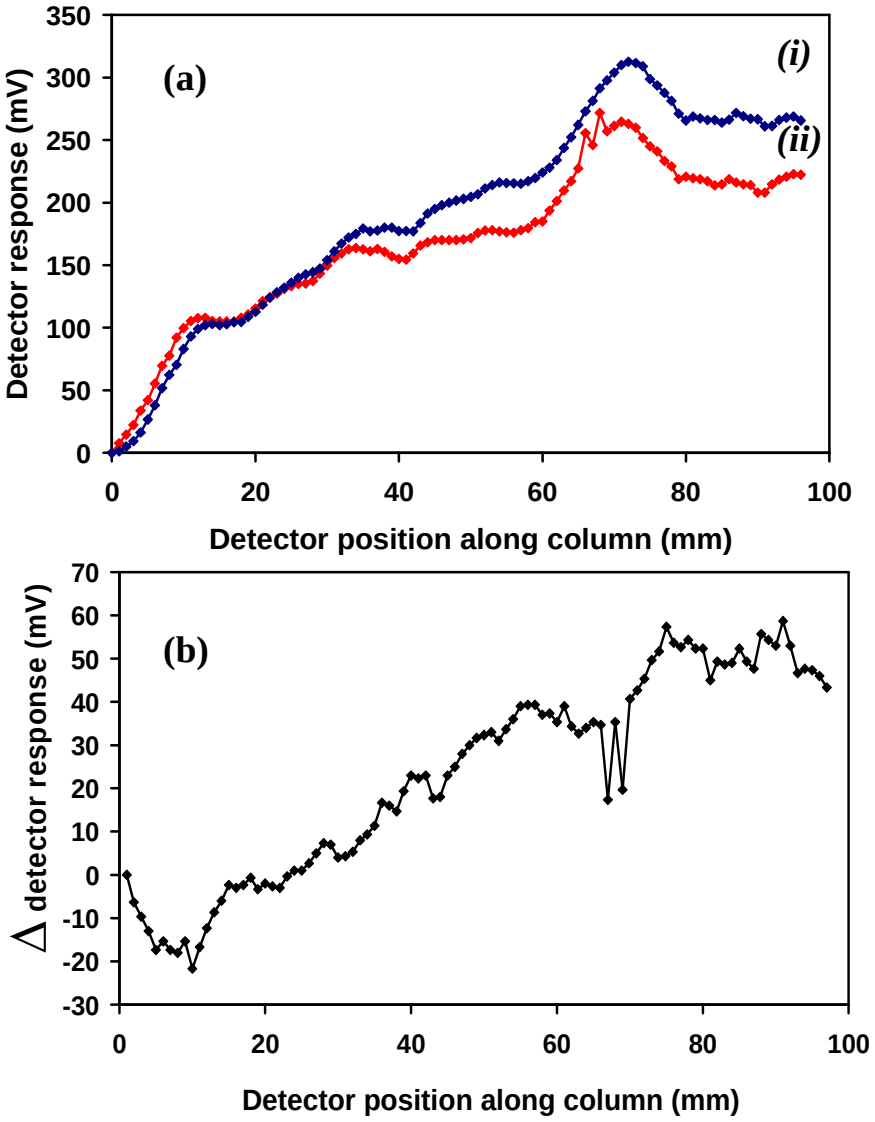

Figure 2.12: *sC^{4}D profile of IDA#1 before (i) and after (ii) Cu^{2+} chelation in scanning buffer 2.5 mM TES, 3 mM ethanolamine, (a). The change in detector response between plot (i) and (ii) is shown in (b).*

A drop in detector response is easily observed which can be explained by the change in counter ions experienced by the immobilised groups. In the scan prior to metal immobilisation, the dissociated ligand would exhibit electrostatic attraction toward passing buffer counter-ions. The counter-ions experienced would likely be H^+, of which the limiting ionic conductance is relatively high (349 S cm^2/eq). In contrast the limiting ionic conductance of Cu^{2+} is much lower (53.6 S cm^2/eq). As a result, the detector response is lowered due to the exchange in counter ions for metal cations. This was also reported by Gillespie *et al*. [12], wherein titrations were performed on-

column, with immobilised IDA and IDA-like groups, which exhibited a change in detector response above pH 7. The detector response generated by the immobilised IDA groups can be explained by Equation 2.3, below.

$$\kappa = c_L \frac{\left(\frac{K_1}{[H^+]} + \frac{K_1 K_2}{[H^+]^2}\right)\left(\Lambda_{COO^-} + \frac{1}{n}\Lambda_{Cat}{}^{n+}\right)}{1000K} \qquad \text{(Equation 2.3)}$$

κ = conductance of ligand functionalised monolithic column, C_L = concentration of bound ligand , K_1 K_2=dissociation constants for carboxyl groups of IDA , Λ_{COO^-} = equivalent ionic conductances of carboxylates, $\Lambda_{Cat}{}^{n+}$ = equivalent ionic conductance of n^+ counter ions , K = cell constant.

As expected the detector response decreased due to the formation of the [IDA-Cu^{2+}] complex, with a lower contribution of ionic conductance from Cu^{2+}. Tsukagoshi *et al.* [16] reported similar effects using EOF measurements in capillary electrochromatography (CEC), where a reduced electroosmotic flow (EOF) was observed for IDA columns in the Cu^{2+} form.

2.3.3.4.Production of GMA-co-*EDMA*-co-*VAL monolithic columns*

If this type of column was to be used in protein applications such as IMAC, the hydrophobic nature of the column would result in non-specific hydrophobic interactions between the protein and the column. As shown in Figure 2.3, a more hydrophilic monomer (glycidyl methacrylate, GMA) was chosen which consists of a methacrylate group, and an epoxide group. The resulting monolith consisted of both pendant epoxide groups and VAL groups. The same co-polymerisation stationary phase gradient fabrication protocol was followed for this monomer, however, due to the change in surface chemistry, a lower detector response was observed overall as seen in Figure 2.13 below.

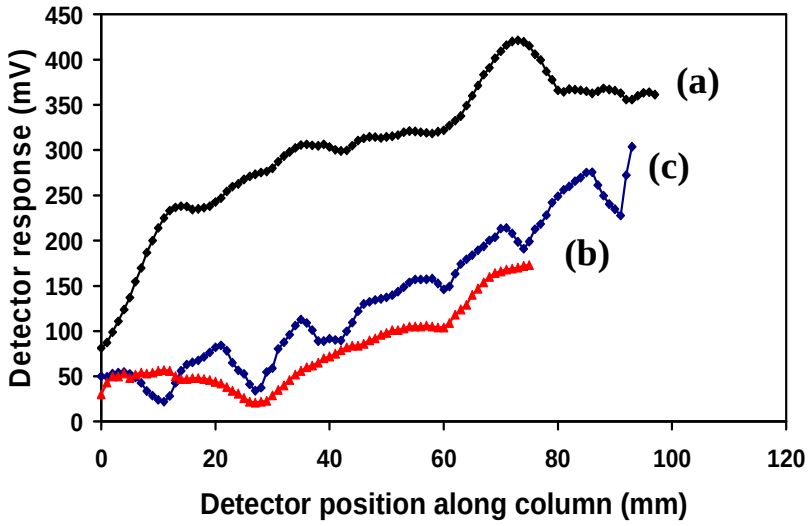

Figure 2.13: *sC^{4}D profiles of IDA#1 (a), GIDA#1 (b), GIDA#2 (c).*

In an attempt to compare BuMA columns to GMA columns, it was necessary to increase the resulting detector response for GMA-*co*-EDMA-*co*-VAL columns. The lower detector response for GIDA#1 indicated a lower proportion of surface expressed VAL groups for IDA immobilisation. The maximum VAL concentration was therefore increased from 2 % to 10 % (Table 2.1 and Figure 2.3). The detector responses for the GMA based monoliths were much lower than that of the BuMA based columns (IDA#1-3) as seen in Figure 2.13.

The increased concentration of VAL had no effect on the gradient profile of GIDA#2 (Figure 2.13 (c)) compared to the gradient profile of GIDA#1 (Figure 2.13 (b)). The gradient profiles for the GMA columns are not ideal and show an irregular pattern, which may be the result of a distortion in monolithic morphology along the column or an inhomogeneous distribution of VAL-IDA upon the surface of the monolith. One possible explanation of the low detector response of the GIDA monolithic columns may be due to low reactivity of GMA in the polymerisation. Factors such as the presence of appropriate hydrogen atoms for hydrogen abstraction (e.g. tertiary and secondary bonded hydrogen atoms) may affect the branching of chains during polymerisation. Generally tertiary bonded hydrogen atoms are preferable for branching in hydrogen abstraction based chain polymerisation reactions, however, secondary bonded hydrogen atoms can also be abstracted, albeit at lower amounts [17]. The BuMA monomer contains a higher proportion of

secondary hydrogen atoms compared to GMA (Figure 2.14), which may account for the poor reactivity exhibited by GIDA monolithic columns in this work.

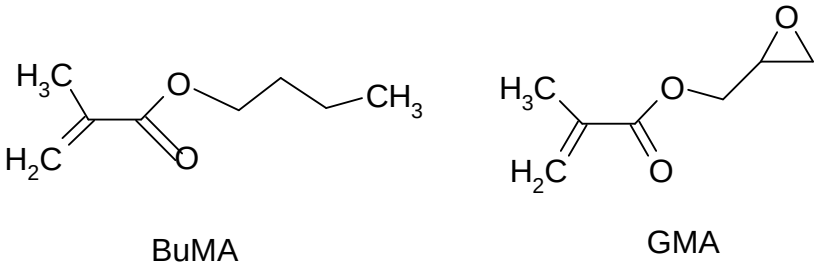

Figure 2.14: *Structures of monomer used in monolith formation.*

2.3.3.5.Chromatographic evaluation of VAL-IDA columns

An eluent of 0.025 m*M* nitric acid was prepared to retain and elute a standard solution of Zn^{2+}. A standard of 1 ppm Zn^{2+} was injected onto the column, and the peak was detected using on-column non-suppressed indirect conductivity detection, via C^4D. The resulting chromatograms are shown in Figure 2.15.

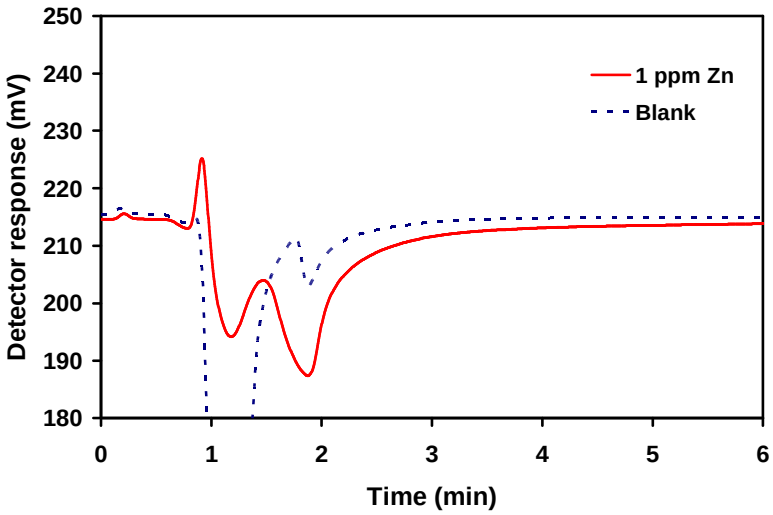

Figure 2.15: *Chromatogram of the retention of Zn^{2+} on a co-polymerised IDA#1 monolithic column. Eluent; 0.025 m*M *nitric acid, 50 nL injection volume, 1 ppm Zn^{2+} standard. Flow of 1 µL/min, blank is deionised water.*

The retention factor, *k*, for the retained analyte was calculated from the chromatogram shown in Figure 2.15: The resulting *k* value of 0.58 indicated retention of the analyte, however, it was a poor result (desirable *k* values range between 1 and 5). If analytes are eluted too quickly from the column the *k* value is < 1, as seen in this

example. The overall capacity of the column was not evaluated, however, from the above chromatogram it can be inferred the capacity, based on *k*, is extremely low. This type of column would not be suitable for use in separations, however, the information obtained from this study will aid the production of future stationary phase gradient columns.

2.3.4. SEM analysis of morphology in co-polymerised stationary phase gradient columns

2.3.4.1. SEM analysis of AMPS co-polymerised monolithic columns

The column denoted SCX#3 was taken for SEM analysis. This column consisted of two discrete sections of functional monomer, 0 % AMPS, and 2 % AMPS. A section of 5 mm from each end of the column was removed for analysis, followed by gold sputter coating. The morphology of the resulting globules was visualised. As seen in Figure 2.16 below, the morphology of the resulting globule system is shifted from smaller to larger globules from 0 % AMPS (a) to 2 % AMPS (b) respectively. This is caused by a change in the solvating ability of the porogen with respect to nuclei formed during the polymerisation. Solvating solvents (e.g cyclohexanol for methacrylate based monoliths) produce monolithic columns with small pore sizes, when compared to non-solvating solvents (e.g. decanol for methacrylate based monoliths) which result in larger pores (discussed in detail in Chapter 1, Section 1.7). In the column segment of 0 % AMPS, the porogen is a solvating solvent for the resulting polymer. In contrast, the 2 % AMPS segment of the monolith contains a non-solvating solvent for the resulting polymer.

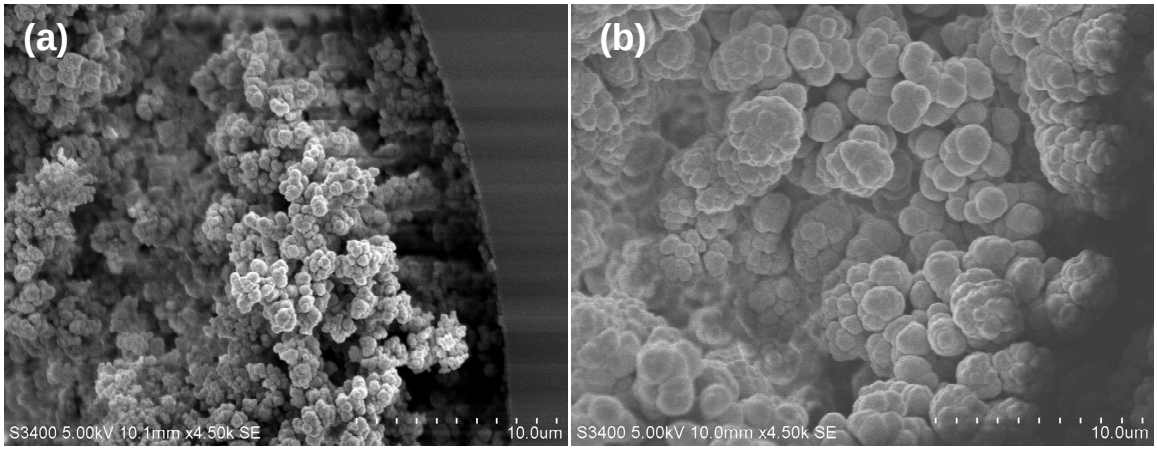

Figure 2.16: *SEM micrographs of SCX#3 containing 0 % AMPS (a), and 2 % AMPS (b), co-polymerised into monolith pre-cursor solution. Magnification 4, 500 x, V_{acc} 5 kV. Secondary electron detection.*

The obvious change in porogen solvation ability with the changing monomer composition across the column can be seen in Figure 2.16, with a variation in pore and globule size for the two sections of column analysed. The monolith is therefore not homogeneous in structure, and a gradient in pore size is evident. From the change in morphology, several problems arise. In chromatographic separations using such a co-polymerised stationary phase gradient, secondary effects such as size exclusion, may be observed. This is obviously not ideal, as any change in separation performance with the column should be solely generated by the presence of the gradient. Also, for profiling columns using sC^4D, the variation in available volume between the electrodes may change with monolith pore size. This may inherently affect the resulting conductive profile. Thus, the variation in morphology is not ideal, and is a fundamental flaw in the production of stationary phase gradients using a co-polymerisation method.

2.3.4.2. SEM analysis of VAL co-polymerised monolithic columns

Samples of column IDA#1 were taken for analysis. Again 5 mm segments from each end of the column were cut and subjected to gold sputter coating. The two samples represented a column segment containing 0 % VAL and 2 % VAL co-polymerised into the monolith structure. From the resulting micrographs in Figure 2.17, a small change in morphology is observed.

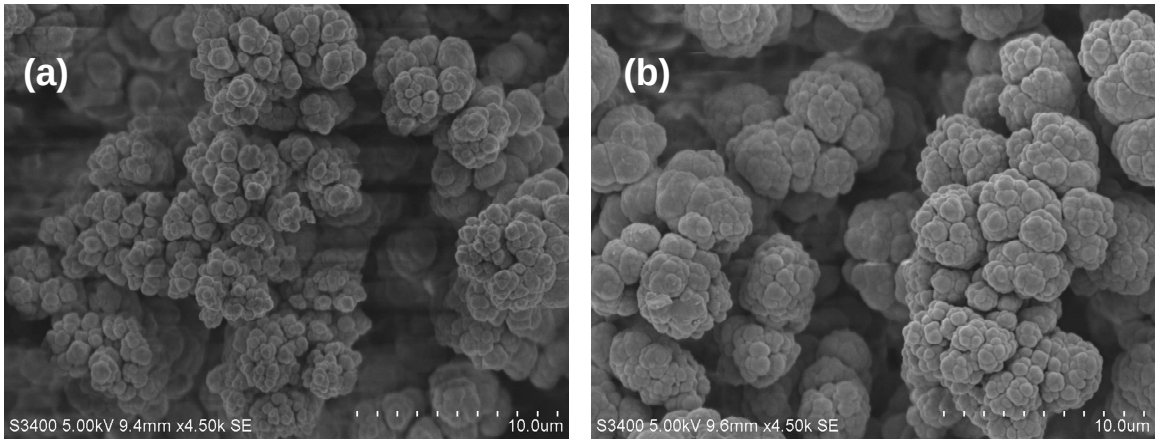

Figure 2.17: *SEM micrographs of 0 % VAL (a) and 2 % VAL (b) co-polymerised into monolith pre-cursor monomer matrix. Magnification 4, 500 x, V_{acc} 5 kV. Secondary electron detection.*

As discussed above, the change in monolith pore size is due to the difference in solvation ability of the porogen during the polymerisation. In a previous report of monolith formation using the co-polymerisation method, the effect of co-monomer on resulting pore size was not investigated, and so, the change in monolith porosity was not monitored. In co-polymerised gradients, where the change in porosity was not monitored, and so the efficiency of the separation cannot be solely based upon the performance of the gradient.

2.4. Conclusions

Scanning C^4D has been presented as a simple and rapid means of visualising monolithic stationary phase gradients, non-invasively, for the first time in the characterisation of stationary phase gradients. Using photo-grafting or segmented co-polymerisation methods, stationary phases incorporating a gradient of charged ion exchange groups have been prepared. Accurate visualisation of the axial coverage of charged groups along the column length permitted columns of different gradient profiles to be directly compared and subtle irregularities in gradient form could be identified. An investigation was carried out using this detection method, in the optimisation of stationary phase gradient production. The use of sC^4D has been shown to expose the location of voids in the stationary phase as well as showing the spatial

distribution of charged functional groups along a polymeric monolithic capillary column. The chromatographic ability of the column was evaluated and deemed not suitable to the purpose of separations due to low capacity. However, the production of a gradient, and its accurate profiling, was achieved. This is a novel demonstration, and with new information regarding the production of low capacity stationary phase gradients, the method can be further optimised for future chromatographic endeavours.

2.5. References

[1] Pucci, V., Raggi, M.A., Svec, F., Fréchet, J., *J. Sep. Sci*., 27, 2004, 779.

[2] Maruška, A., Rocco, A, Kornysova, O., Fanali, S., J. *Biochem, Biophys. Methods*, 70, 2007, 47.

[3] Brennen, R., Yin, H., Killeen, K., *Anal. Chem*. 79, 2007, 9302.

[4] Rohr, T., Hilder, E., Donovan, J., Svec, F., Fréchet, J., *Macromolecules*, 36, 2003, 1677.

[5] Gillespie, E., Connolly, D., Macka, M., Nesterenko, P. N., Paull, B., *Analyst*, 132, 2007, 1238.

[6] Connolly, D., O' Shea, V., Clark, P., O' Connor, B., Paull, B., *J. Sep. Sci*., 30, 2007, 3060.

[7] Hiemenz, P., Lodge, T., *Polymer Chemistry*, Second Edition, CRC press, 2007.

[8] Vesely, D., *International Materials Reviews*, 53, 2008, 299.

[9] Lou, Q., Zao, H., Xiao, X., Guo, Z., Kong, L., Mao, X., *J. Chromatogr. A*, 926, 2001, 255.

[10] Ren, D., Penner, N. A., Slentz, B. E., Inerowicz, I., Rybalko, M., Regnier, F. E., *J. Chromatogr. B*, 1031, 2004, 87.

[11] Zhang, Y., Li, W., Wang, X., Qu, L., Zhao, G., Zhang, Y., *Anal Bioanal Chem* 394, 2009, 617.

[12] Peterson, D. S., Rohr, T., Svec, F., Frechet, J. M. J., *Anal. Chem*., 75, 2003, 5328.

[13] Gillespie, E., Connolly, D., Nesterenko, P., Paull, B., *J. Sep. Sci*., 32, 2009, 2659.

[14] Heilmann, S., Rasmussen, J., Krepski, L., *J. Poly. Sci. Part A: Polm. Chem*., 39, 2001, 3655

[15] Bolanos-Garcia, V., Davies, O., *Biochimica et Biophysica Acta*, 1760, 2006, 1304.

[16] Tsukagoshi, K., Shimadzu Y., Tatsuhiko, Y., Riichiro, N., *J. Chromaotgr. A*, 1040, 2004, 151.

[17] Rånby, B., *Polym. Eng. Sci.*, 38, 1998, 1229.

Chapter 3.0

Production and characterisation of photo-grafted stationary phase gradients upon polymer monoliths.

"Progress is not an illusion; it happens, but it is slow and invariably disappointing."

George Orwell.

3.1. Introduction.

Following column profiling using sC^{4}D, as described in Chapter 2, the technique of on-column C^{4}D was used to observe the separation of a mixture of divalent metal cations. With the mobile nature of C^{4}D the detector cell could be moved along the column, changing the L_{eff} as described previously [1]. As described within Chapter 2.0, the co-polymerisation of a functional monomer resulted in a column incorporating a stationary phase gradient, unsuitable for applications in chromatographic separations due to its low density of surface functional groups. An alternative approach is in the use of photo-initiated grafting procedures to produce a gradient localised at the surface of the monolithic column. However, due to difficulties in using commercially available optical filters (e.g. availability of required optical density), a gradient can be prepared using photo-masking methods and varied photo-grafting energy.

In the process of photo-grafting, the grafting density can be controlled using monomer concentration, and initiating energy. Rohr *et al*. [2], reported that by increasing the energy applied to a column or masked zone of a column, an increase in the density of cross-linked grafted groups would result. Using this information, a photo-grafted gradient was produced by Pucci *et al*. [3], using a commercially available neutral density filter, which provided an attenuation in UV energy axially along the column. The group also used a moving shutter to produce a linear gradient of grafted functional groups along a polymer monolithic column. The characterisation technique used by the group was summarised in Chapter 1, Section 1.16, which ultimately resulted in the destruction of the column by cutting the column into cross-sections.

Similarly, Urbanova *et al*. [4] also reported the use of a moving shutter, in the fabrication of a gradient of hydrophobic monomer (lauryl methacrylate, LMA) across a glass thin layer chromatography (TLC) plate, upon which an immobilised porous polymer layer of glycidyl methacrylate-*co*-ethylene dimethacrylate (GMA-*co*-EDMA) was grafted. The resulting gradient was verified by measuring the contact angle of water, across the TLC plate, which ranged from 0 ° to 135 ° for the hydrophobic "corner" of the TLC plate. The presence of a gradient was confirmed in these two publications [3,4], however, variations in the speed of the moving shutter could result

in variation of the desired gradient profile. In order to detect such variation, a vast number of contact angle measurements would be required, making this approach somewhat impractical.

Using photo-grafting techniques, Gillespie *et al*. [5] investigated the increase in grafting energy upon "zones" of grafted monomer (2-acrylamido-2-methyl-1-propanesulphonic acid, AMPS), using non-invasive sC^4D. With increasing UV irradiation, the detector response of the grafted zone increased to a point, at which a levelling off in the signal occurred (Figure 3.1). The authors reported that the detector response was due to the uppermost layer of grafted polymer of highly cross-linked polymer grafts. The detector response was proportional to the grafting density, which increased with increasing UV irradiation. Using a similar grafting strategy, a column expressing an increase in graft density could be produced using photo-grafting techniques.

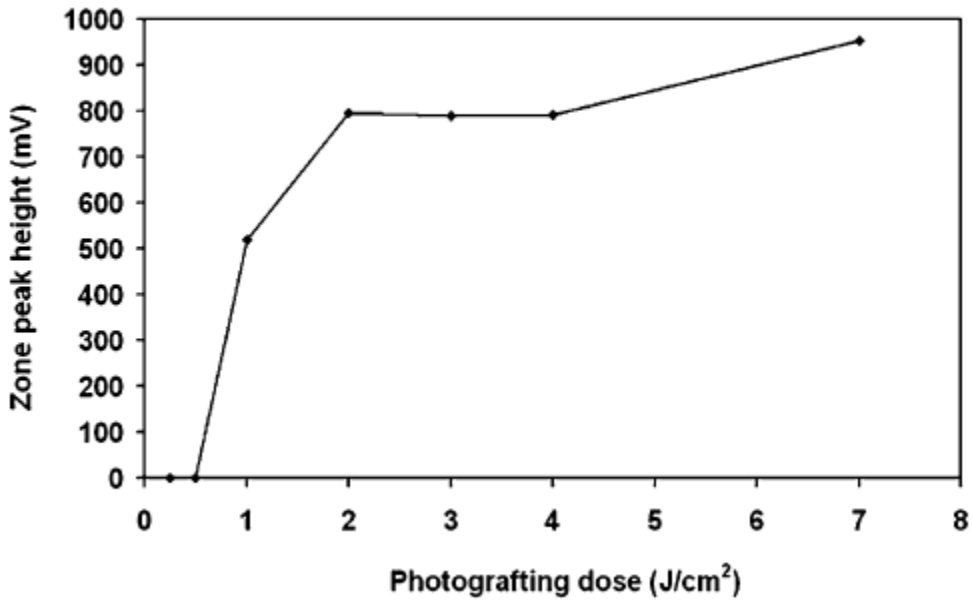

Figure 3.1: *Plot of maximum zone detector response (mV) with respect to the irradiation energy (J/cm^2) used for grafting of zones of AMPS to a poly(BuMA-co-EDMA) monolithic column [5].*

In isocratic elution, there should be no change in the retention factor, *k*, throughout the separation [1,6]. In gradient elution, however, the retention factor changes as the separation progresses, for example with an increase in solvent strength [7]. Conventional gradient programmes consist of an increase in solvent strength, (e.g.

ACN/MeOH concentration for reversed-phase chromatography) over time. To optimise gradient elution protocols, a series of experiments are generally carried out to investigate the effect of varying the solvent strength, upon the retention of the analyte in question. Many groups use this process in an effort to model and predict retention data for a wide range of separations. Reports on retention modelling usually consist of a plot of *k* (*k'*) or log *k* versus a multitude of various factors, such as pH [8] and content of organic modifier (volume fraction, φ) [7,9,10]. During gradient elution, the logarithms of the analyte retention factors decrease gradually with time from the start of the gradient [7].

In 1998, Row [9] reported on different retention models for the dependency of *k* on varying mobile phase composition (i.e. methanol or ACN). In that study, *k* (expressed as capacity factor *k'*) was plotted against the volume fraction of methanol in a reversed-phase separation of a number of analytes, in which the capacity factor decreased with an increase in the volume fraction of organic modifier (methanol) within the mobile phase. In a similar report, Galaon *et al.* [10] constructed a plot of log *k'* versus organic modifier content, which demonstrated a gradual decrease in log *k'* with an increasing volume fraction of organic modifier (ACN) in the mobile phase. This is illustrated below, in Figure 3.2. The change in retention factor, *k*, is determined by the ratio of analyte in the stationary phase, to that of the analyte in the mobile phase. Changing the retention factor would therefore require a change in column capacity, and/or solvent strength.

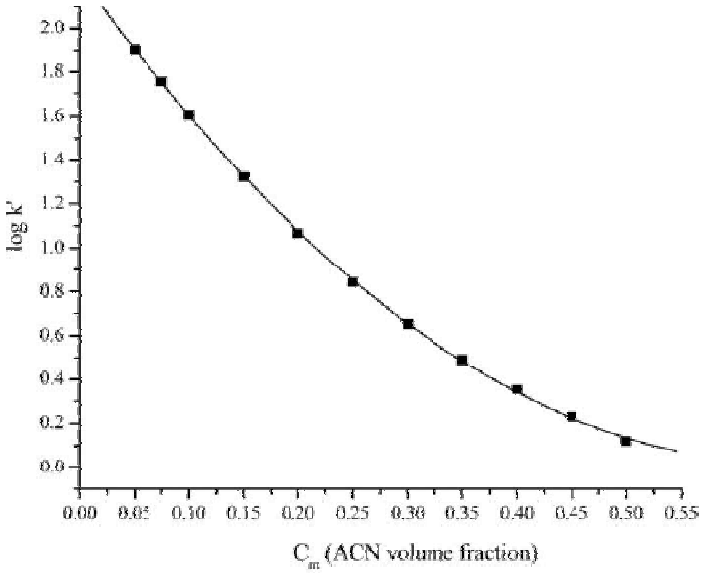

Figure 3.2: *Dependency of log k' of salicylic acid on organic modifier content in mobile phase [10].*

In a similar report, a plot of *k* versus effective column length (L_{eff}) was constructed for a silica monolithic column coated with surfactant in a homogeneous (isotropic) manner, in the separation of anions [1]. With the aid of C^4D, a plot of *k* at various L_{eff} could be constructed and evaluated. The C^4D cell was moved along the column at a spatial constant interval, and the separation was performed at each detector location. From the data generated, the group noted a deviation in *k* across the column, leading to the assumption that the surfactant coating responsible for the separation mechanism was "bleeding" from the column, i.e. the concentration of immobilised surfactant was lower at one end of the column. The group indicated that this type of experiment could be used to improve stationary phase modification methods to achieve a more homogeneous distribution of modifier along the column.

The aim of this work was to prepare a poly(butyl methacrylate-*co*-ethylene dimethacrylate) stationary phase incorporating a gradient of cation exchange groups via photo-initiated surface grafting of functional monomer (sulphopropyl methacrylate), and to map the resulting distribution of functional groups along the column length using sC^4D. In addition the chromatographic performance of the resulting gradient stationary phase was of interest, and so, the C^4D cell was used in stationary mode (i.e. on-column) at numerous on-column *loci* to visualise the on-going separation of a sample mixture of two divalent cations, Mg^{2+} and Ba^{2+}. Since the C^4D cell can be easily moved along a capillary column, it was suitable for the non-invasive evaluation of the chromatographic separation (via retention factor, *k*) occurring on-column [1], which was compared to the relative capacity observed along the column.

3.2. Experimental

3.2.1. Instrumentation

As described in Chapter 2.0, Section 2.2.1 with the following additions. For injection of cation standards onto the column, a 20 nL automated injection valve was used (Vici Valco Instruments Co. Ltd., Switzerland). All chromatographic studies were performed with a Waters nanoAcquity pump (Waters, Milford, MA, USA) at 1 µL/min unless otherwise stated. For the detection of separated divalent cations, C^4D was used as a non-suppressed on-column conductivity detector. The excitation

frequency was set to 2x high, voltage set to -12 dB, gain set to 50 %, and an offset of 001 was used, unless otherwise stated.

3.2.2. Materials and reagents

As described in Chapter 2.0, Section 2.2.2, with the following additions. Lauryl methacyrlate (LMA), sulphopropyl methacrylate potassium salt (SPM), ethylenediamine, nitric acid, and magnesium chloride were purchased from Sigma-Aldrich (Dublin, Ireland) and used as supplied. Barium chloride was purchased from BDH Laboratory Supplies (Poole, England) and used as supplied. Eluents were prepared from 0.25 m*M* and 0.56 m*M* ethylenediamine, titrated to pH 4 using nitric acid (~0.1 m*M*), which was subsequently filtered using 0.45 µm nylon 66 filter paper (Millipore, Bedford, MA, USA).

3.2.3. Scanning C^4D

sC^4D was performed as described previously in Chapter 2.0, Section 2.2.3. Following grafting the columns were washed with a buffer of 10 m*M* ethylenediamine acidified to pH 4, henceforth called Buffer 1. For sC^4D profiling, the columns were scanned in a buffer consisting of 0.25 m*M* ethylenediamine, where the pH was adjusted to approximately pH 4, using dilute nitric acid (0.1 m*M*), henceforth called Buffer 2. This buffer was also used as an eluent for the separation of divalent metal cations. It must be noted that due to the length of column fittings, and the size of the detection cell some areas of columns could not be measured; ~ 5 mm from the end of the column, and ~15-20 mm at the column head.

3.2.4. Vinylisation of fused silica capillary

Fused silica capillary was vinylised using a procedure described previously in Chapter 2.0, Section 2.2.4.

3.2.5. Fabrication of monolithic columns

3.2.5.1. Preparation of BuMA-co-EDMA monoliths for gradient and isotropic columns

In order to create a grafted gradient, a homogeneous monolith must first be fabricated. BuMA-*co*-EDMA monoliths were prepared using a mixture of 24 %

BuMA, 16 % EDMA and 60 % decanol (porogen). The initiator, 2,2-dimethoxy-2-phenylacetophenone (DAP), was present to 1 % w.r.t total monomer concentration. The column housing (fused silica capillary) was filled with this precursor solution, via capillary action, and was sealed using rubber septa. The monolith precursor solution was then subjected to UV initiated polymerisation, *in situ*, using 2 J/cm^2 UV energy. Following polymerisation, the column was washed with methanol for 1 h to remove any un-reacted monomer. Prior to sC^{4}D profiling the column was flushed with water, until a stable detector response was obtained (1 h). In total, eight monolithic columns were fabricated using this technique, as shown in Table 3.1. Introduction of surface functional groups was dependant on post polymerisation modification, and so, the above monolith technique could be used for both gradient and isotropic columns (as defined by Maruška and co-workers [11]). A total of eight monolithic columns were prepared using this method, and were denoted as shown in Table 3.1. The monolithic columns were then modified further, as outlined in section 3.2.5.3.

3.2.5.2. Preparation of LMA-co-EDMA monolith for isotropic column

Another homogeneous monolith was prepared from LMA and EDMA precursors. For the isotropic column, a LMA-*co*-EDMA monolithic column was fabricated using 24 % LMA, 16 % EDMA with a binary porogenic system of 1, 4-butanediol (14.5 %) and 1-propanol (45.5 %). The initiator, DAP, was present to 1 % w.r.t total monomer concentration. The capillary was filled with this mixture and photo-polymerisation was achieved using 2 J/cm^2 UV energy. The column was washed with methanol for 1 h, to remove any un-reacted monomers, followed by water, for 1 h (flow rate 1 µL/min) prior to sC^{4}D profiling. To compare the effect of a gradient upon the separation, a column grafted with a homogeneous (isotropic) density of charged functional monomer across the column was prepared. The resulting columns were further modified as outlined in the following sections.

3.2.5.3. Immobilisation of initiator to polymer monoliths

Both the BuMA-*co*-EDMA and the LMA-*co*-EDMA columns were subjected to two step grafting. The photo-initiator, benzophenone, was immobilised onto the surface as described previously [12]. Briefly, a 5 % solution of benzophenone in methanol was deoxygenated via nitrogen sparging for 10 mins, and was pumped across the column at 1 µL/min for 1 h. The column was end-capped and irradiated

within the range of 0 to 2 J/cm^2 of UV energy as specified in Table 3.1, and was subsequently washed with methanol for 1 h to remove any un-reacted benzophenone. Columns BuMA-Iso 1-4 were reacted with benzophenone using 0 to 1 J/cm^2 UV irradiation. Columns BuMA-Iso 5, BuMA-Grad 2, BuMA-Grad 3, and LMA-Iso 1 were immobilised with benzophenone using 2 J/cm^2 UV irradiation, to increase the uniformity of the resulting detector response, provided by the grafted SCX groups.

Table 3.1: *List of columns fabricated with the dose of UV energy used during photo-grafting procedures. BP stands for benzophenone, SPM is sulphopropyl methacrylate.*

Gradient columns

Column	Monomer	BP dose (J/cm^2)	SPM dose (J/cm^2)		
			Zone 1	Zone 2	Zone 3
BuMA-Grad 1	BuMA-*co*-EDMA	2	1	2	3
BuMA-Grad 2*	BuMA-*co*-EDMA	1	0.25	0.5	0.75
BuMA-Grad 3	BuMA-*co*-EDMA	2	0.25	0.5	1

Isotropic columns

Column	Monomer	BP dose (J/cm^2)	SPM dose (J/cm^2)
BuMA-Iso 1	BuMA-*co*-EDMA	0	0
BuMA-Iso 2	BuMA-*co*-EDMA	1	0.075
BuMA-Iso 3	BuMA-*co*-EDMA	1	0.1
BuMA-Iso 4	BuMA-*co*-EDMA	1	0.25
BuMA-Iso 5	BuMA-*co*-EDMA	2	0.5
LMA-Iso 1	LMA-*co*-EDMA	2	0.5

**Note; A fourth zone was included in which no grafting occurred (before zone of 0.25 J/cm^2), offering a blank for sC^{4}D purposes.*

3.2.5.4. Optimisation of grafting using sC^{4}D

Four columns were prepared to determine the optimum grafting technique and UV energy dose range. The columns denoted columns BuMA-Iso 1 to 4, were prepared as outlined above in Table 3.1. In order to optimise the grafting energy, the UV dose was varied for a number of columns, from 0 J/cm^2 (blank) to 0.25 J/cm^2 in order to determine the lowest amount of UV energy required for grafting. Each column was modified along the entire column length (isotropic) in two distinct steps; immobilisation of initiator (5 % benzophenone), and a grafting of the functional monomer SPM, using a solution of 4 % concentration. Column BuMA-Iso 1 was not modified to provide a "baseline" for future scans. The applied energy doses are summarised in Table 3.1. Following the grafting procedures, the columns were subjected to sC^{4}D profiling at 5 mm intervals in Buffer 2. The detector settings for this experiment were set to 2x high, -6 dB, 50 % gain, 001 offset.

In order to ascertain the maximum energy required for grafting, a single column (BuMA-Grad 1) was grafted with three sequential zones of increasing UV energy, with varying zone length by means of photo-masking (Section 3.2.5.5). The column was scanned in Buffer 2 prior to grafting to provide a reference blank. Zone 1 measured 10 mm in length and was exposed to a dose of 1 J/cm^2 UV energy. Similarly, zone 2 measured 20 mm in length and was exposed to a dose of 2 J/cm^2 UV energy. Zone 3 measured 30 mm in length and was exposed to a dose of 3 J/cm^2 UV energy. Following grafting the column was scanned in Buffer 2, and a plot of detector response versus detector position along column could be constructed.

3.2.5.5. Protocol for the photo-grafting of a stepped gradient

A solution of 4 % sulphopropyl methacrylate (SPM) was prepared in water and was deoxygenated via nitrogen sparging for 10 mins. The SPM solution was pumped across the column, previously immobilised with benzophenone, for 1 h. The column was then end-capped and subjected to the grafting protocol. To allow the exposure of different areas of the column to different UV doses, certain areas must be covered with a photo-mask, during exposure. The column was divided into a number of zones (n =3) named Zones 1, 2 and 3. Each zone was subjected to a dose of UV irradiation, in an additive approach as shown in Figure 3.3. The column was masked exposing a length of 30 mm of monolithic column, designated Zone 1. This segment

was exposed to 0.25 J/cm^2 UV energy. The Zone 2 segment was un-masked, and both Zones (1 & 2) were exposed to another 0.25 J/cm^2 UV energy. The Zone 3 segment of the column was un-masked and all 3 zones were exposed to a final dose of 0.25 J/cm^2 UV energy.

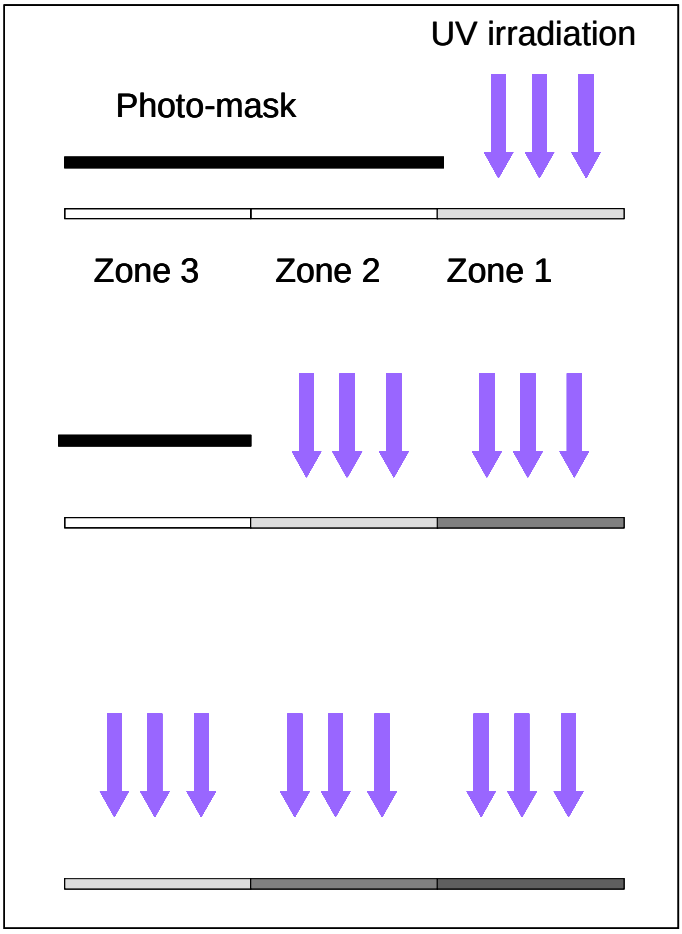

Figure 3.3: *Schematic photo-grafting protocol used in the formation of a stepped gradient. Density of grafted zones illustrated with grey scaling.*

This resulted in a column comprising of three zones, with total grafting UV energy of 0.25, 0.5 and 0.75 J/cm^2 applied, respectively. The described technique could be adapted in order to achieve higher graft density, as seen in Table 3.1. Following the grafting procedure, the column was then washed with methanol for 1 h, to remove any un-reacted monomer. Subsequently, the column was washed with Buffer 1 (10 m*M* ethylenediamine buffer, pH 3.9) for 3 h. The column was then equilibrated in Buffer 2 (0.25 m*M* ethylenediamine, pH 4) prior to sC^{4}D profiling.

3.2.5.6. Grafting the isotropic monoliths

For comparison against the stationary phase gradient column, isotropic columns LMA-Iso 1 and BuMA-Iso 5 were prepared, and following immobilisation of benzophenone, the columns were grafted with 4 % SPM using 0.5 J/cm^2 UV energy. This single dose of UV energy was applied to the entire length of the column, producing a homogeneous ligand density throughout. The column was washed with methanol for 1 h at 1 µL/min, to remove any un-reacted monomers, followed by water at 1 µL/min for 1 h. The column was then flushed with Buffer 1 for 3 h, followed by equilibration with Buffer 2 prior to sC^{4}D profiling.

3.2.5.7. SEM analysis of gradient grafted monolithic column

For SEM analysis, column BuMA-Grad 3 was cut into three cross-sections, corresponding to the zones grafted to the column. A final and fourth cross-section was cut from column BuMA-Grad 2, where no grafting of SPM occurred providing a "blank". The monolithic samples were subjected to gold sputter coating for 2 mins. The samples were mounted, and were analysed using a low accelerating voltage (V_{acc}) in order to view surface features. For comparison, magnification was held constant for each sample.

3.2.5.8. Determination of k with varying effective column length (L_{eff})

In order to determine the effect of the stationary phase gradient upon the retention factor, *k*, sixteen on-column detector positions were assigned. Using the mobile nature of C^{4}D, the detector could be moved to a variety of on-column positions, allowing for the observation of the separation along the length of the column, non-invasively. In this experiment, the selected metals were injected onto the column in triplicate, with each chromatogram recorded using stationary on-column C^{4}D. This was repeated for all sixteen on-column detector positions. Following each set of three separations, the detector was moved by 4 mm to another on-column position, increasing the L_{eff} by a further 4 mm, for all remaining detector positions. The resulting *k* was used to construct a plot of *k* versus L_{eff}. An ideal way to observe the effect of the gradient upon the separation was to change the direction of flow through the column, in order change the shape of the gradient relative to the separation. The chromatograms were recorded at the sixteen detector positions on-column (in triplicate), in both directions of flow through the column, as shown in

Figure 3.4 (a) and (b). In Figure 3.4 (a) the direction of flow is shown to be in the forward direction, whilst (b) illustrates the reversed direction of flow.

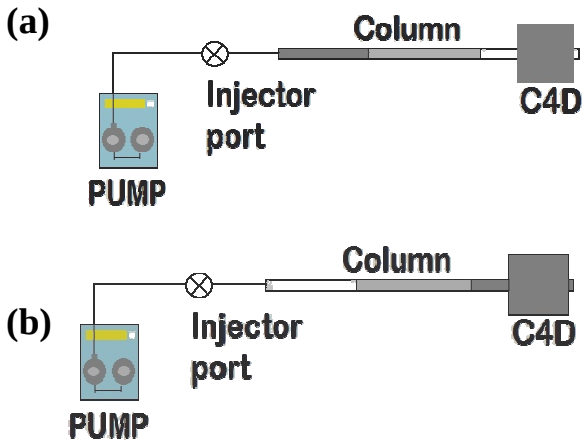

Figure 3.4*: Diagrammatic representation of the forward direction of flow (a), and the reversed direction of flow (b) through column BuMA-Grad 3.*

3.3. Results and discussion

3.3.1. Optimisation of grafting energy using sC^{4}D profiling

Columns BuMA-Iso 1 through to BuMA-Iso 4 were grafted with increasing intensities of UV energy with each column. Column BuMA-Iso 1 was not grafted with functional monomer to provide a reference blank for the columns BuMA-Iso 2 to 4. Following grafting, the columns were profiled using sC^{4}D. In doing so, the resulting detector response was recorded and correlated to the UV energy applied to the grafted column. The resulting plot would therefore illustrate the lowest possible UV energy dose required to obtain grafting of the monomer to the monolithic surface. The resulting plot for can be seen below in Figure 3.5.

It should be noted, as mentioned in Chapter 2, due to the length of fittings on the columns the total column length cannot be measured. Also, due to the dimensions of the detector, approximately 2 mm at the end of the column cannot be measured. The plot in Figure 3.5 illustrates the lowest possible amount of UV energy required for grafting, which is 0.1 J/cm^2. In a similar study [5], investigating the effect of grafting energy upon the resulting detector response, the authors noted that using a grafting energy below an intensity of 1 J/cm^2, no detector response was observed.

They concluded that the required activation energy was not achieved for zones of lower grafting intensity.

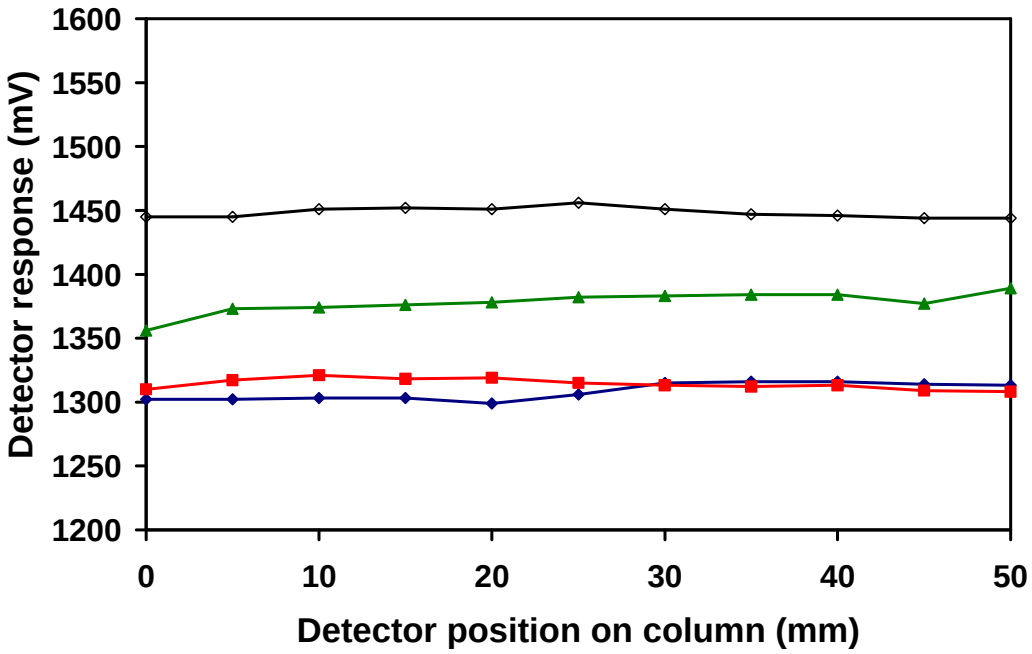

Figure 3.5: *sC^{4}D profiles for BuMA-Iso 1 (—♦—), BuMA-Iso-2 (—■—), BuMA-Iso 3 (—▲—), and BuMA-Iso 4 (—◊—) in Buffer 2. Scans performed in 5 mm intervals at a flow rate of 1μL/min. Grafting UV energy varied with each column as outlined in Table 3.1.*

A similar effect was observed in this work, as UV energy above 0.075 J/cm^2 was required for grafting to occur. The % change in detector response was calculated for each column relative to the blank column BuMA-Iso 1. The detector response of BuMA-Iso 4 (with a UV grafting intensity of 0.25 J/cm^2) resulted in a higher % change in detector response of 10.7 % relative to the blank column (BuMA-Iso 1). Column BuMA-Iso 3 provided a % change in detector response of 5.3 % relative to the blank column, with BuMA-Iso 2 providing only 0.45 % change in detector response. Due to these characteristics, the lowest grafting energy dose for the gradient column was 0.25 J/cm^2.

To find the maximum grafting density, another column, BuMA-Grad 1 was grafted with three zones of sequentially increased UV energy, with 1 J/cm^2, 2 J/cm^2, and 3 J/cm^2. The resulting profile can be seen in Figure 3.6. From the data shown in

Figure 3.6, the blank demonstrated a homogeneous polymer density along the column length.

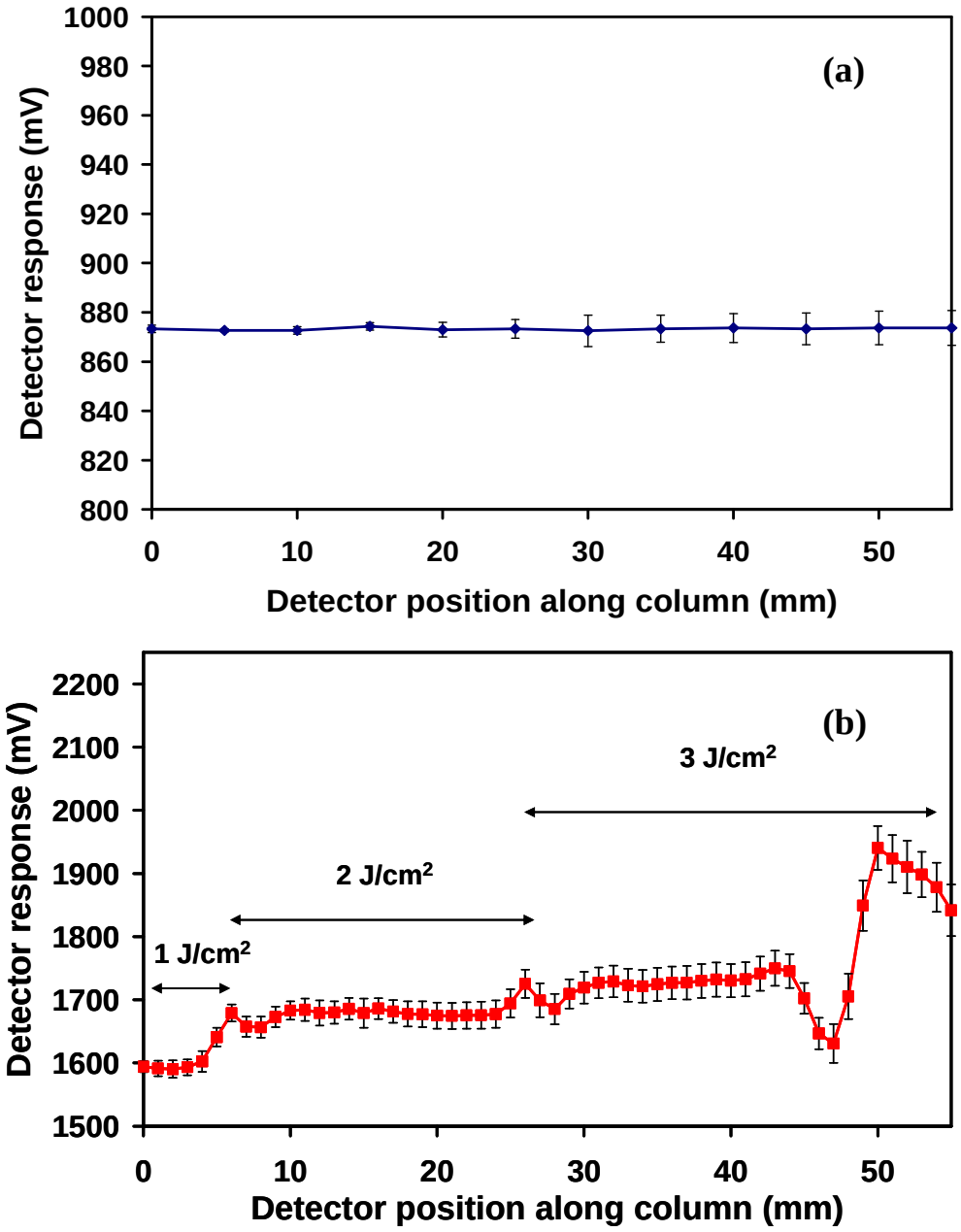

Figure 3.6: *sC⁴D profile of BuMA-Grad 1 prior to (a) and following grafting (b) with SPM. Zone 1 was 10mm of 1 J/cm², Zone 2 was 20 mm of 2 J/cm², and Zone 3 was 30 mm of 3 J/cm². Scans performed in triplicate using Buffer 2, at a flow rate of 1 µL/min.*

All three zones exhibited an increase in detector response relative to the blank column. Zone 1, which was grafted using 1 J/cm² UV energy, resulted in a % change

in detector response of 82 % relative to the blank column. Similarly Zone 2 exhibited a % change of 92 % in detector response with respect to the blank column profile. From Figure 3.6, the observed detector response for the three zones does not change significantly across the column. However, in Zone 3 an increase in detector response (approximately +300 mV) was evident beyond 45 mm. This feature may be due to a section of localised increased grafted SPM, because such a significant increase was not observed across the length of the unmodified zone. The column was scanned in triplicate, with a resulting % RSD for this feature no greater than 2.2 %. In using sC^4D to profile the column, this section of grafting deviation was discovered, which can be removed by cutting the column, which is an obvious benefit of the profiling method.

In the remainder of the column, an increase of ~ 5 % is observed between the average detector responses of each zone. This indicated a levelling off in detector response. Gillespie and co-workers [5] grafted BuMA-*co*-EDMA monoliths with a charged monomer AMPS. Each zone was grafted with increasing UV irradiation, and the resulting conductivity was monitored with sC^4D. With increasing UV irradiation, they discovered the detector response did not increase between the final two zones of 3 J/cm^2 and 5 J/cm^2. They postulated that the resulting detector response was owing to the contribution of conductive groups at the surface of the grafted zone rather than the total number of underlying charged functional groups in a highly cross-linked graft. From the above results, the optimum UV energy doses for grafting therefore lay between 0.25 J/cm^2 and 1 J/cm^2.

3.3.2. Optimisation of gradient grafting, using sC^4D

A BuMA-*co*-EDMA monolith grafted with a number of zones of functional SPM monomer was fabricated first. This column contained 4 zones; Zone 1 (50 mm, 0 J/cm^2), Zone 2 (33 mm, 0.25 J/cm^2), Zone 3 (33 mm, 0.5 J/cm^2), and Zone 4 (33 mm, 0.75 J/cm^2). Zone 1 was masked for the entire grafting procedure, resulting in an unmodified (un-grafted) section of monolith. The column was scanned in Buffer 2 prior to and following the grafting procedure. The resulting plot can be seen below in Figure 3.7. The resulting plot for the column prior to grafting (blank), shows a flat profile across the column indicating the absence of any possible deviations in polymer density. The resulting gradient profile illustrated the sequential increase in graft

density with an increase in UV energy dose. This mirrored the work performed by Gillespie *et al*. [5] where the detector response of grafted zones was compared to the energy applied during grafting procedures.

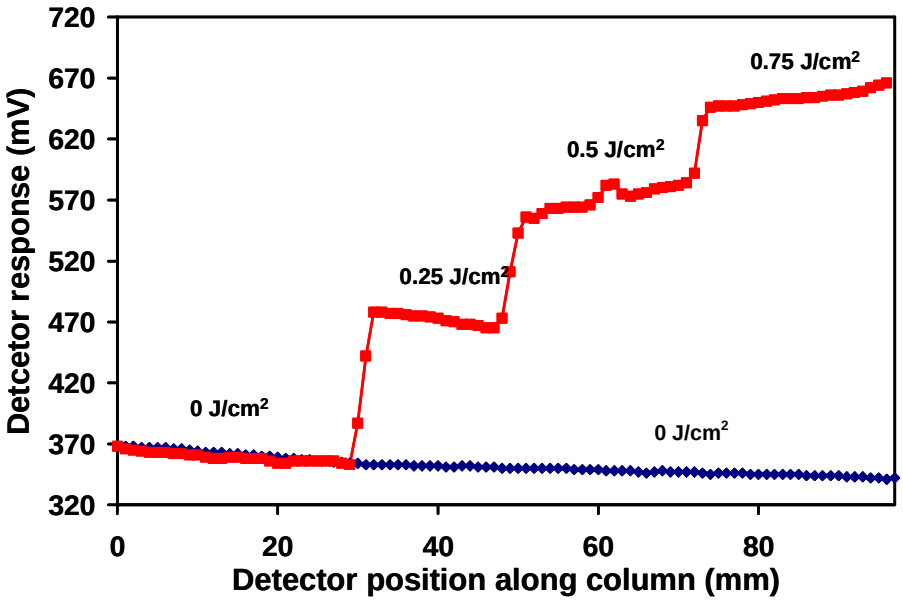

Figure 3.7: *sC^{4}D profile of BuMA-Grad 2 prior to grafting (—♦—) and following grafting (—■—). The signal for SPM was normalised to the blank by taking the difference between the "blank" (Zone 1) of the gradient column and the column prior to grafting, for illustrative purposes. Scan performed once with 1 mm increments, using Buffer 2 at a flow rate of 1 µL/min.*

For a BuMA-*co*-EDMA column grafted with distinct zones of a charged monomer (AMPS), the group noted an increase in detector response for the zones irradiated with an increased dose of UV energy. The same result is noted in this work. From the plot above in Figure 3.7, the resulting detector response increased for zones of increasing UV graft energy, within the desired range.

In order to increase the uniformity of the resulting grafted zone, the irradiation time can be increased. Rohr *et al.* [13] reported the increase in fluorescence intensity of zones, with a sharper boundary definition between adjacent grafted and ungrafted zones. The maximum grafting dose was determined in Section 3.3.1, resulting in a value of ≤ 1 J/cm^2. To avoid using higher grafting energy for the grafting of SPM, the energy dose used in the grafting of benzophenone was increased from 1 J/cm^2, to 2

J/cm^2 in the immobilisation procedure for BuMA-Grad 3. The grafting doses of SPM for BuMA-Grad 3 were increased relative to BuMA-Grad 2, to include 0.25 J/cm^2, 0.5 J/cm^2 and 1 J/cm^2. Following the grafting procedure, the column was scanned in Buffer 2, with the resulting plot shown in Figure 3.8.

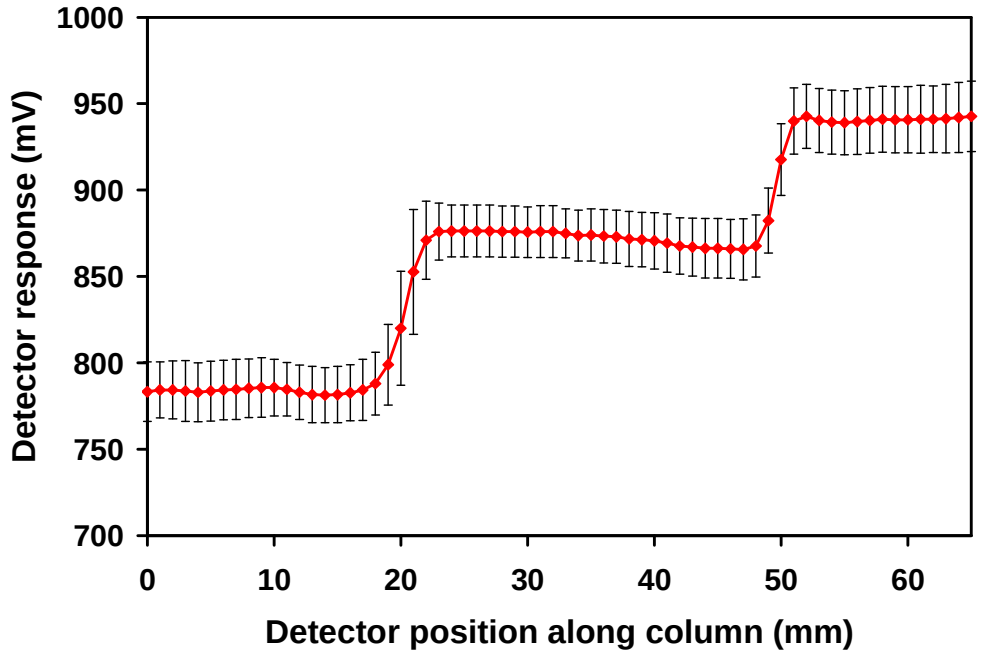

Figure 3.8: *sC^{4}D profile of BuMA-Grad 3 expressing a photo-grafted gradient, with zones grafted using UV energy doses of 0.25 J/cm^2, 0.5 J/cm^2, and 1 J/cm^2, respectively. Scan performed in triplicate in Buffer 2, at 1 mm intervals, with a flow rate of 1 µL/min. Each zone ~ 30 mm in length.*

Again, the three zones of increasing graft density can be easily seen. The resulting plot demonstrates excellent uniformity across each zone of the gradient. The scan was repeated in triplicate and a % RSD of no greater then 4.3 % was observed between replicate scans, indicating a good repeatability between profiling scans. A difference in detector response of approximately 10 % was evident between Zone 1 (0.25 J/cm^2) and Zone 2 (0.5 J/cm^2). Similarly, an increase of 7 % was observed between Zone 2 and Zone 3 (1 J/cm^2). This may be due to the levelling off effect mentioned in Section 3.3.1. Due to the uniformity of the grafted zones in the gradient column BuMA-Grad 3 this column was used in the separation of divalent metal cations (see Section 3.3.5.1).

3.3.3. SEM analysis of grafted columns

The monolith cross-sections were evaluated under a low accelerating voltage to view the surface morphology of the monolith sample. As highlighted in Chapter 2, Section 2.3.4, the formation of a gradient using co-polymerisation resulted in an increase in pore size across the column. By using grafting chemistry, it was expected that no change in pore size across the column would be observed. This was indeed the case, as from the SEM micrographs in Figure 3.9, the globule size remains similar across all four samples, spanning a range of grafting energy including 0 J/cm^2, 0.25 J/cm^2, 0.5 J/cm^2, and 1 J/cm^2. As the pore size is dependent on globule size, it can be inferred that the resulting pore size was not affected by the grafting procedures.

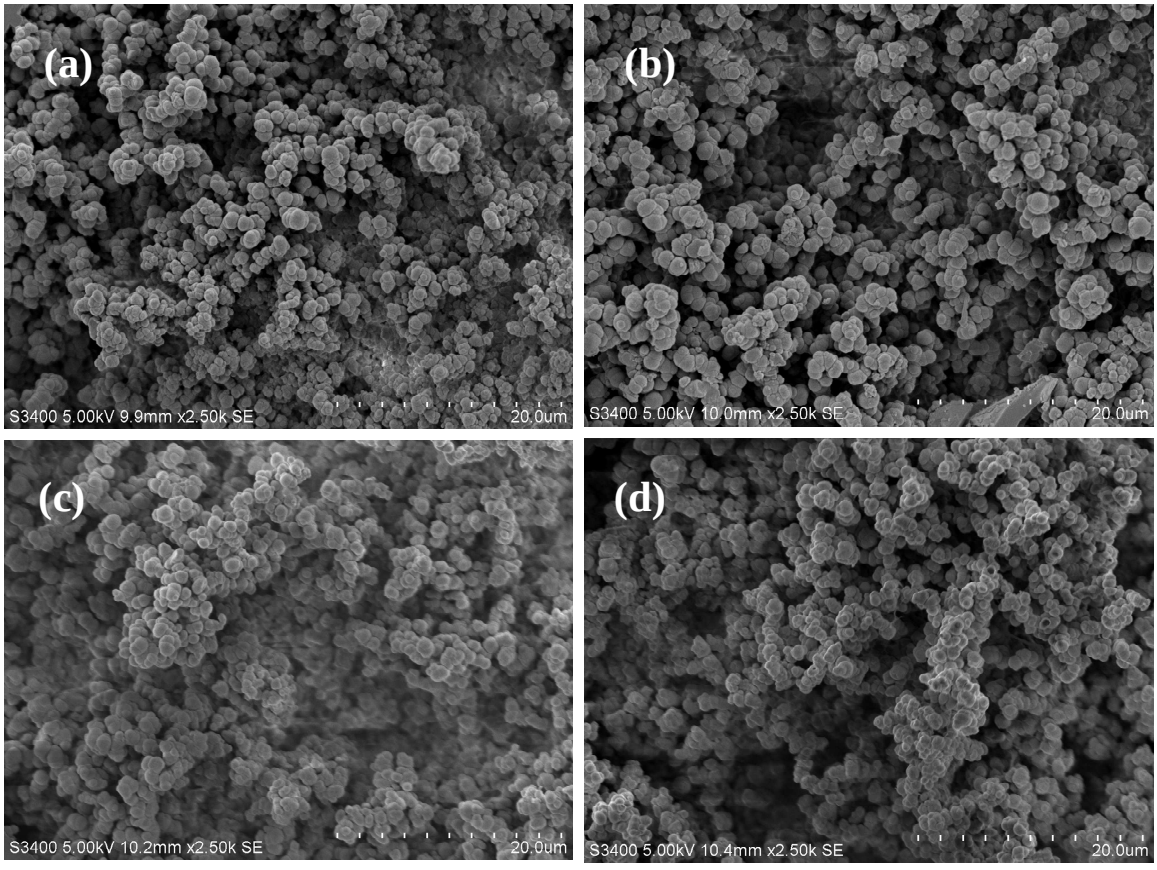

Figure 3.9: *SEM micrographs of monolith samples following grafting. BuMA-Grad 2; unmodified zone (a); BuMA-Grad 3; 0.25 J/cm^2 (b), 0.5 J/cm^2 (c), and 1 J/cm^2 (d). Magnification of 2, 500 x, V_{acc} of 5 kV, working distance ~ 10 mm.*

3.3.4. sC^{4}D profiles of isotropic columns

To cross-validate the presence of a gradient of ion exchange groups upon the stationary phase, a reference isotropic column was fabricated. This column was to incorporate a longitudinal homogeneous density of grafted monomer unlike that with a stationary phase gradient. Columns produced from BuMA (BuMA-Iso 5) and LMA (LMA-Iso 1) monomers were evaluated using sC^{4}D. Each column was grafted in a homogeneous manner along the column i.e. the columns were irradiated with a single dose of UV energy with no masks between the light source and the column. The grafting energy of 0.5 J/cm^2 was used for the isotropic columns. Following grafting, the columns were profiled using sC^{4}D, with the resulting plots shown in Figure 3.10.

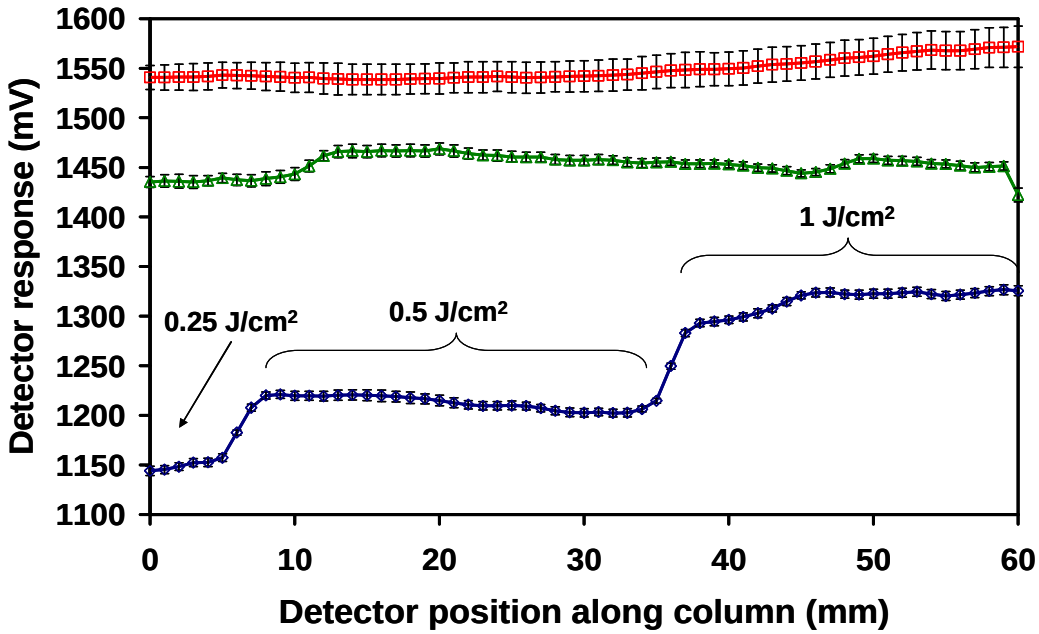

Figure 3.10: *sC^{4}D profiles of the gradient column, BuMA-Grad 3(—◊—), and isotropic columns, BuMA-Iso 5 (—□—) and LMA-Iso (—Δ—) 1. Isotropic columns were grafted with SPM (4 %) using a UV dose of 0.5 J/cm^2. Scans performed in Buffer 2 on the same day, in triplicate. Scans performed at 1 mm intervals at a flow rate of 1 µL/min.*

Firstly, the detector response of the BuMA-Iso 5 column was higher than that of the LMA-Iso 1 column by ~ 100 mV (6.2 %). The lower detector response for the LMA-*co*-EDMA column was possibly due to the change in surface chemistry (C_{12} of LMA versus C_4 of BuMA), and the change in the porous network of the monolithic column,

as a lower detector response indicates an increase in polymer density [14]. The detector response of the grafted isotropic columns was higher than expected, relative to the corresponding anticipated graft density on the gradient stationary phase. A difference of ≥ 200 mV was observed between the 0.5 J/cm^2 zone of the gradient column, and the isotropic columns (~16 % difference between BuMA-Grad 3 and LMA-Iso 1). One possible reason for this deviation may be due to the grafting protocol itself, used in the formation of the gradient. For example, the zone of 0.5 J/cm^2 grafting energy on the gradient column was produced using two sequential grafting steps of 0.25 J/cm^2, which may not be representative of a single dose of 0.5 J/cm^2. For the isotropic columns, the grafting intensity was constant and uninterrupted for the allotted grafting period, unlike that for the gradient column. To eliminate variation due to different preparations of profiling buffer, the columns were scanned on the same day, in the same buffer preparation. For the separation of divalent metal cations, the LMA-Iso 1 column was used alongside the gradient column BuMA-Grad 3. The LMA-Iso 1 column was chosen due to its increased axial ligand homogeneity relative to its BuMA counterpart.

3.3.5. Studies on the chromatographic performance of fabricated monolithic columns

In cation exchange chromatography, eluents consisting of acids such as nitric acid, are suitable for the separation of alkali metals, however, in the separation of divalent alkaline earth metals, these eluents can be ineffective [15]. Divalent cations are more strongly retained by cation exchangers, and thus, require an eluent containing a protonated divalent cation [16,17].

3.3.5.1. Chromatographic separation of divalent metal cations via cation exchange chromatography

In this work, a cation exchanger expressing sulphonic acid groups was used for the separation of alkaline earth metals. An eluent was prepared from acidified ethylenediamine (0.25 m*M*, and 0.56 m*M*), using nitric acid to reduce pH to ~ pH 4. At this pH, the predominant eluent species is that of EnH_2^{2+}, which is suitable for the elution of alkaline earth metals [15,16]. The resulting chromatograms were recorded using non-suppressed on-column C^4D detection. Two columns were selected for this

work, the gradient column BuMA-Grad 3, and the isotropic column LMA-Iso 1. In this experiment, a sample mixture of Mg^{2+} and Ba^{2+} was injected onto both columns in triplicate. With the C^4D cell as close to the column inlet as possible (as allowed for by column fittings), the first set of three chromatograms were recorded. The detector was moved by 4 mm and secured, to increase the L_{eff}. With the L_{eff} increased by 4 mm, the analytes were then injected in triplicate. This was repeated for the entire column lengths of both the gradient (BuMA-Grad 3) and isotropic (LMA-Iso 1) columns. For the gradient column (BuMA-Grad 3), two directions of flow were examined, as outlined in Figure 3.4. Chromatographic separations were first obtained for the gradient column in both directions of flow. Figure 3.11 illustrates the separation of the analytes at a L_{eff} of 28 mm, on the BuMA-Grad 3 column in both directions of flow.

The analyte peaks were detected as negative peaks, due to lower equivalent ionic conductance of the analytes compared to the acidified eluent, as observed by Fritz *et al.* [15]. The effect of direction of the gradient was easily observed from the chromatogram in Figure 3.11.

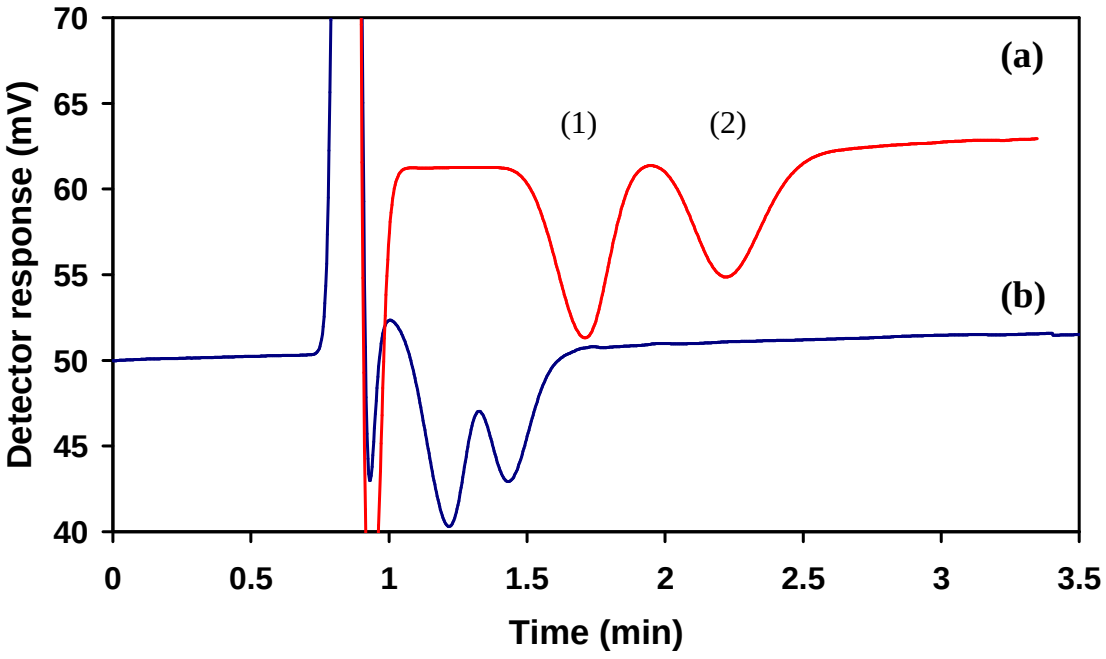

Figure 3.11: *Separation of Mg^{2+}(1) and Ba^{2+} (2) upon BuMA-Grad 3 in both the forward (a) and reversed (b) direction. Eluent 0.25 mM ethylenediamine (pH 4), flow rate 1 µL/min, L_{eff} 28 mm. Signal for (a) offset by + 60 mV, and signal (b) was offset by + 50 mV for illustration.*

The increased graft density, and thus, relative capacity at the inlet of the column in the forward direction (Figure 3.11 (a)), resulted in a separation of the two analytes, with a resolution of 1.26. For ideal separations, the resolution should lie between 1.2 and 1.5. The column in the forward direction of flow indicated sufficient separation with a minimum L_{eff} of only 28 mm.

With the column in the reversed direction of flow, the retention was lower resulting in a resolution of only 0.9 (Figure 3.11 (b)). With the column in the opposite direction of flow, the first zone encountered by the metals was the lowest graft density zone (0.25 J/cm^2). With a lower graft density the relative capacity observed in this column segment would, therefore, also be lowered with respect to the zone of highest grafting energy (1 J/cm^2). From the sC^{4}D profile in Figure 3.10, the higher detector response was indicative of a higher capacity for column LMA-Iso 1 [5]. For this column to exhibit a capacity similar to the overall capacity of the gradient column, the eluent strength was increased from 0.25 m*M* to 0.56 m*M* ethylenediamine. By increasing the eluent strength, the solute-sorbent interactions are reduced (relative to the conditions used in the gradient column) resulting in a lowered observed retention. The separation was also performed on the isotropic column (LMA-Iso 1), with the resulting chromatogram shown in Figure 3.12.

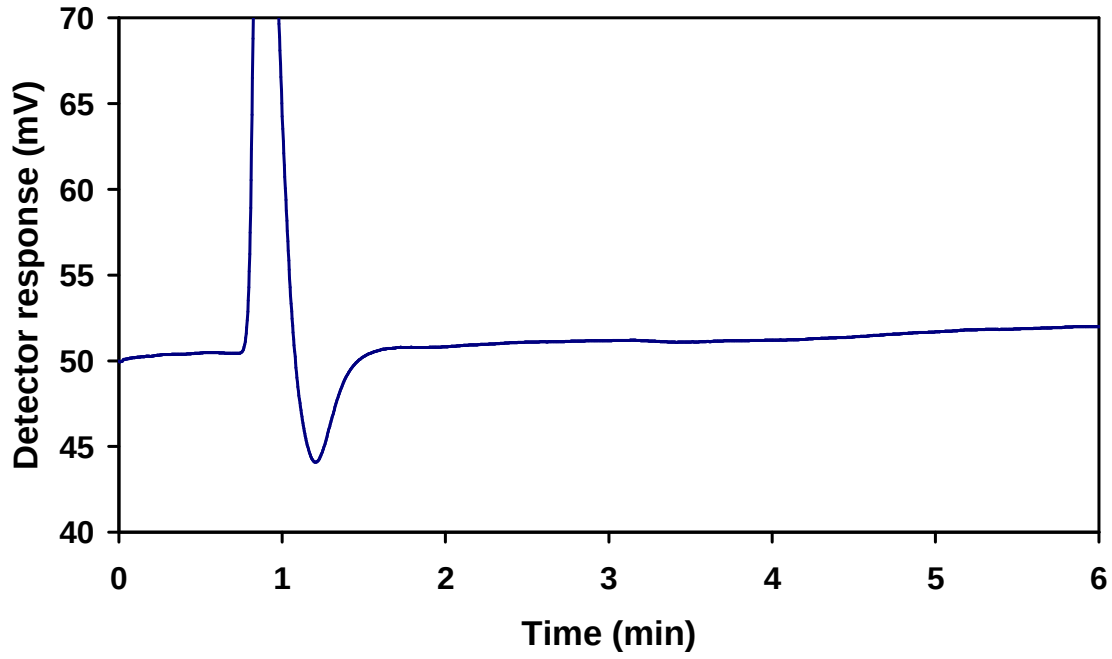

Figure 3.12: *Recorded chromatogram of metal standards of Mg^{2+} and Ba^{2+} onto the LMA-Iso 1 column. Eluent of 0.56 mM ethylenediamine (pH 4), flow rate 1 µL/min, L_{eff} 28 mm.*

Using the isotropic column (LMA-Iso 1) no retention was observed at a L_{eff} of 28 mm. The relative capacity of the column at the L_{eff} of 28 mm was obviously low, relative to the gradient column in both column directions (Figure 3.11). For an effective separation to occur upon the isotropic column (under these conditions) a longer L_{eff} was required. Increasing the L_{eff} to 36 mm resulted in a similar resolution to the gradient column in the forward direction of flow (1.12 and 1.09, respectively). The BuMA-Grad 3 demonstrated better separation compared to the isotropic column.

The L_{eff}, for both BuMA-Grad 3 and LMA-Iso 1 columns, was increased throughout the experiment until the final detector position, with a L_{eff} of 88 mm. A similar separation was expected for the gradient column, as the overall capacity of the column remained constant, independent of the direction of flow through the column. There was a longer retention time for the column in the forward direction of flow, by approximately 0.2 min. When the column was connected in the reversed direction, the entirety of the high capacity zone (1 J/cm^2) was not available as part of the calculable effective column length as shown in Figure 3.4 (b).

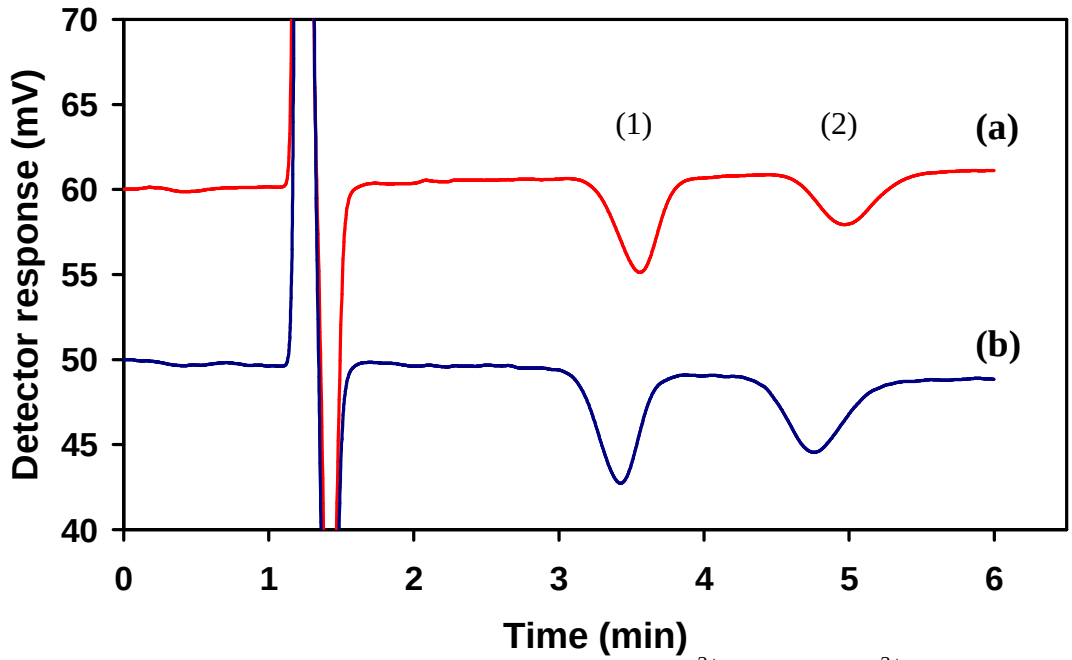

***Figure 3.13**: Chromatogram of a separation of Mg^{2+} (1) and Ba^{2+} (2) on BuMA-Grad 3 in the forward (a) and reversed (b) direction of flow, at a L_{eff} of 88 mm. Eluent 0.25 mM ethylenediamine, flow rate 1 µL/min. Signal (a) offset by +60 mV, and signal (b) offset by +50 mV for illustration.*

The column in the reversed direction did not interact with the total relative capacity of the final zone (1 J/cm^2). This was due to the size of the C^{4}D cell, which unfortunately could not be used on the remaining 2-3 mm of the column. Theoretically, if the separation was measured further (e.g. off-column), it would be expected that the separation time would be similar, with little deviation, for the column in both directions of flow.

The final resolution for the forward direction of flow was 2.22, whilst the resolution in the reversed direction of flow was slightly lower, at 2.12. To better understand the effect of the gradient upon the separation, the separation was performed on the isotropic column also. The reported chromatogram in Figure 3.14 was recorded at a L_{eff} of 88 mm.

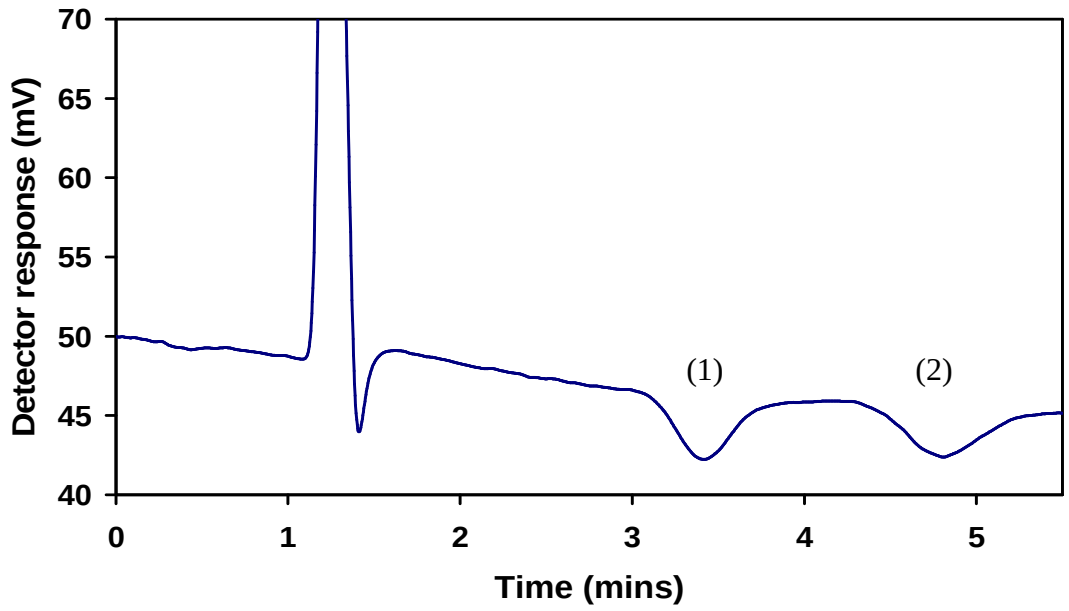

Figure 3.14: *Chromatogram of a separation of Mg^{2+} (1) and Ba^{2+} (2) on LMA-Iso 1. Eluent of 0.56 mM ethylenediamine (pH 4), flow rate 1 µL/min, L_{eff} 88 mm.*

The time required for separation was approximately 5.5 mins, similar to that for the gradient column. In the chromatogram of Figure 3.14 a shift in baseline was evident. As the C^{4}D cell was sensitive to changes in ambient temperature, this may account for the lowering of the baseline throughout the separation. The separation on the isotropic column resulted in a resolution of 2.02, lower than that exhibited by the gradient column (Rs of 2.22). A gradient column could produce a better separation, with a lower concentration of eluent when compared to the isotropic column.

3.3.5.2. Retention factor (k) and effective column length (L_{eff})

During the characterisation of a stationary phase gradient, Maruška and co-workers observed no marked change in retention factor (*k*) on a gradient column in forward and reversed flow directions [11]. When the column was reversed, there should be no change in the final *k* due to the finite amounts of total functional ligand immobilised along the column, regardless of the direction of flow through the column. The method of detection used was off-column, and so the changes in retention factor per unit column length, due to the presence of the stationary phase gradient could not be monitored through the progression of separation, but only following separation using the total column length. The group claimed band focusing occurred, similar to that of "pre-column" pre-concentration, where a large volume of diluted analyte is injected on to a column with a low elution strength solvent. When the column was placed in the forward gradient direction (Figure 3.15 (b)), this type of band compression was expected to occur. Using a reference isotropic column, the group discovered that the strength of the eluent was too strong to pre-concentrate the analytes, at the head of the column. This resulted in a broader zone width at the beginning of the chromatographic run, and so theoretically, resolution and efficiency would be lower.

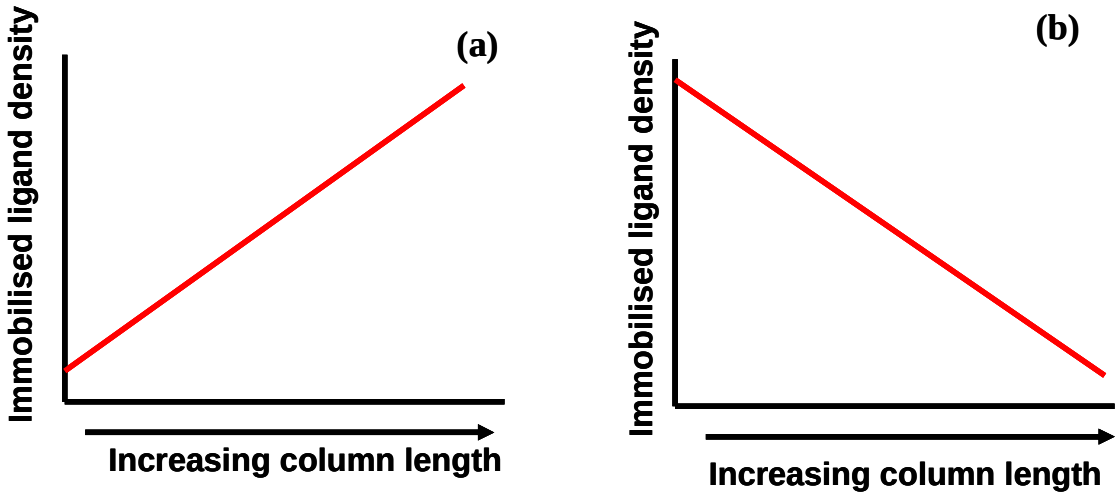

Figure 3.15: *Schematic of a gradient column in a reversed (a) and a forward direction (b), as defined by Maruška et al. [11].*

Alternatively, with the gradient column in the reversed gradient direction of flow (Figure 3.15 (a)) the group expected the chromatographic band to be focussed on-column. At a constant eluent concentration, the change in retention along the

column is attributed to the presence of the gradient of immobilised ligand. As a chromatographic band traverses the gradient with a reversed direction of flow, the band compresses due to the increasing density of immobilised ligand. With the tail of the band experiencing a lower ligand density, there would be fewer interactions between the analyte and the stationary phase with respect to a region of higher immobilised ligand density, resulting in faster elution from that region. The synergy of both processes theoretically results in a compression of the chromatographic band. The group examined this concept with a single column tested in both directions of flow. The group noted no significant change in retention factor or efficiency (plates per meter, N/m) with a change in the direction of flow through the column. This was because the overall capacity of the column was independent of the direction of flow through the column, and so, the same number of analyte-ligand interactions across the column in both column directions would be expected. As the group collected chromatograms off-column, the effects of relative capacity upon the separation were not determined.

In this work, the retention factor, *k*, was calculated from the resulting chromatograms using BuMA-Grad 3. Using the L_{eff}, the change in retention factor along the column could be monitored, thus evaluating the effect of relative capacity upon *k* (due to the grafted zones of increasing ligand density). From the separations recorded at sixteen on-column detector positions, the retention factor was calculated, for both directions of flow through the gradient column as described in Section 3.2.5.8. The resulting plot of *k* versus L_{eff} was expected to yield two curved plots, one concave and the other convex. However, as the gradient is stepped and not linear, the resulting retention factor plots should be similar to concave and convex curves, but should demonstrate a collection of three distinct regions of varying *k*, as outlined in Figure 3.16.

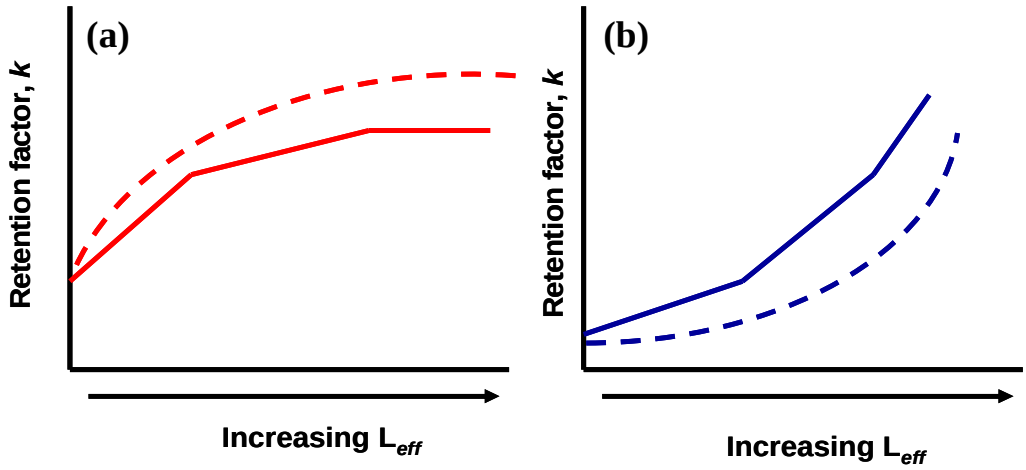

***Figure 3.16**: Theoretical curves for k vs. L_{eff} along a stepped gradient column in the forward direction (a) and in the reversed direction (b). The dotted line indicates the convex plot for a linear gradient, solid line indicates the concave plot for a stepped gradient.*

The gradient column (BuMA-Grad3) was investigated first with the direction of flow as indicated in Figure 3.4 (a), for the first analyte peak, Mg^{2+}. The data is presented in Figure 3.17 below.

The column can be described as having three discreet zones of different relative ion exchange capacity, resulting in a gradient of capacity along the column. As the relative capacity was constant across each zone, this should be reflected in the retention factor. In Figure 3.17 (a), the end of Zone 3 (grafted with 1 J/cm^2) can be seen at approximately 36 mm L_{eff}. For the column in the forward direction, *k* begins to level off from approximately L_{eff} of 66 mm. This coincides with the zone of lowest grafting density, which would not significantly increase *k* along the remainder of the column. The change in retention factor was caused by the increase in relative capacity for that zone. In Figure 3.17 (a) the steepest increase in *k* was observed for Zone 3, where the relative capacity was higher, compared to Zones 2 (grafted with 0.5 J/cm^2) and Zone 1 (grafted with 0.25 J/cm^2) In Zone 3, *k* began to level off, as a lower relative capacity was experienced in this section of the column.

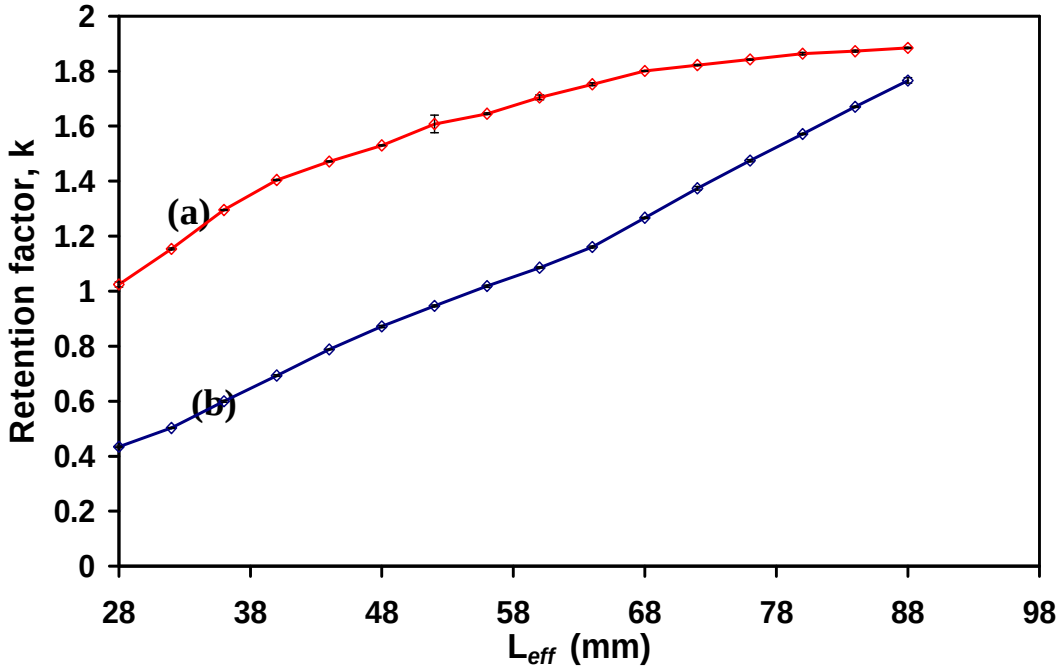

Figure 3.17: *Plot of retention factor,* k, *versus effective column length* L_{eff} *for* Mg^{2+} *in the forward (a) and reversed (b) flow direction on BuMa-Grad 3. Separation conditions: Eluent 0.25 m*M *ethylenediamine (pH 4), flow rate 1 µL/min,* Mg^{2+} *prepared with a concentration of 10 ppm.*

In the reversed direction (Figure 3.4 (b)), the effect is more pronounced, resulting in an incremental increase in *k* along the entire length of the column, which exhibited an almost linear character. Again the boundary between zones was accompanied by a change in the curvature of the resulting plot. For example, at L_{eff} of 36 mm and 66 mm, a change in the curvature of the plot was observed, due to the increase in relative capacity, as the analyte moves through the column to zones of higher grafting density and thus capacity, in the reversed direction. In comparing to work performed on gradient elution with an isotropic stationary phase [6-10], as the content of modifier is increased the retention of analyte along the column is decreased. As the solvent strength in this work is held at a constant concentration throughout the separation, the deviation in *k* is attributed to the relative capacity expressed by each zone.

As noted by Maruška *et al.* [11], there should be no change in the resulting (final) retention factor, following the reversal of flow through the column. Contrary to expectations, in the plot above the final retention factor for the column in both flow directions was not the same. In this work, since the final *k* value was recorded on-

column, and due to the limitations of the detector cell, approximately 2-3 mm of the column could not be measured. This affected the results when the column was in the reversed flow direction (Figure 3.17 (b)), because the column outlet contained a higher relative capacity (grafted with 1 J/cm^2), which would have increased *k* further. As a result, the final *k* values for the column in both directions were not exactly equal, with a difference of 6.3 %. A similar plot was constructed for Ba^{2+}, and is shown below in Figure 3.18. Similar features in the plot were observed, such as the change in curvature of the plot at the boundary of the grafted zones.

The effect of the distinct relative capacity of each zone is more apparent in this plot, particularly for the column in the forward direction (as in Figure 3.4 (a)). As observed above for Mg^{2+} the zone boundaries are reflected in the retention factor, as changes in the curvature of the plot occur at a L_{eff} of 36 mm and 66 mm. In the forward direction of Figure 3.18 (a), the three zones of different relative capacity were easily observed, unlike the column in the reversed direction, where the boundary between Zone 2 and Zone 3 could be as easily observed. Again, the final *k* values were not equal, with a difference of 6.2 %.

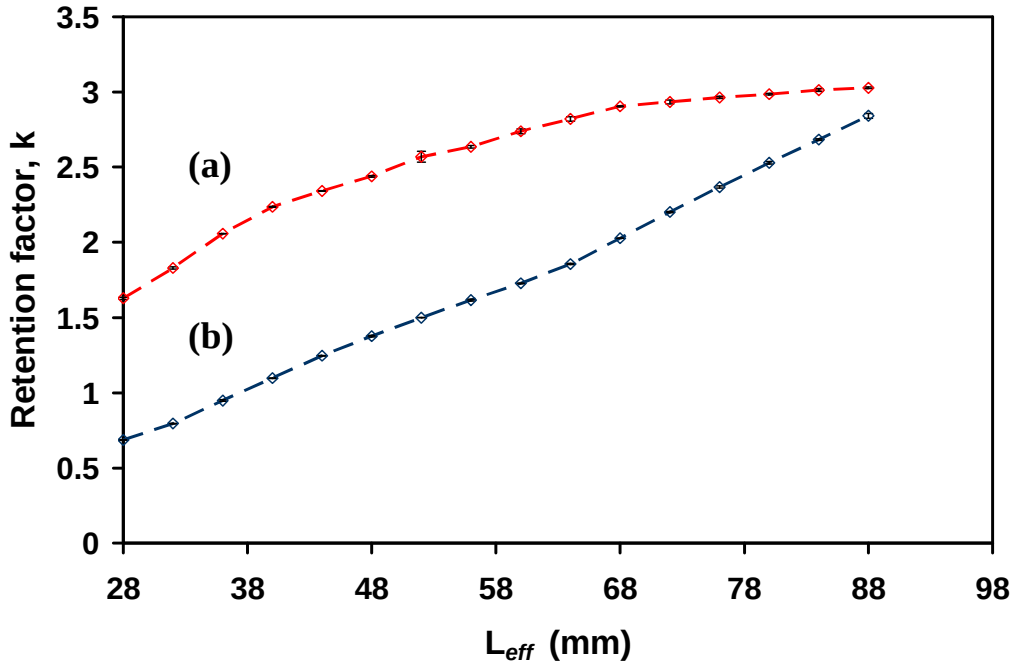

Figure 3.18: *Plot of retention factor,* k, *versus effective column length* L_{eff} *for* Ba^{2+} *in the forward (a) and reversed (b) flow direction of BuMA-Grad 3. Separation conditions: Eluent 0.25 m*M *ethylenediamine (pH 4), flow rate 1 µL/min,* Ba^{2+} *prepared with a concentration of 50 ppm.*

From this work it is to be noted that the presence of the gradient upon the column was determined via the retention factor *k*, with the resulting values for *k* due to the difference in relative capacity along the column.

In a similar report, O' Riordáin *et al*. [1], visualised *k* with varying L_{eff} in the separation of anions, on a surfactant modified silica monolith, using on-column C^4D. From that report, the authors noted an incremental increase in *k* with increasing L_{eff}, which was due to a lower surfactant concentration at the column inlet (Figure 3.19). Under isocratic conditions, with a column expressing a relatively homogeneous distribution of functional groups, a flat profile for *k* with increasing L_{eff} would be expected. From the results presented in this work, the profiles generated by *k* versus L_{eff} clearly indicate distinct zones of differing relative capacity across the column.

An isotropic column was also produced in this work, and was subjected to measurement of the retention factor, *k*, along the column with increasing L_{eff}. As observed above in Figure 3.10, the grafting density for the isotropic column was higher than that of the gradient column. In order to produce similar overall capacity of this column (for comparison to the gradient column), an eluent was prepared with an increased concentration of ethylenediamine (0.56 m*M*) and was adjusted to pH 4.

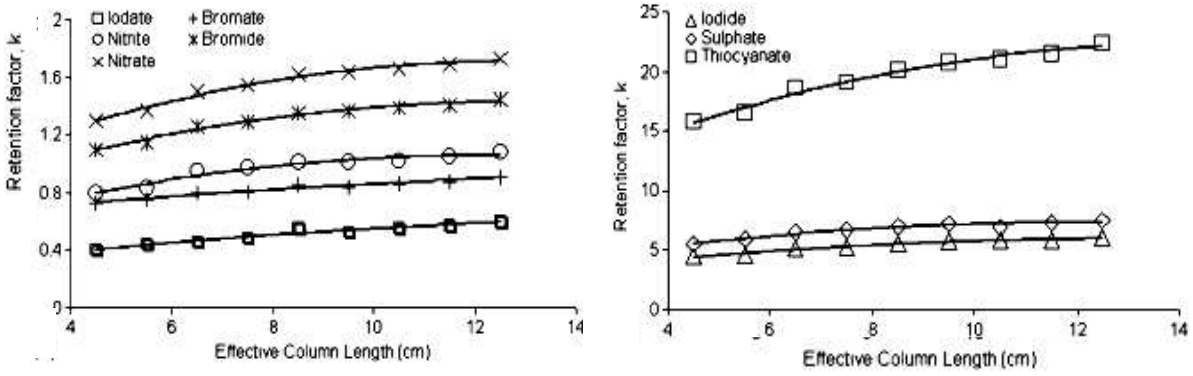

Figure 3.19: *Plot of* k *versus* L_{eff} *on an Onyx™ monolithic column coated with surfactant for anion exchange chromatography. Eluent; 0.5 m*M *phthalic acid (pH 4), at 1 μL/min. Adapted from [1].*

The same procedure was followed for sample injection and data acquisition as outlined above, with sixteen on-column detector positions at 4 mm intervals, and triplicate injections of the analyte mixture. A plot of *k* versus L_{eff} could then be

constructed, as illustrated in Figure 3.20. From the resulting chromatogram at the shortest L_{eff} of 28 mm, there was no retention of the analyte peaks. At a L_{eff} of 32 mm, the first separation was observed, and so, *k* could be determined from this point.

The retention factor for the Mg^{2+} analyte peak (-♦-) demonstrated an incremental increase in *k* along the column. For the plot of the *k* for Ba^{2+} (-■-), the increase in *k* was incremental, unlike the expected behaviour as reported by O' Riordáin *et al.* [1]. The resulting profile for *k* versus L_{eff} for an isotropic column under isocratic conditions should result in a flat profile [1]. From Figure 3.19, *k* for a range of anions separated on a silica monolith resulted in horizontal profiles for *k* along the column length which exhibited a small degree of curvature. The group postulated that this curvature was due to an inhomogeneous coating of surfactant upon the monolith. It may be futile comparing the resulting *k* from a silica monolith with a polymer monolith, due to the increased efficiencies generally observed with silica monolithic columns for ion exchange (this was discussed in Chapter 1, Section 1.3).

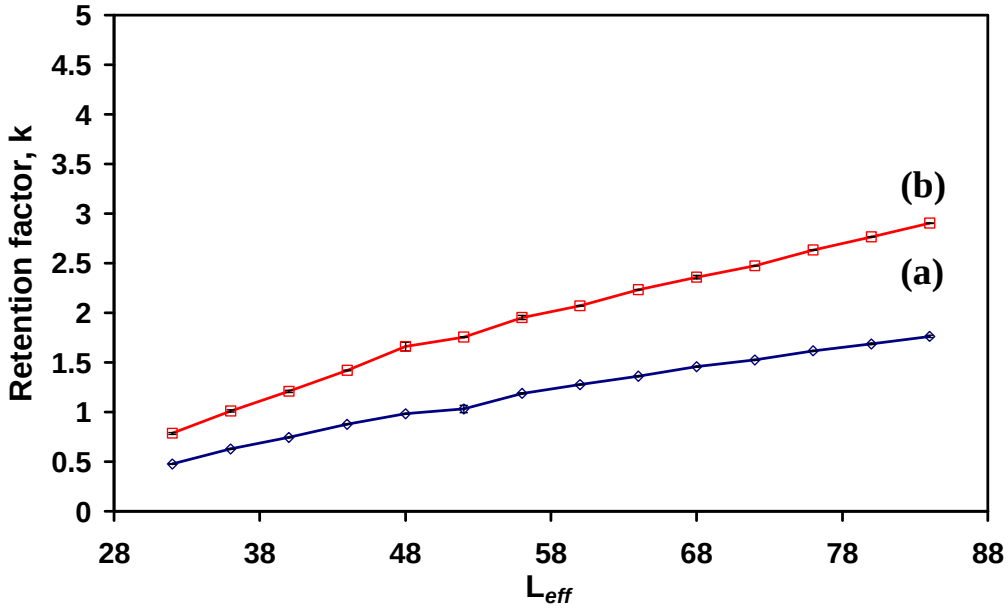

Figure 3.20: *Plot of retention factor,* k, *versus effective column length* L_{eff} *for* Mg^{2+} *(a) and* Ba^{2+} *(b) upon the isotropic column LMA-Iso 1. Separation conditions: Eluent 0.56 mM ethylenediamine (pH 4), flow rate 1 µL/min.*

The plot for *k* versus L_{eff} for the isotropic column resulted in an incremental increase in *k* with increasing columns length, similar to that observed by O' Riordáin *et al.* [1]. This may be indicative of an inhomogeneous graft density of SPM along the isotropic column. From the sC^4D profile in Figure 3.10, the profile of the LMA-Iso 1

column indicated two features upon the monolith at detector positions of approximately 12 mm and 45 mm, which may indicate a localised in-homogeneity of SPM graft density.

What is to be noted, however, from this work is that the generated profiles of *k* versus L_{eff} differ between the isotropic column and the gradient column, indicating a difference in the behaviour of the *k* with constant eluent concentration. As *k* is dependent on the capacity of the column and the eluent concentration, the change in *k* across the column can only be due to the change in relative capacities exhibited in each zone along the gradient column. To conduct such an experiment in the absence of scanning C^4D methods would be difficult, and would no doubt result in the destruction of the columns, to vary L_{eff}.

3.4. Conclusions

Column profiling using sC^4D has been shown as an invaluable tool in the optimisation of a grafting protocol, necessary for the production of a gradient of photo-grafted functional groups (SCX) upon a poly(BuMA-*co*-EDMA) monolithic column. Using a variety of columns, the optimal range of UV energy required for grafting procedures was optimised, using the detector response, generated by the grafted charged functional groups via non-invasive and non-destructive sC^4D.

A gradient of photo-grafted functional groups was then produced upon a single poly(BuMA-*co*-EDMA) monolithic column. The distribution of the grafted gradient was then visualised using the sC^4D approach. With an increase in energy applied along the column, an increase in graft density was expected, as reported previously [2,13]. The resulting gradient column was then subjected to the chromatographic separation of a mixture of two divalent metal cations, Mg^{2+} and Ba^{2+}. The separation was monitored using on-column C^4D, at sixteen on-column detector positions (predetermined test areas). The effect of the gradient upon the separation was determined, following the reversal of flow through the column, whereby the separation process was repeated. The retention factor, *k*, was determined at the on-column detector positions. A plot of *k* versus the effective column length was constructed, and the effect of varying relative capacity (graft density) was investigated.

Using sC^4D, the change in retention factor along the gradient column, in both directions of flow, could be observed. The behaviour of *k* clearly illustrated a change in retention, with differing relative capacities. In comparison to the isotropic column, the gradient column exhibited concave and convex type profiles for *k* with increasing L_{eff}. As *k* is dependent on eluent concentration and column capacity, under constant eluent concentration any deviation in *k* was due to the relative capacity experienced by the analyte in that particular zone. Following chromatographic application, the gradient exhibited shorter analysis times for the separation of Mg^{2+} and Ba^{2+} with similar resolution, compared to an isotropic column of similar capacity. As linear gradients perform better than stepped gradients [11], the grafting protocol must be optimised further in order to produce a linear gradient.

3.5. References

[1] O' Riordáin, C., Gillespie, E., Connolly, D., Nesterenko, P., Paull, B., *J. Chromatogr. A*, 2007, 1142, 185.

[2] Rohr, T., Ogletree, F., Svec, F., Fréchet, J., *Adv. Funct. Mater*., 13, 2003, 264.

[3] Pucci, V., Raggi, M., Svec, F., Fréchet, J., *J. Sep. Sci*., 27, 2004, 779.

[4] Urbanova, I., Svec, F., *J. Sep. Sci*., 34, 2011, 2345.

[5] Gillespie, E., Connolly, D., Paull, B., *Analyst*, 134, 2009, 1314.

[6] Lee, J., Row, K., *Korean J. Chem. Eng.*, 19, 2002, 978.

[7] Jandera, P., Kucerova, Z., Urban, J., *J. Chromatogr. A*, 1218, 2011, 8874.

[8] Heinisch, S., Rocca, J., *J. Chromatogr. A*, 1048, 2004, 183.

[9] Row, K., *J. Chromatogr. A*, 797, 1998, 23.

[10] Galaon, T., Medvedovici, A., David, V., *Sep. Sci. Tech.*, 43, 2008, 147.

[11] Maruška, A., Rocco, A, Kornysova, O., Fanali, S., *J. Biochem, Biophys. Methods*, 70, 2007, 47.

[12] Stachowiak, T., Svec, F., Fréchet, J., *Chem. Mater*., 18, 2006, 5950.

[13] Rohr, T., Hilder, E., Donovan, J., Svec, F., Fréchet, J., *Macromolecules*, 36, 2003, 1677.

[14] Connolly, D., Barron, L., Gillespie, E., Paull, B., *Chromatographia*, 70, 2009, 915.

[15] Fritz, J., Gjerde, D., Becker, R., *Anal. Chem*., 52, 1980, 1519.

[16] Hajos, P., *J. Chromatogr. A*, 2002, 955, 1.

[17] Fritz, J, Gjerde, D., *Ion Chromatography*, 3rd edition, Wiley, 2000.

Chapter 4.0

Fabrication of a cyclic olfein co-polymer optical filter and its application towards the production of novel polymer monolithic columns, with stationary phase gradients.

"*There cannot be a crisis next week. My schedule is already full.*"

Henry Kissinger

4.1. Introduction

Many optical filters are available commercially, fabricated from fused silica substrate, glass or borosilicate glass. However, not all filters are suitable for use in the deep UV range. Using commercially available filters, optimisation can be costly, as choosing the correct optical density to suit the application may require the purchase of numerous filters. The range of optical density is also limited, mainly due to substrate suitability to the working optical range. Both step and continuous gradients are commercially available.

Jiang *et al.* [1] prepared a continuous gradient of poly(ethyleneglycol methacrylate) (PEGMA) on a silicon wafer, with nano-meter thickness, using diffusion controlled surface polymerisation. The wafer may have applications as an optical filter if optimised, for example, if a UV absorptive polymer was grafted to a quartz plate in increasing thickness, resulting in a gradual attenuation in UV energy. This would be an ideal method in the production of a column expressing a gradient of grafted functional groups, or indeed, the production of a column of varying pore sizes.

Collins *et al.* [2] recently produced a polymer monolithic column with a gradient in pore size, using spatially controlled thermal polymerisation, over a period of 16 h. The device used incorporated an array of Peltier thermoelectric units. Each unit within the array could be controlled independently, and so, the units were programmed to increase from 54 °C to 60 °C in 1 °C intervals. Each unit of the array represented a zone along the column, introducing a gradient in average pore size. However with this method, specialised equipment was necessary, with lengthy experimental times required by thermal polymerisation techniques. In contrast, graft polymerisations performed using UV initiation, can be performed rapidly and can be easily controlled [3,4].

Previous attempts in the literature to prepare a photo-grafted gradient, involved the use of a moving shutter [5,6], neutral density gradient filters, and the use of polymer films [6]. However, through utilising commercially available polymer films, the production of a tailored gradient to suit specific applications can be both inexpensive and fast. Pucci *et al.* [6] used a polyester film to attenuate the UV intensity during photo-grafting of a gradient using a moving shutter, to facilitate longer irradiation times. The group reported a drop in UV intensity, from 15 mW/cm^2

to 0.9 mW/cm^2. The use of a moving shutter resulted in a linear gradient, as determined by cross-sectional analysis of the column via electron probe microscopy. In using a moving shutter, possible variations may be introduced to the grafting procedure, due to variable speed of the motorised components. Here, in Chapter 3.0, the work focused on the production of a monolithic stationary phase grafted to express a stepped gradient of functional groups (strong cation exchange), distributed along the column, with subsequent profiling using sC^{4}D. This column was not a linear gradient, and it did not demonstrate ideal properties for applications as a chromatographic phase [7]. The aim of the following investigation was to produce a controlled linear gradient using UV initiated photo-grafting (UV light 254 nm). Since higher surface ligand density is generally observed for photo-grafted columns, a suitable optical filter was designed and applied to the fabrication of photo-grafted stationary phase gradients within monolithic capillary columns. Utilising commercially available cyclic olefin co-polymer (COC) polymer films, the production of a tailored gradient to suit the specific application was carried out. Fabricated columns were subjected to scanning C^{4}D profiling (sC^{4}D), which was used to determine the distribution of the grafted functional groups axially along the column. The sC^{4}D profiling indirectly verified the operation of the filter by profiling the distribution of the photo-grafted gradient resulting from the use of an optical filter.

4.2. Experimental

4.2.1. Instrumentation

As described in Chapter 3.0, Section 3.2.1, with the following additions. A Shimadzu UV mini-1240 UV/VIS spectrophotometer was used for the characterisation of the optical density of polymer films (Mason Technology Ltd., Dublin, Ireland).

4.2.2. Materials and reagents

As described in Chapter 3.0, Section 3.2.2 with the following additions. COC films were kindly donated by Mr. Stuart Harris (Zeon Chemicals Europe Ltd., Vale of Glamorgan, UK). Each film had a protective film, which was removed prior to analysis.

4.2.3. Scanning C^4D

sC^4D was performed as described previously in Chapter 2.0, Section 2.2.3, with the following additions. Detector settings were at a frequency of 2x high, a voltage of -6 dB, 50 % gain, 001 offset, for all experiments including IDA functionalised columns. For the SCX monolith, voltage was lowered to -12 dB, with other settings as outlined above. For measurements taken at 5 mm intervals the detector response was monitored in real time using Tracemon software along with manual recording of each data point at 5 mm increments. For C^4D profiling of IDA functionalised columns, a buffer consisting of 2.5 m*M* TES and 3 m*M* ethanolamine (pH9) (Buffer 1) was used. For the strong cation exchange column (grafted with a gradient of SPM) the sC^4D profiles were performed using 0.25 m*M* ethylenediamine (pH 4). It must be noted that due to the length of column fittings, and the size of the detection cell some areas of columns could not be measured; ~ 5 mm from the end of the column, and ~15-20 mm at the column head.

4.2.4. Vinylisation of fused silica capillary

Fused silica capillary was vinylised using a procedure described previously in Chapter 2.0 Section 2.2.4.

4.2.5. Fabrication of COC film optical filter

4.2.5.1. Spectroscopic analysis of COC polymer films

A spectrophotometer was used to determine the transmission properties of polymer films at a wavelength of 254 nm. A quartz cuvette was used for absorption measurements. To determine the optical transmission of a film, a piece of film was cut to fit the dimensions of the quartz cuvette. To measure a blank in this experiment a clean, empty quartz cuvette was used. To measure absorbance of the films, each film was washed with deionised water, followed by methanol, followed by water. The films were dried using nitrogen flow and lint free tissues. Following the auto zero of a blank cuvette, a test film was placed into a quartz cuvette and the absorbance was measured in triplicate, with blank measurements taken between each reading. There were two grades of film provided; ZF 14 and ZF 16. The ZF 14 films were provided with film thickness varying from 40 μm, 100 μm and 188 μm, whereas ZF 16 films were provided with film thickness of 100 μm and 188 μm. The difference between

these films was the glass transition temperature (T_g) which was 136 °C and 163 °C, respectively. For the analysis of optical density and % T for the gradient, the same procedure was applied. Triplicate readings were taken for each layer of film.

A wavelength of 254 nm was chosen for analysis, as this wavelength was used for all subsequent photo-grafting procedures. The absorption of each film was measured in triplicate. The exact composition of the COC film is proprietary information, and so, some assumptions must be made on the composition. The ZF 14 films are more maleable and flexible than the ZF16 films, which may be due to a change in plasticiser content. This may account for the deviations in UV transmission between the ZF 14 and ZF 16 films of equal thickness.

4.2.5.2. Fabrication of COC film optical filter

The optical density (OD) can be related to % transmission by the following equation:

$$T = 10^{-OD} \times 100 \quad \text{(Equation 4.1)}$$

Following the photometric analysis, the ZF 14 film of thickness 40 µm was deemed a suitable candidate for optical filter development. The absorption of the 40 µm film was measured in the detection cell from a single film through to thirteen film samples in the single cell, (n =1,2,3,….13), resulting in a final total film thickness of 520 µm. The absorbance measurements were used to quantify the OD range achieved by the films. Using this information a prototype filter was prepared to a total length of 130 mm. Each film piece was 10-130 mm long and ~ 40 mm wide. The films were glued along one side of the film, with a thin layer of glue. To compress each film together a holder was fashioned from black card, through which a 5 mm window was cut. The fabrication process is illustrated in the schematic below (Figure 4.1).

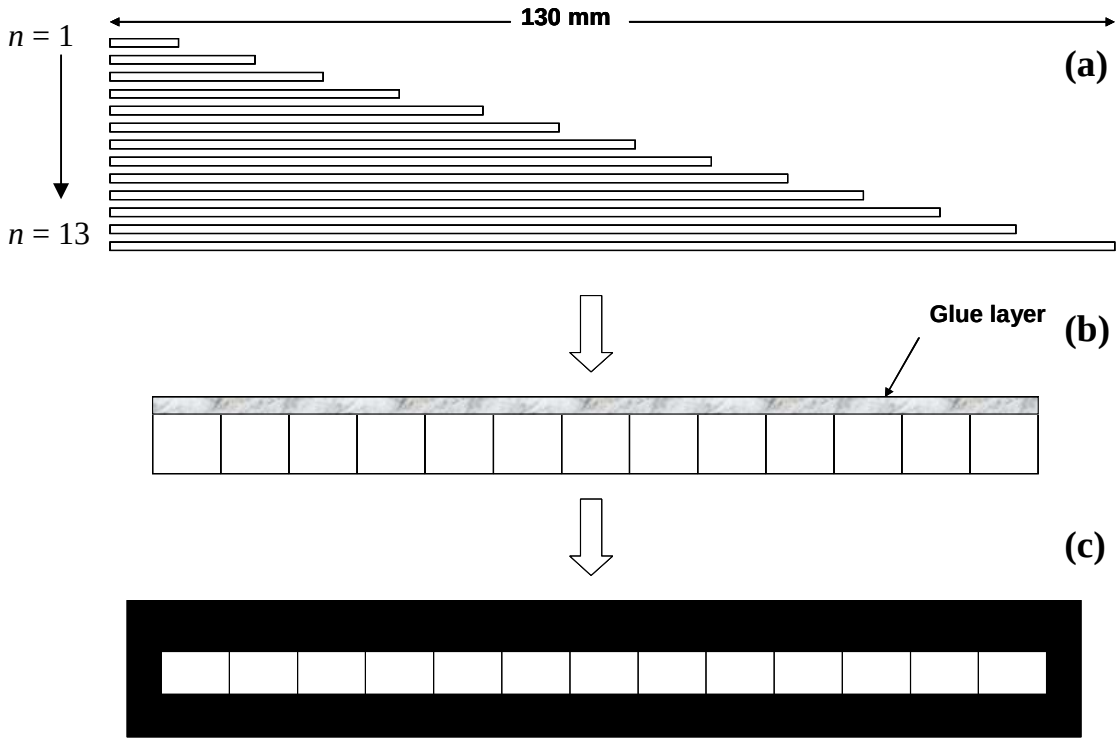

Figure 4.1: *Schematic of COC film optical filter. Each polymer film layer was cut to measure from 10 to 130 mm (a), the films were glued together on one side (b), and finally the films were sealed between pieces of black card (c).*

The glue used was not UV transparent, however, this was not an issue. By gluing a selected region, which was to be situated beneath the filter holder, the glue did not interfere with the UV transmission of the exposed films at the window of the film. A photograph of the resulting filter is shown in Figure 4.2.

Figure 4.2: *Photograph of optical filter used in the production of surface localised, photo-grafted stationary phase gradients.*

4.2.6. Fabrication of polymer monolithic columns for photo-grafting

4.2.6.1. Preparation of monolithic columns

Monolithic columns were fabricated as outlined in Chapter 3.0, Section 3.2.5.1. Three columns labelled hereafter as Columns 1, 2 and 3, were fabricated to evaulate the effectiveness of the optical filter in UV grafting procedures to produce a chlelating IDA stationary phase. Another column (Column 4) was fabricated as a substrate for grafting of SPM to produce a gradient of SCX groups. Each column measured 150 mm to allow the optical filter (which measured 130 mm in length), to be positioned above the column during grafting procedures.

4.2.6.2. Photo-grafting procedure for vinyl azlactone grafting

The immobilisation of benzophenone took place upon the monolith as described previously in Chapter 3.0, Section 3.2.5.3, and [8]. It is known that a grafted layer of poly(ethylene glycol methacrylate) (PEGMA) provides a hydrophilic surface, which is known to minimise non-specific hydrophobic interactions between proteins and the stationary phase [9,10].Therefore, a 0.3 *M* solution of PEGMA was prepared in water and deoxygenated with nitrogen for 10 mins. The solution was pumped across the column for 1 h and the column's ends were sealed. A UV irradiative dose of 1 J/cm^2 was applied to the entire column. The column was then washed with water for 1 h (at 1 μL/min), to remove any un-reacted PEGMA.

To facilitate the immobilisation of PEGMA and VAL, benzophenone was used for two discreet photo-initiation steps and thus was immobilised to the column twice. Initiator (benzophenone) was again immobilised onto the hydrophilised monolith, as above, and a solution of 20 % VAL was prepared in methanol, and was deoxygenated with nitrogen for 10 mins. The solution was pumped across the monolith for 1 h and subsequently irradiated with 1 J/cm^2 UV irradiation through the COC optical filter. The column was then washed with methanol for 1 h (at 1 μL/min) to remove any un-reacted monomer. The column was then washed with water for 1 h prior to sC^{4}D profiling.

4.2.7. Immobilisation of IDA

The IDA ligand was immobilised via reactive VAL groups grafted onto the column as previously described in Chapter 2.0, Section 2.2.7. A solution of 1 *M* ethanolamine was pumped across the column to "end-cap" any un-reacted VAL sites producing neutral 2-hydroxyethylamido groups. The column was washed with water until the effluent reached a neutral pH.

4.2.8. Immobilisation of Cu^{2+} ions

Copper ions were immobilised on to the column by a combination of dynamic and static coating as follows. A solution of copper sulphate pentahydrate was prepared to a concentration of 1 m*M* in 2.5 m*M* TES 3 m*M* ethanolamine buffer (pH 9) (Buffer 2). Buffer 2 was pumped across the column for 3 h to facilitate dynamic coating. For static immobilisation, Buffer 2 was pumped across the column for 1 h, then the column ends were was sealed, and left to react for 1 h. The column was then washed in Buffer 2 for 1 h before washing with water.

4.2.9. Fabrication of a photo-grafted SCX gradient

Using the two-step photo-grafting procedure highlighted in Chapter 3.0, Section 3.2.5.3, a gradient of grafted SPM was fabricated. Benzophenone was immobilised onto the monolith surface as previously described. The column was filled with a deoxygenated 4 % solution of SPM in deionised water. The COC filter was placed between the irradiation source and the column, and grafting occurred using 1 J/cm^2 UV irradiation. The column was washed with deionised water for 1 h to remove any un-reacted monomer. The column was flushed using a buffer of 10 m*M* ethylenediamine (pH 4), and was subsequently equilibrated with a 0.25 m*M* ethylenediamine (pH 4) buffer, in which the column was profiled.

4.2.10. Chromatographic separation of proteins

The isocratic separation of proteins on the SCX gradient monolith was carried out, both in the forward direction (low to high capacity) and the reverse direction (high to low capacity). Two proteins, namely transferrin (0.1 mg/mL) and lysozyme (0.3 mg/mL) were injected onto the column, in both the forward and reversed directions of the gradient. Proteins were eluted using an isocratic eluent of 0.175 *M*

NaCl, and a flow rate of 2 µL/min. The separation was recorded using UV detection at a wavelength of 214 nm.

4.3. Results and discussion

4.3.1. Fabrication of optical filter

4.3.1.1. Photometric analysis of polymer films

The transmission properties of each film were analysed at a wavelength of 254 nm, and are displayed below in Figure 4.3. The manufacturers stated that the % T for each film was equal at a thickness of 3 mm, with no discrimination between film type. This applies principally at wavelengths above 300 nm [11], however, in this work the wavelength of interest was 254 nm. From Figure 4.3 below, it can be seen there was a decrease in transmission with increasing film thickness.

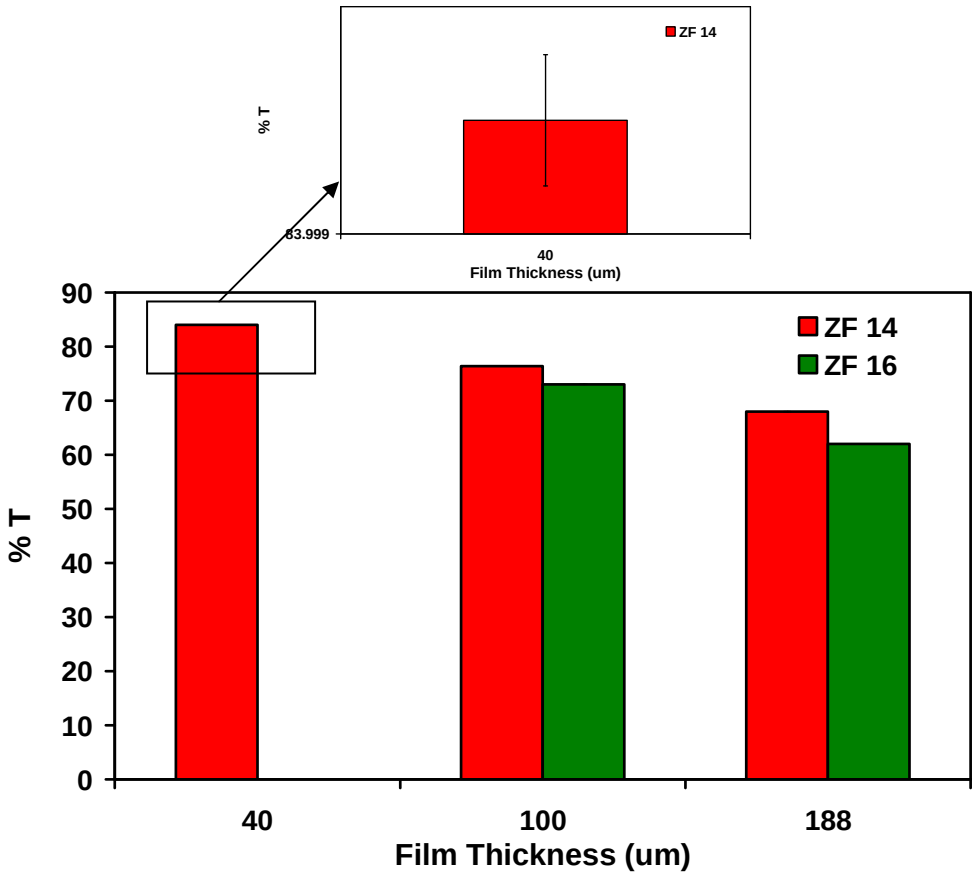

***Figure 4.3**: The % T of UV light at a wavelength of 254 nm, ZF 14 represented by red plots, ZF 16 represented by green plots. Average of triplicate absorbance readings reported, error bars included indicating little deviation (%RSD ≤ 1.7 %). Insert; 40 µm film %T expanded to demonstrate the presence of error bars.*

This was pivotal for the development of an optical filter. The preparation of a gradient of UV light is dependant upon the ability of the filtering material to attenuate the transmission of UV light. However, the attenuation of the films may be caused by a change in plasticiser and/or the monomer concentration in the polymer pre-cursor solution, unintentionally altering the UV transmission range. The 40 µm film exhibited the highest % T at 254 nm of approximately 84 % T.

The % T was measured from multiple (*n*) layers of 40 µm films, where *n* was varied from a single layer to 13 total layers, within the detection cell. Results are shown in Figure 4.4. (a). The % T decreases from 84 % (*n* = 1) to 9 % (*n* = 13). This profile results in a gradient similar to a gradient fabricated by Pucci *et al*. using a neutral density filter [6]. As the graft density is related to the grafting energy applied, the resulting gradient profile should resemble this transmission profile. Equation 4.1 was used to relate % T to OD, resulting in an OD of 1 to 0.1, as illustrated in Figure 4.4 (b).

In previous works ([6] and Chapter 2.0, Section 2.2.5.1), commercial gradient filters were applied to the production of photo-grafted stationary phase gradients, where the OD was obviously an important factor. This factor describes the absorption of the filtering material, and so, when optimising a photo-initiated grafting procedure, this parameter requires the utmost attention. When designing a photo-initiated procedure, the amount of absorption of the material (OD) and its effect upon the wavelength of interest should be known. With an increasing OD, the amount of light transmitted is reduced, resulting in a decrease in grafted chain growth.

Pucci *et al*. used a stepped gradient with an OD of 0.04 to 2.0 over 11 steps [6]. In Chapter 2.0, a continuously variable, filter with an OD of 0.04 to 4 was used, resulting in poor axial control of the graft density along the column length (see Figures 2.4 and 2.5). The OD obtained from the COC filter as seen in Figure 4.4 (b), increased linearly from 0.1 to 1 with a linear regression of 0.9996 (R^2). The reported OD is the result of triplicate measurements. Error bars are included for the standard deviation, with % RSD no greater than 0.6 %.

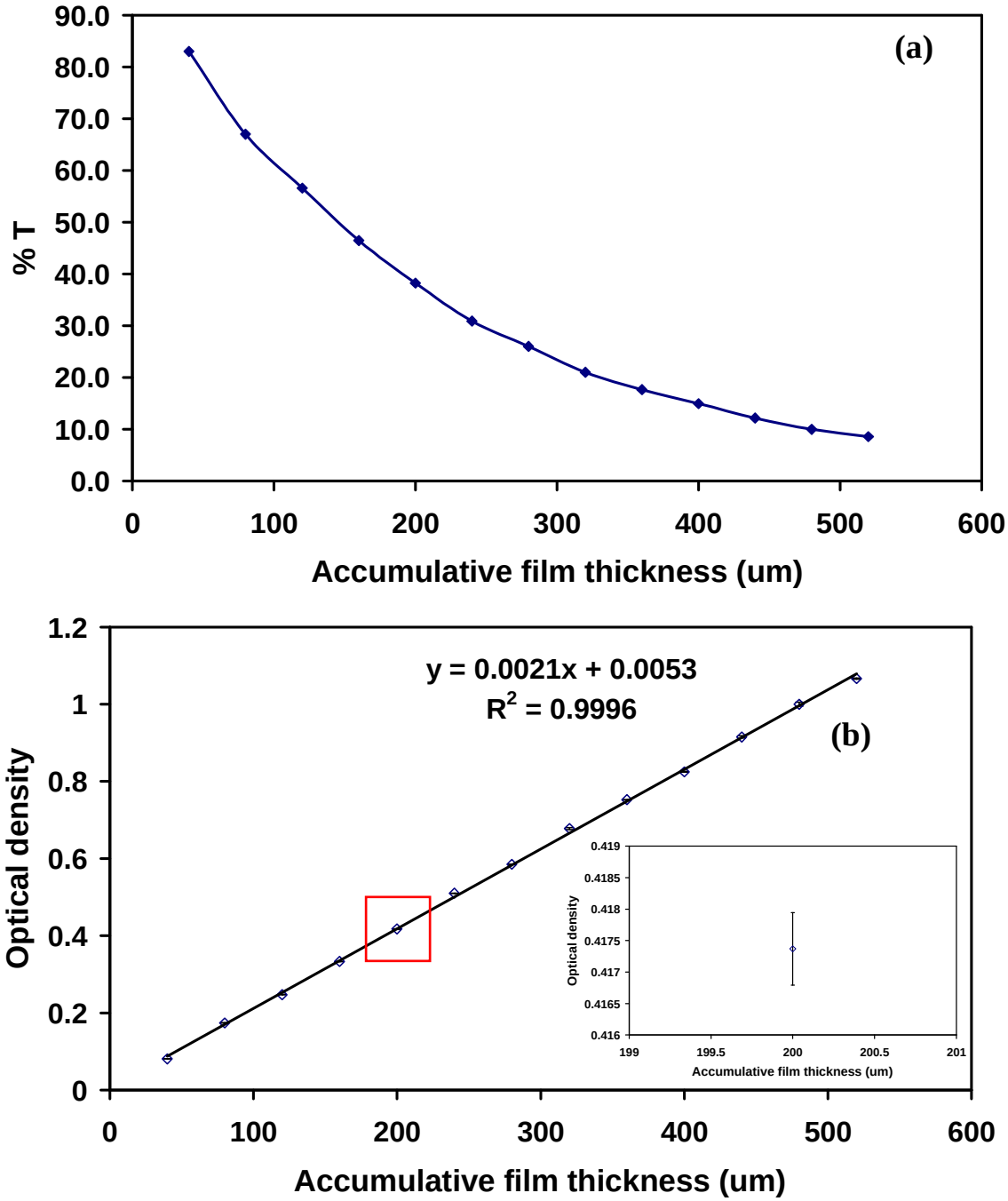

Figure 4.4: *%T for increasing film thickness (a), optical density for 13 layers of 40 µm COC film (b). Insert; film thickness of 200 µm, as indicated by red box, expanded to show error bar.*

The filter was then applied to the production of novel grafted stationary phase gradients. The following diagram in Figure 4.5 illustrates the formation of the gradient during such photo-grafting processes.

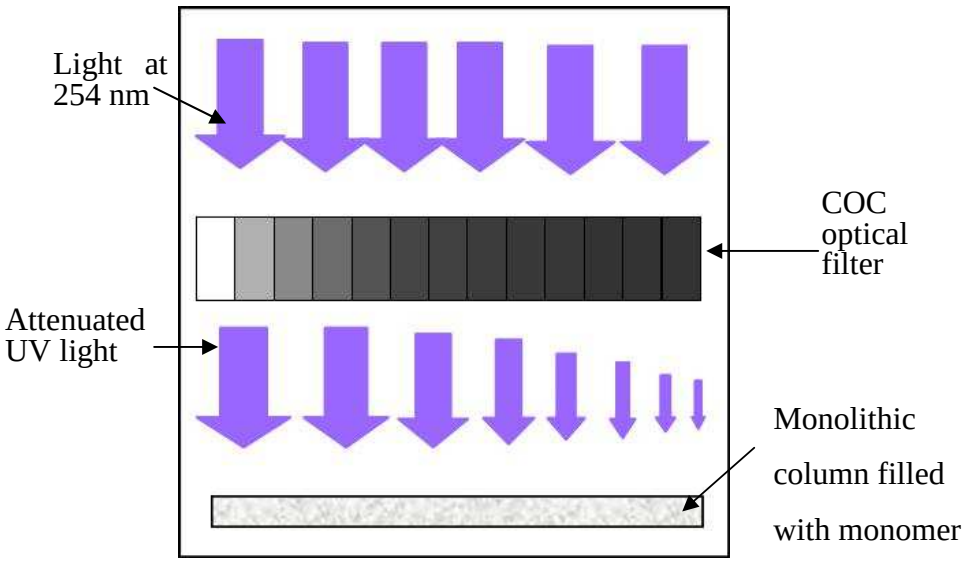

Figure 4.5: *Schematic of the application of the COC film optical filter. Optical density increases from left to right as indicated by grey scaling.*

4.3.2. Fabrication of monolithic columns

4.3.2.1. IDA immobilised stationary phase gradients

Three monolithic columns were prepared for gradient functionalisation, named column 1-3. Prior to the grafting and immoblisation procedures, the columns (columns 1-3) were scanned in 2.5 m*M* TES, 3 m*M* ethanolamine (Buffer 1) thus producing a reference scan (blank). Using this scanning buffer very little changes in detector response could be observed on each blank monolith, due to the lack of charged groups present. The profiles of the blank columns are illustrated in Figure 4.6 below.

In Figure 4.6 small deviations in the monolith bed homogeneity can be seen. This was caused by a local decrease in monolithic bed density. No large increases in signal are observed which would indicate the presence of a break in the stationary phase, or a contaminated section.

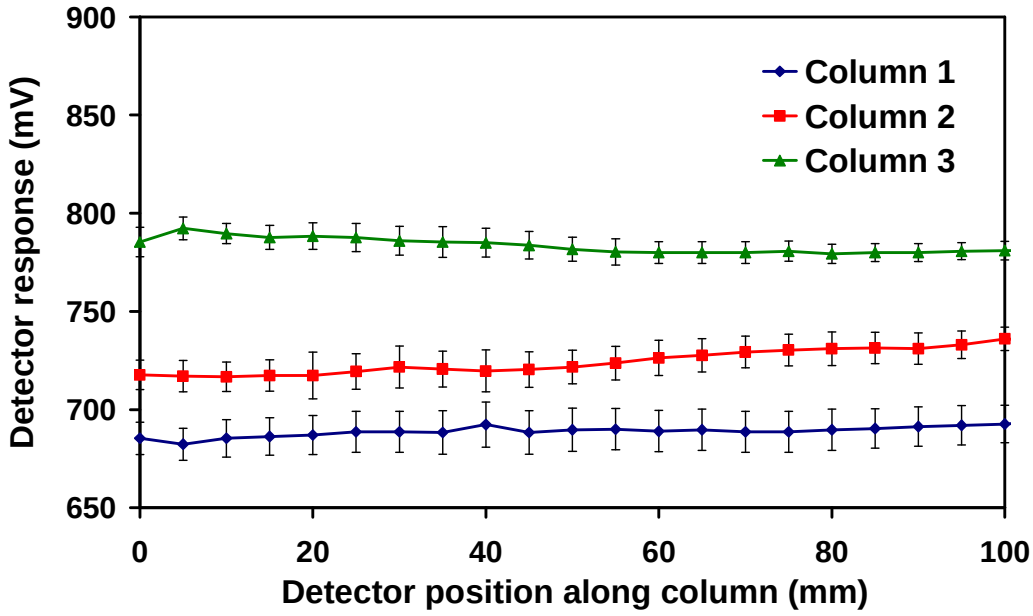

***Figure 4.6**: Columns 1 (-♦-), 2 (-■-) and 3 (-▲-) profiled using sC^{4}D prior to surface grafting of VAL. Flow rate 1 µL/min, 2.5 m*M*, TES 3 m*M *ethanolamine. Columns scanned in triplicate as indicated by error bars. Column signals have been offset by +50 mV each for illustrative purposes only. Column 1 measured 150 mm, columns 2 and 3 measured 140 mm in length.*

As previously reported by Connolly *et al*., a decrease in detector response results from a decrease in the fluid volume in the detection gap [12] between the electrodes. In terms of monolithic columns a decrease in detector response equates to an increase in polymer density, resulting in a decrease of fluid moving through that cross sectional area.

4.3.3. Profiles of grafted gradient columns

To allow surface localised grafting, benzophenone was first grafted to the monolithic column, followed by grafting of PEGMA. The columns were grafted with PEGMA (Figure 4.6) to pre-empt any possible non-specific hydrophobic interactions of proteins with the hydrophobic stationary phase, for applications in protein separations. Following from the study performed by Stachowiak *et al*. [8], the use of a PEGMA monomer reduced non-specific hydrophobic bonding by up to 98 %. In this work a relatively short monomer (of average molecular weight of 300 g/mol) was used to encourage a large surface coverage of PEGMA, reducing any possible steric hindrance among grafted PEGMA groups. The addition of PEGMA to the monolithic

column had no discernible change in conductivity during sC^{4}D profiling, as shown in Figure 4.7. This was due to the neutral charge on the monomer.

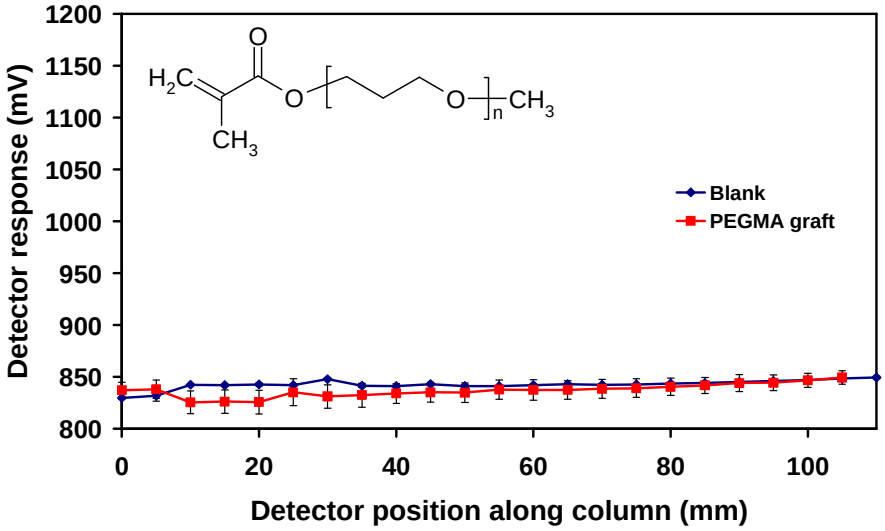

***Figure 4.7**: sC^{4}D profiles of a BuMA-co-EDMA monolithic column prior to grafting of PEGMA (—♦—), and following the grafting of PEGMA (—■—). Column scanned in 2.5 m*M *TES, 3 m*M *ethanolamine at a flow rate of 1 µL/min. Insert, structure of PEGMA.*

The profiles in Figure 4.8 (a-c) demonstrate the production of a gradient of VAL functional groups, further reacted with IDA to create a chelating stationary phase. The plots exhibit a decrease in detector response axially, along the column length. This was due to the decrease in the concentration of IDA graft density. The detector response for each column deviates to a small degree. Each column exhibits < 2.5 % RSD between scans (the C^{4}D cell can be temperature sensitive which may also account for deviations in signal, approximately 10 % change in detector response per 1° C, Figure 4.9).

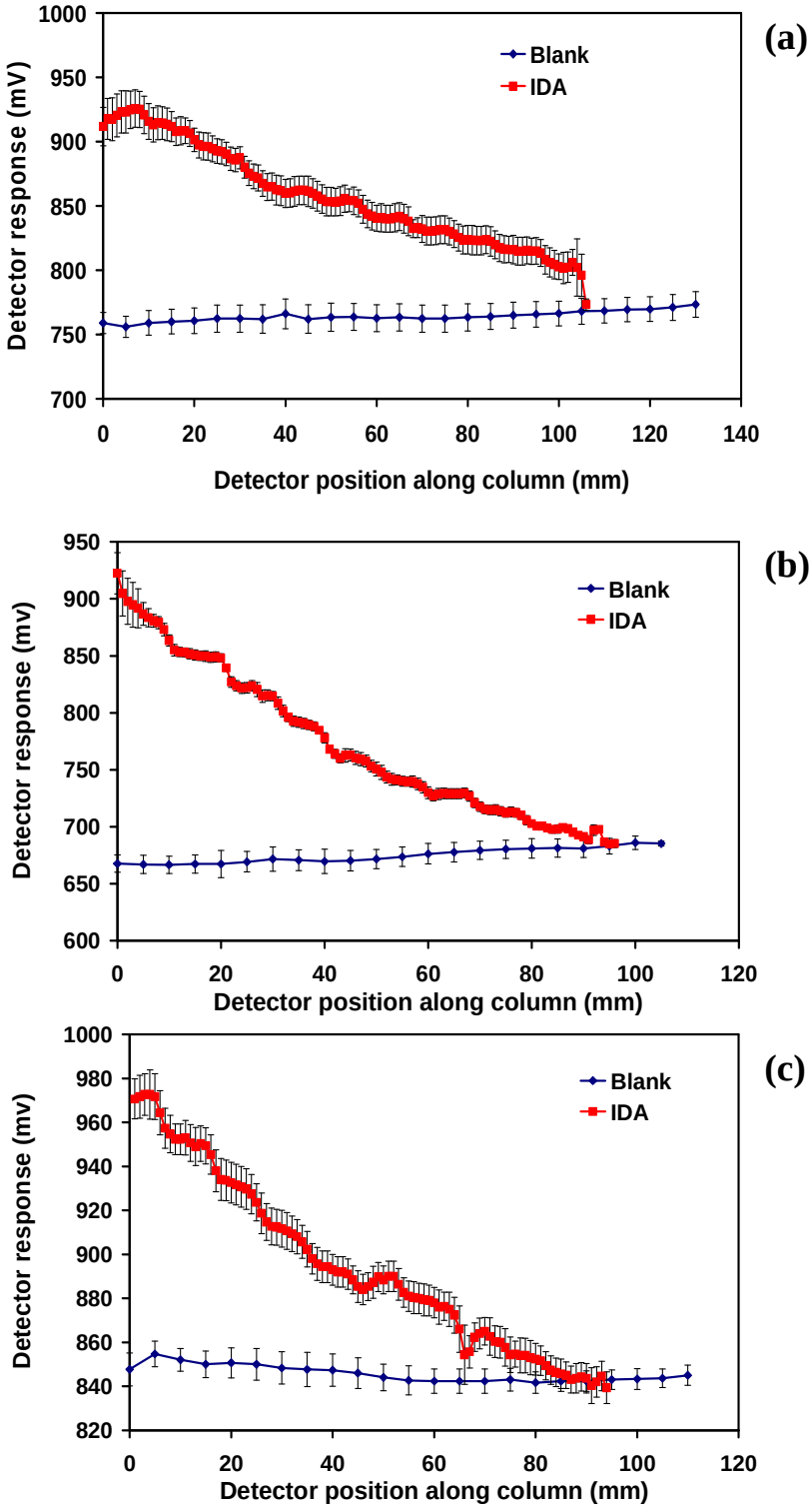

Figure 4.8: *sC^4D profiles prior to and following grafting of VAL and immobilisation of IDA for column 1 (a), column 2 (b), and column 3 (c). Scanning buffer 2.5 m*M *TES 3 m*M *ethanolamine at 1 µL/min. Measurements for sC^4D taken at 5 mm for blank columns conditions and 1 mm for grafted gradient column conditions. Gradient columns were normalised to blank columns by subtraction of excess signal generated by the buffer, for illustrative purposes only.*

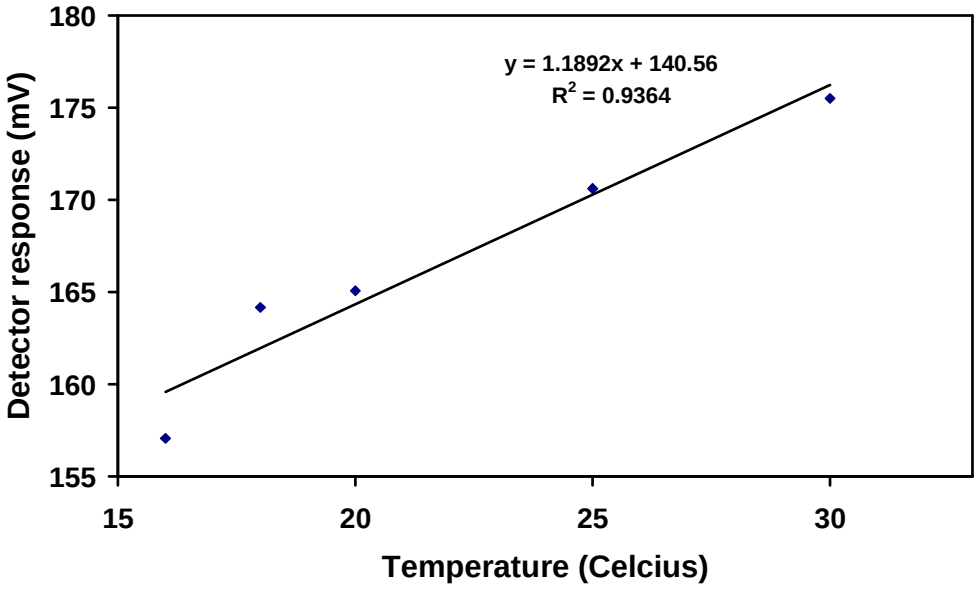

Figure 4.9: *Plot of C^4D response versus temperature for deionised water. Temperature controlled by column oven heater. Detector response measured at 16 °C, 18 °C, 20 °C, 25 °C and 30 °C. Flow rate of 1 µL/min.*

The results demonstrate how utilising a COC filter, a gradient of surface grafted functional groups can be prepared. The fabricated gradients were profiled using sC^4D. Stationary phase gradients were prepared via photo-grafting, using an in-house developed optical filter.

4.3.4. Chelation of copper ions to IDA

In immobilised metal affinity chromatography (IMAC), a trap and release mechanism is applied to separate proteins or peptides expressing histidine residues. For a separation of these molecules a gradient of imidazole [13], or chaotropic agent such as NaCl is often used [14]. In such applications titanium pumps are generally required due to high salt concentrations employed.

The ligand IDA has been used in previous reports for the preparation of IMAC stationary phases, using epoxide ring opening [15,16,17,18]. However, in this work IDA was immobilised using vinyl azlactone chemistry, which also reacts with amines, under mild room temperature conditions, as discussed in Chapter 2.0, Section 2.3.3.1. This method has also been used to immobilise proteins via pendant lysine residues [9,10] and for small molecules expressing free amines [19]. Following a multi-step

grafting fabrication process as described in Section 4.2.6.2, the column was equilibrated in 2.5 m*M* TES, 3 m*M* ethanolamine and was profiled using sC^4D. For this experiment column 1 was used. sC^4D profiles of the column were obtained prior to and following complexation with Cu^{2+} ions. Upon the formation of the chelate, the detector response should be considerably lowered due to the lower equivalent ionic conductance value for Cu^{2+} versus hydrogen based counter-ions, as discussed in Chapter 2.0, Section 2.3.3.3.

The steps involved in the IDA-Cu^{2+} complex formation were described by Nesterenko *et al*. [20] as the "long distance" interaction of electrostatic attraction which facilitates the "short distance" interaction, wherein the metal and ligand form a chelate. For the ligand and a metal to form a chelate, the metal needs to be in close proximity to the ligand. For example, the metal cation is attracted electrostatically to the negative charge on the IDA acetate groups ("long distance interaction"). A stronger ion-pair is formed, and once the metal is in close proximity, it is enveloped by the ligand to form a chelate ("short distance interaction") as water molecules are released. These processes can be seen in the schematic below in Table 4.1.

Table 4.1: *Schematic of formation of a chelate in homogeneous solution but is also applicable to sorption of metal onto a chelate modified surface, such as a column. Adapted from [20].*

Schematic	Event occurring
$M^{y+}{}_{aq} + L^{-}{}_{aq} = [M^{y+}{}_{aq}][L^{-}{}_{aq}]$	Long distance electrostatic attraction
$[M^{y+}{}_{aq}][L^{-}{}_{aq}] = [M^{y+}{}_{aq}L^{-}]$	Formation of ion pair
$[M^{y+}{}_{aq}L^{-}] = [ML^{(y-1)+}] + H_2O$	Formation of chelate with expulsion of water molecules

Where M = metal, y = valency of metal ion, L = ligand.

To allow the two step complex formation to occur, convection was removed (flow was switched off and the column was sealed). In convection mediated immobilisation, such as flushing Cu^{2+} across a monolithic column, the metals are flushed past numerous sites where possible interactions could occur. This may limit the formation

of chelates within reasonable reaction times, resulting in extended reaction times (≥ 12 h) in an attempt to produce as many complexed sites as possible. When convection is removed, the metals are not flushed beyond possible sites through the column, but are allowed to diffuse and interact with immobilised ligands. In using this mechanism, reaction can occur in as little as one h.

In Chapter 2.0, the change in detector response of the column following chelation, was found to have a maximum value of 60 mV, localised only to the area of highest functional monomer composition, i.e. the decrease in detector response was not reflected along the entire column length (Figure 2.12). This indicated a low surface concentration of immobilised copper ions along the column, with a localised increase with respect to the region of highest VAL co-monomer concentration.

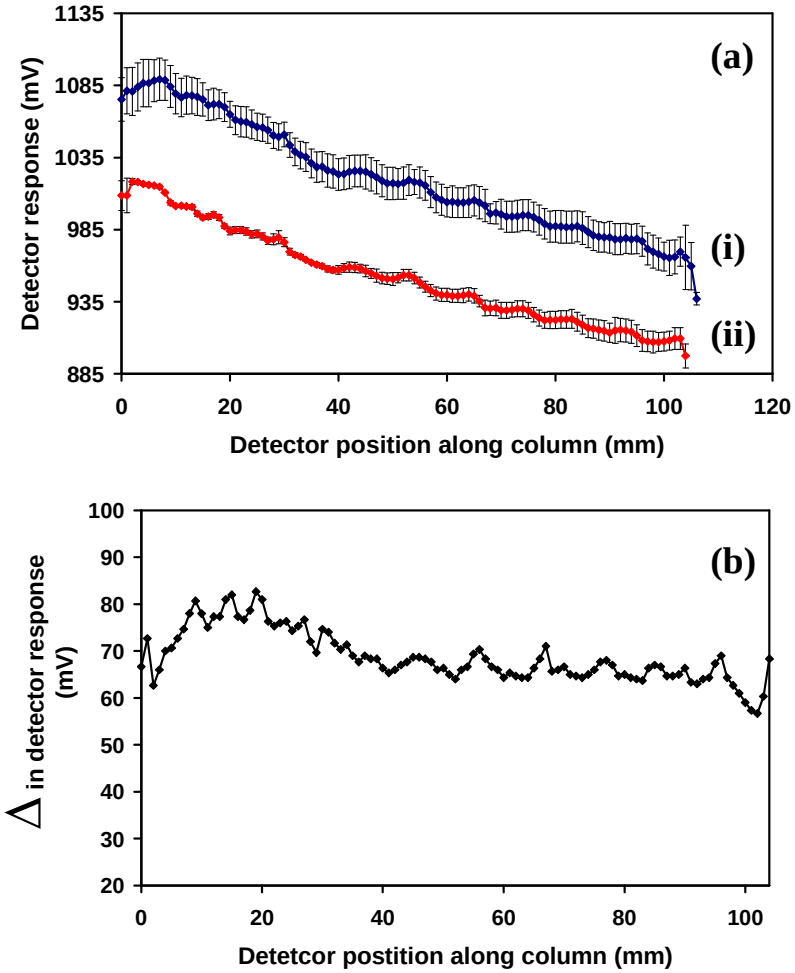

Figure 4.10: *sC^4D profiles of column 1 in IDA form (a)(i), and following complex formation (a)(ii). Change in detector response versus detector position along column, difference in detector response following chelation (b). Plots measured in triplicate, error bars included. Scan performed in 2.5 m*M *TES, 3 m*M *ethanolamine at a flow rate of 1 µL/min.*

From Figure 4.10 the reduction in detector response was much larger than previously reported with a VAL co-polymerised stationary phase gradient. The column was scanned in triplicate prior to and following chelate formation, with both column conditions exhibiting excellent scan repeatability with <2 % RSD and 1 % RSD, respectively. The stability of the on-column complex results in a lower % RSD. This enhanced stability was caused by the chelate effect, wherein the increase in entropy favours complex formation. When the complex is formed there is no counter-ion exchange process, which may also account for a higher standard deviation in sC^4D profiles involving free, un-reacted acetate groups of IDA.

In a CEC application of an IDA modified monolithic stationary phase, Tsukagoshi and co-workers reported the reduction in EOF upon binding of Cu^{2+} to the IDA stationary phase [21]. In this work, the difference in detector response is maintained along the entire column at approximately 70 mV ± 10 mV, as shown in Figure 4.10 (b). The horizontal nature of this plot indicates a constant presence of copper ions complexed to the monolith surface, along the entire column length. This indicates the complexation of all available IDA sites across the column. The success of the complexation step was examined using column 3. The column was treated with both methods for copper immobilisation, i.e. dynamic (in the presence of flow) and static immobilisation. Using sC^4D profiles the method producing the most effective complexation was determined as illustrated in Figure 4.11.

The sC^4D profiles in Figure 4.11 above demonstrate the increase in complex formation following static immobilisation versus dynamic immobilisation, as indicated by a further decrease in detector response along the column. Following the dynamic immobilisation step, where copper ions were flushed across the column for 3 h, the detector response was lower for approximately 30 mm of the initial column length. This indicated incomplete immobilisation of Cu^{2+}, with most complex formation events occurring at the column inlet (0 to 30 mm of sC^4D profile, Figure 4.11).

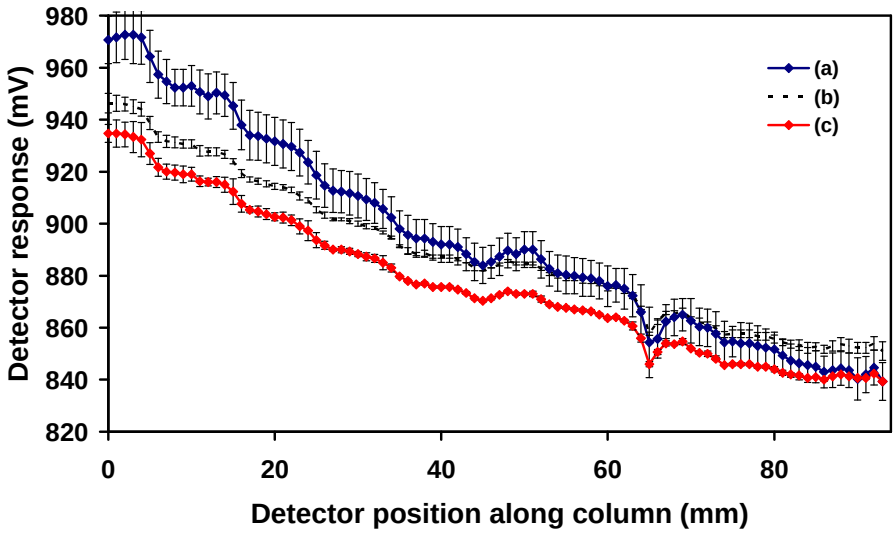

Figure 4.11: *sC^{4}D profile of column 3 in IDA form (a), following complex formation using dynamic (b) and static immobilisation (c). The difference between the final data points in (b) and (c) was used to adjust the sC^{4}D response of (c), to account for variation in background detector response. Triplicate scans reported, error bars included.*

Following static immobilisation, where the column was filled with a solution containing copper ions and sealed, a further drop in detector response was seen across the entire length of the column. From the resulting sC^{4}D plots, the difference in conductivity could be determined across the column. Similar to results generated from column 1, the difference in detector response resulted in a horizontal plot (50 mV ± 10 mV) for Δ in detector response versus detector position along column. This is shown below in Figure 4.12. This indicated complex formation across the entire column length, again, as seen with column 1. By utilising the static method of copper ion immobilisation, higher surface concentrations of copper ions would be expected.

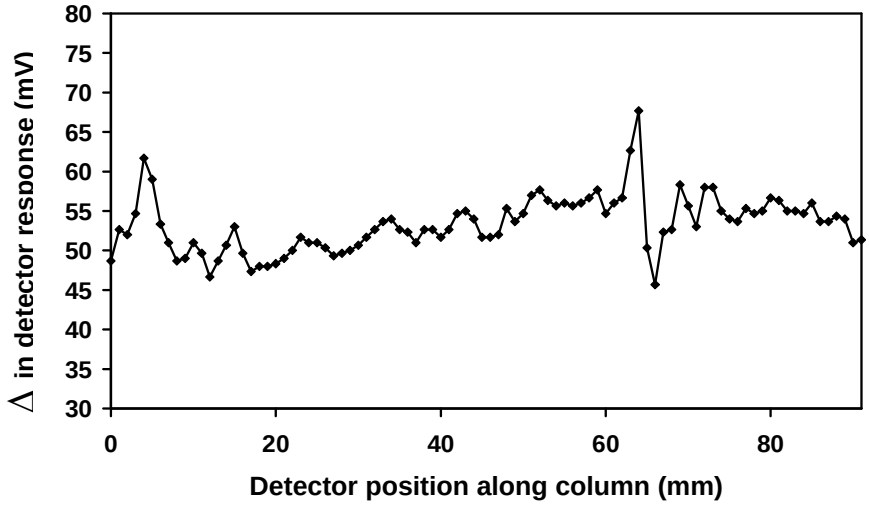

Figure 4.12: *Change in detector response across column 3 between plot (a) and plot (c) of Figure 4.11. Measurement from triplicate scan in 2.5 mM TES, 3 mM ethanolamine at a flow rate of 1 µL/min.*

In Figure 4.12 above, the deviation in signal at approximately 64 mm can also be seen in the profiling of the column in IDA form, and was likely due to a localised decrease in column permeability (i.e with increased polymer density).

In utilising photo-grafting methods the surface availability of IDA groups is greatly increased, and the density of the grafted groups can be controlled [3,4]. The increase in capacity, from a co-polymerisation method to a surface modified method, may improve the separation performance of monolithic IMAC columns, however, to confirm this, further investigaton is required. The optical filter produced in this report is not specific to the fabrication of IMAC columns, and may be applied to any polymerisation/grafting procedure at 254 nm, as described in the following section.

4.3.5. Production of SCX gradient

To illustrate the variety of selectivities that can be produced using this method, the COC optical filter was applied to the production of a strong cation exchange monolith. Using SPM, a gradient of sulphonic acid groups was immobilised to the surface of a BuMA-*co*-EDMA monolithic column using the in-house developed COC optical filter (column 4). Following fabrication, the SCX gradient column was flushed with 10 m*M* ethylenediamine (pH 4) for 3 h. The column was then equilibrated in

0.25 m*M* ethylenediamine (pH 4), which was subsequently used to profile the column (scanning buffer). The column was scanned at 5 mm intervals prior to grafting for the (blank). Increments of 1 mm were used to visualise the gradient axially along the column, using sC^4D profiling, as seen in Figure 4.13.

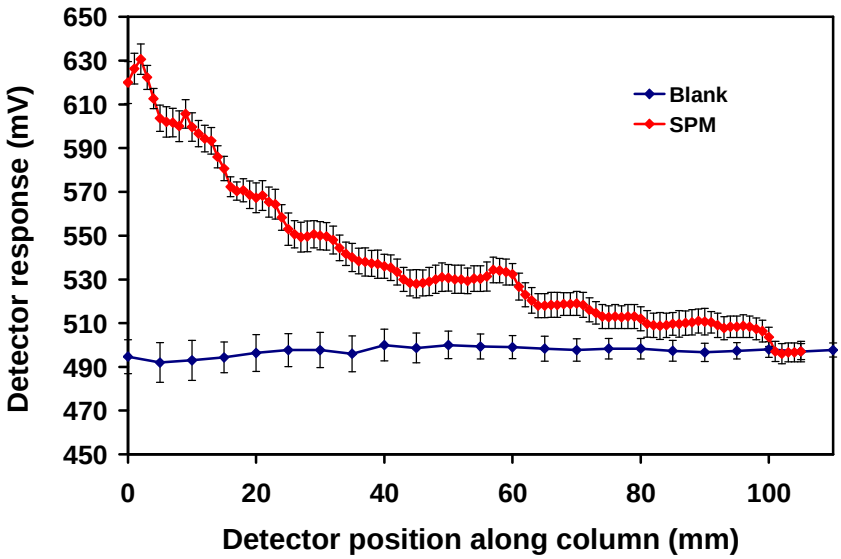

Figure 4.13: *sC^4D profile of SPM gradient produced via photo-grafting with the in house built COC optical filter. Column scanned in 0.25 m*M *ethylenediamine (pH 4) at a flow rate of 1 µL/min.*

The gradient can easily be seen in the scanning buffer. The change in detector response along the column with comparison to the blank was similar, as seen with those columns prepared with a VAL grafted gradient (Figure 4.8). This method of column grafting can be useful for the production of numerous selectivities, in trying to obtain enhanced separations.

4.3.6. Chromatographic application of SCX stationary phase gradient

The application of the gradient stationary phase was required in order to identify evidence of band focussing under isocratic eluent conditions. It was postulated that as peak broadening occurs when the band travels along the length of the chromatographic column, a low to high longitudinal capacity could act to counter this process through limited peak focussing. With a column displaying a high to low longitudinal capacity (reversed direction), it is proposed that an opposite effect may

occur, and that band broadening may even be accentuated. Transferrin was unretained on the SCX gradient monolith in both directions, and thus acted as a column void marker. Lysozyme was retained relatively strongly albeit with considerable peak tailing, due to the isocratic mobile phase conditions used. Figure 4.14 shows the two sets of chromatograms, with Figure 4.14 (a) showing the chromatograms obtained in the high to low capacity (reversed) direction, and Figure 4.14 (b) showing the same sample following chromatography in the low to high capacity (forward) direction. From these preliminary studies, evidence of peak focussing can be seen. Using the peak width at half height (W½), a decrease of 26% was observed for chromatogram Figure 4.14 (b), despite the fact that the overall SCX capacity experienced by the protein band in both chromatograms remained equal. In fact the relative improvement in peak shape for lysozyme seen when chromatographed in the forward direction was sufficient to resolve the main protein peak from a small impurity peak in the standard, thus confirming a positive effect on chromatographic efficiency.

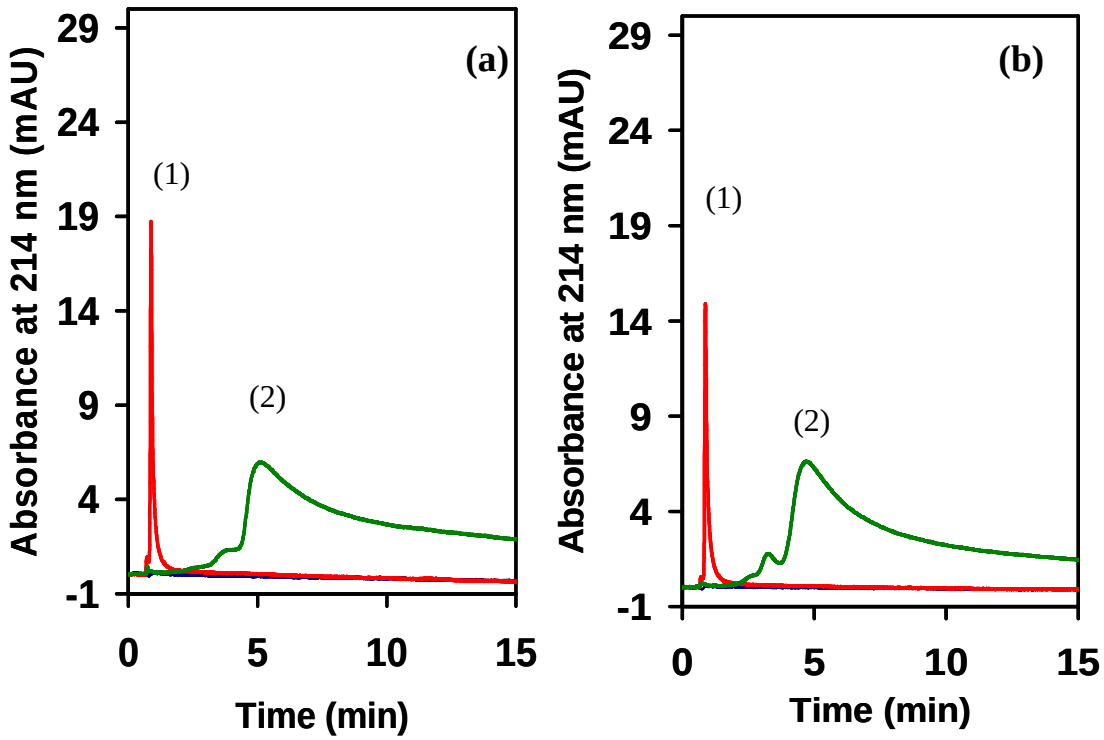

Figure 4.14: *Chromatograms of transferrin (1) and lysozyme (2) obtained under isocratic eluent conditions (0.175 M NaCl) on a SCX gradient stationary phase monolith, flow direction from high to low capacity (a), same protein standards under same eluent conditions, with flow direction from low to high capacity (b).*

4.4. Conclusions

For the first time, an optical filter based upon COC films has been fabricated and applied to the production of photo-grafted stationary phase gradients. Previous methods of gradient fabrication using co-polymerisation of functional monomer via thermal polymerisation, require lengthy reaction times (≥16 h), with a low and often sporadic surface coverage of desired functional group chemistry. Alternatively, commercially available optical filters could be used, however, optimisation of optical density may be a costly task. Using inexpensive commercially available polymer films, a novel optical filter was prepared. Photometric analysis was performed on the material, and a decrease in UV transmission (at a wavelength of 254 nm) was obtained with an increase in film thickness. An optical filter was fabricated and an optical density of 1 to 0.1 was obtained. The filter was successfully applied to the production of photo-grafted stationary phase gradients of IDA and SPM selectivities. Once produced, the IDA column was treated with Cu^{2+} to form a chelated stationary phase.

The corresponding reduction in detector response was profiled using sC^4D. In comparison to previous stationary phase gradient production via co-polymerisation, the grafting method has provided better coverage, and an evenly distributed decrease in detector response upon the formation of [IDA-Cu^{2+}] complex. To prove the usefulness of the filter, a gradient of differing chemistry was also prepared resulting in a gradient of SCX material. The columns were profiled using non-invasive sC^4D. Using this method of characterisation, the distribution of charged IDA and sulphonic acid groups could be spatially determined in both column selectivities produced herein. The application of sC^4D to the characterisation of photo-grafted stationary phase gradients, produced using this novel filter, was itself novel, as no previous reports on such a fabrication method exist. In using an immobilised gradient, pump conditions such as mixing time, re-equilibration time, and solvent compressibility (when using nano- and micro- fluidics [22]) do not require consideration. With further optimisation, stationary phase gradients produced using this approach may enhance chromatographic zone focusing, and increase peak capacity. An increase in separation performance with a stationary phase gradient was demonstrated previously [6]. Maruška and co-workers also observed increased separation efficiencies with the use

of a gradient of hydrophobic properties [7]. With further optimisation, a gradient of grafted functional groups or polymer density may be used to enhance separations.

The effect of the gradient upon a separation was also investigated using the SCX gradient column. Two proteins were separated using the gradient column with an isocratic mobile phase (0.175 *M* NaCl). In changing the direction of the gradient through which the separation is performed, a decrease in peak width (W½) of 26 % was observed in the low to high capacity direction relative to the high to low capacity direction of the gradient. This is encouraging for the future development of gradient stationary phases.

Using this type of column modification, a number of future applications may also be investigated, particularly in the production of a gradient of porosity in monolithic columns. As previously mentioned, Collins *et al*. used a thermal gradient to produce a gradient of porosity within a monolithic column over a period of 16 h [2]. By varying photo-polymerisation activation energy using an optical filter such as the one produced here, a column exhibiting a gradient of porosity can be produced easily and rapidly, and profiled non-invasively using sC^4D, with possible applications in size exclusion chromatography.

4.5. References

[1] Jiang, D., Huang, X., Qiu, F., Luo, C., Huang, L.L., *Macromolecules*, 43, 2010, 71.

[2] Collins, D., Nesterenko, E., Connolly, D., Vasquez, M., Macka, M., Brabazon, D., Paull, B., *Anal. Chem*., 83, 2011, 4307.

[3] Rohr, T., Ogletree, D., Svec, F., Fréchet, *J., Adv. Funct. Mater*.,13, 2003, 264.

[4] Rohr, T., Hilder, E., Donovan, J., Svec, F., Fréchet, J., *Macromolecules*, 36, 2003, 1677.

[5] Urbanova, I., Svec, F., *J. Sep. Sci*., 34, 2011, 2345.

[6] Pucci, V., Raggi, M.A., Svec, F., Fréchet, J., *J. Sep. Sci*., 27, 2004, 779.

[7] Maruška, A., Rocco, A., Kornysova, O., Fanali, S., *J. Biochem. Biophys. Methods*, 70, 2007, 47.

[8] Stachowiak, T., Svec, F., Frechet, J., *Chem. Mater*., 18, 2006, 5950.

[9] Logan, T., Clark, D., Stachowiak, T., Svec, F., Fréchet, J., *Anal Chem*. 79, 2007, 6592.

[10] Krenkova, J., Lacher, N., Svec, F., *Anal. Chem*., 81, 2009, 2004.

[11] http://www.zeonex.com/applications_zeonorfilm.asp (access 08 Dec 2011).

[12] Connolly, D., Barron, L., Gillespie, E., Paull, B., *Chromatographia*, 70, 2009, 915.

[13] Ren, D., Penner, N., Slentz, B., Inerowicz, H., Rybalko, M., Regnier, F., *J. Chromatogr. A*, 1031, 2004, 87.

[14] Lou, Q., Zou, H., Xiao, X., Guo, Z., Kong, L., Mao, X., *J. Chromatogr. A*, 926, 2001, 255.

[15] Iwata, H., Saito, K., Furusaki, S., *Biotechnol. Prog*., 7, 1991, 412.

[16] Oshima, T., Kanemaru, K., Tachiyama, H., Ohe, K., Baba, Y., *J. Chromatogr. B*, 876, 2006, 116.

[17] Kanemaru, K., Oshima, T., Baba, Y., *Reactive & Functional Polymers*, 70, 2010, 103.

[18] Zachariou, M., Hearn, M., *Biochemistry*, 35, 1996, 202.

[19] Gillespie, E., Connolly, D., Nesterenko, P., Paull, B., *J. Sep. Sci*., 32, 2009, 2659.

[20] Nesterenko, P., Jones, P., Paull, B., *High performance Chelation Ion Chromatography*, RSC publishing, 2011.

[21] Tsukegoshi, K., Shimadzu, Y., Tamane T., Riichiro, N., *J. Chromatogr. A*, 1040, 2004, 151.

[22] Brennan, R., Yin, H., Killeen, K., *Anal. Chem*., 79, 2007, 9302.

Chapter 5.0

Production and characterisation of monolithic stationary phases, with segmented functionality.

“I'm an idealist. I don't know where I'm going, but I'm on my way.”

Carl Sandburg

5.1.Introduction

Polymer monolithic columns have been used in the past to produce columns expressing dual [1] or multiple functionalities [2]. However, transfer of such technology to packed columns can be difficult. Multi-dimensional columns have been produced for multi-dimensional protein identification technology (MudPIT), using packed capillary columns [3,4]. In this technique a capillary column is packed with two separate stationary phases, resulting in a column containing both ion exchange and reversed-phase packing materials. However, problems in maintaining packing pressure whilst changing particle slurry mixtures can be challenging. Photo-grafting of polymer monolithic columns can provide an alternative to packing technologies, when attempting to produce a multi-dimensional column within a single column housing.

An inherent problem encountered with polymeric monolithic columns, is the lack of meso-pores in the structure. As meso-pores (and micro-pores) contribute greatly to monolithic surface area, polymer monoliths generally exhibit low surface area [5,6]. For example Svec *et al.* [7] reported the fabrication of a poly(GMA-*co*-EDMA) monolith with a surface area of ~ 10 m^2/g, which was further used to separate a mixture of myoglobin, ovalbumin, cytochrome C and lysozyme. Viklund *et al.* [8] produced a poly(GMA-*co*-EDMA) monolith with a surface area of ~35 m^2/g, however, due to the low permeability of the column it could not be applied to chromatographic separations. Instead the group used a column with a surface area of 8.2 m^2/g in the separation of myoglobin, chymotrypsinogen, and lysozyme. In an attempt to increase the surface area of a polymer monolith, Santora *et al.* [9] prepared monolithic columns with very high surface areas (~800 m^2/g) using 100 % divinylbenzene in the polymerisation mixture, however, since surface area is inversely proportional to permeability, this also resulted in poor permeability of the monolith [10].

Urban *et al.* [6] also investigated alternative methods to increase surface area, whereby hyper-cross-linking was used. The group produced columns of poly(styrene-*co*-vinylbenzyl chloride-*co*-divinyl benzene), with extremely high surface areas of >650 m^2/g. In this fabrication process, the polymer monolith exhibiting macro-pores is further reacted to contain an extensive network of additional meso- and micro-

pores, using Friedel Crafts alkylation *in situ*. In a column with no hyper-cross-linking, the separation of benzene derivatives resulted in a peak for uracil, and the co-elution of 6 other analytes (benzene, toluene, ethylbenzene, propylbenzene, butylbenzene, and amylbenzene). Using a shorter hyper-cross-linked column, the same separation was performed, and resulted in the separation of all of the analytes outlined above. Using the hyper-cross-linked column a plate count of 73, 000 N/m was obtained for uracil.

Due to the high surface to volume ratio of nano-particles [11], they can be used to increase the surface area of polymer monoliths, either by encapsulation within the monolith [12,13,14] or by surface attachment [15,16]. Hilder *et al.* [15] reported the use of latex nano-particles expressing quaternary amine functionality, to increase surface area upon a poly(BuMA-*co*-AMPS-*co*-EDMA) monolithic column, where surface expressed sulphonic acid groups facilitated sites for coulombic interaction. Using this approach an increase in surface area of approximately 30 % was reported by the authors. Krenkova *et al.* [11] investigated the use of commercially available hydroxyapaptite nano-particles, encapsulated within a poly(2-hydroxyethyl methacrylate-*co*-EDMA) monolith. In this process, a solution of nano-particles was added to the monolith pre-cursor monomer solution. By varying the concentration of nano-particles incorporated into the monolith pre-cursor solution, the morphology of the monolith changed, expressing smaller average pore sizes. As pore size is inversely proportional to surface area [8], it can be inferred that the surface area increased with increasing nano-particle content. The binding capacity of the monolith was determined using frontal analysis of a 0.5 mg/mL solution of lysozyme. The binding capacity was found to increase with increasing nano-particle content, thus increasing the surface area.

Other nano-materials have been incorporated into polymer monoliths to increase separation efficiencies for small molecules on polymer monoliths. Chambers *et al.* [14] synthesised a monomer which contained a fullerene ([6,6]-phenyl-C_{61}-butyric acid-2-hydroxyethyl methacrylate) which was subsequently used as a co-monomer in the fabrication of poly(GMA-*co*-EDMA) and poly(BuMA-*co*-EDMA) monoliths. The columns were subjected to analysis of benzene derivatives with the peak for benzene resulting in an efficiency of 110, 000 N/m. In a separate report [16] the same group prepared a poly(GMA-*co*-EDMA) monolith, which was subsequently aminated. The amination facilitated the capture of carboxylated multi-walled carbon

nano-tubes via electrostatic attraction. Using this column the group performed separations of benzene derivatives, with efficiencies up to 44, 000 N/m obtained.

Gold nano-particles are commonly attached to polymer monoliths using either amine [17,18] or thiol [19,20] based immobilisations. Alwael *et al.* [17] immobilised gold nano-particles onto EDMA monoliths contained within polypropylene pipette tips, using amine based immobilisation. By preparing these monolith materials in pipette tips, they can be used for *in-tip* solid phase extraction (SPE) applications. The group immobilised a carbohydrate binding protein (lectin) to the gold modified monolith. The immobilised lectin was selective for galactose, and so the monolith tips were applied to the selective extraction of desialylated transferrin from an *E. Coli* cell lysate, spiked with desialylated transferrin. The resulting chromatograms (performed on a reversed-phase monolith) demonstrated no interference from the cell lysate material, which contained no glycoproteins.

Cao *et al.* [19] demonstrated the versatility of immobilised gold nano-particles. Using a single method for attachment of gold to the poly(GMA-*co*-EDMA) monolith, the immobilised nano-particles could be further modified with additional functional groups. The authors demonstrated that a number of different functionalities could be expressed upon the gold modified monolith using exchangeable ligands, thus resulting in tailored chemistries for specific applications. For example, mercaptopropionic acid was flushed across the gold modified column, producing a carboxylic acid functionality. The column was washed subsequently with mercaptoethanol (resulting in hydroxyl functionality), which was further reacted with cysteamine to finally produce a column expressing amine functionality. Similarly a solution of octadecanethiol was flushed across the gold modified column, producing a stationary phase suitable for reversed-phase chromatography. Using an aqueous solution of sodium-2-mercaptoethansulphonate, strong cation exchange functionality could be produced on the monolith.

In 2010, Xu *et al.* [20] reported the fabrication of a poly(GMA-*co*-EDMA) monolith, subsequently modified to bear thiol groups, using either sodium sulphide (NaHS) or cysteamine. The column was modified with gold using two methods of nano-particle attachment, either through flushing the pre-formed nano-particles through the column, or by *in situ* reduction of gold chloride and sodium citrate. The group opted for *in situ* reduction, resulting in a faster immobilisation time, however this immobilisation technique can lead to lower concentrations of immobilised gold

[19]. The column was used for the selective trapping of cysteine containing peptides, with subsequent separation on a commercially available Acclaim PepMap packed capillary column (150 mm x 75 µm ID, 3 µm particle diameter with 100 Å pore diameter) with C_{18} functionality. Krenkova *et al.* [11] have also investigated the use of nano-particles for bioaffinity chromatographic applications. Iron oxide nano-particles were immobilised to a poly(GMA-*co*-EDMA) monolith functionalised with quaternary amine groups. The column was applied to the enrichment of phosphopeptides (following tryptic digestion), using analytes of β-casein and α-casein.

Photo-grafting has been used in monolithic column research to obtain numerous selectivities, upon morphologically optimised monolithic structures [1,2,21]. In 2003, Peterson *et al.* [1] produced a dual function device, incorporating a hydrophobic segment suitable for SPE, and a micro-reactor (immobilised trypsin) on a polymer monolithic column. The hydrophobic SPE zone facilitated the trapping of proteins. Visualisation of the SPE segment relied on the capture of fluorescently tagged protein (casein), which does not represent the total amount of immobilised protein [22]. Logan *et al.* [2] used a multi-step photo-masking procedure in order to produce a poly(BuMA-*co*-EDMA) monolithic column expressing three distinct zones of different enzymes. Both methods were discussed in detail, in Chapter 1, Section 1.12.5.

Scanning electron microscopy (SEM) is used predominantly in the visualisation of nano-particles on monolithic phases. In the use of SEM imaging, the column must be destroyed for analysis, rendering it useless for future application. In previous chapters, the fabrication of monolithic columns expressing a longitudinal spatial variation in surface chemistry was investigated. The production of such advanced stationary phases requires finely tuned grafting techniques, which may be adapted for the production of other stationary phase modes, such as multi-dimensional stationary phases, wherein a stationary phase consisting of two (or more) distinct and orthogonal chemistries can be produced.

The aim of the present chapter is to develop a dual function monolith column via photo-grafting techniques, and to introduce gold nano-particles to a defined section of the monolith column suitable for micro solid phase extraction (µSPE). The fabricated columns with a dual function were non-invasive and non-destructive characterised using sC^4D profiling, throughout all stages of development and also as a

quality control step for the fabricated columns [23]. Photo-masking and photo-grafting techniques will be used to produce a zone of nano-agglomerated monolith upon an otherwise unmodified monolith. Poly(BuMA-*co*-EDMA) and poly(LMA-*co*-EDMA) monoliths were grafted with reactive monomers such as vinyl azlactone (VAL) and epoxide groups (via GMA), in order to produce an aminated surface suitable for gold nano-particle attachment for possible future applications in bioaffinity chromatography. Such a detailed investigation has not been previously performed on a column presenting two distinct stationary phases, one of which incorporating gold nano-particles. The profiling technique (sC^4D) was also used to cross-validate the presence of gold nano-particles across the entire nano-agglomerated monolith segment.

5.2. Experimental

5.2.1. Instrumentation

As described in Chapter 2.0, Section 2.2.1 with the following changes. A Mistral Column Oven 880 (Spark Holland, The Netherlands) was used for thermal modification of photo-grafted epoxy groups. A PEEK loop of approximately 300 µL, was filled with gold nano-particle solution, and was placed between the pump and the column, to introduce gold nano-particles to the column. A Hitachi S-5500 field emission SEM (Hitachi, Maidenhead, UK) used for FE-SEM imaging. For chromatographic studies, a Dionex Ultimate 3000 capillary LC system was used, with a split flow rate of 1: 101, delivering a flow rate of 2 µL/min. Protein standards were prepared at 50 µg/mL for ribonuclease B, insulin, and bovine serum albumin. The proteins were injected onto the column via 120 nL loop. For separation, a hold up time of 5 minutes was applied, followed by a 10 minute gradient from 100 % A (5 % ACN, 0.1 % TFA) to 100 % B (95 % ACN, 0.1 % TFA). Proteins were detected using UV detection at a wavelength of 214 nm.

5.2.2. Materials and reagents

As described in Chapter 2.0, Section 2.2.2 with the following additions. Gold(III) chloride trihydrate, trisodium citrate, and nitric acid (67 %) were purchased from Sigma-Aldrich (Dublin, Ireland) and used as supplied.

5.2.3. Scanning C^4D

For sC^4D profiling, the column was equilibrated with water and was scanned prior to immobilisation procedures. Intervals of 5 mm were used for profiling of the preliminary test columns. Prior to sC^4D profiling, the pendent amines were protonated using a flush of HNO_3. The acid was flushed across the columns for 1 hour followed by water until the effluent reached a neutral pH. The columns were then equilibrated with water prior to sC^4D profiling. By protonating the amine groups, the charge can be easily observed with sC^4D. Following the subsequent immobilisation of gold nano-particles, the monolithic columns were scanned in deionised water.

5.2.4. Vinylisation of fused silica capillary

Fused silica capillary was vinylised using a procedure described previously in Chapter 2.0, Section 2.2.4.

5.2.5. Fabrication of monolithic columns

5.2.5.1.Fabrication of butyl methacrylate columns

A total of ten monolithic columns consisting of BuMA-*co*-EDMA, were prepared for the optimisation of grafting procedures. Each monolith was prepared as described in Chapter 2.0, Section 2.2.5.1. Three columns named column BuMA-V1, BuMA-V2, and BuMA-V3 were fabricated, for VAL photo-grafting using UV light at 254 nm. To investigate the effect of varying VAL concentration during photo-grafting, two more columns were produced, named columns BuMA-V30 and BuMA-V40. Columns BuMA-G1, BuMA-G2 and BuMA-G3 were fabricated for GMA grafting procedures. The final columns measured 100 mm in length (for grafting optimisation). Following fabrication the monolithic columns were equilibrated in water prior to sC^4D profiling. The optimised grafting and amination procedure was then extended to LMA-*co*-EDMA monolithic columns, in the preparation of analytical columns for chromatographic applications. A list of all fabricated monoliths with a naming convention can be seen in Table 5.1.

5.2.5.2. Fabrication of lauryl methacrylate columns

A total of seven LMA-*co*-EDMA monoliths were prepared. Columns LMA-G1, LMA-G2, and LMA-G3 (see Table 5.1) were used in the preliminary optimisation of photo-grafting methods. These columns were prepared to a length of 100 mm each, with 50 mm dedicated to the immobilisation of gold nano-particles, followed by 50 mm of reversed-phase selectivity. The fourth and fifth columns, column LMA-A1 and column LMA-A2 were fabricated as analytical columns, for future chromatographic applications. Columns LMA-A1and LMA-A2 were fabricated with a total length of 200 mm, comprising of a 50 mm zone intended for solid phase extraction (after gold nano-particle immobilisation), and a 150 mm reversed-phase zone (C_{12}) intended for subsequent separations. The monoliths were produced using a monomer mixture of 24 % LMA and 16 % EDMA, with a binary porogen system of 14.5 % 1,4-butanediol, 45.5 % 1-propanol. The photo-initiator DAP was present at 1 % w.r.t. the total % monomer present. Following deoxygenation, the capillary housing was filled with monomer pre-cursor solution using capillary action, and the ends of the column were sealed. A dose of UV energy measuring 2 J/cm^2 was applied to the columns. Following polymerisation, the columns were washed with methanol to remove any un-reacted monomer. When investigating the effect of varying GMA concentration during photo-grafting, two final columns were fabricated namely LMA-G5 and LMA-G30.

5.2.5.3. Fabrication of poly(styrene-co-divinyl benzene) monoliths

Using thermal polymerisation methods, two poly(styrene-co-divinyl benzene) (PSDVB) monoliths were prepared as described by Premstaller *et al.* [24]. A porogen system of decanol (56 %), and tetrahydrofuran (4 %), were used. Styrene was present at 20 %, with the cross-linker, divinyl benzene, present at 20 %. The polymerisation was initiated at 70 ˚C for 24 hours using 2.5 % AIBN. The column was washed with methanol for 3 hours at 10 µL/min, to remove any unreacted monomer. These columns were used in the investigation of immobilisation of gold nano-particles upon blank unmodified monolithic columns. The two columns were named PS-Blank 1 and PS-Blank 2, as seen in Table 5.1.

Table 5.1: *Composition of monoliths and grafted monomer for amination and gold nano-particle immobilisation.*

Monolith	Column name	Total column length (mm)	Grafted monomer
BuMA-*co*-EDMA	BuMA-V1	100	VAL
BuMA-*co*-EDMA	BuMA-V2	100	VAL
BuMA-*co*-EDMA	BuMA-V3	100	VAL
BuMA-*co*-EDMA	BuMA-V30	N/A	VAL
BuMA-*co*-EDMA	BuMA-V40	N/A	VAL
BuMA-*co*-EDMA	BuMA-G1	100	GMA
BuMA-*co*-EDMA	BuMA-G2	100	GMA
BuMA-*co*-EDMA	BuMA-G3	100	GMA
BuMA-*co*-EDMA	BuMA-Blank 1	N/A	N/A
BuMA-*co*-EDMA	BuMA-Blank 2	N/A	N/A
LMA-*co*-EDMA	LMA-G1	100	GMA
LMA-*co*-EDMA	LMA-G2	100	GMA
LMA-*co*-EDMA	LMA-G3	100	GMA
LMA-*co*-EDMA	LMA-G5	N/A	GMA
LMA-*co*-EDMA	LMA-G30	N/A	GMA
LMA-*co*-EDMA	LMA-A1	200	GMA
LMA-*co*-EDMA	LMA-A2	200	GMA
PSDVB	PS-Blank 1	N/A	N/A
PSDVB	PS-Blank2	N/A	N/A

5.2.6. Modification of methacrylate monolithic columns

Photo-masking has been described previously as an effective means to selectively pattern sections of a monolithic column [1,2,22]. All columns were marked into two distinct zones using a permanent marker. The first zone was to contain the solid phase extraction material, as immobilised gold nano-particles can be used to selectively extract cysteine containing peptides [19]. The second zone was to contain the separation phase (e.g. C_4 or C_{12}). Using photo-masking and photo-grafting this could be easily achieved.

The solid phase extraction zone consisted of gold nano-particles immobilised to the column via amine chemistry, facilitated by photo-grafted VAL or photo-grafted GMA. For both modification types, the columns were first immobilised with benzophenone as described previously [22]. Briefly, a 5 % solution of benzophenone in methanol was deoxygenated with nitrogen, prior to being flushed across the column for 1 hour. The column's ends were sealed, and a photo-mask was placed on the column housing, exposing the area ultimately intended to contain the grafted zone, as shown in Figure 5.1. The exposed section of the column was then subjected to 1 J/cm^2 of UV energy, and was subsequently washed with methanol, to remove any un-reacted monomers.

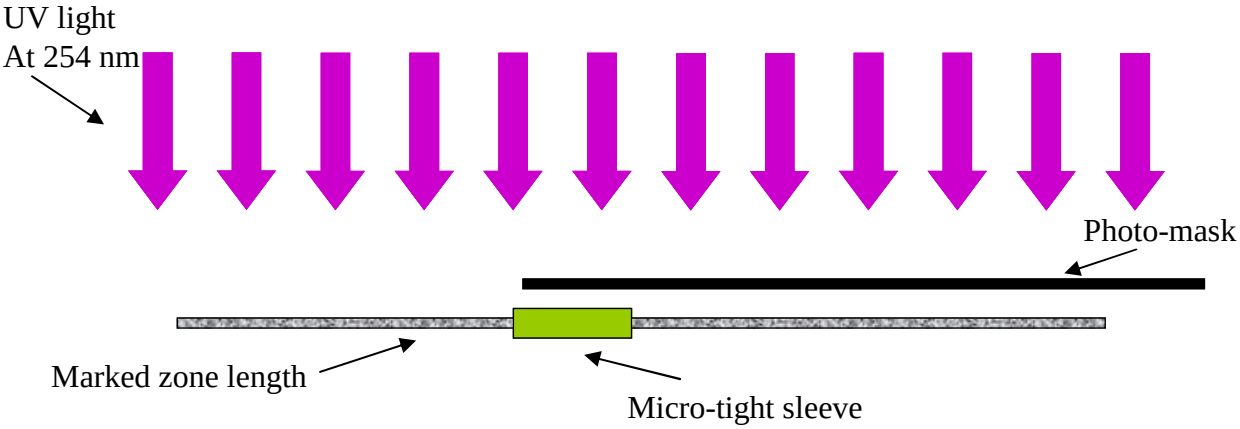

Figure 5.1: *Schematic of the photo-grafting protocol used to produce a single zone of grafted functionality. Micro-tight sleeve used to promote a sharp boundary during photo-grafting procedures.*

Connolly *et al.* [18] prepared poly(BuMA-*co*-EDMA) monoliths, which were modified to express wither amine or thiol functional groups. Comparing amine to thiol immobilisation protocols, amine immobilisation resulted in a higher coverage of nano-particles. Thiol based modification resulted in dimers, trimers, and larger clusters of nano-particles, with large spaces between them. In this work gold nan-particles were immobilised via amine chemistry, as outlined below.

5.2.6.1.Amination via vinyl azlactone chemistry

For the optimisation of the photo-grafting procedure, a solution of 20% VAL was prepared in methanol and deoxygenated with nitrogen. The column was flushed with this solution for 1 h. Again the photo-mask was applied to the same length of column as outlined above in Figure 5.1. The exposed zone was subjected to 1 J/cm^2 UV energy, and the column was then subsequently washed with methanol, to remove any un-reacted monomer. To aminate the grafted zone, a solution of 1 *M* ethylenediamine was prepared in deionised water, and flushed across the active poly(VAL) sites for 3 h, at a flow rate of 1µL/min and at room temperature. The lone pair from the amine group acts as a neutral nucleophile resulting in immobilisation, via a ring opening reaction. Following amination, the column was subsequently washed with water until the effluent reached a neutral pH. A schematic of the reaction is shown in Figure 5.2 (a).

5.2.6.2.Amination via epoxy ring chemistry

An alternative to using azlactone ring chemistry is the opening of the epoxide ring in a grafted polymer, such as poly(GMA). Using a base at elevated temperatures (60 °C to 70 °C) has been reported numerous times in the literature for the immobilisation of amine containing compounds [2,25]. In this work, the immobilisation of benzophenone was performed as described previously in Section 5.2.6. A 15 % GMA solution was prepared in methanol and deoxygenated using nitrogen sparging for 10 minutes. The solution was flushed across the monolith for 1 hour, and the column was subsequently sealed. The column was masked to expose a segment of 50 mm, equal to that of the previous immobilisation step. A UV dose of 1 J/cm^2 was applied to the exposed segment of column, which was subsequently washed with methanol to remove any un-reacted monomer. The column was profiled using sC^{4}D in deionised water.

For amination of the epoxide group, a 1 *M* solution of ethylenediamine was flushed across the monolith at 70 ˚C for 16 hours, at a flow rate of 0.167 µL/min. The column was washed with water to remove any excess base. A schematic of the reaction scheme is shown in Figure 5.2 (b).

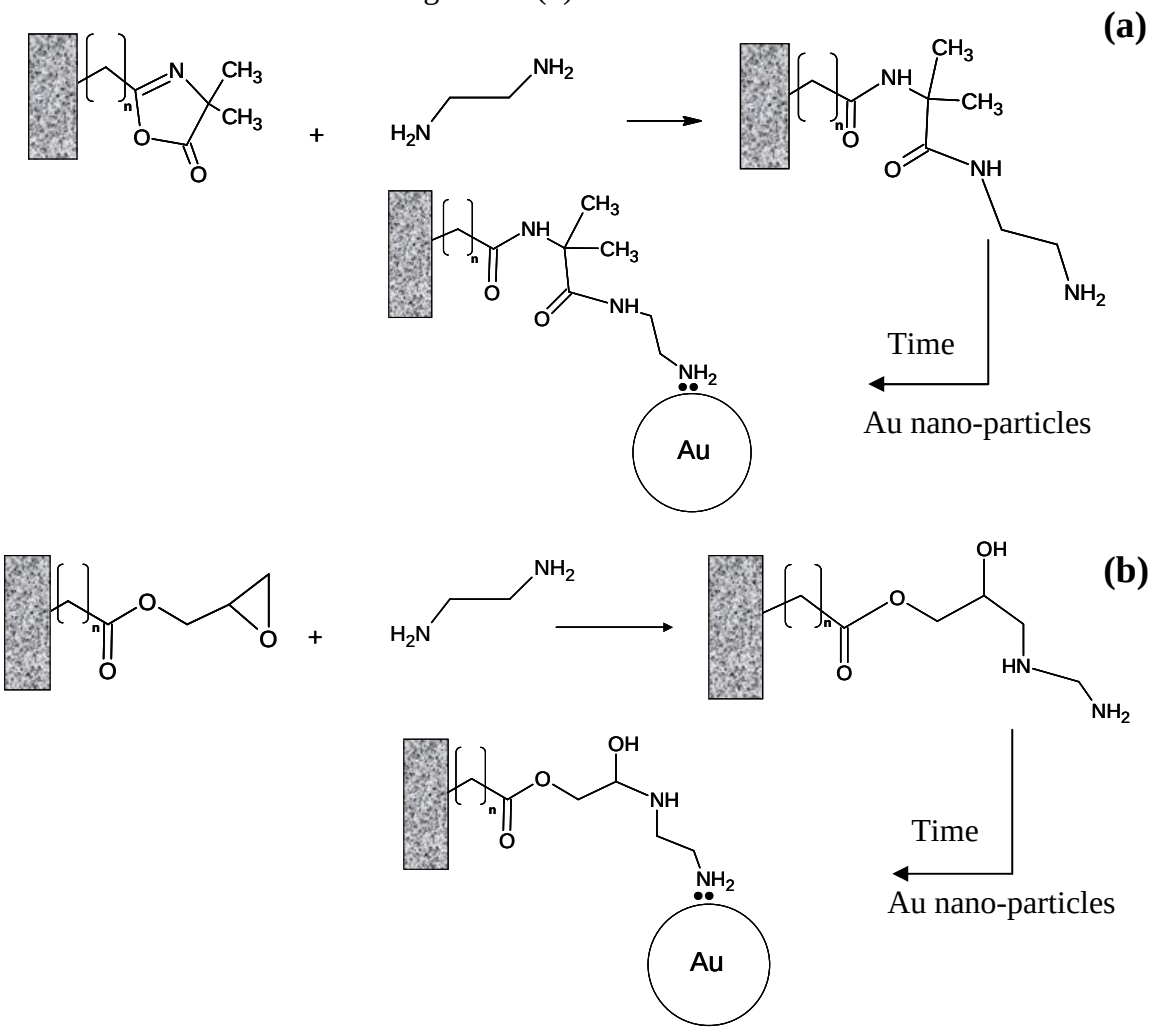

Figure 5.2: *Reaction scheme for the immobilisation of ethylenediamine and gold nano-particles upon a VAL grafted monolithic column (a), and an epoxide ring of photo-grafted GMA groups (b).*

A schematic of the experimental set-up is shown in Figure 5.3. The syringe was filled with 1 *M* ethylenediamine and placed on the syringe pump, which was then connected to some capillary tubing (25µm ID). Within the oven, the base was pumped through the column towards the waste vial. The un-reacted ethylenediamine was pumped through some fused silica capillary (25 µm ID) to a waste vial.

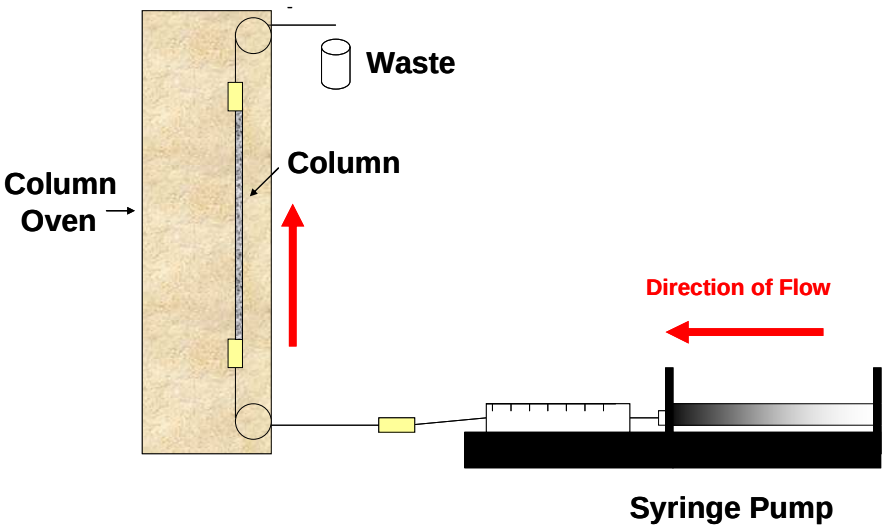

Figure 5.3: *Schematic of the experimental setup used for the immobilisation of ethylenediamine.*

5.2.6.3.Immobilisation of nano-particles

Citrate stabilised gold nano-particles (20 nm) were prepared as described by Frens [26]. Using UV-VIS spectrometry the maximum absorbance (λ_{max}) of the gold nano-particle-citrate suspension was measured across the UV-VIS spectrum (wavelengths of 800 to 200 nm) (Figure 5.4). The presence of gold nano-particles could be visualised by eye due to the characteristic colour of gold nano-particles of 20 nm (200 Å) diameter (Table 5.2). To create a defined boundary between the gold-modified and reversed-phase sections of the column, it was imperative that the zone boundary was not altered throughout the photo-grafting procedures. The column was connected to a loop containing nano-particles, which were subsequently pumped across the column, until the moving "plug" of the gold solution reached the pre-determined zone boundary. As reported by Frens [26] the size of the fabricated nano-particles resulted in different colours (Table 5.2). The nano-particles were deemed to be fully immobilised when the column bed turned a deep burgundy colour, as reported previously [17,20]. The direction of flow through the column was reversed and water was flushed through the column to remove any interstitial citrate.

Table 5.2: Relationship between gold nano-particle size and colour.

Diameter (Å)	Colour
160	Orange
245	Red
410	Red
715	Dark red
975	Violet
1470	Violet

5.2.7 Chromatographic application

To investigate the use of the modified monolithic phases for the retention of proteins, for either trap and release applications, or for on-capillary sample clean-up, a series of individual protein standards were injected onto the column, with the gold nano-particles located at the column inlet. The selected proteins, bovine serum albumin and insulin, were chosen due to the large number of thiols and lysine residues within the molecules. Prior to, and immediately following, each protein injection, blank injections (mobile phase) were also injected onto the column and an ACN mobile phase gradient applied to the monolith. In order to elute the trapped proteins, the column was disconnected from the system and flushed with 4 *M* 2-mercaptoethanol for 1 h. The column was then reconnected to the system and flushed with 100 % A for 15 mins to remove any interstitial mercaptoethanol. A blank was injected and the gradient programme was applied as outlined in Section 5.2.1.

5.3. Results and discussion

In order to verify the presence of goln nano-particles a number of characterisation techniques can be used such as UV-VIS spectrometry or imaging techniques susch as SEM.

5.3.1. UV-VIS analysis of gold nano-particles

Using a scanning range of 800 to 200 nm a spectrum of the gold suspension was recorded. The spectrum showed a characteristic absorprtion peak at

approximately 520 nm, similar to that reported by Šlouf and co-workers [27]. The resulting spectrum is shown in Figure 5.4.

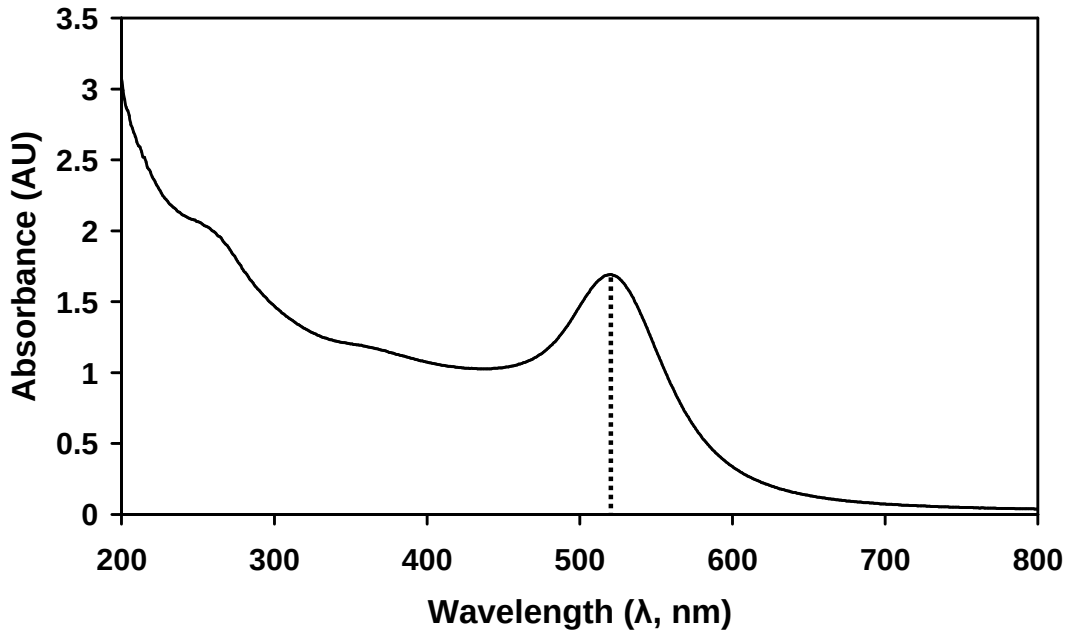

Figure 5.4*: UV-VIS spectrum of gold nano-particles suspended in citrate. Scanning range from 800 nm to 200 nm in wavelength.*

This spectrum demonstrated the successful fabrication of the gold nano-particle suspension. Following the immobilisation of gold nano-particles upon the separation media, characterisation techniques such as FE-SEM and sC^4D were used as outlined in the following sections.

5.3.2. FE-SEM analysis of gold nano-particle coverage

5.3.2.1. BuMA-co-EDMA with aminated photo-grafted VAL

In an attempt to optimise the surface coverage of gold nano-particles, the mechanism for amination was investigated. By increasing the surface density of grafted VAL, an increase in amination can occur resulting in a higher surface concentration of nano-particles. Concentrations of 20 %, 30 % and 40 % VAL were grafted onto a number of columns, to ascertain which concentration provided the highest coverage of nano-particles. The resulting coverage with respect to VAL concentration is shown in Figure 5.5.

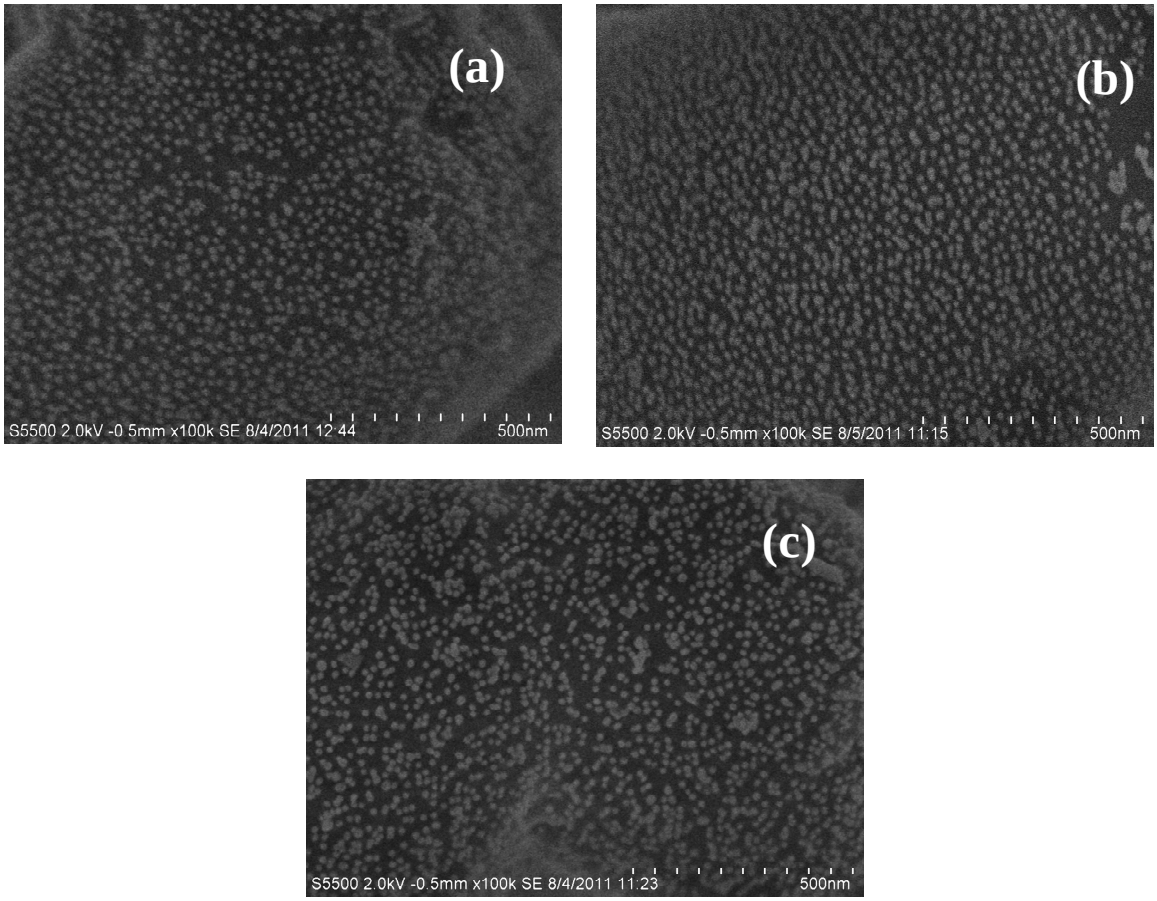

Figure 5.5: *FE-SEM micrographs of BuMA-co-EDMA monolithic columns grafted with 20 % VAL (a), 30 % VAL (b), and 40 % VAL (c), with subsequent amination and gold nano-particle attachment as outlined above.* V_{acc} *2 kV, magnification 100, 000 X.*

Using a square of 500 nm in length and width (area 250, 000 nm^2), the number of nano-particles were counted using the three FE-SEM micrographs from Figure 5.17. Columns grafted with a zone of 20 % VAL expressed approximately 296 nano-particles in the defined region. Using a higher concentration of VAL (30 %) the nano-particle count in an area of the same magnitude was higher at ~370 nano-particles in the defined region. However, on increasing the concentration of VAL further to 40 % VAL resulted in a drop in the number of nano-particles in the defined region, with approximately 330 nano-particles in the defined region.

As the concentration of functional monomer was increased an effect known as self screening occurs during photo-grafting, wherein the monomer begins to absorb the applied polymerisation energy leaving little to the photo-initiator [28]. This

resulted in a lower concentration of available energetic free radicals and thus immobilised polymer. Above 30 % VAL the effect of self screening was observed resulting in lower concentration of surface immobilised gold nano-particles. From the FE-SEM images it was evident that 30 % VAL produced the highest coverage of gold nano-particles, however, due to the termination of production of VAL, 20% solutions were used. A concentration of 20 % VAL provided sufficient coverage of gold nano-particles, whilst minimising the occurrence of self screening of the monomer during photo- grafting.

5.3.2.2. BuMA-co-*EDMA and LMA-co-EDMA columns grafted with GMA*

Using a 15 % GMA solution, grafting of GMA was carried out on both BuMA-*co*-EDMA monoliths, and LMA-*co*-EDMA monoliths. For possible future application in bioaffinity phases, LMA-*co*-EDMA monoliths are anticipated to be more suited to the separation of proteins in the reversed-phase, due to increase in available surface area (as determined from SEM images), which ay increase retention and separation efficiency. In this case, BuMA-*co*-EDMA monoliths were investigated first, with the grafting procedure later extended to LMA-*co*-EDMA monoliths. Using FE-SEM imaging, the resulting coverage of gold nano-particles could be observed. Figure 5.6 demonstrated coverage of gold nano-particles upon a BuMA-*co*-EDMA monolith, grafted with 15 % GMA, and subsequently aminated.

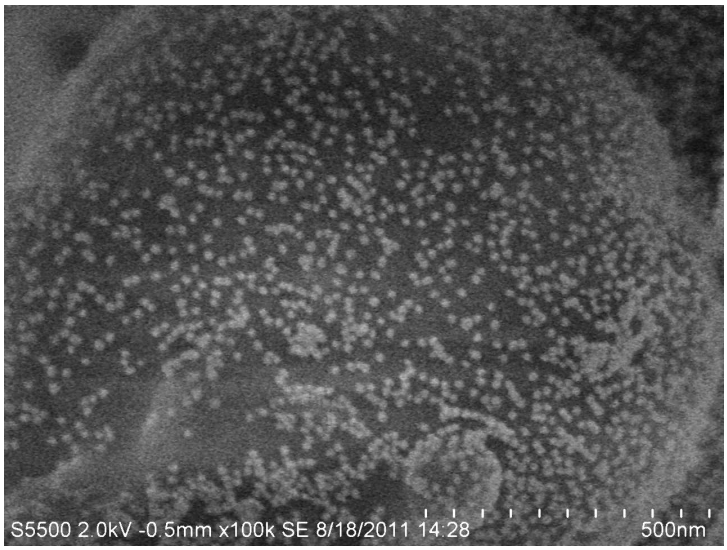

Figure 5.6: *FE-SEM of BuMA*-co-*EDMA grafted with 15 % GMA, aminated with 1* M *ethylenediamine, and treated with gold nano-particles.*

Using a defined square of 500 nm in length (are 250, 000 nm^2), the number of nano-particles present was counted. From the SEM micrograph in Figure 5.6, the area in question contained ~315 nano-particles within the defined area. This is higher than the column grafted with 20 % VAL (296 nano particles). This is also indicative of a higher concentration of aminated groups immobilised to the surface of the monolith. The grafting of GMA groups to the monolith surface was then extended to LMA-*co*-EDMA monolith columns. Following amination and nano-particle attachment, the column was subjected to FE-SEM imaging. Using a 15 % GMA monomer solution for grafting upon LMA-*co*-EDMA columns, produced a significantly more uniform coverage of gold nano-particles across the monolith surface when compared to BuMA-*co*-EDMA monolith (Figure 5.6). Using a defined square, of 500 nm in length (described above), the number of nano-particles were counted. The aminated LMA-*co*-EDMA monolith contained a much higher concentration of nano-particles compared to BuMA-*co*-EDMA monoliths, with 376 nano-particles within the defined region. This may be due to hydrogen abstraction differences, as outlined in Chapter 2, Section 2.3.3.4. Briefly, tertiary bonded hydrogen atoms are preferable for branching in hydrogen abstraction based chain polymerisation reactions, such as grafting. However, secondary bonded hydrogen atoms can also be abstracted, albeit at lower amounts [29]. Monoliths comprising of BuMA-*co*-EDMA, exhibit a lower concentration of secondary hydrogen atoms compared to LMA-*co*-EDMA monoliths, which may account for the increase in coverage of nano-particles. The resulting FE-SEM micrograph is shown in Figure 5.7.

The resulting FE-SEM micrograph demonstrated extremely uniform coverage across the sample section of monolith. In Figure 5.7, a section of unmodified column was observed, along the curvature of a globule in the foreground of the image. As the coating procedure was performed in a single direction (i.e. across the SPE zone), some sections of monolith would not have been exposed to the flow of gold nano-particles, resulting in small sections of unmodified column, particularly close to curved features of the monolith.

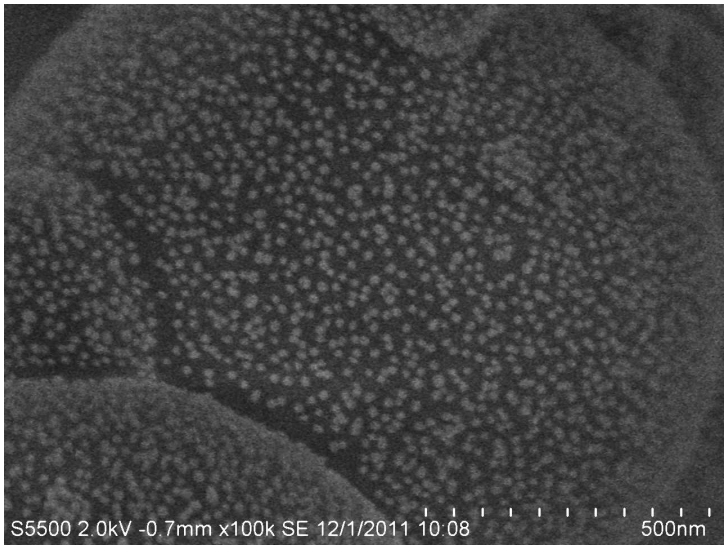

Figure 5.7: *FE-SEM of LMA-co-EDMA grafted with 15 % GMA, aminated with 1* M *ethylenediamine, and treated with gold nano-particles.* V_{acc} *2kV, magnification 100, 000 X.*

To investigate the effect of varying graft monomer concentration, prior to amination, two more LMA-*co*-EDMA columns (LMA-G5 and LMA-G30) were prepared and solutions of GMA with a concentration of 5 % and 30 % respectively, was grafted to each column. The column was aminated as outlined above and gold nano-particles were immobilised upon the aminated sites. The resulting FE-SEM images are shown in Figure 5.8. Using the method outlined previously for counting nano-particles, the surface coverage within a defined area was calculated (250, 000 nm^2). The column grafted using a 5 % GMA solution produced approximately 350 nano-particles in this area (Figure 5.8 (a)). This is lower than that of the 15 % GMA column (~380 nano-particles). The column grafted with 30 % GMA exhibited a slightly higher surface coverage at ~ 400 nano-particles in the same defined area (Figure 5.8 (b)). This was a 5 % change in nano-particle coverage between grafting solutions of 15 % and 30 % GMA, which was not deemed to be statistically significant. A concentration of 15 % GMA was subsequently used throughout the experiment.

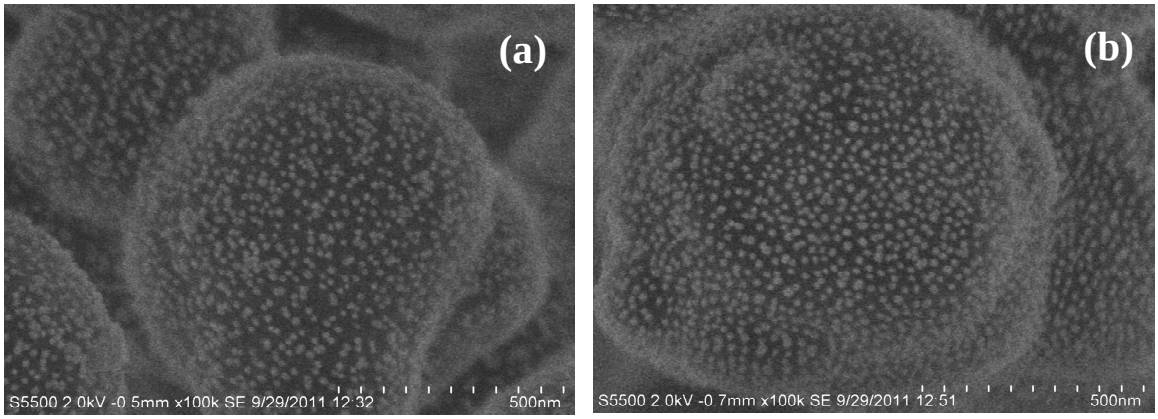

Figure 5.8: *FE-SEM micrographs of LMA-co-EDMA columns grafted with 5 % GMA (a) and 30 % GMA for amination with subsequent gold nano-particle immobilisation. V_{acc} 2 kV, magnification 100, 000 X.*

5.3.2.3. FE-SEM imaging of the boundary between the μSPE section and the unmodified section of monolith

According to the sC^4D profiles, the boundary between the SPE column segment, and the remainder of the column, spans a distance no greater than 1 mm. To verify this observation, a BuMA-*co*-EDMA monolith grafted with 20 % VAL, aminated and modified with gold nano-particles was taken for FE-SEM analysis. For this investigation, the SPE zone was cut from the column, with approximately 10 mm of unmodified column attached. This is illustrated in Figure 5.9 below.

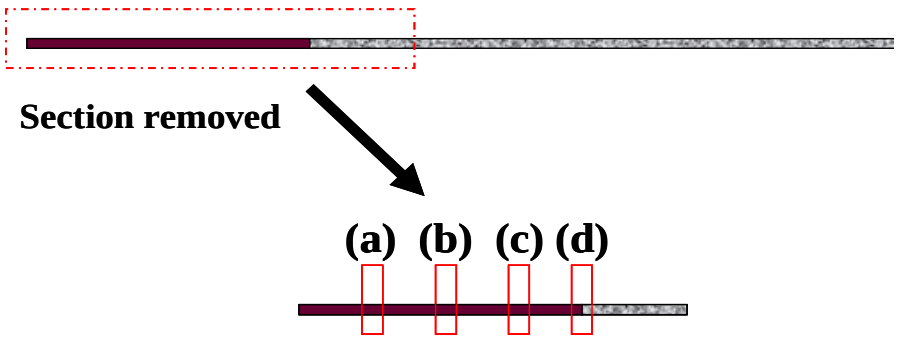

Figure 5.9: *Schematic of the sampling process used to determine the effectiveness of the boundary. Cross-sections denoted as (a)-(d). Section (d) contains no modification, and thus was a blank. Total length of gold zone was 50 mm.*

The column segment was further cut into four cross-sections, incorporating both the gold modified μSPE segment and the unmodified "blank" column segment [Figure 5.9 (d)]. The resulting micrographs are shown in Figure 5.10. Across the samples (a) to (c), the coverage of nano-particles is similar indicating a homogeneous coverage across the SPE zone.

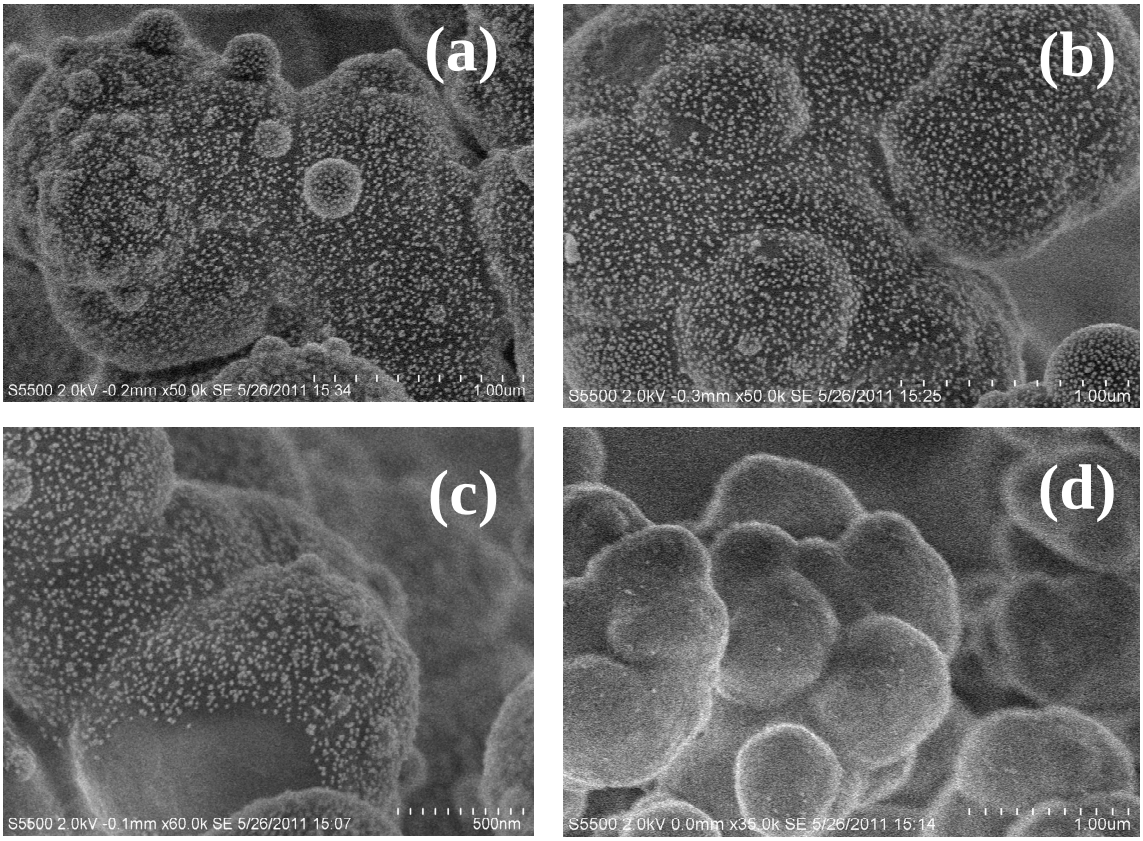

Figure 5.10: *FE-SEM micrographs of BuMA-co-EDMA monolith grafted with 20 % VAL, aminated and modified with gold nano-particles. Cross-sections of column, with (a)-(d) as explained in Figure 5.9 above.* V_{acc} *2 kV, magnification 50, 000 X (a) and (b), 60, 000 X (c), and 35, 000 X (d).*

In Figure 5.10 (c) a patch of unmodified column can be seen in the centre foreground, in which the globule was sliced during sample preparation for FE-SEM imaging. In Figure 5.10 (d) the section of column directly following the gold modified zone can be seen. Compared to micrographs in Figure 5.10 (a) to (c), there is little or no coverage of gold upon this section of column, with approximately 1-2 nano-particles in an area of 250, 000 nm^2 (as used for coverage evaluation in Section 5.3.2.1), with

most of the sample demonstrating no gold nano-particles. This verified the "sharp" division of the monolith into two distinct functionalities, as observed with sC^4D profiling.

5.3.3. FE-SEM imaging of polymer monolithic columns treated directly with gold nano-particles

5.3.3.1.Methacrylate monoliths

To determine the effect of possible gold immobilisation upon an unmodified monolithic column, two BuMA-*co*-EDMA columns, named BuMA-Blank 1 and BuMA-Blank 2 respectively, were treated directly with the gold nano-particle solution. Following washing in deionised water, the column was dried for FE-SEM imaging. The resulting micrographs are shown in Figure 5.11.

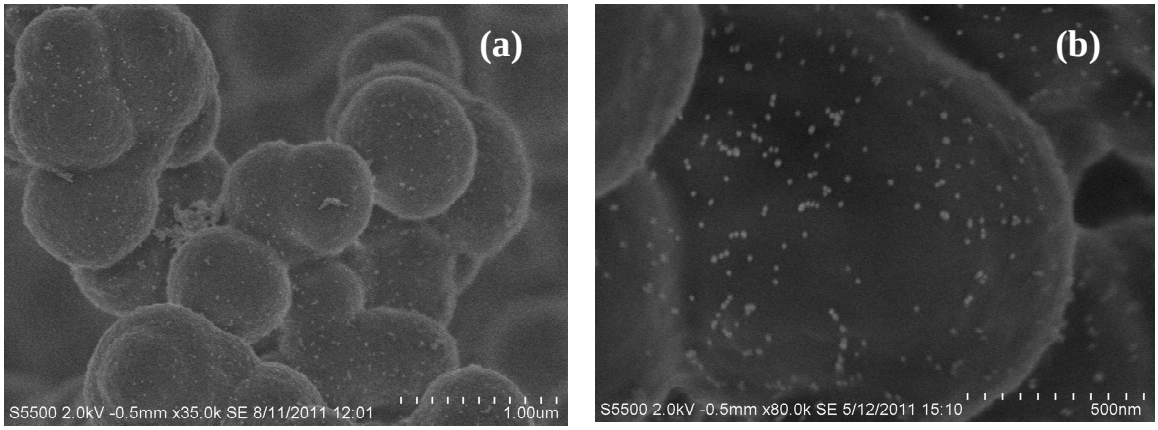

Figure 5.11: *FE-SEM micrograph of Column BuMA-Blank 1 (a) and BuMA-Blank 2 (b) following gold nano-particle immobilisation.* V_{acc} *2 kV, magnification 35, 000 X (a), 60, 000 X (b).*

From the micrographs in Figure 5.11, the immobilisation of gold nano-particles was evident upon unmodified BuMA-*co*-EDMA monolithic columns. The coverage was sporadic, with clusters of nano-particles presented as dimers, trimers and some larger clusters. As with previous gold modified columns, the number of nano-particles within a square of length 500 nm (area 250, 000 nm^2) was counted. Across the two columns tested, an average in nano-particle coverage within the defined area was <50 nano-particles. In comparison to immobilised-gold via amine lone pairs, the unmodified column exhibits a much lower surface coverage (<50 nano-particles

versus ~300 nano-particles). The coverage on the columns in Figure 5.11 was non-uniform, with nano-particles accumulating in large clusters within the crevices of the monolith scaffold. Methacrylic monoliths contain carbonyl groups which are polarised, due to the slightly positive charge on the carbon and the slightly negative charge on the oxygen. The stabilised gold nano-particles carry a negative charge due ot the stabilising citrate ligands. The carbonyls of the citrate may cause a dipole-dipole interaction with the carbonyls of the polymer. This may account for the sporadic nature of the gold nano-particle coverage on the unmodified methacrylic polymers. To determine if this mechanism was indeed responsible for the non-specific interaction, two more columns were fabricated using monomer pre-cursors which did not contain carbonyls, i.e. PSDVB.

5.3.3.2. PSDVB monoliths

Monoliths consisting of PSDVB (columns PS-Blank 1 and PS-Blank 2) were fabricated, and flushed with the gold nano-particle suspension. The columns were then sampled for FE-SEM imaging, with the resulting images shown in Figure 5.12.

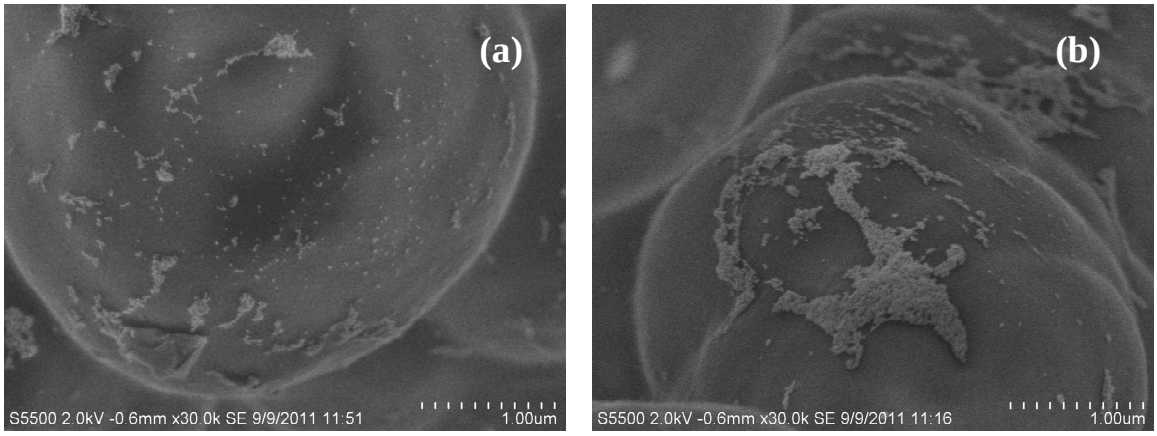

Figure 5.12: *FE-SEM micrographs of column PS-Blank 1 (a) and PS-Blank 2 (b) following gold nano-particle treatment.* V_{acc} *2 kV, magnification 30, 000 X.*

Unlike columns BuMA-Blank 1 and BuMA-Blank 2, the resulting coverage in columns PS-Blank 1 and PS-Blank 2 is patchy, with larger accumulations of clusters between the crevices and niches of the monolith structure. This was particularly evident in Figure 5.12 (b). The coverage of nano-particles does not resemble that of the methacrylate based monoliths. The number of nano-particles could not be counted

due to the large agglomerations present. Nonetheless, the coverage on the unmodified PSDVB columns was not reminiscent of the gold-modified aminated column zones, as seen in Section 5.3.2. The immobilisation of gold upon unmodified PSDVB columns could not be due to the polar interactions postulated above. The mechanism of immobilisation in this instance may be due to interactions between the citrate capped gold nano-particles with the high electron density of the benzene rings within the polymer structure. The reasons for immobilisation must be investigated further before a definite mechanism can be elucidated.

By determining the extent of nano-particle coverage upon unmodified columns, the high surface coverage observed upon modified methacrylate based columns, could be attributed to the surface expression of aminated grafted groups alone.

5.3.4. sC^{4}D profiles of photo-grafted columns

5.3.4.1. sC^{4}D of aminated photo-grafted VAL columns

The columns BuMA-V1, BuMA-V2, and BuMA-V3 were scanned prior to any modifications having taken place. As observed from the plots in Figure 5.13, the longitudinal homogeneity of the columns is evident and no voids were observed in the stationary phase. It must be noted that due to the length of column fittings, and the size of the cell some areas could not be measured; ~ 5 mm from the end of the column, and ~15-20 mm at the column head.

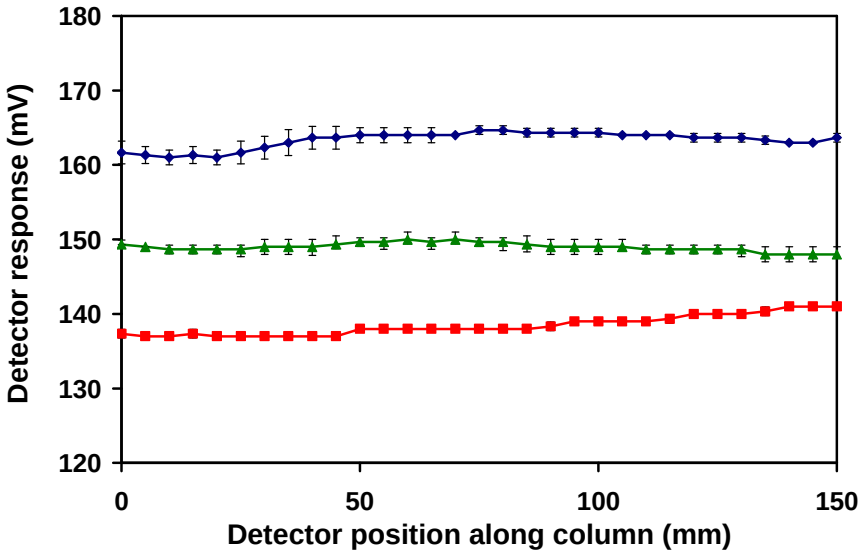

Figure 5.13: *sC^{4}D profiles of columns BuMA-V1(—♦—), BuMA-V2 (—■—) and BuMA-V3 (—▲—), prior to photo-grafting of VAL. Columns were scanned in triplicate in deionised water, average reported, including error bars. Scans performed at 5 mm intervals in deionised water, at a flow rate of 1 µL/min.*

In order to visualise covalently attached ethylenediamine, the pendant amines were protonated, by treatment with nitric acid (100 m*M*) as outlined above in Section 5.2.3. The pK_a of ethylenediamine is ~pH 9, so below this pH the amine groups should be protonated. As the sC^{4}D profile is constructed using deionised water as the scanning buffer, the pH is not sufficiently high to cause deprotonation of the charged amines. By protonating the amines, the ionic conductance is increased, enhancing the detector response of the aminated zone, designated for nano-particle immobilisation. The resulting profiles indicated an increase in detector response in the aminated zone, as shown in Figure 5.14.

The grafted zone was indicated by an increase in detector response, with the zone spanning 0 to 35 mm from the column fittings. Along each photo-grafted zone, an increase in detector response was observed, following amination and protonation of the pendant amine groups, by approximately 30 mV (± 5 mV) for each column (columns BuMA-V1 to BuMA-V3). The change in detector response expressed as % change was calculated using the detector response of the highest data point of the aminated zone and the lowest data point of the remainder of the column.

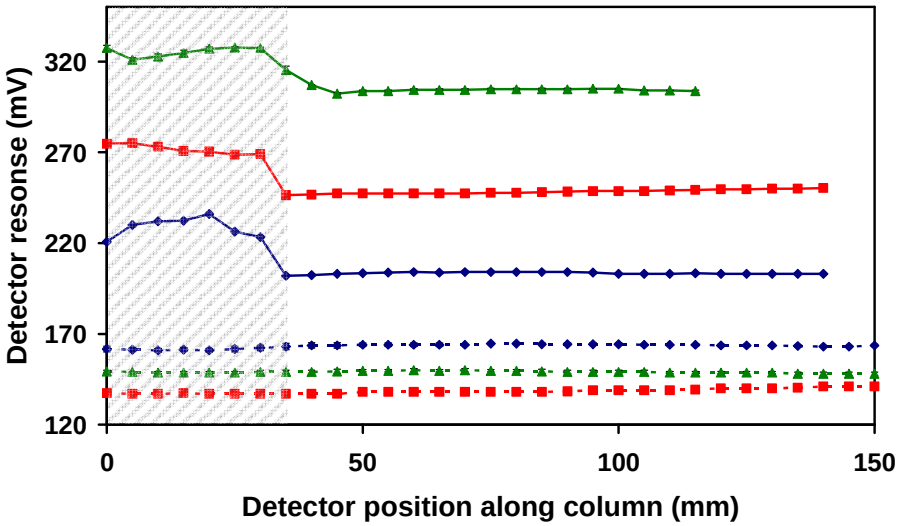

Figure 5.14: *sC^{4}D profiles of columns BuMA-V1 (—♦—) column BuMA-V2 (—■—) and column BuMA-V3 (—▲—) following protonation of aminated zone, versus sC^{4}D profiles of column BuMA-V1 (--♦--) Column BuMA-V2 (--■--) and column BuMA-V3 (--▲--) prior to grafting. Scans for protonated columns (indicated by solid line) offset by +50 mV, +100 mV and + 150 mV, respectively, for illustration. Scans performed in triplicate in deionised water, at 5 mm increments, with a flow rate of 1 µL/min. Section of column corresponding to aminated zone indicated by shading.*

This translated to an average % change of 15.7 % ±1.3%, across the three columns. The plateau in the resulting detector response spanned the length of the aminated zone, with a distinct drop in detector response at the boundary between the grafted zone and unmodified column. This indicated that the photo-grafting procedure and subsequent amination, was a success. However, in column BuMA-V3 (—▲—), a shallow decline in detector response was observed between 30 and 45 mm. This may be due to an error in maintaining the length of the zone during the multiple grafting procedures required for the fabrication process of such columns.

A boundary, spanning no more than 5 mm (as 5 mm intervals were used in these preliminary stages) resulted (this was further investigated in the case of the analytical column A1, in Section 5.3.4.4). By using sC^{4}D to construct a profile of the charged zone on the column, deviations in the resulting profile (as a product of the photo-grafting procedures) could be observed. This can be used as a quality control technique during the fabrication process.

5.3.4.2. sC^4D profiles of aminated photo-grafted GMA columns

Following amination of epoxide groups grafted to the monolith, the pendant amines were protonated as outlined above in the previous section. An increase in detector response relative to the grafted SPE segment of the column was observed, following protonation of the attached amines. This may result from an increase of ionic conductance, caused by the presence of the additional proton [Figure 5.15 (—■—)]. The resulting profiles are show in Figure 5.15.

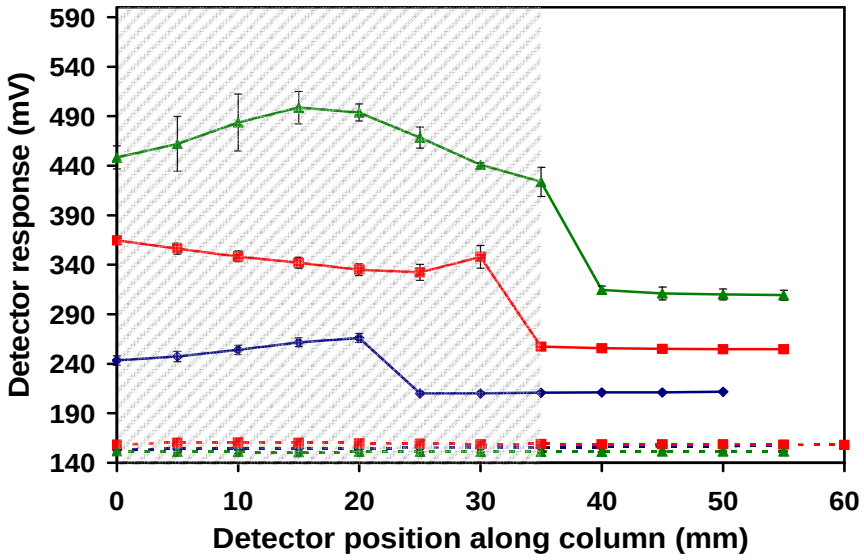

Figure 5.15: *sC^4D profiles of columns BuMA-G1 (—♦—) column BuMA-G2 (—■—) and column BuMA-G3 (—▲—) following protonation of aminated zone, versus sC^4D profiles of column BuMA-G1 (--♦--) column BuMA-G2 (--■--) and column BuMA-G3 (--▲--) prior to grafting. Scans for protonated columns (indicated by solid line) offset by +50 mV, +100 mV and + 150 mV respectively, for illustration. Scans performed in triplicate in deionised water, at 5 mm increments, with a flow rate of 1 µL/min. Section of column corresponding aminated zone indicated by shading.*

The resulting detector response across the aminated zone was similar to that observed with columns of aminated photo-grafted VAL. Columns grafted with GMA with subsequent amination, exhibited an increase in detector response of ≥ 60 mV. The % change in detector response was calculated and resulted in an average % change of 38 % ±10%. This standard deviation may be due to excessive washing time for column BuMA-G1 with respect to the remaining columns BuMA-G2 and BuMA-G3. The increase in detector response was much higher in the GMA aminated columns compared to the VAL aminated columns (15.7 % ± 1.3 %).

The sC^4D profile of column BuMA-G3 (—▲—) indicated a much higher detector response compared to that of columns BuMA-G1 and BuMA-G2, which was likely caused by a decrease in washing time prior to scanning. All three columns do, however, demonstrate a plateau profile corresponding to the aminated zone of the column. This trend was also observed for columns grafted with VAL, following amination and protonation of the amine groups. It should be noted that due to cutting of the columns between the photo-grafting and amination processes, the SPE zone length of 50 mm could not be maintained for each column. This resulted in a shortened column length for column BuMA-G1 in Figure 5.15.

5.3.4.3. sC^4D profiles of LMA-co-EDMA columns grafted with GMA

Using the grafting chemistry outlined above, LMA-*co*-EDMA monoliths were grafted with GMA, resulting in surface expressed epoxide groups. The columns were then subjected to amination, and subsequent protonation for sC^4D visualisation. The resulting profiles are shown in Figure 5.16. Following the trend observed with previous columns, an increase in response along the grafted zone was observed following amination. The increased detector response across three columns resulted in a % change of 32.5 % ± 6.95 %. This increase was higher than that reported for aminated VAL grafted column (15.7 % ± 1.3%), and similar to that of BuMA columns grafted with GMA (38 % ± 10%). Column BuMA-G3 demonstrated a lower increase in detector response relative to columns BuMA-G1 and BuMA-G2. This may be a reflection of a lower density of grafted GMA. Nonetheless, the profiles of the LMA-*co*-EDMA monoliths grafted with GMA, do follow trends as observed with both VAL and GMA grafted BuMA monoliths. A significant increase in detector response along the aminated zone was observed following amination and a flush of nitric acid.

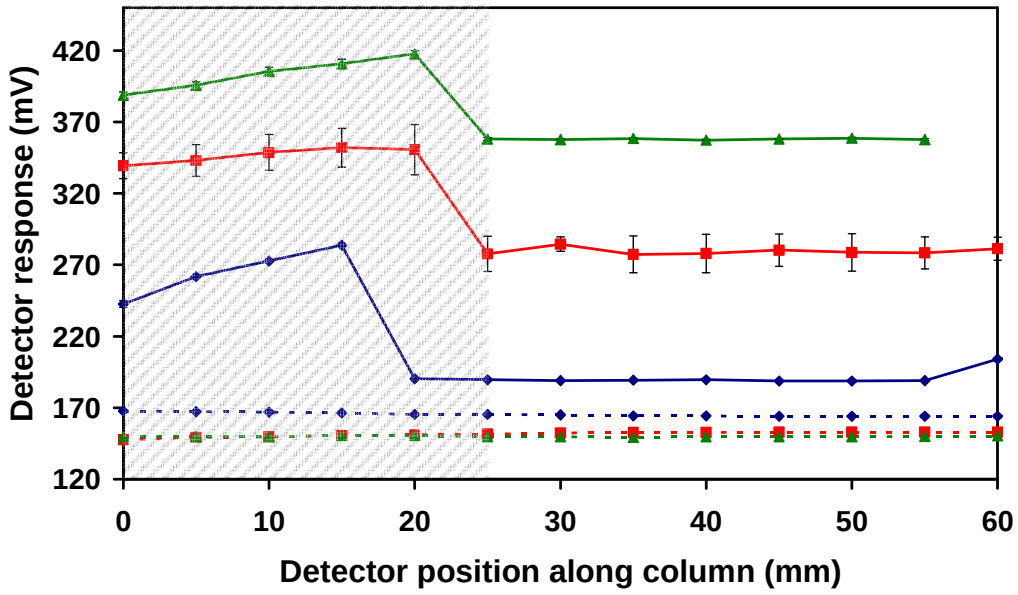

Figure 5.16: *sC^4D profiles of columns LMA-G1 (—♦—) column LMA-G2 (—■—) and column LMA-G3 (—▲—) following amination of GMA, and protonation, versus sC^4D profiles of unmodified column LMA-G1 (--♦--) column LMA-G2 (--■--) and column LMA-G3 (--▲--). Scans for protonated columns (indicated by solid line) offset by +50 mV, +100 mV and + 150 mV respectively, for illustration. Scans performed in triplicate in deionised water, at 5 mm increments, with a flow rate of 1 µL/min. Section of column corresponding to aminated zone indicated by shading.*

5.3.4.4.sC^4D profiles of an analytical LMA-co-EDMA column grafted with GMA

For future chromatographic applications, column LMA-A1 measuring 200 mm in length was produced, with a 50 mm zone designated for grafting in order to produce a zone of SPE material, prior to the separation segment of the column. The column was subjected to sC^4D profiling throughout the modification processes as outlined above. For sC^4D profiling, 1 mm increments were used to record the profile of the column. Firstly the column was grafted to express epoxide groups via poly(GMA) grafts. The column was then subjected to amination, with subsequent protonation of pendant amines, prior to sC^4D profiling. The resulting profile is shown in Figure 5.17.

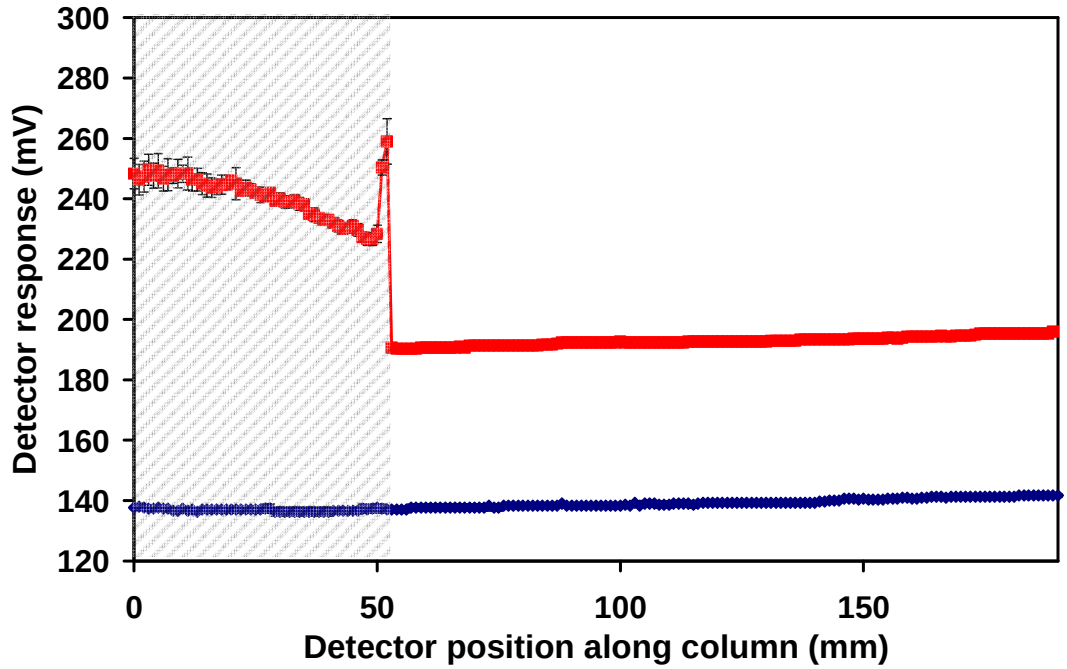

Figure 5.17: *sC^{4}D profiles of column A1 prior to grafting occurring (—♦—), and following amination and protonation (—■—). Scan of grafted column (—■—) was offset by 50 mV for illustration. Scans performed in triplicate in deionised water, at 1 mm increments, with a flow rate of 1 µL/min. Section of column corresponding to aminated zone indicated by shading.*

By mapping the distribution of charge across this section of column with sC^{4}D, the success of the grafting procedure could be evaluated. Along the zone of aminated grafted poly(GMA), the detector response increased by approximately 70 mV from the unmodified monolith to the maximum value in the aminated zone. The boundary between the grafted and unmodified column sections could be seen to span no greater that 1 mm, as the detector response decreased from 259 mV to 190 mV (% change in detector response of 33.33 %), between the detector position of 51 and 52 mm. The sharp increase in detector response before the boundary, at a distance of 51 mm may be due to a localised increase in GMA graft intensity reflected in an increase in the presence of amines, and thus an increase in detector response. This data point exhibits a % RSD of no greater than 3.7 % across the three individual sC^{4}D scans, indicating it is indeed a permanent feature. This feature was also observed on a second column, column-A2, as seen in Figure 5.18.

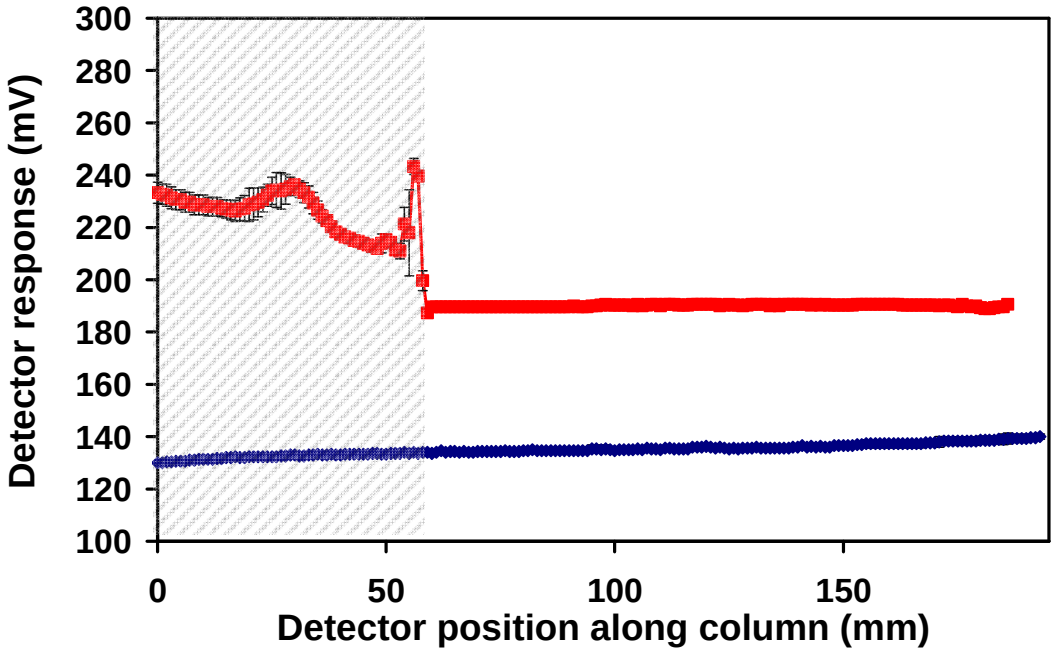

Figure 5.18: *sC^{4}D profiles of column LMA-A2 prior to grafting occurring (—♦—), and following amination and protonation (—■—). Scan of grafted column (—■—) was offset by 50 mV for illustration. Scans performed in triplicate in deionised water, at 1 mm increments, with a flow rate of 1 µL/min. Section of column corresponding to aminated zone indicated by shading.*

Both columns LMA-A1 and LMA-A2 exhibited similar deviation along the aminated zone (±7.5 and ±8.07 mV, respectively). Again column LMA-A2 exhibited a similar peak in detector response at the boundary between the aminated and unmodified zones of the column. As this feature was observed for two individual columns, it can be inferred that it was a side effect of the photo-masking process. In addition, Gillespie *et al.* [30] used similar photo-masking techniques to graft zones of AMPS, using masks to separate each zone boundary form the next zone. The boundaries of zones grafted with the charged monomer also exhibited a sharp increase in detector response, relative to the total length of the zone, resulting in a "u" type profile across the grafted zone. In this work, a single mask was used to distinguish the boundary between the grafted and unmodified segments of the column, which resulted in the peak in detector response at the zone boundary. As such an increase was observed in both instances of grafting, it can be inferred that this sharp increase is a side effect of using (possibly reflective) masks defining zone boundaries.

5.3.5. sC^{4}D profiles of gold modified columns

5.3.5.1.Modification of aminated zones with gold nano-particles

Following amination, the columns were flushed with gold nano-particles (20 nm), until the entire zone turned a characteristic burgundy colour [17]. Following washing, the column was again scanned, and the detector response of the gold-modified zone was mapped. The resulting sC^{4}D profiles are shown in Figure 5.19. The detector response for the modified zone decreased upon the immobilisation of gold nano-particles. Following the reaction with the gold nano-particles, the ionic conductance of the zone was reduced. The detector response along the aminated zone prior to gold immobilisation was due to the protonated amines. The amines are attachment sites for the incoming gold, and so for attachment of the gold nano-particles the amines can no longer be protonated.

In the profile for column BuMA-V3, the detector response of the reversed-phase segment of the column produced an inhomogeneous conductive profile, unlike previous scans. Variation in ambient temperature and possible fouling of the electrodes due to residue on the capillary from zone marking (permanent marker) during the acquisition of sC^{4}D data, may have contributed to this variation.

Similarly, columns BuMA-G1 to BuMA-G3 were flushed with gold nano-particles until the entire SE column segment was a characteristic burgundy colour. The columns were washed, and equilibrated with deionised water prior to sC^{4}D profiling. The resulting profile for the columns demonstrated a minor decrease in detector response along the entire aminated column segment, compared to the profile of the protonated aminated segment. The sC^{4}D profiles are shown in Figure 5.20.

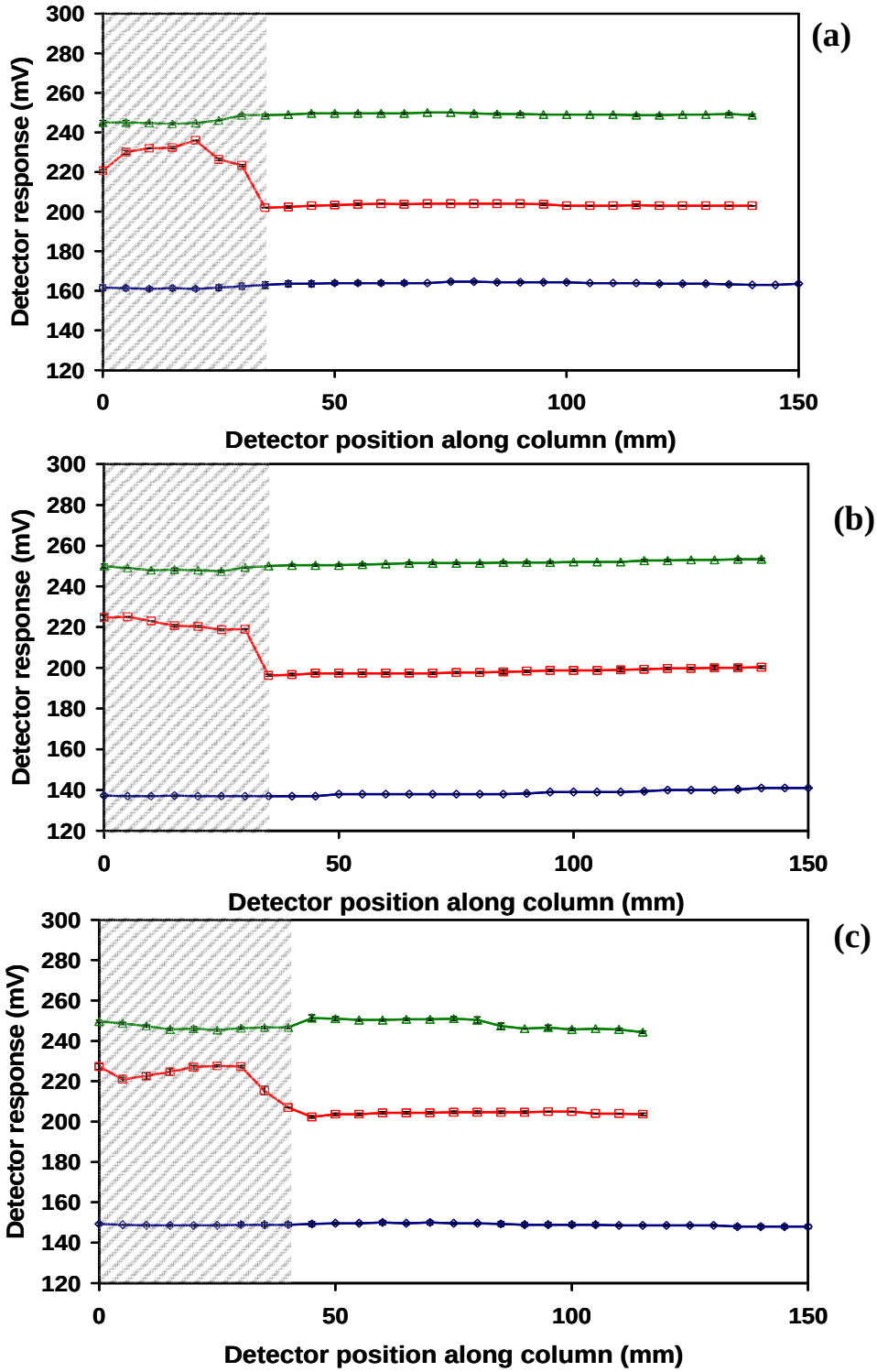

Figure 5.19: *sC^{4}D profiles of columns BuMA-V1 (a), BuMA-V2 (b), and BuMA-V3 (c). Each plot contains a profile of the unmodified column (—◊—), following amination (—□—) offset by + 50 mV, and following gold nano-particle immobilisation (—Δ—) offset by + 100 mV. Triplicate scans reported, open data points to illustrate presence of error bars. Scans performed at 1 µL/min at 5 mm intervals. Section of aminated column highlighted with shading.*

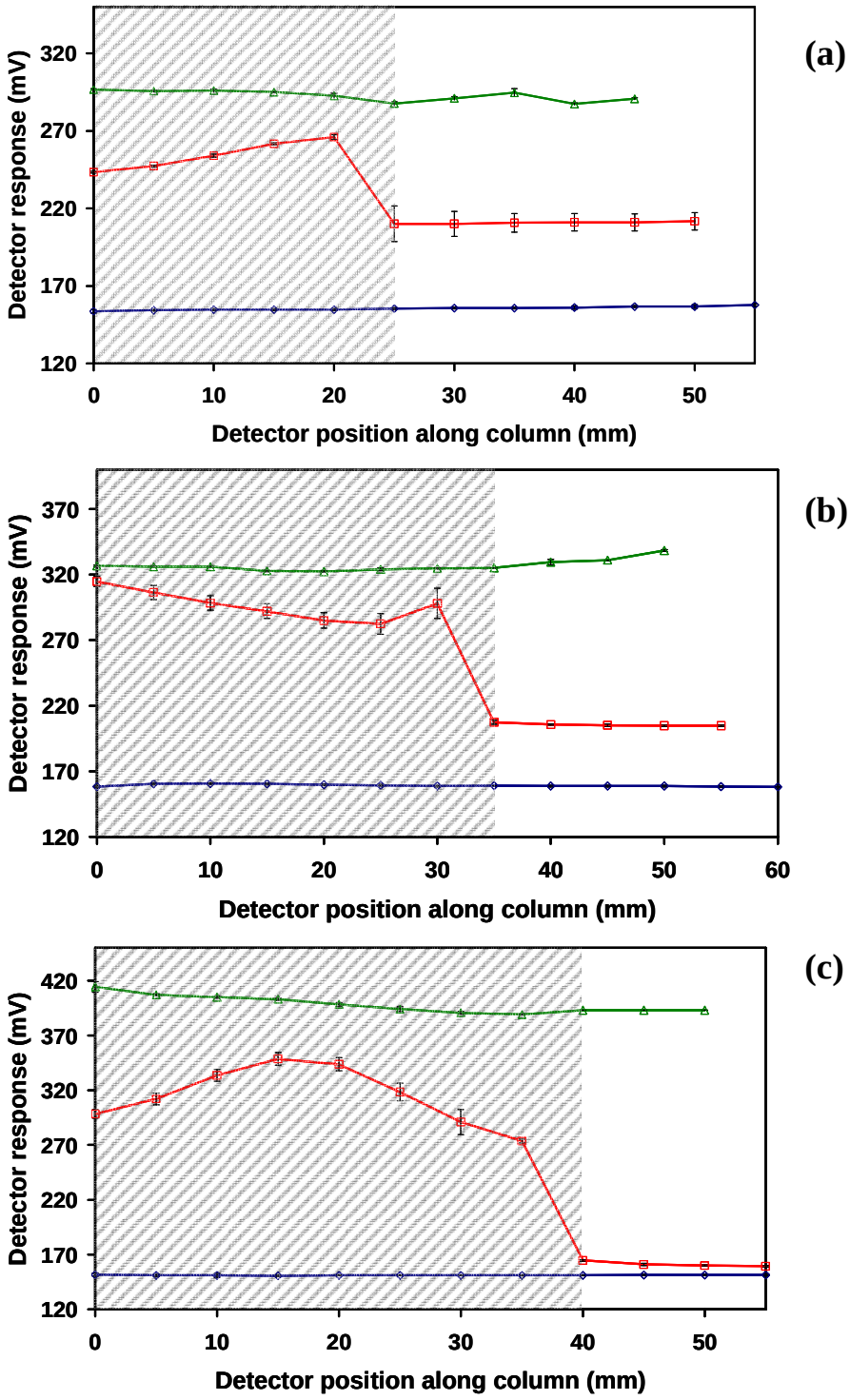

Figure 5.20: *sC^{4}D profiles of columns BuMA-G1 (a), BuMA-G2 (b), and BuMA-G3 (c). Each plot contains a profile of the unmodified column (—◊—), following amination (—□—) offset by + 50 mV (a & b) and 25 mV (c), and following gold nano-particle immobilisation (—Δ—) offset by + 150, + 175, and 250 mV, respectively. Triplicate scans reported, open data points to illustrate presence of error bars. Scans performed at 1 µL/min at 5 mm intervals. Section of aminated column highlighted with shading.*

As observed with VAL grafted columns, a decrease in detector response was observed upon the attachment of gold nano-particles to the aminated zone. From Figure 5.6, the profile for column BuMA-G1 was shorter than previous scans, due to cutting of the column during the gold modification process. As the ethylenediamine was easily observed along the column, it can be inferred that all the available pendant amines were reacted with gold nano-particles, as the detector response across the SPE zone was horizontal and flat, showing no signs of increased conductivity resulting from unmodified amines.

The immobilisation protocol was then extended to LMA-*co*-EDMA monoliths. Following the immobilisation and washing procedures, the columns LMA-G1, LMA-G2, and LMA-G3 were profiled using sC^4D. The resulting profiles are shown in Figure 5.21. Following gold nano-particle immobilisation, the detector response along the aminated zone decreased. The detector response across the aminated SPE zone in Figure 5.21 decreased following gold nano-particle immobilisation. Again this was consistent with profiles obtained for previous columns.

The analytical column (LMA-A1) was also subjected to gold nano-particle modification as outlined above. The profiling was performed using 1 mm increments, which gave a more detailed profile of the grafted zone. The resulting profile is shown in Figure 5.22

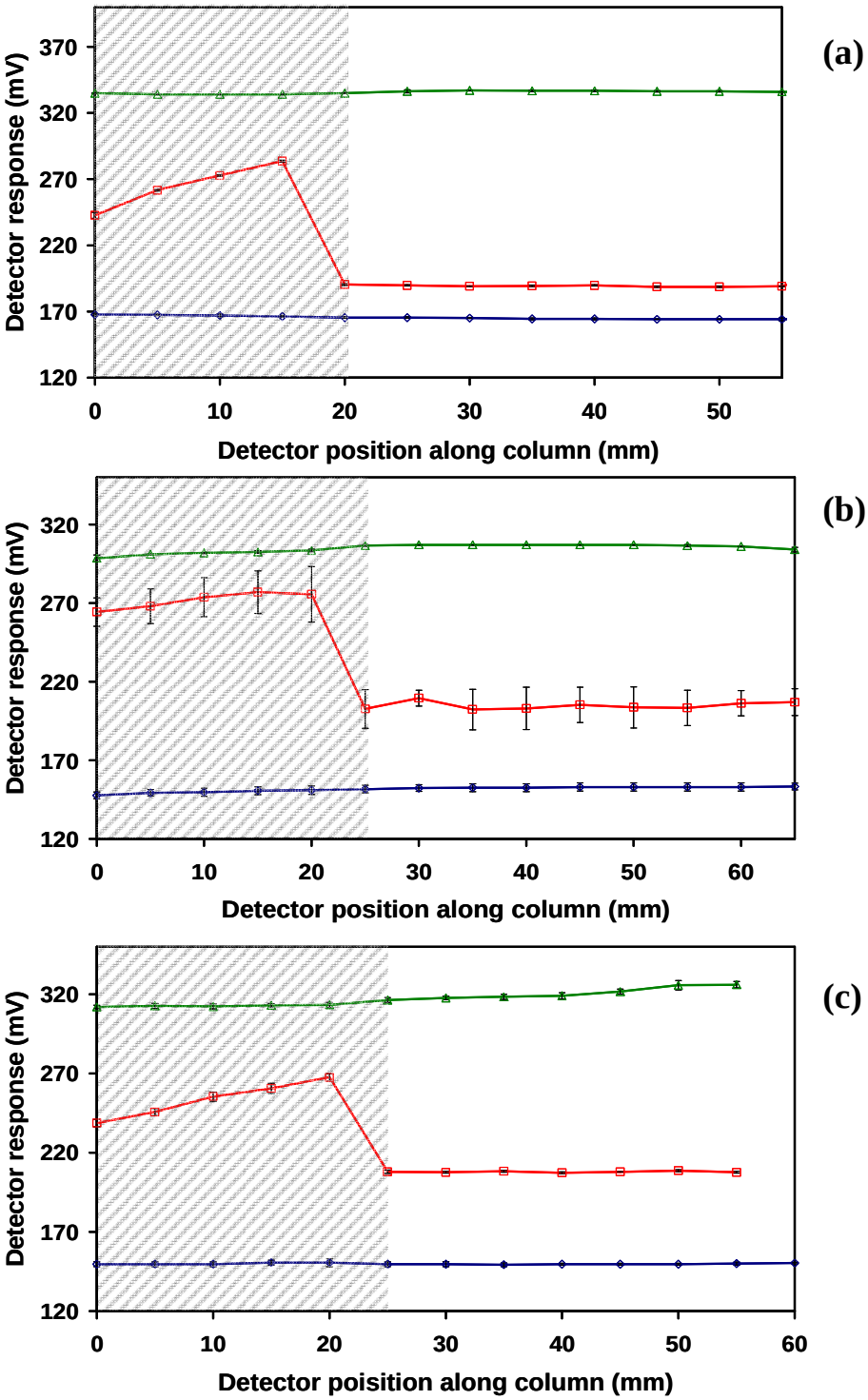

Figure 5.21: *sC^{4}D profiles of columns LMA-G1 (a), LMA-G2 (b), and LMA-G3 (c). Each plot contains a profile of the unmodified column (—◊—), following amination (—□—) offset by + 50 mV (a & c) and 25 mV (b), and following gold nano-particle immobilisation (—Δ—) offset by + 200 (a), and + 150 mV (b& c) respectively. Triplicate scans reported, open data points to illustrate presence of error bars. Scans performed at 1 µL/min at 5 mm intervals. Section of aminated column highlighted with shading.*

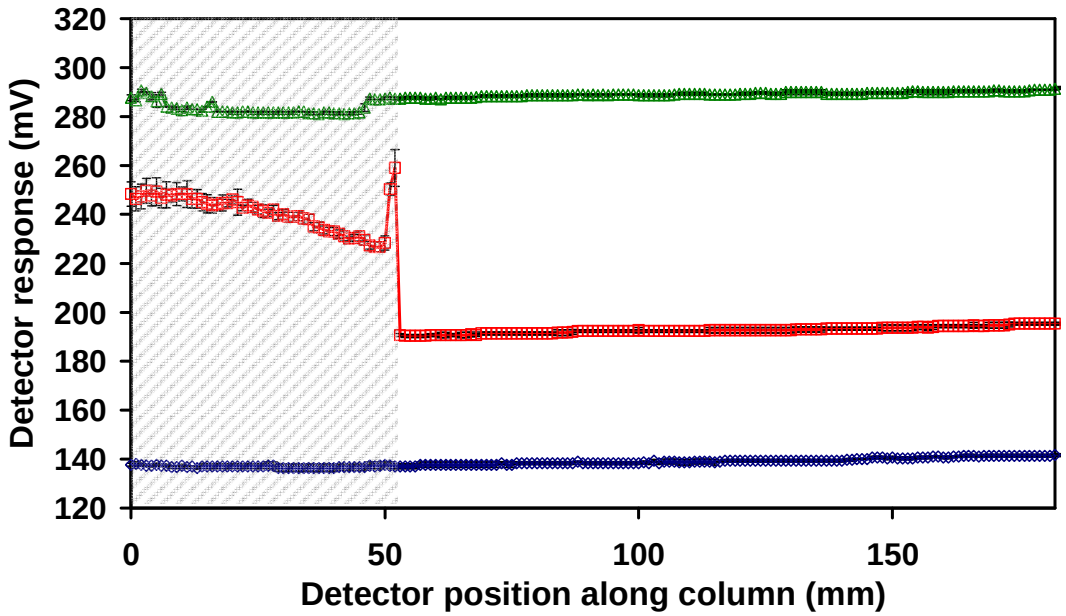

Figure 5.22: *sC^{4}D profiles of column LMA-A1, in the unmodified column form (—◊—), following amination and protonation (—□—) offset by + 50 mV and following gold nano-particle immobilisation (—Δ—) offset by + 150 mV. Triplicate scans reported, open data points to illustrate presence of error bars. Scans performed at 1 µL/min at 1 mm intervals. Section of aminated column highlighted with shading.*

Following the modification of the aminated zone with gold nano-particles, the sC^{4}D profile was indicative of the attachment of gold onto the charged amine groups. The resulting sC^{4}D profile demonstrated that all the available amines had been reacted with, as the significant increase in detector response corresponding to the presence of charged amines was absent. The boundary between the two zones spanned no greater than 1 mm, as in previously profiled grafted and amination steps. This indicated that the boundary was sustained throughout the experiment, evaluating the photo-masking procedure.

The columns demonstrated the characteristic colour associated with gold nano-particle immobilisation, a deep red/burgundy colour as described previously [17]. Using a digital microscope, an image of the column LMA-A2 following gold modification, was recorded (Figure 5.23)

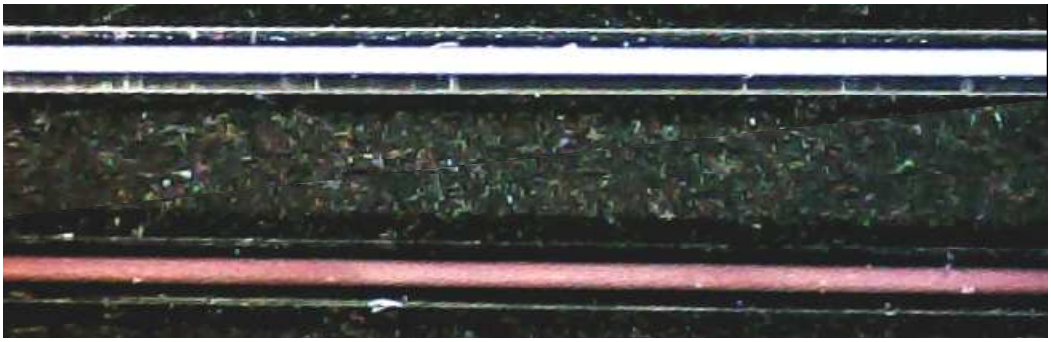

Figure 5.23: *Digital microscope image of two columns; blank LMA-co-EDMA monolithic column (a), zone of grafted monolith with subsequent amination and gold nano-particle immobilisation LMA-A2 (b). Magnification was 250 X.*

In Figure 5.23 (a), an unmodified BuMa-*co*-EDMA monolith in 100 µm i.d. PTFE coated capillary is shown, which exhibited a continuous white colour. In contrast, Figure 5.23 (b) the gold modified section of the monolith exhibited a dark red colour, indicative of the immobilisation of gold nano-particles. The colour observed is also continuous across the sample length, indicating no deviation in nano-particle coverage. This confirmed the presence of gold as observed with sC^4D profiling of the columns.

A distinct boundary between the SPE section of the column, and the remainder of the column was present, as identified using sC^4D profiling. Due to the colouration of the SPE zone, the boundary between the two column sections could be easily visualised. To demonstrate the sharp boundary obtained by this procedure, an image was recorded using a digital microscope, which is shown in Figure 5.24.

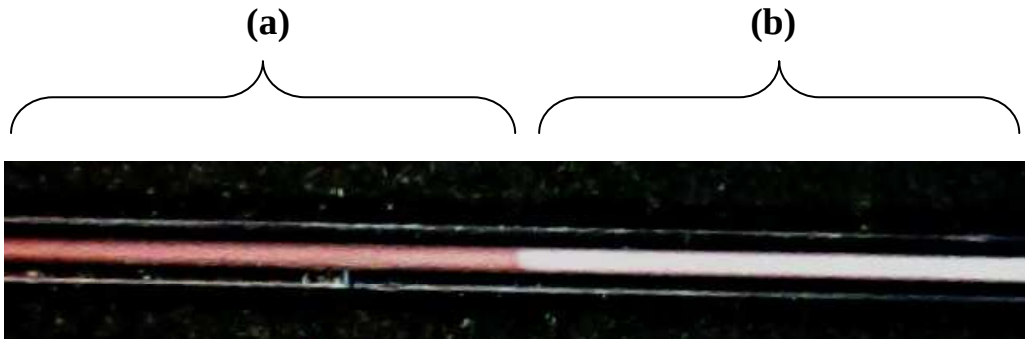

Figure 5.24: *Digital microscope image of the boundary between the gold modified SPE segment of the column (a), and the remaining reversed-phase segment of the column (b). Magnification 250 X.*

5.3.6. Reproducibility of sC^{4}D profiling

To study the reproducibility of sC^{4}D profiling on a dual function monolith, column A1 was used, following immobilisation of gold nano-particles. This column was scanned in triplicate using 1 mm increments. Error bars are included for each data point as shown in Figure 5.25. The response along the length of the column was very reproducible with a % RSD of no greater than 1.9 %. The low variation in detector response along the dual function column indicated excellent reproducibility with three replicate profiles.

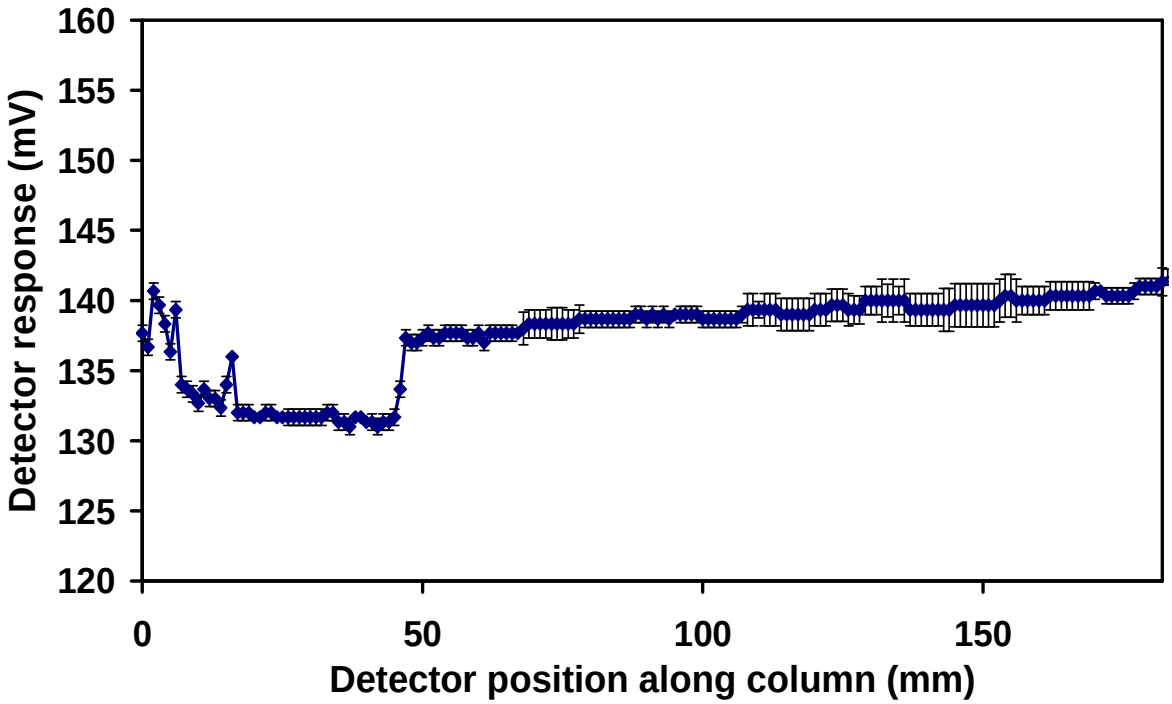

Figure 5.25: *sC^{4}D profile of Column A1 following gold nano-particle immobilisation. Column scanned in triplicate, with error bars included for each data point. A % RSD of less than 1.9 % was evident.*

5.3.7. Chromatographic application

The injection of the blank solutions following loading of the protein standards, and the application of an ACN gradient demonstrated that no detectable protein was eluted from the gold nano-particle modified region (i.e. in the absence of the competing thiol containing species in the mobile phase), indicating the strong interaction between the gold nano-particles and the protein. Protein standards, namely insulin and bovine serum albumin (0.1 mg/mL), were loaded onto the gold nano-particle modified inlet of the LMA-*co*-EDMA monoliths (column LMA-A1), and

following a blank gradient run, eluted from the gold nano-particles modified zone onto the start of the bare LMA-*co*-EDMA monolith section using 4 *M* 2-mercaptoethanol, where the protein was retained via reversed-phase sorption. At this point an ACN gradient was once again applied and the protein was eluted from the monolith. Figure 5.26 shows the series of chromatograms, namely pre- and post protein loading blanks and the reversed-phase elution and separation of the protein standard (bovine serum albumin, BSA) and insulin. The eluted protein band showed a number of individual peaks, reflecting both the purity of BSA standards and the likely presence of dimers and aggregates, which have been reported previously for proteins immobilised upon nano-particles [31]. However, the chromatogram clearly shows the unmodified zone of LMA-*co*-EDMA monolith is capable of separation of multiple components within the trapped protein band, thus demonstrating that both trapping and subsequent reversed-phase separation of proteins is indeed possible upon such segmented phase monoliths.

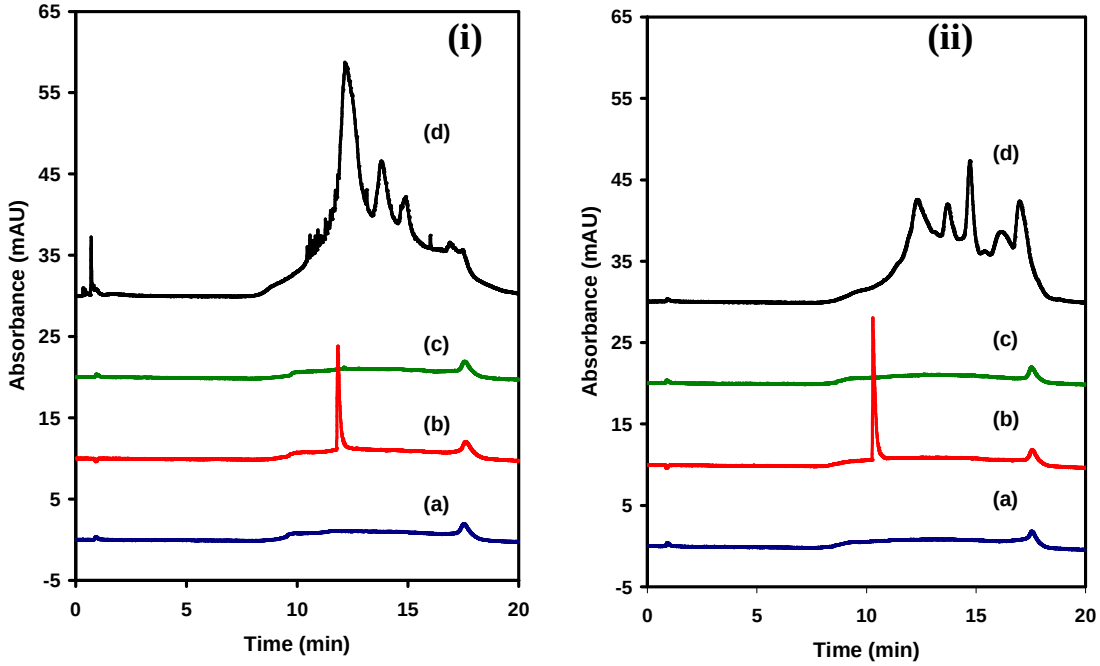

Figure 5.26: *Sequence of chromatograms generated on the gold nano-particle reversed-phase column. Blank prior to protein injection (a), protein standard showing breakthrough to reversed-phase column, blank prior to elution of trapped protein (c), elution of trapped protein (d). Retention of bovine serum albumin (i), retention of insulin (ii). Flow rate 2 µL/min, UV detection at 214 nm.*

5.4.Conclusions

For the first time, polymer monolithic columns expressing a zone of immobilised gold nano-particles and a reversed-phase segment within a single column was produced. Using photo-grafting techniques, the fabrication of an aminated zone was possible, with subsequent non-invasive evaluation of the grafting procedure using sC^4D. By flushing the pendant amines with a solution of 100 m*M* nitric acid, the amines were protonated. With profiling based on conductivity, the protonated amines exhibited an increase in detector response, relative to the bare unmodified section of the polymer monolith. This resulted in a plateau type profile. Upon the addition of gold nano-particles, the detector response decreased to a level below the unmodified monolith. With photo-masking, a sharp boundary, no greater then 1 mm as profiled by sC^4D, was produced and maintained throughout the experiment. The use of sC^4D in the fabrication process of the monolith was vital, in determining the extent of amination and success of the photo-grafting procedures. This was a novel application of sC^4D, as it has not been used in conjunction with immobilised nano-particles previously in the literature.

Using FE-SEM imaging, the coverage of the gold nano-particles could be evaluated. Columns photo-grafted with a zone of GMA and aminated using ethylenediamine, produced a higher coverage than those photo-grafted with VAL functional groups. The effect of amine modification on columns was also evaluated with respect to gold nano-particle coverage. Blank columns did show some coverage of nano-particles, however, this was mostly sporadic with agglomerations accumulated between crevices of the monolith structure.

The analytical column LMA-A1 was used for some chromatographic applications which demonstrated the ability of the column to effectively trap proteins. Proteins could then successfully be eluted, and the column could be regenerated for subsequent use for another protein. This is a novel column type and may have possible further applications in sample clean up, pre-concentration and separation of biomolecules [18], and polycyclic aromatic hydrocarbons (PAH's) [32].

5.5.References

[1] Peterson, D., Rohr, T., Svec, F., Fréchet, J., *Anal. Chem.*, 75, 2003, 5328.

[2] Logan, T., Clark, D., Stachowiak, T., Svec, F., Fréchet, J., *Anal. Chem*., 79, 2007, 6592.

[3] Wolters, D., Washburn, M., Yaters III, J., *Anal. Chem*., 73, 2001, 5683.

[4] Washburn, M., Wolters, D., Yates III, J., *Nat. Biotechnol*., 19, 2001, 242.

[5] Svec, F., 2010, *J. Chromatogr. A*., 1217, 2010, 902.

[6] Urban, J., Svec, F., Fréchet, J., *Anal. Chem*., 82, 2010, 1621.

[7] Svec, F., J. Fréchet, *Anal. Chem*., 64, 1992, 820.

[8] Viklund, C., Svec, F., Fréchet, F., *Biotechnol. Prog*., 13, 1997, 597.

[9] Santora, B., Gagne, M., Moloy, K., Radu, N., *Macromolecules*, 34, 2001, 658.

[10] Svec, F., Tennikova, T., Deyl, Z., *Journal of Chromatography Library*, *Monolithic Materials*, Vol. 67, First edition , 2003.

[11] Krenkova, J., Foret, F., *J. Sep. Sci.*, 34, 2011, 2106.

[12] Li, Y., Chen, Y., Xiang, R., Ciuparu, D., Pfefferle, L., Horváth, C., Wilkins, J., *Anal. Chem*., 77, 2005, 1398.

[13] Krenkova, J., Lacher, N., Svec, F., *Anal. Chem*., 82, 2010, 8335.

[14] Chambers, S., Holcombe, T., Svec, F., Fréchet, J., *Anal. Chem*., 83, 2011, 9478.

[15] Hilder, E., Svec, F., Fréchet, J., *J. Chromatogr. A*., 1053, 2004, 101.

[16] Chambers, S., Svec, F., Fréchet, J., *J. Chromatogr. A*., 1218, 2011, 2546.

[17] Alwael, H., Connolly, D., Clarke, P., Thompson, R., Twamley, B., O' Connor, B., Paull, B., *Analyst*, 136, 2011, 2619.

[18] Connolly, D., Twamley, B., Paull, B., *Chem. Commun*., 46, 2010, 2109.

[19] Cao, Q., Xu, Y, Liu, F., Svec, F., Fréchet, J., *Anal. Chem*., 82, 2010, 7416.

[20] Xu, Y., Cao, Q., Svec, F., Fréchet, J., *Anal. Chem*., 82, 2010, 3352.

[21] Rohr, T., Hilder, E., Donovan, J., Svec, F., Fréchet, J., *Macromolecules*, 36, 2003, 1677.

[22] Stachowiak, T., Svec, F., Fréchet, J., *Chem. Mater*., 18, 2006, 5950.

[23] Walsh, Z., Vázquez, M., Benito-Lopez, F., Paull, B., Macka, M., Svec, F., Diamond, D., *Lab Chip*, 10, 2010, 1777.

[24] Premstaller, A., *Anal. Chem*., 72, 2000, 4386.

[25] Svec, F., Fréchet, J., *Anal. Chem*., 64, 1992, 820.

[26] Frens, G., *Nature, Physical Science*, 241, 1973, 20.

[27] Šlouf, M., Kužel, R., Matěj, Z., *Z. Kristallogr. Suppl*. 23, 2006, 319.

[28] Augistine, V., Stachowiak, T., Svec, F., Fréchet, J., *Electrophoresis*, 29, 2008, 3875.

[29] Rånby, B., *Polym. Eng. Sci*., 38, 1998, 1229.

[30] Gillespie, E., Connolly, D., Paull, B., *Analyst*, 134, 2009, 1314.

[31] Crotts, G., Park, T., *J. Controlled Release*, 44, 1997, 123.

[32] Wang, H., Campiglia, A., *Anal. Chem*., 80, 2008, 8202.

Chapter 6.0

Final conclusions and summations.

"Veni, Vidi, Vici"

Julius Caesar

From the work presented herein, the use of sC^{4}D is demonstrated as a viable technique for the characterisation of polymeric monolithic columns expressing a co-polymerised stationary phase gradient. This profiling technique has never been reported for use in the characterisation of polymeric monolithic columns, incorporating a gradient of functional monomer. Previous methods of column characterisation required destructive and invasive techniques, such as scanning electron microscopy (SEM). To ascertain the surface concentration of specific functional groups, methods such as SEM with energy dispersive X-ray detection is used, again a destructive technique. Profiling the column with sC^{4}D has proven to be a valuable asset, and due to changes in equivalent ionic conductance values, the concentration of surface available functional groups can be evaluated, non-invasively and non-destructively. The method provides a rapid technique to visualise the distribution of a gradient of co-polymerised ionised functional monomer, and can aid in the evaluation of the viability of columns fabricated with such an approach.

In an attempt to produce a column with a gradient of selectivity, grafted upon the surface of a polymeric monolithic column, photo-grafting techniques were performed. Using sC^{4}D, the distribution of grafted functional groups could be easily visualised and characterised. The ability to use the C^{4}D as an on-column detector proved invaluable in the visualisation of the effect of a gradient upon a separation. By varying the on-column position of the detector, the separation of two analytes could be monitored, in a non-destructive manner. This monitoring of a separation on a gradient stationary phase had not previously been documented. The non-contact and non-destructive approach of C^{4}D allowed the characterisation of the column under varying conditions, such as a change in plumbing orientation. By changing the orientation of the column plumbing, and with the use of C^{4}D, the optimum positioning of the column could be determined. This novel application of C^{4}D can aid in the optimisation of gradient shape, monomer concentrations used (i.e. to increase or decrease capacity), and can be an additional tool in the visualisation of on-column effects such as band broadening.

In polymeric monolithic columns, the techniques used to produce a longitudinal change in surface chemistry are varied, and can have numerous negative effects on separations, due to inadequate characterisation during fabrication.

In an attempt to produce a linear photo-grafted gradient of selectivity upon a polymeric monolithic column, an optical filter was developed and fabricated using commercially available polymer films. The production of such a filter had not been previously documented. The application of the filter to the production of tailored stationary phase gradients in polymeric monolithic columns is also a novel feature. The distribution of ionised functional groups longitudinally along the column was rapidly visualised, with no interference to the column structure, using sC^{4}D. In comparison to stationary phase columns produced using co-polymerisation, using method of static immobilisation of copper ions, a higher concentration of copper ions could be immobilised to surface localised chelating ligands, as determined by C^{4}D. The optical filter demonstrated an improvement towards the fabrication of viable stationary phase gradient columns. The use of such an optical filter may produce monolithic columns with varying pore size distributions, in rapid photo-initiated processes, with possible applications in size exclusion chromatography. The use of the optical filter in such an application has yet to be demonstrated.

Two dimensional techniques are growing in popularity due to the ability to perform separations using two orthogonal methods, in a single column or device. Nano-particles are becoming a growing interest to researchers, and so present new challenges in characterisation techniques. Scanning C^{4}D was used to accurately, and non-invasively, profile columns following each step in the fabrication process. Following amination, sC^{4}D could map the charged amine groups expressed on the surface. The equivalent ionic conductance of the aminated zone was profoundly reduced upon the application of gold nano-particles. The scanning of a column containing immobilised nano-particles has not yet been reported in the literature, and so presents a novel application of sC^{4}D. This methodology can also be applied to the production of numerous other devices. For example, a column consisting of iron oxide nano-particles followed by a reversed phase section of stationary phase, may be useful in the extraction and separation of phosphopeptides. Similarly, using two types of nano-structures, such as iron oxide nano-particles and gold nano-particles, could be immobilised to a polymer monolith to produce a column suited for multi-affinity chromatography (e.g. phosphopeptides and cysteine containing peptides). Accurate positioning of graft sites and immobilisations can be accurately mapped using sC^{4}D.

In conclusion, the use of C^4D, whether in scanning mode or stationary mode, has been an invaluable tool in the profiling and characterisation of stationary phases in capillary housed monolithic columns. The non-invasive and non-destructive method of sC^4D is advantageous, as the chemistry occurring within the column can be visualised and profiled without interference or destruction of the monolithic column. In using sC^4D for the visualisation of surface available functional groups, the fabrication of monolithic columns exhibiting a longitudinal increase of selectivity could be validated, and adapted to allow for a more ideal, linear gradient shape. The use of C^4D in the investigation of stationary phases for enhanced separation ability, or applications, is clearly demonstrated as a powerful analytical tool in the characterisation and profiling of stationary phases for use in separation science.